Metabolic liver disease and hepatocellular cancer: exploring the role of AKR1C1 and POR

Ismael Quirin Huber

Lincoln College
University of Oxford

A thesis submitted for the degree of Doctor of Philosophy

Trinity 2023

Abstract

Non-alcoholic fatty liver disease (NAFLD) is the hepatic manifestation of the continuing epidemic of metabolic disease including obesity and type 2 diabetes mellitus (T2DM). Currently, approximately 25% of the population and over 80% of obese individuals or those with T2DM have NAFLD with varying degrees of severity. The underlying cellular mechanisms contributing to the natural history of the condition still remain poorly understood and research into molecular targets remains a priority with no approved treatment currently available. As a consequence, NAFLD is the most rapidly growing cause of hepatocellular cancer (HCC) and accounts for more than 15% of liver transplants due to liver failure or progression to HCC.

Steroid hormones and the enzymes that metabolize them are believed to play a key role in metabolic liver disease and disease progression. Aldo-keto reductase 1C1 (AKR1C1), acting mainly as a 20α-HSD, plays a pivotal role in inactivating progesterone and has been implicated in multiple cancers including ovarian, bladder and non-small lung cancer (NSCLC). Cytochrome p450 reductase (POR) acts as an electron shuttle, facilitating the transfer of electrons from co-factors like NADPH to cytochrome p450 (CYP) enzymes and has been incidentally found to cause liver steatosis in mice knockout studies. Both AKR1C1 and POR are highly expressed in the liver but any potential pathogenic role has remained almost completely unexplored in liver disease.

High expression and activity of AKR1C1 showed significant association with HCC and poor prognosis in patients diagnosed with HCC. In contrast, in hepatoma cell lines, HepG2 and Huh7, knockdown of AKR1C1 with siRNA and CRISPR showed very little effect on differential gene expression and does not cause any changes in proliferation or cell motility. I have for the first time shown that AKR1C1 is probably unlikely to play a role in HCC development and progression.

Patients with NAFLD showed significant attenuation of POR expression and activity as well as compensatory up regulation of CYP7A1 and CYP7B1 expression. Furthermore, mice and HepG2 cell line fed with NAFLD inducing diet and media, showed lower POR expression on both mRNA and protein level. Gene silencing of POR in hepatoma cell line showed increased fatty acid oxidation (FAO) on transcriptional, protein and biomarker level, disturbed cholesterol metabolism and an increase of the alternative bile acid synthesis pathway. I provided the first evidence of a regulatory role for POR in metabolic homeostasis and that their might be potential for POR activity to serve as a non-invasive clinical marker in metabolic liver disease.

Metabolic liver disease and hepatocellular cancer: exploring the role of AKR1C1 and POR



Ismael Quirin Huber

Lincoln College

University of Oxford

A thesis submitted for the degree of

Doctor of Philosophy

Trinity 2023

To mum and dad

Acknowledgements

Firstly, I would like to thank my supervisors Prof Jeremy Tomlinson, Dr Nikolaos Nikolaou and Prof Leanne Hodson for their constant guidance, their instructions in the lab and their willingness to help. Their encouragement and trust instilled me with the necessary confidence to overcome all the challenges I faced throughout my studies.

To all my colleagues in the JWT group and OCDEM who have helped with my experiments or analysis in any way, big or small. Nick, thanks for not just being my supervisor and closest advisor in the lab but also for the friendship, your patience and the laughter that made my time at OCDEM all the more enjoyable. Anastasia, Laura, Tom M, Tom P, Hamish thank you for your ideas, discussions and presentation during our lab meetings. Also, I would like to thank Elsbeth for helping me with countless little things and training me up on the GC-MS. Moreover, I would like to express my gratitude to Jake for the countless discussions and brainstorming sessions over dinner, the laughter and friendship, as well as the help with generating the CRISPR plasmids. Many thanks also to Ellie, for always having an open ear and making life in and out of the lab a bit more fun, especially during times of COVID-19.

To my parents, Barbara and Felix, your unwavering support, love, and encouragement have been the bedrock of each and every successful step I have taken. From the earliest days you instilled me with curiosity and a passion to explore the unknown and taught me how to be kind, ambitious, independent but above all grateful, even for the small things in life. Thank you.

Finally, thanks to to all my friends in the UK and back in Switzerland. Above all, to Tobi, despite the distance, you have supported me in every situation, being not just a friend but family.

I extend my sincere appreciation to the Berrow Foundation and the Radcliffe Department of Medicine for their generous financial support. The Berrow Foundation Lord Florey Scholarship was crucial to fund my doctoral studies, and I am honored to have been a beneficiary of their support.

Abstract

Non-alcoholic fatty liver disease (NAFLD) is the hepatic manifestation of the continuing epidemic of metabolic disease including obesity and type 2 diabetes mellitus (T2DM). Currently, approximately 25% of the population and over 80% of obese individuals or those with T2DM have NAFLD with varying degrees of severity. The underlying cellular mechanisms contributing to the natural history of the condition still remain poorly understood and research into molecular targets remains a priority with no approved treatment currently available. As a consequence, NAFLD is the most rapidly growing cause of hepatocellular cancer (HCC) and accounts for more than 15% of liver transplants due to liver failure or progression to HCC.

Steroid hormones and the enzymes that metabolize them are believed to play a key role in metabolic liver disease and disease progression. Aldo-keto reductase 1C1 (AKR1C1), acting mainly as a 20α-HSD, plays a pivotal role in inactivating progesterone and has been implicated in multiple cancers including ovarian, bladder and non-small lung cancer (NSCLC). Cytochrome p450 reductase (POR) acts as an electron shuttle, facilitating the transfer of electrons from co-factors like NADPH to cytochrome p450 (CYP) enzymes and has been incidentally found to cause liver steatosis in mice knockout studies. Both AKR1C1 and POR are highly expressed in the liver but any potential pathogenic role has remained almost completely unexplored in liver disease.

High expression and activity of AKR1C1 showed significant association with HCC and poor prognosis in patients diagnosed with HCC. In contrast, in hepatoma cell lines, HepG2 and Huh7, knockdown of AKR1C1 with siRNA and CRISPR showed very little effect on differential gene expression and does not cause any changes in proliferation or cell motility. I have for the first time shown that AKR1C1 is probably unlikely to play a role in HCC development and progression.

Patients with NAFLD showed significant attenuation of POR expression and activity as well as compensatory up regulation of CYP7A1 and CYP7B1 expression. Furthermore, mice and HepG2 cell line fed with NAFLD inducing diet and media, showed lower POR expression on both mRNA and protein level. Gene silencing of POR in hepatoma cell line showed increased fatty acid oxidation (FAO) on transcriptional, protein and biomarker level, disturbed cholesterol metabolism and an increase of the alternative bile acid synthesis pathway. I provided the first evidence of a regulatory role for POR in metabolic homeostasis and that their might be potential for POR activity to serve as a non-invasive clinical marker in metabolic liver disease.

Contents

List of Figures **x**

List of Tables **xiii**

List of Abbreviations **xiv**

1 Introduction **1**

1.1 Liver . . . 2
1.1.1 Histology . . . 2
1.1.2 Liver cells . . . 3
1.1.3 Liver function . . . 5
1.1.4 Liver lipid metabolism . . . 6
1.1.5 Liver bile acid metabolism . . . 9
1.1.6 Liver steroid metabolism . . . 11
1.2 Bile acids . . . 11
1.2.1 Synthesis . . . 12
1.2.2 Function . . . 12
1.2.3 Involvement in disease . . . 16
1.3 Steroid hormones . . . 17
1.4 Non-alcoholic fatty liver disease . . . 18
1.4.1 Pathogenesis . . . 19
1.4.2 NAFLD and steroid hormones . . . 22
1.5 Liver Cancer . . . 23
1.5.1 Pathogenesis . . . 24
1.5.2 Liver cancer and NAFLD . . . 27
1.5.3 Liver cancer and steroid hormones . . . 27
1.6 Aldo-Keto Reductase 1C1 . . . 28
1.6.1 Aldo-Keto Reductase 1C . . . 28
1.6.2 Function . . . 28
1.6.3 Tissue expression . . . 29
1.6.4 Structure . . . 29
1.6.5 AKR1C1 and Cancer . . . 30
1.6.6 AKR1C1 and HCC . . . 31
1.7 Cytochrome p450 reductase . . . 33
1.7.1 Function . . . 33
1.7.2 Mechanism . . . 34
1.7.3 Structure . . . 35

1.7.4 POR and human phenotype 35
1.7.5 POR and mouse phenotype 37
1.8 Aims and objectives 38

2 Methods **39**
2.1 Cell lines 40
2.2 Cell culture 40
2.3 Cloning 41
2.4 Transformation 41
2.5 Transfection 42
2.6 Gene manipulation 42
2.6.1 Transient knockdown 42
2.6.2 Stable CRISPR/Cas9 knockdown 44
2.6.3 Overexpression 44
2.7 Pregnanediol-3-Glucuronide Competitive ELISA 45
2.8 Gene expression 46
2.8.1 RNA extraction 46
2.8.2 RNA sequencing 47
2.8.3 Reverse Transcription Polymerase Chain Reaction 49
2.8.4 Quantitative Polymerase Chain Reaction 50
2.9 Protein expression 51
2.9.1 Protein extraction 51
2.9.2 Protein quantification 52
2.9.3 Western blotting 52
2.10 Biochemical measurements 54
2.10.1 Sample preparation 54
2.10.2 Glucose 55
2.10.3 TAG 55
2.10.4 NEFA 55
2.10.5 Cholesterol 56
2.11 D-3-Hydroxybutyrate 56
2.12 Lipid measurements 56
2.12.1 Lipid extraction 56
2.12.2 Gas chromatography 58
2.12.3 Gas chromatography-mass spectrometry 58
2.13 Bile acids quantification 59
2.13.1 Total bile acid assay 59
2.13.2 Liquid chromatography–mass spectrometry of bile acids . . . 59
2.14 Statistical analysis 60
2.15 Outsourced methods 61

3 Characterisation of AKR1C1 in humans **62**
3.1 Introduction . . . 62
3.1.1 AKR1C1 in cancer . . . 62
3.1.2 AKR1C1 in NAFLD . . . 63
3.1.3 AKR1C1 urinary steroid ratios . . . 63
3.1.4 Hypothesis and aims . . . 65
3.2 Methods . . . 66
3.2.1 Data mining . . . 66
3.2.2 Liver biopsies . . . 66
3.2.3 Urine samples . . . 67
3.3 *AKR1C1* expression in HCC . . . 69
3.4 *AKR1C1* expression in NAFLD . . . 71
3.5 Functional AKR1C1 activity in humans . . . 74
3.6 Discussion . . . 77

4 AKR1C1 in hepatocellular model **80**
4.1 Introduction . . . 81
4.1.1 AKR1C1 in liver cancer . . . 81
4.1.2 Hypothesis and aim . . . 82
4.2 Methods . . . 83
4.2.1 Cell culture . . . 83
4.2.2 Pharmacological AKR1C1 inhibition . . . 83
4.2.3 Pregnanediol-3-Glucuronide Competitive ELISA . . . 83
4.2.4 Transient knockdown . . . 85
4.2.5 CRISPR/Cas9 . . . 86
4.2.6 Overexpression . . . 86
4.2.7 MTS cell proliferation and viability assays . . . 86
4.2.8 Chemotoxicity assays . . . 87
4.2.9 Wound healing assay . . . 87
4.3 AKR1C1 expression in hepatoma cell lines . . . 88
4.4 Pharmacological inhibition . . . 88
4.5 Transient knockdown . . . 89
4.5.1 siRNA variants . . . 89
4.5.2 Dose optimisation . . . 89
4.6 Stable knockdown . . . 90
4.7 Overexpression . . . 92
4.8 RNA sequencing . . . 94
4.9 Proliferation and chemo resistance . . . 98
4.10 Motility . . . 102
4.11 Discussion . . . 104

5 Characterisation of POR in human and rodent NAFLD model 108
5.1 Introduction . . . 108
5.1.1 POR deficiency . . . 108
5.1.2 POR in NAFLD . . . 109
5.1.3 POR urinary steroid ratio . . . 110
5.1.4 Hypothesis and aims . . . 110
5.2 Methods . . . 111
5.2.1 Liver biopsies . . . 111
5.2.2 Urine samples . . . 112
5.2.3 Mouse husbandry and experimental design . . . 113
5.2.4 Mouse tissue collection . . . 114
5.2.5 Cell culture . . . 115
5.2.6 OPLA2 lipid loading . . . 115
5.3 POR in patients with NAFLD . . . 116
5.3.1 *POR* mRNA expression . . . 116
5.3.2 POR activity . . . 118
5.3.3 CYP mRNA expression . . . 119
5.4 POR in rodent NALFD model . . . 121
5.5 POR in fat loaded cell model . . . 121
5.5.1 Optimisation of lipid loading . . . 121
5.5.2 POR mRNA and protein expression after lipid loading . . . 121
5.6 Discussion . . . 124

6 Actions of POR on metabolic pathways 127
6.1 Introduction . . . 127
6.1.1 Hypothesis and aims . . . 129
6.2 Methods . . . 130
6.2.1 Cell culture . . . 130
6.2.2 Transient knockdown . . . 130
6.2.3 Overexpression . . . 130
6.2.4 Biochemical measurements . . . 130
6.2.5 Lipid measurements . . . 131
6.2.6 AdipoRed assay . . . 131
6.2.7 Bile acid quantification . . . 131
6.2.8 Proliferation assay . . . 131
6.3 POR expression in HepG2 cell line . . . 133
6.4 Transient knockdown . . . 133
6.5 Overexpression . . . 134
6.6 RNA sequencing . . . 135

6.7 Lipid metabolism 140
6.7.1 Triacylglycerol 142
6.7.2 Cholesterol 146
6.8 Bile acid metabolism 149
6.9 Glucose metabolism 154
6.10 Discussion 157

7 Discussion **162**
7.1 Conclusion and discussion 162
7.2 Future experiments and directions 167
7.2.1 AKR1C1 in HCC and as prognostic marker 167
7.2.2 POR and fibrosis 168
7.2.3 POR and bile acids 169
7.2.4 POR and nuclear receptor activation 169
7.2.5 POR activity for clinical diagnostics 169

Appendices

References **172**

List of Figures

1.1 Functional anatomical liver model 3
1.2 Histology of the liver: hepatic lobules 4
1.3 *de novo* lipogenesis and TAG synthesis 8
1.4 Regulation of fatty acid metabolism in the liver 9
1.5 Micelles formed by bile acids 13
1.6 Bile acid synthesis pathways 13
1.7 FXR regulatory pathway 15
1.8 Progression of NAFLD: different stages of disease 20
1.9 NAFLD pathogenesis 21
1.10 Impact of steroid hormones on hepatic lipid homeostasis 22
1.11 5-year cancer survival in men and women 2013-2018 in England . . 24
1.12 AKR1C1 tissue expression 30
1.13 3D protein structure of AKR1C1 31
1.14 AKR1C1 isoform protein sequence 32
1.15 POR electron transfer 34

2.1 Transient knockdown with siRNA and overexpression using DNA plasmid 43
2.2 AKR1C1 GFP tagged clone 45

3.1 Urinary glucocorticoid metabolites as proxy for AKR1C1 activity . 63
3.2 Urinary pregnanetriol metabolites as proxy for AKR1C1 activity . . 64
3.3 Expression of AKR1C1 in HCC patients and impact on overall survival 70
3.4 Expression of *AKR1C1* in patients with NAFLD 71
3.5 Expression of *AKR1C1* in female patients with NAFLD 72
3.6 Urinary glucocorticoid metabolome in cirrhosis and liver cancer . . 73
3.7 Urinary glucocorticoid metabolome in NAFLD 75
3.8 Cortol and cortolone α/β ratio 76

4.1 Progesterone metabolite Pregnanedio-3-glucuronide 84
4.2 5-PBSA concentration in bovine aortic endothelial cells 85
4.3 AKR1C1 expression in HepG2 and Huh7 88
4.4 Pregnandiol-3-Glucuronide (PDG) reduction after treatment with 5-PBSA 89
4.5 Optimisation of siRNA variant and dose of *AKR1C1* mRNA knockdown in Huh7 and HepG2 90
4.6 Transient AKR1C1 knockdown model in Huh7 and HepG2 cells . . 91
4.7 CRISPR/Cas9 gRNA optimisation in HepG2 and Huh7 92

4.8 Stable *AKR1C1* knockdown: *AKR1C1* mRNA and protein in HepG2 92
4.9 AKR1C1 overexpression: protein in HepG2 93
4.10 Fluorescence of GFP and AKR1C1-GFP 94
4.11 Principal component analysis: transient *AKR1C1* knockdown . . . 95
4.12 Differential gene expression of *AKR1C1* siRNA-transfected cells . . 96
4.13 Cell cycle genes in *AKR1C1* siRNA-transfected HepG2 cells 96
4.14 Cell cycle genes in multiple AKR1C1 inhibition model 97
4.15 Principal component analysis and differential gene expression of CRISPR/Cas9 *AKR1C1* knockdown 97
4.16 Proliferation of HepG2 and Huh7 after *AKR1C1* siRNA knockdown 98
4.17 Proliferation of HepG2 and Huh7 after pharmacological AKR1C1 inhibition 99
4.18 Cell viability after Sorafenib treatment and siRNA knockdown or pharmacological inhibition of AKR1C1 100
4.19 Sorafenib treatment after universal *AKR1C1* siRNA knockdown . . 101
4.20 Wound healing assay after *AKR1C1* siRNA knockdown 102
4.21 Wound healing assay after *AKR1C1* CRISPR/Cas9 knockdown . . 103

5.1 17α-hydroxylase and 21-hydroxylase in steroid metabolism and synthesis 111
5.2 *POR* mRNA expression in patients with NAFLD 116
5.3 *POR* mRNA expression in female patients with NAFLD 117
5.4 Inverse POR activity ratio from urinary metabolites 118
5.5 *CYP7A1* mRNA expression in patients with NAFLD 119
5.6 *CYP7B1* mRNA expression in patients with NAFLD 120
5.8 Lipid loading optimisation of HepG2 cells 123
5.9 POR mRNA and protein expression after lipid loading 123

6.1 POR mRNA and protein expression in HepG2 cells 133
6.2 *POR* siRNA knockdown optimisation in HepG2 cell line 134
6.3 POR overexpression in HepG2 cell line 135
6.4 Number of expressed genes and PCA analysis of *POR* siRNA vs scrambled control siRNA transfected HepG2 cells 136
6.5 Differential expression of *POR* vs scrambled control siRNA-transfected HepG2 cells 137
6.6 DysGeNET mapping and CNET plotting of transcriptomic profile . 138
6.7 PPAR pathway in *POR* siRNA transfected HepG2 cells 140
6.8 Total and phosphorylated AMPK and ACC protein in *POR* siRNA-transfected HepG2 cells 141

6.9 *CPT1A* and FASN expression in in *POR* siRNA-transfected HepG2 cells . . . 141
6.10 Intracellular TAG and phospholipids in *POR* siRNA-transfected HepG2 cells . . . 142
6.11 Cellular lipid quantification with AdipoRed . . . 143
6.12 DNL in POR or scrambled control siRNA-transfected HepG2 cells . 144
6.13 Lipid uptake and β-oxidation by HepG2 cells . . . 145
6.14 TAG composition in *POR* siRNA-transfected HepG2 cells . . . 146
6.15 Impact of POR knockdown on cholesterol biosynthesis and uptake . 147
6.16 *CYP7A1* and *LDLR* expression in *POR* siRNA-transfected HepG2 cells . . . 148
6.17 Total cellular and media cholesterol and cholesterol ester in POR si RNA-transfected HepG2 cells . . . 149
6.18 Bile acid biosynthesis KEGG pathway . . . 150
6.19 qPCR of bile acid biosynthesis genes in *POR* siRNA knockdwon HepG2 cells . . . 151
6.20 Bile acid concentration in media of *POR* siRNA-transfected HepG2 cells . . . 151
6.21 Individual bile acids in media of *POR* siRNA-transfected HepG2 cells 152
6.22 12α-hydroxylated and non-12α-hydroxylated bile acids in *POR* siRNA transfected HepG2 cells . . . 153
6.23 Bile acids in POR overexpressed HepG2 cells . . . 153
6.24 12α-hydroxylated and non-12α-hydroxylated bile acids in POR over-expressed HepG2 cells . . . 154
6.25 Genes of glucose metabolism in *POR* siRNA-transfected HepG2 cells 155
6.26 Glucose in media of *POR* siRNA-transfected HepG2 cells . . . 155
6.27 Impact of low and high glucose culture media on POR expression in HepG2 cells . . . 156
6.28 *CYP51A1* mRNA expression in *POR* siRNA transfected HepG2 cells 159

7.1 Hypothesis of disturbed FXR pathway . . . 165
7.2 *MBOAT7* expression in *POR* siRNA transfected HepG2 cells . . . 168

List of Tables

1.1 Steroid hormones and liver steatosis in animal models 23
1.2 Gene mutation frequency in HCC 26
1.3 List of AKR1C1 substrates 28

2.1 Western blot anti-bodies 54

3.1 Urinary product-substrate ratios of steroid hormones 65

4.1 Guide RNA of stable *AKR1C1* knockdown 86

6.1 POR knockdown: top 40 expressed CYP genes 139

List of Abbreviations

3-OHB 3-hydroxybutyrate

5-PBSA . . . . 3-Bromo-5-phenylsalicylic acid

5αTHF 5α-tetrahydrocortisol

ACC . . . . . Acetyl-CoA carboxylase

AKR . . . . . Aldo-keto reductases

AKR1C . . . . Aldo-Keto Reductase 1C

AKR1C1 . . . Aldo-Keto Reductase 1C1

ALIOS . . . . American lifestyle-induced obesity syndrome

AMPK . . . . AMP-activated protein kinase

ARE . . . . . Antioxidant response element

ASBT . . . . . Apical sodium dependent transporter

BA . . . . . Bile acids

BSA . . . . . Bovine serum albumin

BSEP . . . . . Bile salt export pump

CA . . . . . Cholic acid

CAH . . . . . Congenital adrenal hyperplesia

Cas9 . . . . . CRISPR associated protein 9

CBG . . . . . Corticosteroid-binding globulin

CDCA . . . . . Chenodeoxycholic acid

cDNA . . . . . Complementary DNA

CE . . . . . Cholesterol ester

ChREBP . . . Carbohydrate responsive element-binding protein

CMV . . . . . Cytomegalovirus

COMT . . . . Catechol-O-methyl transferases

CPT1 . . . . . Carnitine palmitoyl-CoA transferase I

CRAC . . . . . Cholesterol recognition/interaction amino acid consensus sequence

CRISPR . . . Class 2 Clustered Regularly Interspaced Short Palindromic Repeat

crRNA . . . . CRSIPR RNA

CYP . . . . . cytochrome p450s

CYP27A1 . . 27-hydroxylase

CYP51A1 . . Lanosterol 14α-demethylase

CYP7A1 . . . Cholesterol 7α-hydroxylase

CYP7B1 . . . Oxysterol 7α-hydroxylase

CYP8B1 . . . Sterol 12α-hydroxylase

DAG . . . . . Diglyceride

DC . . . . . detergent compatible

DCA . . . . . Deoxycholic acid

DHEA . . . . Dehydroepiandrosterone

DMEM . . . . Dulbecco's Minimum Essential Medium

DNL . . . . . *de novo* lipogenesis

ELOVL . . . . Fatty acid elongase

ESAM . . . . . Endothelial cell adhesion molecule

FA . . . . . Fatty acids

FAD . . . . . Flavin adenine dinucleotide

FAMEs . . . . Fatty acid methyl esters

FAO . . . . . Fatty acid oxidation

FASN . . . . . Fatty acid synthase

FFA . . . . . Free fatty acids

FGF19 . . . . . Fibroblast growth factor 19

FGFR4 . . . . Fibroblast growth factor receptor 4

FMN . . . . . Flavin mononucleotide

FPKM . . . . Fragments Per Kilobase of transcript per Million mapped reads

FXR . . . . . Farnesoid X receptor

FXRE . . . . . FXR response element

G6PD . . . . . Glucose-6-phosphate dehydrogenase

GC . . . . . Gas chromatography

GC-MS . . . . Gas chromatography-mass spectrometry

GEPIA . . . . Gene Expression Profiling Interactive Analysis

GFP . . . . . Green fluorescent protein

GLA . . . . . Gamma-linolenic acid

GO . . . . . Gene Ontology

GPBAR1 . . . G protein-coupled bile acid receptor 1

GPCR . . . . . G protein-coupled receptors

gRNA . . . . . Guide RNA

GYS1 . . . . . Glycogen synthase 1

HBV . . . . . Hepatitis B virus

HCA . . . . . Hepatocellular adenoma

HCC . . . . . Hepatocellular carcinoma

HCV . . . . . Hepatitis C virus

HDL . . . . . High-density lipoprotein

HFD . . . . . High fat diet

HNE Hydroxy-2-nonenal

HO-1 . . . . . Heme oxygenase 1

HPRT . . . . . Hypoxanthine-guanine phosphoribosyltransferase

HRP . . . . . Horseradish peroxidase

HSC . . . . . Heaptic stellate cells

HSD . . . . . Hydroxysteroid dehydrogenase

HSD3B7 . . . 3β-hydroxysteroid dehydrogenase type 7

HTGL . . . . . Hepatic triglyceride lipase

IBAT . . . . . Ileal bile acid transporter

IBD . . . . . Inflammatory bowel disease

IR . . . . . Insulin resistance

IS . . . . . Internal standard

JNK . . . . . c-Jun N-terminal kinase

KEGG . . . . . Kyoto Encyclopedia of Genes and Genomes

L1CAM . . . . L1 cell adhesion molecule

LB . . . . . Lysogeny broth

LCA . . . . . Lithocholic acid

LRH-1 . . . . . Liver receptor homolog-1

LTA . . . . . Lipoteichoic acid

LXR . . . . . Liver X receptor

MAG . . . . . Monoglyceride

MASH . . . . Metabolic dysfunction-associated steatohepatitis

MASLD . . . . Metabolic dysfunction-associated steatotic liver disease

MGB . . . . . Minor groove binder

MRP2 . . . . . Multidrug resistance-associated protein 2

MS . . . . . Mass spectrometer

mTOR . . . . Mammalian target of rapamycin complex

MTS . . . . . CellTiter 96® AQueous One Solution Cell Proliferation Assay

NADPH . . . Nicotinamide cofactor

NAFLD . . . . Non-alcoholic fatty liver disease

NAS . . . . . NAFLD Activity Score

NASH . . . . . Non-alcoholic steatohepatitis

NEFA . . . . . Non-estesterified fatty acid

NF-κB . . . . . Nuclear factor-κB

NRF2 . . . . . Nuclear factor erythroid 2-related factor 2

NSCLC . . . . Non-small cell lung cancer

padj . . . . . p-value corrected for mutliple testing

PAM . . . . . Protospacer adjacent motif

PCK1 . . . . . Phosphoenolpyruvate carboxykinase 1

PCR . . . . . Polymerase chain reaction

PD . . . . . Pregnanediol

PDG Pregnanediol-3-Glucuronide

PEPCK . . . . Phosphoenolpyruvate carboxykinase

PGC-1α . . . . Peroxisome proliferator-activated receptor gamma coactivator 1α

PL . . . . . Phospholipids

POR . . . . . Cytochrome p450 reductase

PORD . . . . . Cytochrome P450 oxidoreductase deficiency

PPAR . . . . . Peroxisome proliferator-activated receptors

PUFA . . . . . Polyunsaturated fatty acids

PVDF . . . . . Polyvinylidene diflouride

PXR . . . . . Pregnane X receptor

PYGL . . . . . Glycogen phosphorylase L

RIPA . . . . . Radioimmunoprecipitation assay

RISC . . . . . RNA-induced silencing complex

ROS . . . . . Reactive oxygen species

RT . . . . . Reverse transcription

RT-PCR . . . Reverse transcription Polymerase Chain Reaction

RXR . . . . . Retinoid x receptor

S1PR2 . . . . . Sphingosine-1-phosphate receptor 2

SCD . . . . . Stearoyl-CoA desaturase

SDR . . . . . Short-chain dehydrogenase

SHGB . . . . . Sex hormone-binding globulin

SHP . . . . . Small heterodimer partner

SIM . . . . . Single ion monitoring

siRNA . . . . . Short interfering RNA

SLD . . . . . Steatotic liver disease

SPE . . . . . Solid-phase extraction

SREBP . . . . Sterol regulatory element-binding proteins

SULTs . . . . . Sulfotransferases

T2DM . . . . . Type 2 diabetes mellitus

TAG . . . . . Triglyceride

TBS . . . . . Tris-Buffered Saline

TCA . . . . . Tricarboxylic acid cycle

TGS . . . . . Tris/Glycine/SDS

THE . . . . . Tetrahydrocortisone

THF . . . . . tetrahydrocortisol

TLR4 . . . . . Toll like receptor 4

tracrRNA . . Trans-activating crRNA

UDCA . . . . . Ursodeoxycholate

UGT . . . . . UDP glucuronosyltransferases

UHPL . . . . . Ultra High Performance Liquid Chromatography

VLDL . . . . . Very low density lipoprotein

1 Introduction

Contents

1.1 Liver 2
1.1.1 Histology 2
1.1.2 Liver cells 3
1.1.3 Liver function 5
1.1.4 Liver lipid metabolism 6
1.1.5 Liver bile acid metabolism 9
1.1.6 Liver steroid metabolism 11
1.2 Bile acids 11
1.2.1 Synthesis 12
1.2.2 Function 12
1.2.3 Involvement in disease 16
1.3 Steroid hormones 17
1.4 Non-alcoholic fatty liver disease 18
1.4.1 Pathogenesis 19
1.4.2 NAFLD and steroid hormones 22
1.5 Liver Cancer 23
1.5.1 Pathogenesis 24
1.5.2 Liver cancer and NAFLD 27
1.5.3 Liver cancer and steroid hormones 27
1.6 Aldo-Keto Reductase 1C1 28
1.6.1 Aldo-Keto Reductase 1C 28
1.6.2 Function 28
1.6.3 Tissue expression 29
1.6.4 Structure 29
1.6.5 AKR1C1 and Cancer 30
1.6.6 AKR1C1 and HCC 31
1.7 Cytochrome p450 reductase 33
1.7.1 Function 33
1.7.2 Mechanism 34
1.7.3 Structure 35
1.7.4 POR and human phenotype 35
1.7.5 POR and mouse phenotype 37
1.8 Aims and objectives 38

1.1 Liver

The liver is the largest gland, the largest intestinal and central metabolic organ of the human body. It is located directly under the diaphragm mostly in the right upper quadrant of the abdomen but extends over stomach to the left and is covered by the thoracic cage. Weighing between 970 to 1'860 g and 600 to 1'770 g in men and women respectively the liver accounts for approximately 2 to 3% of body weight [1, 2]. The liver consists of left and right liver, which can morphologically be further divided into four lobes: left, right, caudate and quadrate lobes. The functional anatomical model by Claude Couinaud divides the liver into eight segments with each having an individual portal triad branch [3] (Figure 1.1). In the clinical setting the functional anatomy is more relevant. The liver has a unique dual blood supply through the hepatic artery and the portal vein, which collects the blood from the intestines. Both vessels drain into the hepatic sinusoids where the oxygen-rich and nutrient-rich blood mix at a ratio of 25% and 75%. Deoxygenated blood is then collected in the central venules from which it drains into the hepatic vein leading back to the right atrium of the heart via inferior vena cava [4, 5]

1.1.1 Histology

Histologically the liver is built up of small hepatic lobules of the size of 1-2 mm. They have a roughly hexagonal shape and consist of the portal triad in the portal field at each corner, a central vein and hepatocytes arranged in linear cords parallel to the sinusoids which form the capillary bed between the vessels (Figure 1.2). The portal field is formed by branches of the hepatic artery and hepatic portal vein, the billiary ductules, lymphatic vessel and a branch of the vagus nerve. Sinusoids are discontinuous capillaries with pores in the endothelial lining which allow the blood plasma as well as serum proteins to pass through into the perisinoidal space. The contents of the perisinoidal space then drain as

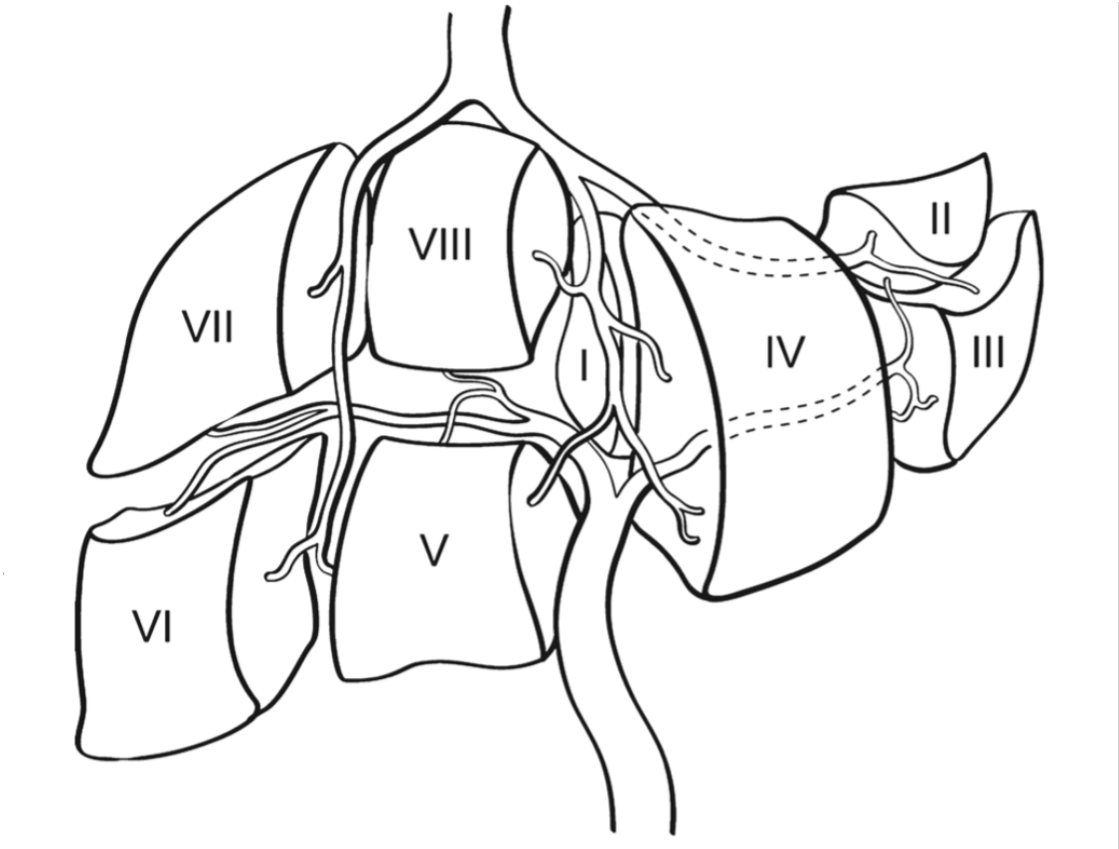


Figure 1.1: The eight liver segments according to the functional anatomical model by Claude Couinaud as shown in The Eighth Edition AJCC Cancer Staging Manual ([6]).

lymph into the lymphatic vessels of the liver. The other side of the perisinoidal space is formed by the basal side of a singular layer of hepatocytes. Hepatocyte microvilli extend into the perisinoidal space and increase the surface area for diffusion. Thereby, they facilitate the absorption of proteins, toxins and other plasma components. Over the apical membrane, hepatocytes secret bile into bile canaliculi formed by two adjacent cells [7].

1.1.2 Liver cells

Liver tissue is formed by two major cell types: parenchymal hepatocytes making up around 55-65% of cells and 80% of liver volume and nonparenchymal cells. Nonparenchymal cells consist of sinusoidal endothelial cells and Kupfer cells lining the sinusoids but also hepatic stellate cells (HSC) occupying the perisinoidal space (space of Disse) in between hepatocytes and sinusoid [8].

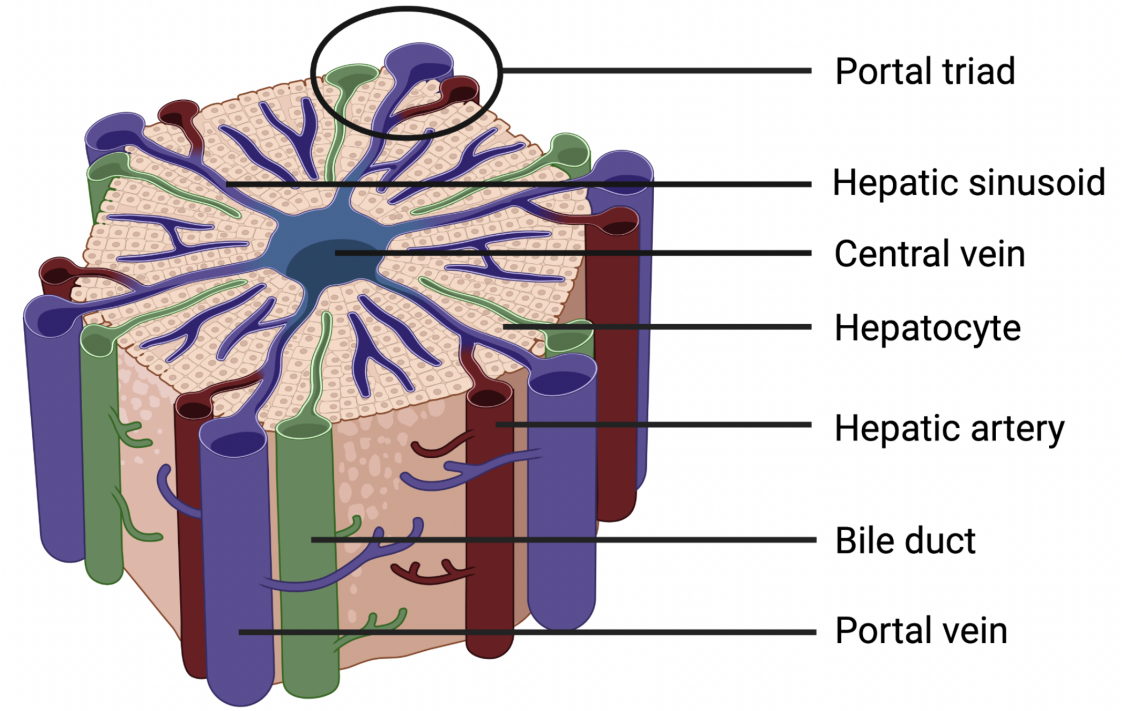


Figure 1.2: Classical structure of a hepatic lobule showing the portal triad (hepatic artery, portal vein and bile duct), the hepatic sinusiod with decreasing oxygen concentrations the closer to the hepatic vein. Hepatocytes are radially ordered with bile canaliculi in between. Created with BioRender.com.

Hepatocytes

Hepatocytes have a life span of approximately 5-months, and possess the ability to regenerate; a property uniquely found in the liver. Hepatocytes have a volume of around 3.4 x 10^{-9} cm^3 and due to their mitochondria rich cytoplasma containing large amounts of rough endoplasmatic reticulum and ribosome, they appear eosinophilic with basophilic granules [9]. Further, they possess a prominent smooth endoplasmatic reticulum which is important in lipid synthesis, steroid metabolism and contains a vital enzyme for gluconeogenesis, glucose-6-phosphatase. Underlining the importance of hepatocytes in an abundance range of metabolic functions performed by the liver ranging from gluconeogenesis, protein-, lipid- and bile synthesis over the storage of glycogen and lipids to detoxification [9, 10].

Hepatic stellate cells

HSC (Ito cells) are located in the perisinoidal space and are symmetrically distributed. They make up only around 8% of liver cells but have a variety of different functions. HSC store 80% of total body vitamin A in lipid droplets. With their cytoplasmatic processes they are believed to be able to regulate sinusoidal blood flow and as antigen presenting cells, they can activate a T cell response. Normally they are in a quiescent state. Liver injury and cellular can cause them to switch to an active state and transdiferantiate to a myofibroblast. As such they proliferate, contract and produce extracellular matrix and collagen scar tissue, therefore playing an important role in the formation of cirrhosis [11–13].

Kupfer cells

Kupffer cells are liver specific macrophages that self-sustain. They line the sinusoid walls and clear the blood of pathogens, noxious substances and old or damaged red blood cells. Kupfer cells sit on a reticulin layer and develop protrusions within the cytoplasm, which facilitate phagocytosis [14]. Through their macrophage CRIg receptor Kupfer cells are able to directly recognise and bind lipoteichoic acid (LTA) on gram-positive bacteria [15]. As innate immune cells with a role in wound healing but also as a proinflammatory mediator they play an important role in various liver diseases [16].

1.1.3 Liver function

The liver is structured so that it can perform a large number of different activities including synthesis, breakdown, storage and detoxification of a range of substances. It is a vital part of glucose, protein and lipid metabolism as well as storing fat-soluble vitamins and trace elements such as iron and copper. Furthermore, it is responsible for the production of bile which allows secretion of fat-soluble toxins. To be able to clear the blood effectively from toxins, the liver receives approximately 25% of resting cardiac output, corresponding to 1.5 l / min of blood. [4, 5, 17].

1.1.4 Liver lipid metabolism

The liver is the central organ in lipid metabolism and controls *de novo* lipogenesis (DNL), lipolysis and fatty acid oxidation (FAO) *via* key regulators including transcription factors, such as sterol regulatory element-binding proteins (SREBPs), peroxisome proliferator-activated receptors (PPARs), and liver X receptors (LXRs), as well as signaling pathways, such as AMP-activated protein kinase (AMPK), and mammalian target of rapamycin complex 1 (mTORC1).

de novo lipogenesis

DNL is the process of synthesising fatty acids (FA) from acetyl-CoA, primarily derived from glucose. Glucose enters the hepatocyte through the glucose transporter, GLUT2 and is broken down via glycolysis into pyruvate within the cells. Subsequently, pyruvate is transported to the mitochondria and converted to acetyl-CoA by pyruvate dehydrogenase [18]. As acetyl-CoA cannot cross the mitochondrial membrane it is fed into the tricarboxylic acid cycle (TCA), crosses the membrane as citrate, and *via* ATP-citrate lyase and oxaloacetate converted back to acetyl-CoA [19]. The conversion of acetyl-CoA to malonyl-CoA is facilitated by the rate limiting enzyme acetyl-CoA carboxylase 1 (ACC1) located in the cytosol. Another isoform, ACC2, localized to the outer membrane of mitochondria inhibits the activity of carnitine palmitoyl-CoA transferase I (CPT1), leading to a subsequent decrease in mitochondrial FAO (Figure 1.4) [20]. Afterwards, fatty acid synthase (FASN) catalyzes the enzymatic reactions, seven cycles of malonyl-CoA addition to an acetyl-CoA primer, ultimately yielding the saturated 16-carbon FA palmitate from malonyl-CoA [21, 22]. Palmitate can then be elongated or desaturated by fatty acid elongase (ELOVL) or stearoyl-CoA desaturase (SCD) respectively to generate very long chain FA (>16 carbon atoms) or palmitoleate. ELOVL6, present in human liver, elongates C16:0 and C16:1 to the respective C18 form [23]. DNL regulation is primarily orchestrated by sterol regulatory element-binding protein 1c (SREBP1c) and carbohydrate responsive element-binding protein (ChREBP) *via* transcriptional regulation of ACC and FAS [24]. Within the liver, all FA including

dietary and synthesized FA are believed to be pooled in one common FA pool before being partitioned in two pathways: esterification or oxidation [25]. When FA are esterified to a glycerol molecule, they produce monoglyceride/monoacylglycerol (MAG), diglyceride/diacylglycerol (DAG) and triglyceride/triacylglycerol (TAG) for storage or to be transported to peripheral tissue as part of very low density lipoprotein (VLDL).

Lipolysis

The breakdown of stored triglycerides into glycerol and free fatty acids (FFA) is another essential component of liver lipid metabolism. The FFA released during lipolysis can be used directly for energy production or can be re-esterified back into triglycerides. Hepatic triglyceride lipase (HTGL) is mainly expressed at the surface of hepatocytes and the endothelial cells in the hepatic sinusoids [26]. The process of lipolysis occurs in a highly regulated and sequential manner. HTGL hydrolyses TAG to DAG, followed by further hydrolysis to MAG, resulting in the release of a FA at each step. Finally, MAG is hydrolyzed, leading to the liberation of the last FA and glycerol. Furthermore, HTGL also hydrolyses phospholipids contained in lipoproteins [27].

Fatty acid oxidation

Breaking down FA to produce energy for the liver itself or indirectly for other tissues *via* the production of ketone bodies (β-hydroxybutyrate, acetoacetate and acetone) [28]. FAO (β-oxidation) occurs in the mitochondria, where FA are converted into acetyl-CoA. Long chain FA are linked to CoA on the outer membrane of the mitochondria but need the rate limiting enzyme CPT1 to be transported to the mitochondrial matrix. β-oxidation proceeds in 4 steps and cleaves 2 carbons each cycle to form acetyl-CoA and 5 ATP molecules. The acetyl-CoA produced can then enter the TCA for further energy production. As described in Section 1.1.4 ACC2 inhibits CPT1 via malonyl-CoA production and thereby the translocation of FFA into the mitochondrial matrix. ACC2 is further inhibited by phosphorylation through AMPK (Figure 1.4. Activation of PPARα on the other hand increases

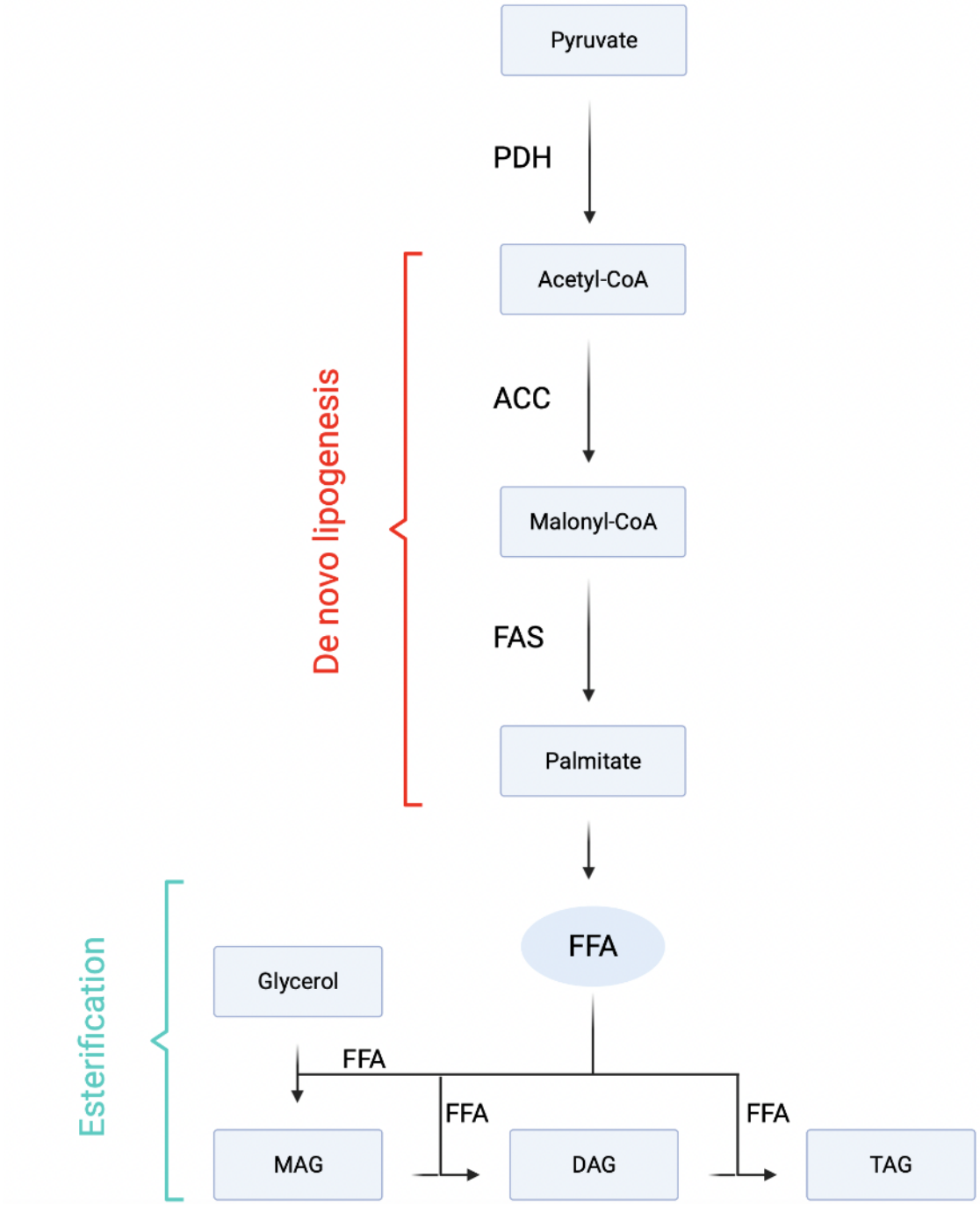


Figure 1.3: The synthesis of TAG is dependent on A) DNL, which produces FFA from pyruvate via acetyl-CoA and malonyl, and B) the esterification of FFA to a glycerol molecule. Created with BioRender.com.

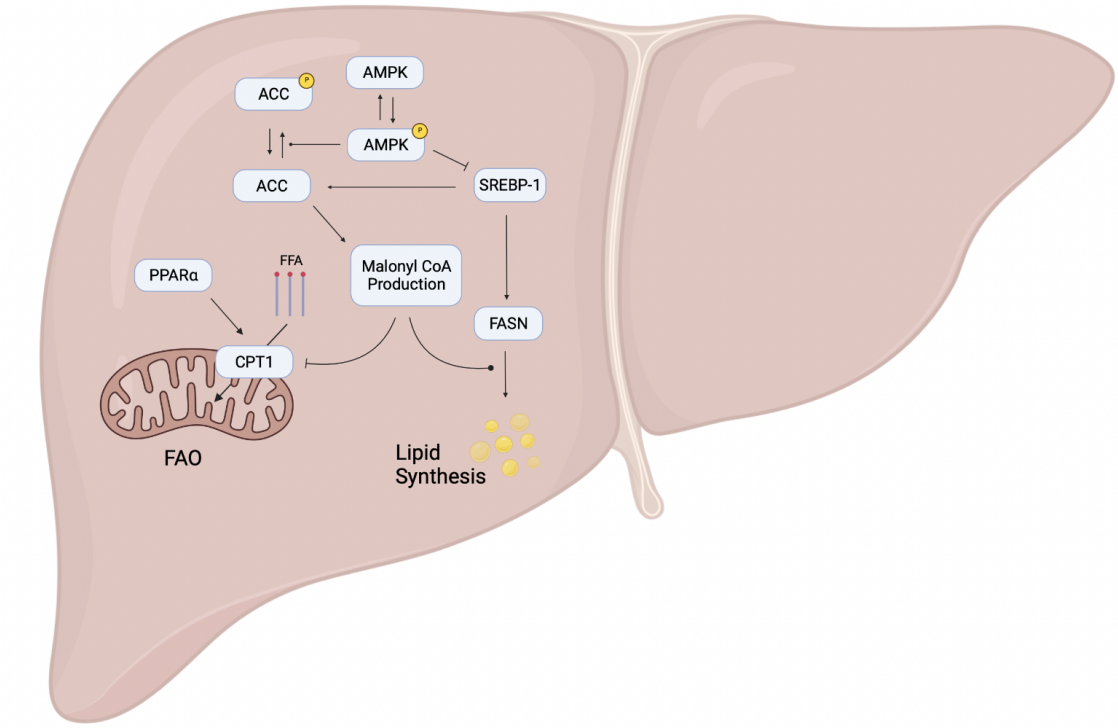


Figure 1.4: The liver is a central player in the lipid metabolism which is regulated via key pathways such as AMPK and PPARα. The phosphorylation of AMPK and thereby ACC1 limits the rate of malonyl production and inhibits lipid synthesis. Upon phosphorylation ACC2 loses the capacity to inhibit CPT1 via its malonyl production on the outer membrane of the mitochondria which in turn drives fatty acid oxidation (FAO). Additionally, CPT1 is up-regulated upon PPARα activation. In reverse, unphosphorylated AMPK and ACC drive SREBP-1 and malonyl production leading to increased lipid synthesis and inhibition of FAO. Created with BioRender.com.

CPT1 expression and promotes β-oxidation [29, 30]. Deregulation of FAO can lead to a variety of metabolic disorders, highlighting the importance of this process in maintaining metabolic health. Under normal conditions, the liver typically stores minimal quantities of TAG as they are primarily stored in lipid droplets in adipocytes. The FA uptake of the liver is proportional to circulating concentration of FA and therefore during conditions of prolonged heightened energy availability increased FA uptake and storage can be observed [31].

1.1.5 Liver bile acid metabolism

The liver plays a vital role in bile acid (BA) metabolism, which is a crucial process for the digestion and absorption of dietary fats and fat-soluble vitamins A, D, E and

K. BA are a group of steroidal compounds synthesised in the liver through a series of hydroxylation and oxidation steps. The adult human liver converts approximately 500 mg of cholesterol to primary BA each day [32]. Once synthesized, BA can be conjugated with glycine or taurine to form bile salts. These are then actively transported from hepatocytes into the bile canaliculi using the bile salt export pump (BSEP), multidrug resistance-associated protein 2 (MRP2) and other transporters [33]. From the bile canaliculi, bile salts, along with other components of bile, flow into the bile ducts within the liver. These progressively merge to form the common hepatic duct, which leads to the gallbladder or directly to the small intestine via the common bile duct. When needed for digestion, the gallbladder contracts and releases bile into the small intestine where they emulsify fats and enhance FA absorption. Through the enterohepatic circulation, BA can be reabsorbed in the distal ileum through transporters such as ileal bile acid transporter (IBAT) and recycled for re-utilisation [33]. In the intestines, bacteria, mostly of colonic origin, can convert primary BA through deconjugation, dehydroxylation, dehydrogenation and epimerization to secondary BA such as deoxycholic acid (DCA) and lithocholic acid (LCA). Some of these secondary BA are passively absorbed in the colon and transported back to the liver via the portal venous circulation. The recycled BA make up around 95% of all BA and consist of a mixed pool of primary and secondary BA, with only 5% newly synthesised [32]. BA also act as important signaling molecules and metabolic regulators in the liver, contributing to the maintenance of metabolic homeostasis and can modulate inflammatory as well as fibrotic response via their effects on various signaling pathways including farnesoid X receptor (FXR), pregnane X receptor (PXR), G protein-coupled bile acid receptor 1 (GPBAR1), and sphingosine-1-phosphate receptor 2 (S1PR2). BA are implicated in metabolic diseases and could play an important role in elucidating the pathophysiology of liver diseases and developing therapeutic interventions [34–37].

1.1.6 Liver steroid metabolism

The liver metabolises steroids in two phases. Phase 1 is the oxygenation, dehydrogenation or reduction by the cytochrome p450s(CYPs) superfamily, short-chain dehydrogenases (SDR) and aldo-keto reductases (AKRs) respectively. Thereafter steroid metabolites are conjugated by, for example, the addition of sulphate or glucuronide group in phase 2 by enzymes including sulfotransferases (SULTs), catechol-O-methyl transferases (COMT) and UDP glucuronosyltransferases (UGTs). Phase 1 enzymes from the CYP superfamily mainly oxidise steroids by introducing oxygen into the steroid ring. This facilitates the breakdown of cholesterol by other enzymes into BAs which can subsequently be excreted by the liver in bile [38]. The AKR1C family of enzymes reduce different carbonyl groups of steroid hormones through their hydroxysteroid dehydrogenase (HSD) activity. This allows them to inactivate or potentiate steroid hormone action. This is not limited to naturally occurring or unconjugated steroids but also affects synthetic therapeutic and conjugated steroids, indicating that phase 1 and 2 are not occurring in a strictly sequential manner [39–42]. The property of nicotinamide cofactor (NADPH) dependent reduction is shared with the SDRs, even though their protein has a dissimilar fold [43, 44].

1.2 Bile acids

BA, which are steroidal in structure, are synthesised as the two major primary BA, cholic acid (CA) and chenodeoxycholic acid (CDCA), within the liver [45]. Through conjugation with glycine or taurine anionic bile salts are generated (i.e. glycocholic and taurocholic acid) and this increases their hydrophilicity [35, 46]. Historically, BA were primarily recognized for their role in emulsifying dietary fats and aiding in their digestion and absorption in the small intestine. Over time, BA have emerged as key signaling molecules involved in energy homeostasis, glucose metabolism, lipid metabolism, and inflammation. Furthermore, alterations in bile acid metabolism

have been implicated in the pathogenesis of several metabolic disorders, such as obesity, diabetes, and non-alcoholic fatty liver disease (NAFLD) [47, 48].

1.2.1 Synthesis

BA synthesis happens either via the neutral (classic) or the acidic (alternative) pathway [34]. The biosynthesis involves a series of enzymatic reactions which are mostly located in hepatocytes for the neutral pathway. It is responsible for producing 50-90% of all BA [49–51]. The neutral pathway involves the rate limiting enzyme cholesterol 7α-hydroxylase (CYP7A1) which converts cholesterol into 7α-hydroxycholesterol which in turn is converted to 7α-hydroxy-4-cholesten-3-one by 3β-hydroxysteroid dehydrogenase type 7 (HSD3B7). The enzymatic reaction with sterol 12α-hydroxylase (CYP8B1) then determines the fate of the precursor molecules which will become CA. Subsequently, critical enzyme reactions are catalysed by AKR1D1, AKR1C4 and mitochondrial sterol 27-hydroxylase (CYP27A1) to create both CA and CDCA. The acidic pathway can occur in liver, macrophages and almost all tissues due to widespread expression of both CYP27A1 and CYP7B1 but the first few steps often take place in macrophages [35, 36, 52, 53]. The initial step is depending on CYP27A1 converting cholesterol to 27-hydroxycholesterol. Afterwards, Oxysterol 7α-hydroxylase (CYP7B1) and then HSD3B7 further catalyse the reactions to produce 3α,7α-dihydroxy-5β-cholestanoic acid and 7α-hydroxy-3-oxo-4-cholestanoic acid which feeds back into the classic pathway in the liver for CDCA synthesis. CA and CDCA make up around 80% of all BA [54]. Some of these primary BA are then conjugated with glycine or taurine to increase water solubility before secretion. In humans 80% of bile salts consist of taurocholic acid and glycocholic acid [55].

1.2.2 Function

Conjugated bile salts, being amphiphiles, have both a hydrophobic and hydrophilic side enabling them to function as surfactants [57]. The hydrophobic part interacts with lipids, while the hydrophilic part interacts with water. The emulsification of

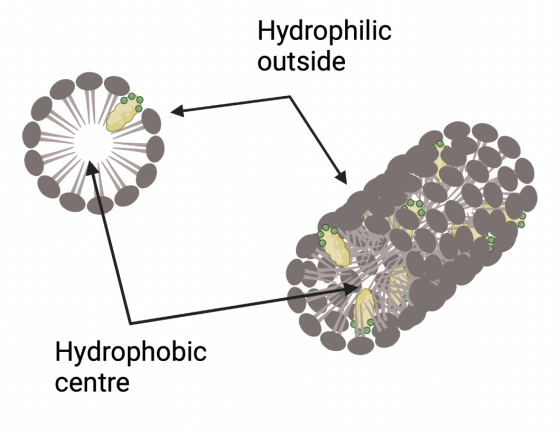


Figure 1.5: Mixed bile acid-fatty acid micelle and a mixed cylindrical micelles both with hydrophilic outside and a hydrophobic centre. Adapted from Stamp et al, Issues in Toxicology 2008 [56]. Created with BioRender.com.

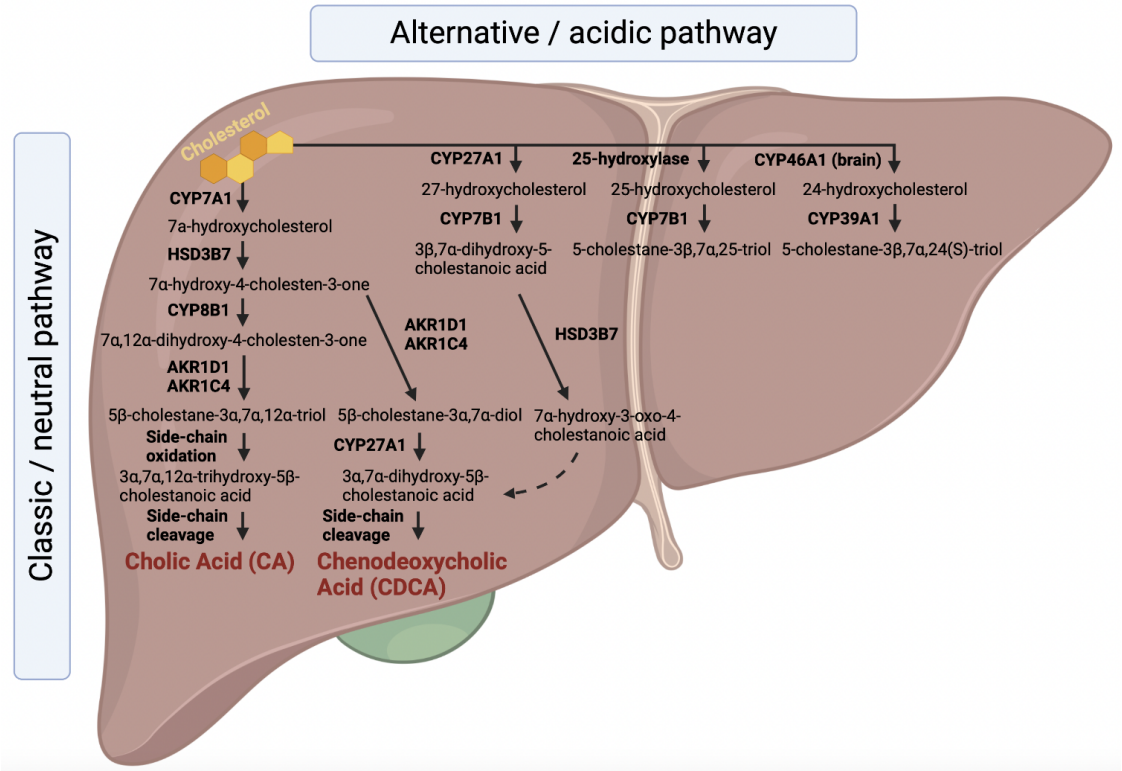


Figure 1.6: Bile acid synthesis in the liver is possible via the classic or the alternative pathway. The classic pathway results in the production of cholic acid (CA) and chenodeoxycholic acid (CDCA) whereas the alternative pathway via CYP27A1 (27-hydroxylase) almost exclusively produces CDCA. The 25-hydroxylase and 24-hydroxylase led pathway have a minor production capacity and produce BA intermediates. Created with BioRender.com.

lipids in water by BA creates significantly more surface area for water-soluble lipase to break down lipids to FA, cholesterol, phospholipids and form micelles together with BA (Figure 1.5. Furthermore, BA play a crucial role in maintaining cholesterol homeostasis and safeguarding the liver against the buildup of cholesterol, TAG and toxic metabolites through bile excretion. Vital for flow solubilisation of bile, BA help to detoxify the liver from bilirubin, lipophilic steroid and drug metabolites as well as heavy metals [56]. The detergent properties of BA also work to disrupt bacterial membranes and, thereby, display an antimicrobial effect. Acting in both a bacteriostatic and bactericidal fashion on bacteria, BA can influence microbiome composition and prevent overgrowth [58]. It has been shown *in vivo* that the viability of Staphylococcus aureus as well as Lactobacillus and Bifidobacterium species are decreased by BA [59, 60]. In reverse, changes in the microbiome induced by high fat diet can also affect secondary bile acid composition which has been shown to also present in human disease with inflammatory bowel disease and cystic fibrosis [61, 62]. As mentioned above, BA are important signaling molecules and play a role as metabolic regulators in the liver. They activate nuclear receptors FXR, PXR and vitamin D receptor, and G protein-coupled receptors (GPCRs) GPBAR1 and S1PR2 [36, 63].

Bile acids and FXR

Primary and secondary BA, CDCA, CA, DCA and LCA are natural ligands of FXR. The nuclear receptor can be activated by both CDCA and CA, with CDCA acting as the more potent agonist of FXR. Further, CDCA, CA, DCA and ursodeoxycholate (UDCA) can upregulate protein expression of FXR [64]. Upon binding of BA, FXR translocates from the cytoplasm to the nucleus and undergoes a conformation change in its ligand binding domain. In the nucleus it forms a heterodimer complex with retinoid x receptor (RXR) and subsequently binds to FXR response element (FXRE). Through the FXRE in the promotor of *PPARA*, BA can activate the PPARα pathway and thereby suppress lipogenesis and activate FAO [65, 66].

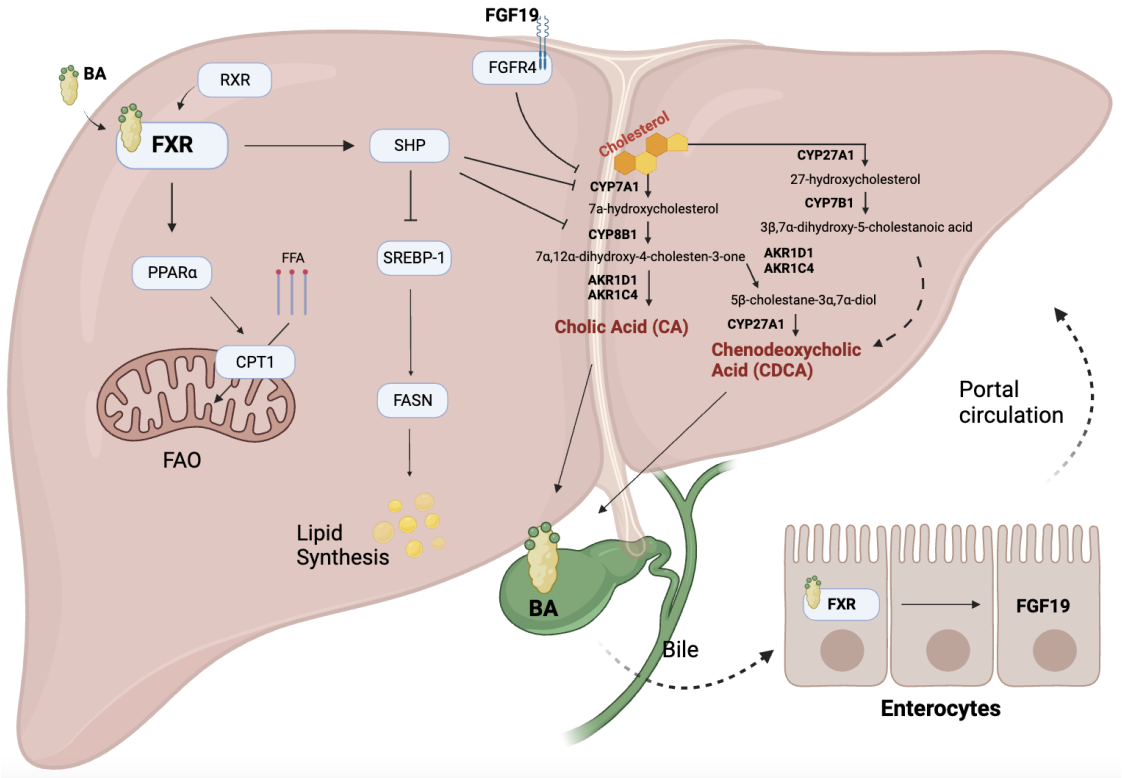


Figure 1.7: FXR translocates into the nucleus upon BA binding and forms a heterodimer with RXR. Downstream it increases FAO via PPARα and inhibits DNL as well as bile acid biosynthesis via SHP dependent SREBP-1 and CYP7A1 inhibition, respectively. Further, intestinal FXR activation leads to the release of FGF19 which in turn activates FGFR4 responsible for further CYP7A1 inhibition. Created with BioRender.com.

Furthermore, FXR activation influences carbohydrate metabolism and is believed to have a positive effect on plasma glucose and improve insulin sensitivity as shown in rodent experiments [66]. There are further redundant mechanisms to regulate bile acid synthesis (for example via PXR) but FXR plays a crucial role in regulating bile acid biosynthesis and cholesterol metabolism through a negative feedback loop [67]. FXR suppresses *CYP7A1* expression, the rate limiting step in the classic bile acid biosynthesis, via the increase of intestinal fibroblast growth factor 19 (FGF19), a ligand for the fibroblast growth factor receptor 4 (FGFR4) found on hepatocytes. Downstream, the activation of FGFR4 starts a c-Jun N-terminal kinase (JNK) signalling cascade which inhibits the transcription of *CYP7A1* [68]. In addition, FXR increases transcription of small heterodimer partner (SHP) which leads to a direct inhibitory interaction with the liver receptor homolog-1 (LRH-1), a nuclear

receptor that positively drives expression. SHP binding of LRH-1 therefore directly suppresses the expression of the *CYP7A1* gene [69, 70]. It has been proposed that there is differential inhibition by hepatic and intestinal FXR for CYP8B1 and CYP7A1, respectively [71]. Absorption of BA in the small intestine is also regulated by FXR. Inhibition of apical sodium dependent transporter (ASBT), one of the central transporters of BA in the small intestine, follows a similar inhibitory mechanism involving SHP as described above [72]. FXR is also a negative modulator of inflammation and fibrosis. It specifically inhibits hepatic inflammatory signalling of NF-κB and has been shown to prevent inflammation in both HepG2 cells, primary hepatocytes and *in vivo* in FXR-null mice [73]. Furthermore, studies were able to show that inflammation due to liver injury could be suppressed by synthetic FXR agonists obeticholic acid and GW4064 [74, 75], and lately a phase 3 trial with obeticholic acid reported positive interim results showing lower levels of fibrosis in NASH patients [76].

1.2.3 Involvement in disease

Congenital disorders of bile acid synthesis

Disorders of bile acid synthesis can be broadly classified as primary or secondary. Primary bile acid synthesis disorders involve congenital deficiencies in enzymes such as CYP7A1, AKR1D1 and 3β-HSD. These congenital defects in bile acid synthesis lead to an accumulation of potentially hepatotoxic atypical BA if they don't function as substrates of BSEP. In addition, the missing negative feedback loop, can lead to the production of large quantities of such compounds which in turn can cause hepatic necrosis. Other rare primary disorders include impaired conjugation enzymes leading to an increased amount of unconjugated BA. Secondary disorders encompass bile acid transport disorders such as MDR3 deficiency and low gamma-GT familial intrahepatic cholestasis, impaired cholesterol supply as in the Smith-Lemli-Optiz syndrome, or impaired peroxisome function. Typically, bile acid synthesis disorders lead to lipid deficiency and fat-soluble vitamin malabsorption [77–80].

Secondary bile acids in disease

Differences in the microbiome can lead to changes in the composition of the secondary bile acid pool and secondary BA in turn have been implicated in a variety of diseases ranging from colon cancer, inflammatory bowel disease (IBD), gallstones and metabolic disorders such as NAFLD. Elevated levels of DCA and LCA have been linked with colorectal cancer and gallstone formation. Interestingly, humans in contrast to rodents don't have the enzymatic capability to break down DCA. Therefore, DCA levels are highly dependent on formation and absorption in the colon [81] Furthermore, *in vitro* and *in vivo* experiments have shown DCA to potentially have pro-carcinogenic effects [82]. IBD studies have shown clear dysbiosis induced differences with lower secondary BA and a relative increase of primary BA [82]. So far, cause or consequence is unclear, but early *in vitro* experiments indicate an increase of permeability of the intestinal barrier function, even though there are conflicting results [83, 84]. BA might further impact NAFLD through elevated biosynthesis but a shift towards proportionally higher levels of FXR antagonistic DCA compared to agonistic CDCA [85]. This was further underlined with lower serum levels FGF19 within the same patient population.

1.3 Steroid hormones

There are five types of steroid hormones: glucocorticoids and mineralocorticoids are synthesised in the adrenal cortex and can be clustered as corticosteroids; androgens, estrogens and progesterone on the other hand are grouped as sex steroids or gonadal steroids. These different classes of hormones all play a crucial role in regulating carbohydrate, lipid and protein metabolism, salt and fluid homeostasis, inflammation and immune function as well as development of secondary sexual characteristics and reproduction. Synthesis of these lipid-based hormones derives from cholesterol in the adrenal or gonads and allows them to pass through cell membranes. For transport in the blood they are often bound to carrier proteins such as sex hormone-binding globulin (SHBG) or corticosteroid-binding globulin (CBG).

They can either free themselves of their solubilizing carrier protein to passively cross the cell membrane or taken into the cell through endocytosis by binding as a complex to megalin [86]. Once in the cell they bind as a free molecule to the cytosolic or nuclear steroid receptors. The nuclear receptor, a large metalloprotease, will dimerise upon binding of steroids to a DNA binding unit and subsequently enter the nucleus. In the nucleus it can bind specific DNA sequences and induce transcription of its target genes, the delayed genomic response. Steroids can also stabilise mRNA through post-transcriptional regulation leading to higher availability of target mRNA or have non-genomic more immediate effect through interaction with GPCR-linked proteins. It is believed that this interaction happens through the cholesterol recognition/interaction amino acid consensus sequence (CRAC) [87, 88].

1.4 Non-alcoholic fatty liver disease

The continuing epidemic of metabolic disease including obesity, type 2 diabetes mellitus (T2DM) and the hepatic manifestation, NAFLD, puts an ever-increasing burden on society. NAFLD is currently present in approximately 25% of the population at varying severity and over 80% in obese patients or those with T2DM [76, 89]. It is a spectrum of disease which ranges from simple steatosis, meaning >5% of liver weight comprised of fat, through to steatosis with an inflammatory phenotype, non-alcoholic steatohepatitis (NASH), and eventually fibrosis and cirrhosis in the absence of excess alcohol consumption (Figure 1.8). In June 2023, it has been decided to rename NAFLD to metabolic dysfunction-associated steatotic liver disease (MASLD) and metabolic dysfunction-associated steatohepatitis (MASH) under the umbrella of steatotic liver disease (SLD) by the American Association for the Study of Liver Diseases (AASLD), La Asociación Latinoamericana para el Estudio del Hígado (ALEH) and the European Association for the Study of the Liver (EASL). MASLD is diagnosed as hepatic steatosis and at least one of the five cardiometabolic risk factors including excess abdominal obesity, diabetes, hypertension, high triglyceride or low high-density lipoprotein (HDL) cholesterol levels. Furthermore, to facilitate sub-grouping a new category, MetALD, was created

for patients with MASLD who consume excessive amounts of alcohol, 140 g/week and 210 g/week for females and males respectively. Patients without a cardiometabolic riskfactor and no other underlying cause are diagnosed with cryptogenic SLD [90]. To facilitate better understanding and ensure consistency with the cited literature I will keep referring to NAFLD for the content of this thesis.

Today, we are still missing a clear understanding of what mechanisms drive development and progression of disease even though progressed NAFLD carries a significant risk of development of hepatocellular carcinoma (HCC) alongside increased cardiovascular mortality [91]. NAFLD is the most rapidly growing cause of HCC but already today, accounts for more than 15% of liver transplants due to liver failure or progression to HCC and is, therefore, already the second most common indication for liver transplantation in the US [76, 92]. Current therapy of NAFLD is limited to life style changes and treating co-existing metabolic conditions such as diabetes, obesity, high blood pressure and high cholesterol. Therefore, the continued rise puts emphasis on the need to better understand underlying disease mechanisms to find new approaches to treating such a complex multivariate disease. Importantly, there is also a need for further improvements of diagnostic or staging solutions through bio-markers to increase accuracy with less invasive procedures compared to the current standards such as elevated liver enzymes, ultrasound, fibroscan or biopsy.

1.4.1 Pathogenesis

Our knowledge is still limited to the multiple-hit hypothesis which propagates that genetically predisposed individuals develop NAFLD through multiple hits such as epigenetic factors, intestinal microbiota, insulin resistance, nutritional factors and adipose tissue secretion [93]. Further, it is not fully understood why the liver starts to accumulate lipids but the following processes are implicated: an increase of dietary FA, lipolysis leading to an increased delivery of FA to the liver, heightened DNL, a reduction in FAO and a reduction in TAG secretion as part of VLDL [94, 95]. Events leading to increased FA influx into the liver such as insulin resistance (IR) and obesity are therefore associated with the development and progression of

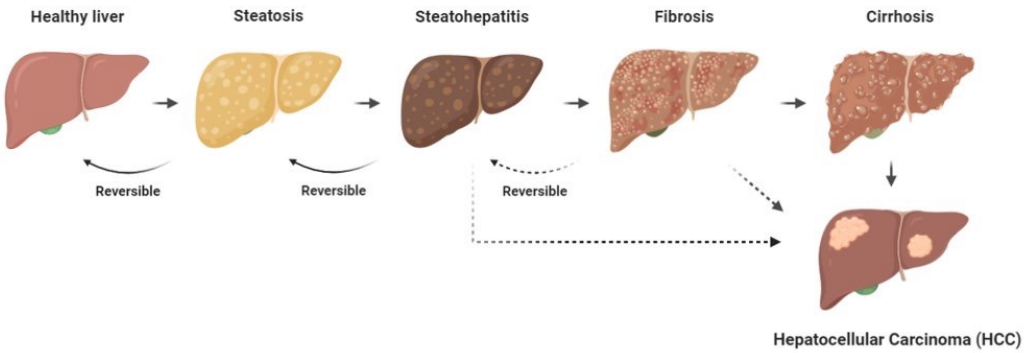


Figure 1.8: Progression of NAFLD from simple steatosis to cirrhosis and HCC. The initial stage demonstrates steatosis, where fat accumulates within liver cells. As the disease progresses, inflammation and liver cell damage occur leading to non-alcoholic steatohepatitis (NASH). Subsequent stages show the progression of fibrosis, ranging from mild to advanced fibrosis with different extent of scarring and liver dysfunction present. At the advanced stages, the likelihood of HCC development drastically increases and patients with cirrhosis should be screened regularly. Created with BioRender.com.

NAFLD. IR is believed to significantly contribute to steatosis and occur early on in NAFLD development [96]. The occurrence of IR leads to a decrease in insulin receptor substrate activation and thereby to an impaired Akt phosphorylation. This in turn results in an attenuation of glucose uptake *via* GLUT4 in skeletal muscle and adipose tissue, accompanied by a decrease in muscle glycogen synthesis overall leading to hyperglycaemia [97]. IR and steatosis in patients with NAFLD, regardless of inflammation phenotype, are both associated with an increase in CD36, a FA translocase [98]. In addition, the progression of NAFLD towards an inflammatory NASH phenotype might also be partly driven by obesity related adipose dysfunction, as such can lead to the release of pro-inflammatory cytokines [99]. Bariatric surgery and subsequent changes in IL-1 in adipose tissues might prove as a protective measure against developing NASH from simple steatosis [100, 101].

Within the hepatocytes, alteration in lipid metabolism such as lipid processing, increased DNL or impaired hepatic lipid export and oxidation result in the synthesis and accumulation of TAG in the cytoplasm [25]. DNL seems to be a key player with an increase in parallel with liver fat content in patients with metabolic syndrome and accounts for up to 25% of TAG compared to 10% in patients with low hepatic

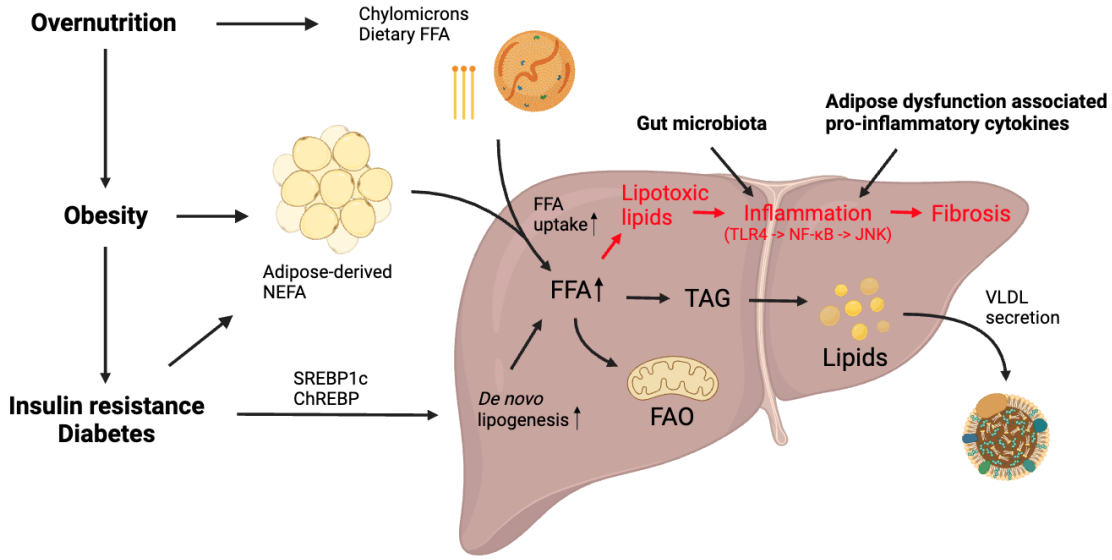


Figure 1.9: NAFLD and the progression to NASH is believed to be caused in genetically predisposed individuals including epigenetic factors, intestinal microbiota, insulin resistance, nutritional factors and adipose tissue secretion which lead to disturbed lipid homeostasis and inflammation. Obesity and IR are believed to significantly drive NAFLD development due to FFA accumulation via increased FFA uptake, persisting DNL and potentially decreased FAO and VLDL secretion. Inflammation can then arise from accumulated FFA which cause lipotoxicity in combination with other triggers such as adipose dysfunction associated cytokines. Created with BioRender.com.

fat content [102]. Furthermore, DNL shows less variability throughout the day in patients with NAFLD and is even elevated in fasting periods [103]. These functional changes are accompanied by increased pro-lipogenic expression patterns in the liver [104, 105]. Overall, lipotoxicity can arise due to an overload of FFA, phospholipids and ceramide, formed from palmitate, which might further interfere with insulin signaling and mitochondrial function and cause liver damage [97, 106, 107]. The excess FFA activate pattern recognition receptors, such as toll like receptor 4 (TLR4), which in turn activate nuclear factor-κB (NF-κB) and the JNK signalling pathways [108]. Persisting NF-κB and JNK activation might subsequently lead to progression of NAFLD towards NASH and cirrhosis. Recent multiomics studies managed to identify 18 sequence variants associated with NAFLD, among others were *GPAM*, *GCKR*, *PNPLA3*, *TM6SF2* and *MTARC1*. Many of them involved in lipid metabolism and emphasising the central role these processes play in the pathogenesis of NAFLD [109].

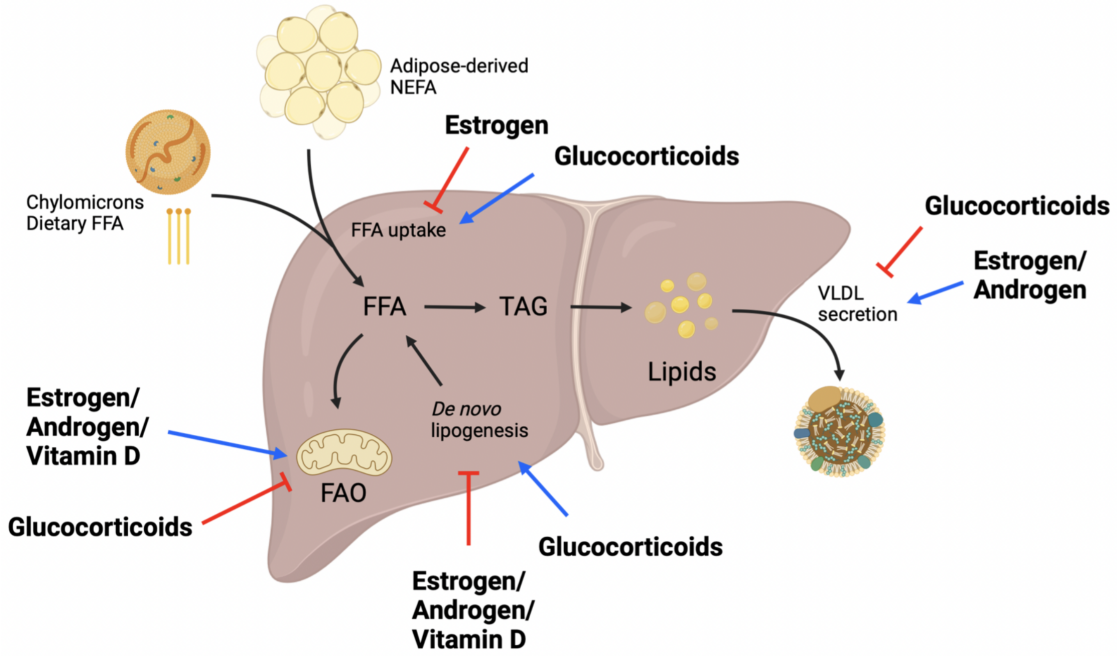


Figure 1.10: Lipid homeostasis is partially regulated by steroid hormones by determining the fate of hepatic fatty acids. Legend: blue (activation), red (inhibition), non-esterified fatty acid (NEFA), free fatty acid (FFA), triacylglycerol (TAG), very-low-density lipoprotein (VLDL), fatty acid oxidation (FAO). Adapted from Yang et al., Metabolites 2021 [110]. Created with BioRender.com.

1.4.2 NAFLD and steroid hormones

Four major pathways regulate lipid homeostasis: uptake of circulating lipids, FAO, *de novo* lipogenesis, secretion of lipids in the form of VLDL. Steroid hormones as stated in Chapter 1.3 are important regulators of carbohydrate and lipid metabolism. Dysregulation of these has therefore been implicated in metabolic phenotype, hepatic lipid accumulation and by effect NAFLD as they regulate the fate of hepatic lipids [110]. The impact of individual steroid hormones or the receptors on hepatic lipid metabolism and steatosis has been extensively explored in animal model (Table 1.1) and is summarised in Figure 1.10. However, there is still a need for more research to properly understand the underlying mechanisms and differences between male and female sex, e.g. androgen deficiency in men but excess in women are associated with NAFLD. In addition, glucocorticoid excess is associated with NAFLD in both sexes. [111].

Table 1.1: Steroid hormones and liver steatosis in animal models. Legend: ↑ increased; ↓ decreased, high fat diet (HFD). Table adapted from Yang et al. 2021 ([110]), Table 1.

Steroid Hormone	Models	Major Phenotypes
Estrogen	Female ERα-deficient mice fed HFD for 10 weeks	Liver weight, hepatic steatosis, and ALT ↑
	Male hepatic ERα-deficient mice fed HFD for 12 weeks	Hepatic steatosis and insulin resistance ↑
	Ovariectomized mice treated with E2 and fed HFD for 6 weeks	Hepatic steatosis and insulin-mediated suppression of VLDL secretion ↓
Androgen	Male hepatic AR-deficient mice fed HFD for 8 weeks	Body weight, hepatic steatosis, and insulin resistance ↑
Glucocorticoid	db/db mice (diabetes model) treated with GR shRNA for 14 days	Hepatic steatosis, and critical genes for lipid storage and transport ↓
	Sprague Dawley rats treated with exogenous corticosterone and fed HFD for 16 days	Hepatic steatosis, fatty acids uptake of liver, and ALT ↑
Mineralocorticoid	Myeloid MR-deficient ob/ob mice (obesity model)	Hepatic steatosis, lipogenesis, and insulin resistance ↓
	Aldosterone synthase-deficient mice fed HFD for 12 weeks	HFD-induced hepatic steatosis ↓
Vitamin D	C57BL6 mice fed a high-fat/ high-sucrose diet followed by treatment with vitamin D for 15 weeks	Hepatic steatosis and hepatic DNL ↓
	Sprague Dawley rats fed HFD followed by treatment with vitamin D for 16 weeks	Liver weight, hepatic steatosis, and ALT ↓

1.5 Liver Cancer

Worldwide, liver cancer is the 6th most common type of cancer when considering general incidence and the 4th most common cause of cancer-related death [112]. Furthermore, primary liver cancer has shown one of the fastest rates of increase in incidence, of up to 50%, in the past decade and numbers of primary liver cancer are projected to rise further until 2030 in the western world. In contrast to the decrease of overall cancer death rates, the death rate due to liver cancer has increased since 2000. Possible explanations are a lack of adequate early diagnosis and lack of effective treatments [113–116] leading to one of the lowest 5-year survival rates for any type of cancer, 13% for male and 10% for female patients in the UK (Figure 1.11).

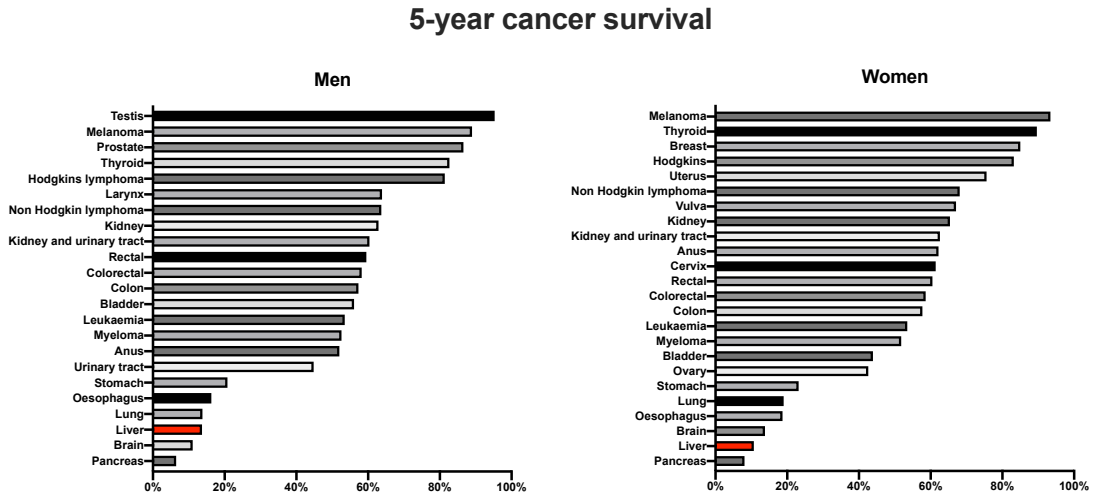


Figure 1.11: 5-year cancer survival in men and women diagnosed with cancer in 2013 and followed up until 2018 in England. Data from Office for National Statistics, 2019 [117].

There are several different forms of primary liver cancer. HCC is the most common (80%), but others such as cholangiocarcinoma and rare forms, like liver angiosarcoma and hepatoblastoma, are also classed as types of primary liver cancer [118]. The most common driver of primary liver cancer is underlying liver disease, including hepatitis B (HBV), hepatitis C (HCV), alcoholic liver disease and NAFLD. Whilst in the developing world the burden of HCC relates to chronic viral liver disease, in the western world the increase in HCC incidence coincides with the epidemic of metabolic disorders [119]. With currently no effective licensed treatment for NAFLD, unlike HCV, NAFLD-associated HCC incidence is likely to rise and present an even bigger global health care burden [120].

1.5.1 Pathogenesis

In western countries, more than 90% of HCCs develop in cirrhotic livers and is tightly linked with chronic liver injury [121]. HCC pathogenesis is a multistep process driven by a spectrum of underlying liver diseases including HBV, HCV, ALD and NAFLD but also hemochromatosis and exposure to aflatoxin. The continuous injury of hepatocytes leads to a constant cycle of chronic inflammation, necrosis and increased cell proliferation. In an attempt to constantly regenerate liver tissue, this

cycle results in fibrosis and cirrhosis. Cell clusters of hyperproliferative hepatocytes form hyperplastic regenerative nodules. The continuing damage-repair-cycle with a heightened state of cell turn over can further lead to the accumulation of successive genetic and epigenetic alterations which benefit proliferation, cell survival, invasive growth and genetic instability. These newly acquired properties can then cause the formation of low-grade dysplastic nodules which in turn can further progress to high-grade dysplastic nodules or the malignant form, HCC [122]. In patients without cirrhosis the molecular development of HCC can be due to the same chronic liver diseases which have not developed cirrhosis yet or other reasons such as viral insertions into the genome or malignant transformation from hepatocellular adenoma (HCA). Viral DNA insertion leading to molecular alterations, is an important factor of hepatocarcinogenesis of HBV patients. Integration of HBV often happens at specific hot-spots in our genome which are actively transcribed and it seems to target genes important in cell proliferation, survival and immortalization with the most prominent being: TERT, MLL2, CCNA2 and CCNE1 [123–126]. Not only specific genes can be influenced but chromosomal translocation, deletion and duplication have been associated with HBV insertion [127]. Furthermore, HBV expresses HBx viral protein which seems to increase reactive oxygen species (ROS) and affects transcription of a variety of oncogenic genes by direct interaction or epigenetic modification (e.g. hyper- or hypomethylation) [128, 129]. The hyperproliferative hepatocytes in HCA are more likely to accumulate alterations which can lead to an increased likelihood for the development of HCC when compared to normal liver tissue. However, HCA still has a low frequency of malignant transformation with around 4-5%. 95.6% of HCA that underwent malignant transformation have been observed to be bigger than 5cm in diameter with the frequency of progression to HCC in small adenomas being even lower. [130].

In HCC, no cancer-specific oncogene has been identified but a series of somatic mutations or gene amplifications seem to function as gatekeepers or HCC drivers. These gatekeeper and driver mutations, so called trunk mutations, are identified in higher proportion already in early cancer development and represent the most

Table 1.2: Frequencies of gene mutation in HCC. Table adopted from Ding et al. 2017 ([131]).

Pathways	Genes	Function	Frequency (%)
Telomere maintenance	TERT	Maintaining telomere length	47.1
Cell cycle control	TP53	Tumour suppressor	28-36
	CCND1	Cell proliferation	7.2
	CDKN2A	Cell cycle regulator	7.2
WNT-β-catenin signalling	CTNNB1	Transcriptional regulator	17-37
	AXIN1	Signal transducer	4-14
Oxidative stress	NFE2L2	Transcriptional regulator	6.4
	KEAP1	Proteinase adaptor	8
Chromatin remodelling	ARID1A	Chromatin remodelling	16.8
	ARID2	Chromatin remodelling	5.6
AKT-mTOR-MAPK pathway	RPS6KA3	kinase	2-10
	PTEN	Tumour suppressor	3
	FGF19	Metabolic regulation factor	5
	PI3KCA	Effector of PTEN-AKT pathway	2-4
JAK/STAT signalling	JAK1	kinase	5
Angiogenesis	VEGFA	Tumour proliferation	3.8

commonly altered genes in HCC which include mutated TERT promoter, TP53 and CTNNB1 genes [122]. Other affected genes in HCC are ARID1A, ARID2, AXIN1 and CDKN2A as well as amplifications in VEGFA and FGF19/CCND1 [132–134] A property of trunk mutations is that they are often ubiquitously expressed in HCC cells of a single carcinoma and in 90% of clonal lesions/intrahepatic metastasis. In a study 90% of HCCs had at least one ubiquitously expressed mutation. Multiple cancer lesions often harbour different trunk mutations and show a very different mutational profile. This is in line with the observation that HCC has a high intertumour heterogeneity, indicating the they are often of non-clonal origin but represent two different HCC entities [122]. HCC also have a high intratumour heterogeneity [135]. Sampling a single cancer lesion in different locations results in very different mutational profiles with the exception of trunk mutations. These strongly varying mutations are summarised as private mutations. This further supports the idea of a branched evolutionary development of HCC with trunk mutations as gatekeeper and drivers. Other differentially expressed genes in HCC were most commonly of importance to metabolic processes or immune response underlining the importance of the tumour microenvironment and changes in anti-tumour immunity [136].

1.5.2 Liver cancer and NAFLD

In multiple western countries including the US, UK and France, NAFLD is considered the fastest growing cause of HCC [137]. Further, genetic polymorphisms such as *GCKR*, *MBOAT7 PNPLA3* and *TM6SF2* which have been flagged as risk factors for NAFLD are independently associated with HCC [138]. NAFLD induced lipotoxicity and oxidative stress is believed to be a key driver in the pathogenesis of HCC from NAFLD, which has a proportionally high ratio of HCC in patients without cirrhosis. This leads to later discovery and therefore cancers are often in more advanced stages when diagnosed [138–140]. More recently, dysbiosis with increased intestinal permeability and reduced immune surveillance via CD4 and CD8 suppression have been implicated to lead to HCC development in NAFLD [141, 142]. In patients with NAFLD, the HCC risk is associated with male gender, Hispanic ethnicity, older age, diabetes and smoking as shown in population-based studies [143, 144].

1.5.3 Liver cancer and steroid hormones

Steroid hormones are of particular interest in HCC pathogenesis due to a clear gender disparity [118]. HCC was found to express androgen receptor, oestrogen receptor and progesterone receptor with negative staining for the latter showing a significant association with overall survival [145]. A recent large-scale study showed that androgen but also oestrone and oestradiol levels were associated with increased risk to develop liver cancer, with the exception of dehydroepiandrosterone (DHEA), which seemed to be protective in men [146]. The precise role of steroid hormones in HCC has yet to be elucidated but is of great interest considering the association of hyperandrogenism, including 11-oxygenated androgens, and insulin resistance and the rise of NAFLD related HCC [147, 148].

Table 1.3: List of AKR1C1 substrates

Enzyme	Substrates	Products	kcat/KM (min^{-1} mM^{-1})	References
AKR1C1	**Steroids**			
	Progesterone	20α-Hydroxy-4-pregnen-3-one	210-980	[151, 154, 155]
	Pregnanolone		3000	[151]
	5α-DHP		2400	[156]
	20α-Hydroxy-5α-pregnan-3-one		860	[156]
	3α-Hydroxy-5α-pregnan-20-one		2200	[156]
	Androsterone		9	[152]
	5α-Androstane-3,17-dione		70	[152]
	5α-DHT	3α-Diol/ 3β-Diol	70-180	[40, 152]
	5α-DHT glucuronide		33	[40]
	5α-DHT sulfate		140	[40]
	Synthetic steroids			
	Tibolone	3β-Hydroxy-tibolone	1200	[39]
	Norethynodrel	3β-Hydroxy-norethynodrel	450	[39]
	Dydrogesterone	20α-hydroxy-9b,10a-pregna-4,6-dien-3-one	1200	[154]
	Lipid peroxidation			
	4-Hydroxy-2-nonenal	1,4-Dihydroxy-2-nonene	270	[157]
	Prostaglandin			
	Prostaglandin E2	PGF2α	0.34-39	[151, 158]
	Prostaglandin D2	9α-, 11β-PGF2	0.11-240	[151, 158]
	Retinaldehyde			
	9-cis-retinaldehyde	9-cis-retinol	370	[159]

1.6 Aldo-Keto Reductase 1C1

1.6.1 Aldo-Keto Reductase 1C

The Aldo-Keto Reductase 1C (AKR1C) subfamily is part of the AKR superfamily 1 and, in humans, is formed by AKR1C1, AKR1C2, AKR1C3 and AKR1C4, with all four showing HSD isoform activities. This subfamily plays an important role in the steroid hormone, lipid aldehyde, prostaglandin and retinoid metabolism as well as chemical carcinogen metabolism [149]. AKR1C1-AKR1C4 all have the potential to work as 3-, 17- and 20-ketosteroid reductase. Even though they show overlapping activities AKR1C1, AKR1C2, AKR1C3 and AKR1C4 act predominantly as 20α-HSD, 3α-HSD3, 17β-HSD and 3α-HSD1, respectively [150]. All four isoforms of AKR1C are ubiquitously expressed in humans, except for AKR1C4 which is almost exclusively expressed in the liver. Expression levels in the liver of all AKR1Cs are equally high [151–153].

1.6.2 Function

AKR1C1 acts mainly as a 20α-HSD and plays a pivotal role in inactivating progesterone by catalysing the reduction to 20α-dihydroprogesterone. In addition, AKR1C1 shows low catalytic activity as a 3α-HSD and 3β-HSD reducing 5α-DHT

to 3α-Diol and 3β-Diol. Its 17β-HSD activity is relatively low with 9 kcat/Km when reducing androsterone [41, 152, 153]. AKR1C1 is not only important in steroid hormone metabolism, but is a key player in reducing lipid peroxides. Compared to other AKRs, AKR1C1 was found to NAD(P)(H) dependently reduce 4-hydroxy-2-nonenal (HNE), a product of lipid peroxidation causing cytotoxicity, genotoxicity and hepatotoxicity, to 1,4-dihydroxy-2-nonene with high specificity [157, 160]. It was further observed that HepG2 human hepatocellular carcinoma cells had higher *AKR1C1* mRNA levels after being exposed to HNE, indicating a self-regulation of oxidative stress through AKR1C1 [157]. In addition, AKR1C1 might be involved in the regulation of subcutaneous fat metabolism. It has been shown that the missense variant p.(Leu213Gln) in AKR1C1, causing a partial loss-of-function and lower catalytic 20α-HSD activity, leads to an increase in subcutaneous fat deposition [161].

1.6.3 Tissue expression

AKR1C1 is ubiquitously expressed in humans. When comparing different tissues, the strongest expression of AKR1C1 is found in liver, fat, intestines, lung, adrenal gland and kidney; low levels of expression have also been observed in heart, muscle, peripheral blood lymphocytes, brain, mammary glands, uterus and testis [151–153]. Within the liver itself, AKR1C1 is clearly spatially localised as part of liver zonation with higher gene and protein expression in the pericentral compared to the periportal region [162, 163].

1.6.4 Structure

AKR1C1 shares an (α/β)8-barrel motif with the other members of the AKR1C subfamily and has a high amino sequence identity of 81.7% -97.8% with AKR1C2, AKR1C3 and AKR1C4. AKR1C1 and AKR1C2 differ only in seven amino acids and only one of them in the binding pocket of the protein [158, 164–166].

There are five splice variants of AKR1C1, three of which encode protein: AKR1C1-201 (A6NHU4), AKR1C1-202 (Q04828) and AKR1C1-203 (H0Y804). AKR1C1-202 (full-length isoform) functions as 20α-HSD. It consists of 323 amino

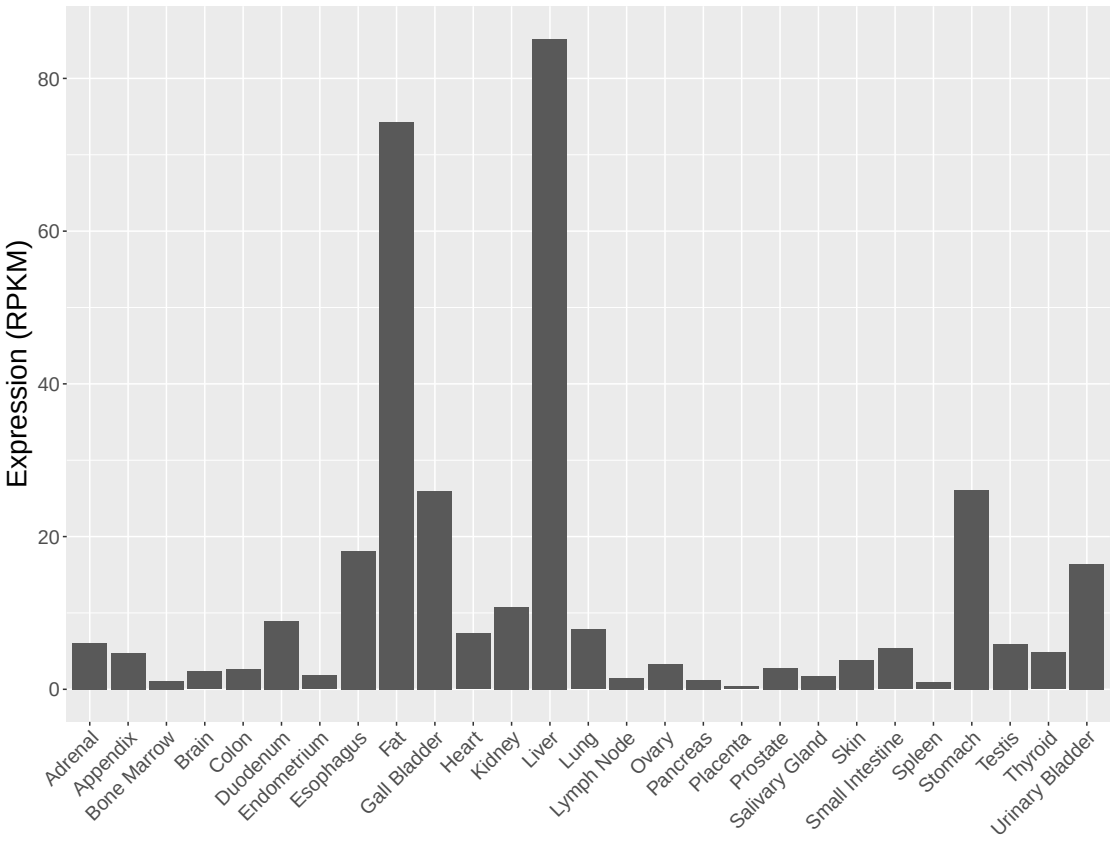


Figure 1.12
Ubiquitous expression of AKR1C1 in humans with prominent peaks in liver and adipose tissue. Data from Fagerberg et al., 2014 ([153])

acids with a calculated weight of 37 kD. The other two protein-encoded variants are computationally calculated to be 205 and 248 amino acids in length, weighing 23 and 28 kD respectively [168].

1.6.5 AKR1C1 and Cancer

AKR1C1 has been found to be differentially expressed and/or to be associated with aggressive growth and chemo resistance in a range of cancers, including breast, prostate, bladder, lung and head and neck tumours [170–174]. Even though AKR1C1 is most highly expressed in the liver, research looking into its role in liver cancer is lacking. Data are now emerging to suggest that it might have a role in the pathogenesis and natural history of HCC.

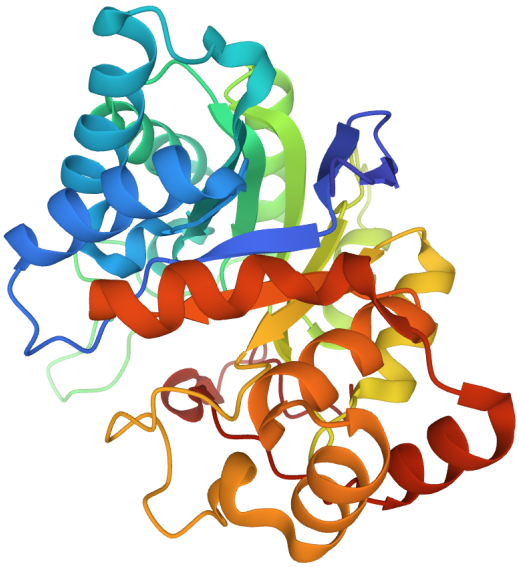


Figure 1.13: 3D protein structure of AKR1C1, Figure: PDB ID: 3NTY, El-Kabbani et al., 2011 ([167])

1.6.6 AKR1C1 and HCC

In a very recent study, AKR1C1 has been included as one of six lipid metabolism-related genes to establish HCC risk prognosis model due to poor HCC outcome being associated with increased AKR1C1 expression through both single cell RNA sequencing and protein data from the Human Protein Atlas (HPA) [175]. Interestingly, AKR1Cs (AKR1C3 and AKR1C4) have been found to be more highly expressed on protein level in patients with high compared to low inflammatory activity in NAFLD, potentially contributing to HCC-underlying disease [176]. Furthermore, a study specifically classifying by underlying liver diseases observed that HCC arising from hereditary haemochromatosis had increased AKR1C1 expression. The liver damage caused by hereditary haemochromatosis is mainly

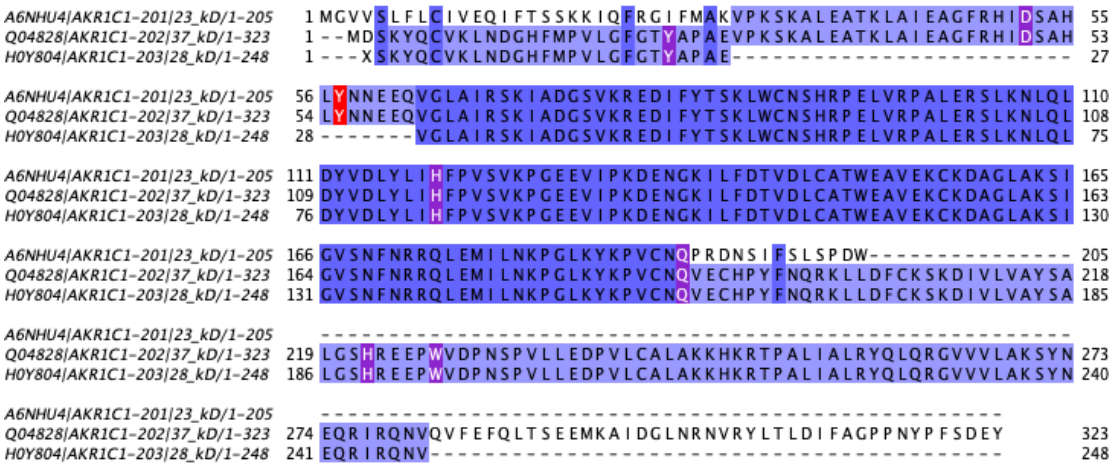


Figure 1.14: AKR1C1 isoform protein sequence; blue: conserved, violet: binding site, red: active site. Figure created with Jalview using data from Bateman, 2019 ([169])

based on an oxidative stress mechanism leading to oxidised cellular proteins, lipids and DNA bases compared to HCV and HBV, which are mainly driven by inflammation and viral DNA integration [136]. This increase in oxidative stress in HCC could well be one of the reasons for increased AKR1C1 expression when looking at this on a molecular level. AKR1C1 increases during oxidative stress, exposure to ROS, and appears to be up-regulated by exposure to HNE, a product of lipid peroxidation through oxidative stress [157, 177]. Nuclear factor erythroid 2-related factor 2 (NRF2) appears to regulate AKR1C1 expression [178, 179]. Therefore, the up-regulation of AKR1C1 expression could be explained by NRF2 overexpression in HCC, which correlates with differentiation, metastasis and tumour size [180]. Overexpression of NRF2 has been shown to increase transcriptional activity of genes containing the antioxidant response element (ARE) in their promotor, one of these being AKR1C1. This has further been confirmed in HepG2 cells where ARE has been identified in the proximal promotor of AKR1C1 [181]. Up-regulation of AKR1C1 as an antioxidative element is further supported by its reductive potential of HNE [157]. Interestingly, HCC may develop a mechanism to evade apoptosis via a decrease of oxidised cardiolipin and its oxidation product HNE which can trigger intrinsic cell death [182]. Consistent with this, NRF2 activation and high

expression of AKR1C1 is associated with resistance to ferroptosis induced by HCC first line chemotherapeutic treatment Sorafenib [183, 184].

While AKR1C1 is a specific enzyme with direct catalytic activity on lipids and hormonal metabolites, we further explored a second target, cytochrome p450 reductase (POR) which affects a broad range of enzymes and functions more as a global regulator of steroid hormones.

1.7 Cytochrome p450 reductase

POR is a membrane-bound protein on the cytoplasmic side of the endoplasmic reticulum (ER) which is responsible for the electron transfer from NADP(H) to cytochrome p450s (CYPs), cytochrome b5, heme oxygenase (HO) and very likely other enzymes. POR is a 677 amino acid long protein and encoded by the POR gene on the long arm of chromosome 7 at 7q11.23. The gene is 50kb and consists of 16 exons of which 2-16 code for protein [185–187].

1.7.1 Function

POR has an influence on the metabolism of a broad range of endogenous and exogenous molecules especially via cytochrome p450s (CYPs). Mitochondrial (type 1) CYPs rely on ferredoxin reductase and ferredoxin and are independent of POR but all 50 microsomal (type 2) CYPs require POR for the electron transfer from electron donors such as NADPH to allow them to catalyze oxidation reactions on their substrates [188]. POR therefore impacts drug metabolism, steroid and bile acid synthesis, vitamin D, retinoic acid, and the metabolism of polyunsaturated fatty acids (PUFAs) to active or inactive cell signalling molecules. Knockout of POR has been shown to be embryonically lethal in mice probably due to extrahepatic lack of electron transport [189]. Interestingly, liver-specific knockout of POR is permissible to life and yields phenotypically, reproductively normal mice with reduced capacity for hepatic drug metabolism [190]. Heme oxygenase 1 (HO-1), the rate limiting step in heme catabolism, also requires POR to catalyse the degradation of heme to biliverdin, ferrous iron and carbon monoxide [191, 192]. Furthermore, POR serves as

redox partner for cytochrome b 5 [193, 194], squalene monooxygenase [195] and fatty acid elongase [196]. POR-dependent enzymes, such as squalene monooxygenase and CYP7A1, are essential for both cholesterol and bile acid synthesis [190, 197].

1.7.2 Mechanism

POR is a diflavin oxidoreductase which catalyses the electron flow in the form of hydride migration from NADP(H) to the flavin adenine dinucleotide (FAD) group, and further through direct interflavin electron exchange onto the flavin mononucleotide (FMN) group which in turn can transfer the electron to an external acceptor like CYPs (Figure 1.15). *In vivo*, POR normally cycles between 1- and 3-electron reduced states whereas *in vitro* it can be reduced to a 4-electron state with excess NADP(H) [198–201]. From a human perspective, we tend to have POR in a FAD – FMNH· semiquinone resting state and transfer electrons to acceptors from the FAD – FMNH2 semiquinone state [202].

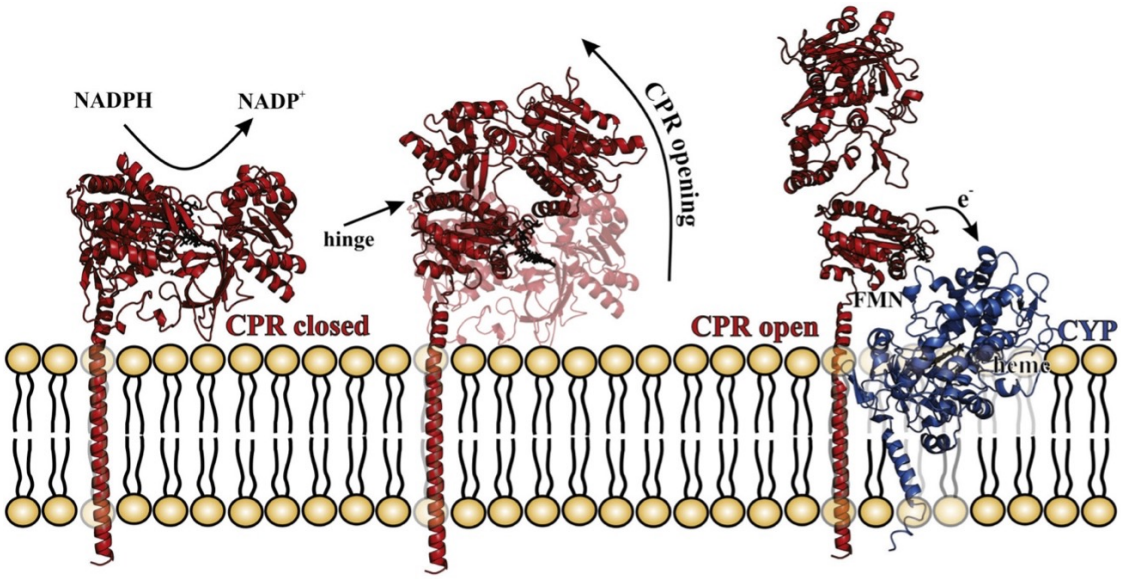


Figure 1.15: POR opens upon the reduction of its flavin by NADPH and afterwards is stabilised by the binding of a CYP enzyme. After binding, POR can transfer electrons from FMN to the heme of CYP. Figure by Šrejber et al. 2018 ([203])

1.7.3 Structure

POR is composed of three structural domains which are made up of the FMN- (N-terminus) and FAD/NADP(H)-binding domain (C-terminus) and are linked together through the connecting domain. The latter ensures the relative orientation of the other domains and through the proper alignment enables efficient electron transfer between the two flavins. The closest distance between the two flavins is around 4 Å. It is believed that a bowl-shaped area close to the FMN-binding site is docking site of CYPs or cytochrome b5 or heme oxygenase. The FMN-binding site is formed through a parallel five-stranded β-sheet with the FMN at the C-terminal ending of the β-sheet and five α-helices surrounding it. The FAD/NADP(H)-binding domain is made up of an anti-parallel flattened β-barrel a five-stranded parallel β-sheet in between α-helices. The connecting domain consists mostly of α-helices. The N-terminus of the enzyme is highly exposed to proteolytic cleavage and therefore very variable [204, 205].

1.7.4 POR and human phenotype

More than 50 missense mutations with A287P and R457H, being the most common mutations in European and Japanese individuals, respectively. The rather severe missense mutation A287P and R457H can cause Antley-Bixler syndrome, virilization and genital anomalies. [206, 207]. Interestingly, a case report of a chinese patient with a R457H missense mutation presented more similar to mild variants which lead to a phenotype similar to polycystic ovary syndrome in women or hypogonadism in men. [208, 209]. Typically, missense mutations lead to impaired steroidogenesis through changes in the co-factor binding or functional region of POR as seen with Y459H and V492E mutants showing diminished FAD binding [210]. Complete loss of functions mutation are most likely not permissible to life in humans. Knockout experiments in mice have shown to be embryonically lethal [189, 211]. Furthermore, POR is a strongly polymorphic gene with at least 140 SNPs present in different ethnic groups. Polymorphisms often affect less relevant structural parts of POR leading to less pronounced changes in activity. The most common variant A503V is

found in around 28% of all human alleles and causes a 40% reduction of CYP17A1 activity. There are substantial differences between different ethnic groups in the frequency of polymorphisms. Eg A503V is present in 40%, 26.4%, 19.1%, and 37.5% of Japanese, White, African American, and Chinese individuals, respectively. Other polymorphisms in the POR promotor region at -152 lead to a 50% lower transcription of POR [206, 212]. POR is particularly relevant as it can affect the activity of all microsomal CYPs and thereby not only impacts steroid hormone and bile acid metabolism but also impairs drug and xenobiotics metabolism in humans. Already polymorphisms have a significant impact on CYP activity as shown in drug metabolism studies. POR polymorphisms and mutations Y181D, R457H, Y459H, V492E, R616X, A287P, C569Y and V608F cause a 65% - 99% loss of CYP3A4 activity compared to wild type [213], whereas K49N, A115V and G413S show an 31% to 65% increase of CYP3A4 activity [214]. CYP2D6 was also shown to be affected: A503V decreased activity and the Q153R mutation increased activity *vs.* wild type [215]. On top, A503V and Q153R increased all three CYP2C9 isoforms activity levels [216]. A case study of POR deficiency shows transcriptionally up-regulated CYPs but revealed diminished activity levels of multiple CYPs including CYP3A4 upon *in vivo* testing [217]. These wide-ranging effects have also been implicated to impact on HCC as suggested in multiple studies. Low POR expression has been associated with poor HCC prognosis and it was shown in mice that a POR increase through glucose-6-phosphate dehydrogenase (G6PD) knockdown went hand in hand with an increase in ferroptosis-related proteins and significantly lower tumour growth [218]. On the other hand, the rs10954732 (G > A) POR polymorphism, in parallel with lower CYP2E1 activity, was associated with higher hepsin levels, a 69% decreased HCC susceptibility and a prolonged overall survival (median 220 *vs.* 437 days) [219]. Moreover, the rs1057868 (TT/CT *vs.* CC) POR polymorphism was significantly associated with HCC overall survival in cancers arising from HBV [220]. Even though POR activity seems to play an essential role for normal liver function, so far no-one has specifically looked at the impact of POR activity on human liver phenotype in the context of NAFLD.

1.7.5 POR and mouse phenotype

As described above, knock out of POR is lethal to mice but liver specific knock out yields seemingly normal, reproductive mice with unaffected growth and survival rates [189, 190, 221]. Only when bred with other hepatic Por-null mice, the fertility and litter size were reduced [221]. In contrast, the CYP enzymatic activity of hepatic Por-null mice was severely impaired. 6β-hydroxylation, 7α-hydroxylation and 16β-hydroxylation were shown to be around 0-10% of the activity observed in wild type animals for both male and female. Furthermore, hepatic POR knock out also effects drug metabolism by CYP enzymes as shown with acetaminophen and phenobarbital. This attenuation of CYP activity was reflected by an increase of CYP mRNA and protein, which could go up to 450% and >500% in male and female mice, respectively [190, 221]. A post mortem analysis identified hepatomegaly with higher fat content compared to wild type animals which makes POR a particularly interesting target for NAFLD research [190, 221]. For drug metabolism studies, hepatic POR knock out was used to suppress remaining activity of rodent CYP enzymes in humanised liver models. This helps to better predict human xenobiotic metabolism and discover differences in interspecies CYP metabolism such as human specific metabolite M28 of gefitinib [222].

1.8 Aims and objectives

The overarching aim of my thesis is to explore AKR1C1 and POR in the context of metabolic liver disease and primary liver cancer. So far, such research has been very limited even though AKR1C1 and POR are involved in steroid, retinoid and bile acid metabolism which are important regulators of metabolic phenotype. The understanding of the precise role of steroid hormones and their metabolites in NAFLD and HCC is still missing. Therefore, unraveling the particular contribution of steroid metabolizing enzymes is likely to add significant mechanistic insight into the pathogenesis of metabolic liver disease and HCC. Having selected two different targets, AKR1C1 having a direct, specific impact on steroids and lipids and POR being a more global regulator with downstream consequences on a very wide variety of enzymes, we hope to further the understanding in such multifactorial diseases.

The aims of this thesis are:

- Use clinical samples from patients with HCC and NAFLD to identify evidence for dysregulation of AKR1C1 activity.
- Define the impact of genetic manipulation of AKR1C1 expression on cellular proliferation, chemo-resistance and cell motility in a hepatocellular model.
- Test clinical samples from patients with NAFLD to show evidence for dysregulation of POR activity.
- Define the impact of a NAFLD inducing diet or treatment on POR in rodents and cell line respectively.
- Define the role of POR in hepatocellular lipid, glucose and bile acid metabolism.

2 Methods

Contents

2.1 Cell lines . . . 40
2.2 Cell culture . . . 40
2.3 Cloning . . . 41
2.4 Transformation . . . 41
2.5 Transfection . . . 42
2.6 Gene manipulation . . . 42
2.6.1 Transient knockdown . . . 42
2.6.2 Stable CRISPR/Cas9 knockdown . . . 44
2.6.3 Overexpression . . . 44
2.7 Pregnanediol-3-Glucuronide Competitive ELISA . . . 45
2.8 Gene expression . . . 46
2.8.1 RNA extraction . . . 46
2.8.2 RNA sequencing . . . 47
2.8.3 Reverse Transcription Polymerase Chain Reaction . . . 49
2.8.4 Quantitative Polymerase Chain Reaction . . . 50
2.9 Protein expression . . . 51
2.9.1 Protein extraction . . . 51
2.9.2 Protein quantification . . . 52
2.9.3 Western blotting . . . 52
2.10 Biochemical measurements . . . 54
2.10.1 Sample preparation . . . 54
2.10.2 Glucose . . . 55
2.10.3 TAG . . . 55
2.10.4 NEFA . . . 55
2.10.5 Cholesterol . . . 56
2.11 D-3-Hydroxybutyrate . . . 56
2.12 Lipid measurements . . . 56
2.12.1 Lipid extraction . . . 56
2.12.2 Gas chromatography . . . 58
2.12.3 Gas chromatography-mass spectrometry . . . 58
2.13 Bile acids quantification . . . 59
2.13.1 Total bile acid assay . . . 59
2.13.2 Liquid chromatography–mass spectrometry of bile acids 59
2.14 Statistical analysis . . . 60

2.15 Outsourced methods 61

2.1 Cell lines

HepG2 is an immortalized hepatocellular carcinoma cell line that was derived from the liver tissue of a 15-year-old Caucasian male from Argentina in 1975. HepG2 cells are non-tumorigenic with a high proliferation rate and exhibit an epithelial-like morphology. They show many differentiated hepatic functions and secrete many major plasma proteins. They have been successfully used in large scale cultivation systems [223].

Huh7 is an immortalized hepatocellular carcinoma cell line that was derived from the liver tissue of a 57-year-old Japanese male with well-differentiated liver cancer in 1982 [224]. Huh7 cells are epithelial-like, tumorigenic and have a point mutation (codon 220 of Exon 6) in TP53 which leads to accumulation of this protein due to a longer half-life [225–227]. These cells were often used to investigate HCV and hepatoma due to its high susceptibility to HCV [228].

2.2 Cell culture

HepG2 and Huh7, two adherent human hepatoma cell lines, were cultured in 75 cm2 non-pyrogenic polystyrene flasks using 15 ml of culture media. Culture media consisted of Dulbecco's Minimum Essential Medium (DMEM) supplemented with 10% Foetal Bovine Serum, 1% Penicillin/Streptomycin and 1% non-essential amino acids. Cells were grown at 37°C in 5% CO2 until reaching 70-80% confluence. At this point cells were trypsinized in 3 ml Tryple Express (Invitrogen, Paisley, UK) and re-seeded into fresh flasks. For experiments, cells were seeded in Costar® 24 well plate (Corning, Flintshire, UK) at 1.6 x 10^5/ml and 1.4 x 10^5/ml for HepG2 and Huh7 respectively, in 500 µl culture media. Cells were frozen at -80°C for later RNA and protein extraction. If media was collected, it was frozen at -80°C for later analysis.

2.3 Cloning

Guide RNA (gRNA) oligonucleotides were ordered from IDT (Integrated DNA Technologies BVBA, Leuven, Belgium) and amplified using PCR. Afterwards, single stranded gRNAs were inserted into the RP-418 Cas9 Puromycin plasmid (plasmid map in lab archives) using Gibson Assembly. First, RP-418 was digested with BsmBI. 5 µg of vector was prepared together with 1 µl BsmBI, 4 µl Tango buffer (including BSA) and 0.4 µl of 100 mM stock of Dithiothreitol. The mixture was topped up to 40 µl with nuclease-free water. In a PCR tube, 20 ng of the vector (1 µl) was prepared with 0.5 µl 40nM gRNA oligo and 1.5 µl of 2x Gibson Assembly buffer and left to assemble for 1-4 hours at 50 °C. 3 µl were then transformed in 50 µl of competent cells and plasmid was sequenced.

2.4 Transformation

50 µl Alpha-Select Gold Efficiency cells (Bioline, Luckenwalde, Germany) were used for bacterial transformation and 1-3 µl of plasmid were added to the competent cells before leaving them on ice for 45 min. Cells were then put in a water bath for 30 sec at 42 °C. After heat-shocking, 500 µl of lysogeny broth (LB) growth medium were added to the tube, which was placed for 1 h into a 37 °C incubator while shaking. 50 µl bacterial solution was plated on a LB agar plate containing 100 µg/ml Ampicillin and incubated upside down for 12-16 h. A single colony was isolated and added to a 50 ml falcon tube containing 15 ml of LB with 100 µg/ml Ampicillin. The tube was shaken in the incubator overnight for 12-16 h and then centrifuged for 15 min at 800 g. The plasmid was then isolated using the commercially available QIAprep Spin Miniprep Kit (QIAgen, Manchester, UK). Quantity and quality of plasmids was assessed using a NanoDrop® ND-1000 UV-Vis Spectrophotometer (Thermo Scientific, Hemel Hempstead, UK). The absorbance ratio 260/280 nm was used to evaluate purity and only DNA samples with a ratio between 1.8 and 2.2 were used in further experiments.

2.5 Transfection

Transfection is a method to introduce nucleic acids into eukaryotic cells in order to either express or inhibit a gene. In this context, the gene and protein function, expression or interaction can be studied. Transfection can be achieved through a variety of chemical, biological, or physical methods and can be divided into transient and stable transfection. During transient transfection there is no integration of nucleic acid into the genome. Therefore, the genetic material only remains in the cell for a limited period of time and will not be passed on to the next generation during cell division. To achieve optimal results cells are harvested between 24h and 96h after transient transfection. In stable transfection, on the other hand, the foreign nucleic acid is integrated into the genome or maintained as an episomal plasmid which replicates with eukaryotic cells. This will allow for the study of long-term effects as the cells will persistently express or inhibit the transfected gene. Cells need to be selected as only few cells integrate the transfected nucleic acid. By also transfecting a selectable marker (e.g. gene for drug resistance), a specific treatment can be used to select for successful transfection after an initial recovery period. In general, the observed effects of stable transfection tend to be lower than in transient transfection.

2.6 Gene manipulation

There are a variety of techniques to reduce or increase expression of specific genes. It can be achieved transiently via mRNA degradation or plasmid insertion and more permanently by DNA manipulation with techniques such as CRISPR/Cas9.

2.6.1 Transient knockdown

Experiments can be conducted with short interfering RNA (siRNA), a double-stranded RNA. SiRNA can be introduced into cells by lipofection to silence genes through repression of transcription. Liposome transfection uses positively charged lipids to form aggregates with negatively charged siRNA, enabling the siRNA

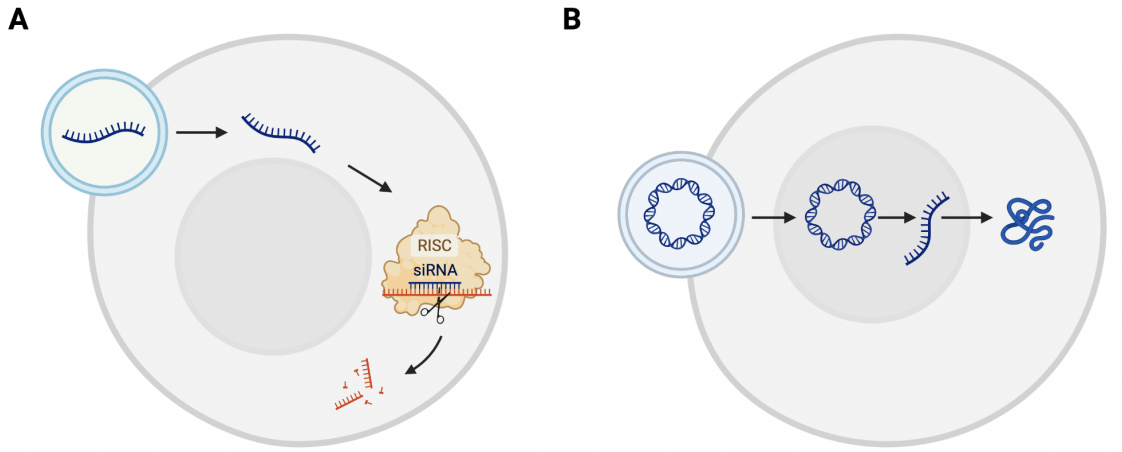


Figure 2.1: A) Transient knockdown of a specific protein can be achieved via transfection of siRNA into the cell, where it binds to the RISC which will degrade the complementary target mRNA of each specific siRNA. B) Overexpression of a specific protein can be achieved via transfection of DNA plasmid containing a expression vector, often a CMV promoter, and the gene coding for the specific protein. The plasmid will produce mRNA which in turn will be converted to protein by the cell leading to the overexpression of the desired protein. Created with BioRender.com.

to pass through the cell membrane. After being transfected into cells, siRNA binds to the RNA-induced silencing complex (RISC) which will unwind the siRNA into single strands. As part of the RISC, siRNA can then bind complementary target mRNA sequences and label them for degradation through cleavage by the RISC (Figure 2.1A).

For transient knockdown cells were seeded in 24-well plates at 1.6 x 10^5/ml and 1.4 x 10^5/ml for HepG2 and Huh7, respectively. After 24h, at 60-80% confluence cells were transfected. Media was changed to DMEM supplemented with 1-10% FBS and 1% non-essential amino acids. 1.25 µl/well Lipofectamine RNAiMAX (Thermo Scientific, Hemel Hempstead, UK) was diluted in 25 µl /well Opti-MEM medium in 1.5 ml tubes. A 10 µM siRNA stock of control and gene of interest was diluted to desired concentrations of 10, 20 or 40 nM in 25 µl Opti-MEM medium in 1.5 ml tubes. All tubes were vortexed and centrifuged. Then the diluted RNAiMAX was transferred into tubes containing diluted siRNA. These were vortexed and centrifuged again and left to incubate at room temperature for 5min. 50 µl/well of siRNA-lipid complex was then added dropwise to cells. 48h post transfection media

was replaced with phenol red free DMEM supplemented with 1% non-essential amino acids, 1% sodium pyruvate and 1% L-Glutamine.

2.6.2 Stable CRISPR/Cas9 knockdown

Cell lines can be generated with the gene editing potential of Class 2 Clustered Regularly Interspaced Short Palindromic Repeat (CRISPR) and the CRISPR associated protein 9 (Cas9), which form a sort of adaptive immune system for bacteria and archaea. An engineered CRISPR system is used to co-express a gRNA and an endonuclease Cas9. The gRNA consists of a CRSIPR RNA (crRNA) and a trans-activating crRNA (tracrRNA) which contain a target sequence followed by a protospacer adjacent motif (PAM) and a scaffold sequence for Cas9 binding, respectively. If the gRNA has sufficient homology with the target DNA it will start annealing and allow Cas9 to cleave the target DNA 3-4 nucleotides upstream of PAM resulting in a double-strand break. These breaks will most likely be repaired by non-homologous end joining often causing deletions, insertions or frameshift mutations which in turn can lead to the intended loss-of-function mutations in the targeted gene.

2.6.3 Overexpression

Overexpression of a gene can be achieved by introduction of genetic material into the cell. The gene of interest can be transfected as a plasmid containing an expression vector followed by the gene of interest. The expression vector, e.g. Cytomegalovirus (CMV) promoter, is a region of DNA controlling transcription of genes. The plasmid can be inserted via lipofection. Most plasmids contain a green fluorescent protein (GFP) region to control for successful transfection.

For overexpression, cells were seeded in a 24-well plate at 1.6 x 10^5/ml and 1.4 x 10^5/ml for HepG2 and Huh7, respectively. At 60-80% confluence cells were transfected, around 24h post seeding. Media was changed to DMEM supplemented with 10% FBS and 1% non-essential amino acids. A tube with 50 µl/well of Opti-MEM was prepared and 500 ng/well of plasmid DNA containing a CMV promoter, the gene of interest and GFP region was added (Figure 2.2. At a 2:1 ratio, 1

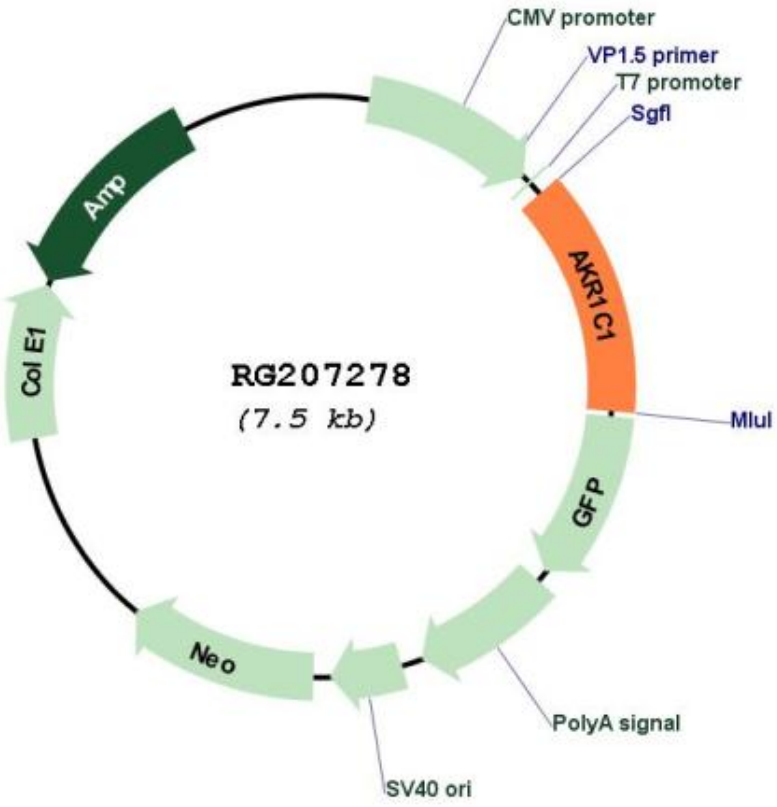


Figure 2.2: Plasmid map of AKR1C1 clone with a pCMV6-AC-GFP vector.

ml/well of X-tremeGENE HP DNA (Sigma-Aldrich, Gillingham, UK) transfection reagent was added and left to incubate for 15 min. 50 µl of plasmid-lipid complex were then added dropwise to each well. 24h post transfection of a GFP containing plasmids, cells were imaged under a fluorescence microscope to control for green fluorescence as a marker of successful transfection. 48h post transfection media was replaced with phenol red free DMEM supplemented with 1% non-essential amino acids, 1% sodium pyruvate and 1% L-Glutamine.

2.7 Pregnanediol-3-Glucuronide Competitive ELISA

Enzyme-linked immunosorbent assays are commonly used to identify antibodies, antigens, proteins, peptides and hormones in a variety of biological samples. These

samples are added to a specially absorbent plate which binds the target. The immobilized target can then be complexed with a detection antibody linked to an enzyme. This allows to quantify the target via enzymatic activity measurement. This general principle does not directly translate to all different forms of ELISAs that exist (direct, indirect, sandwich, reverse and competitive (inhibition)). The competitive ELISA e.g. measures lower enzymatic activity the higher the substrate concentrations are because substrate and detection enzyme compete to bind the same antibody binding site.

To measure AKR1C1 activity we used a commercial solid-phase Pregnanediol-3-Glucuronide (PDG) Competitive ELISA kit (Invitrogen, Paisley, UK) which was cell media compatible. First, 50 μl of standard curve between 0.781ng/ml and 50ng/ml PDG, negative control or samples were added into wells. Then PDG conjugate and PDG Antibodies were added to each well and the plate left to incubate for 2 hours at room temperature with shaking. The ELISA plate was thoroughly washed with 1X wash buffer before 100 μl of the chromogen TMB substrate was added to each well. This will cause the substrate solution to turn blue. After 30min incubation at room temperature without shaking, 50 μl of stop solution was added which will stop the enzymatic reaction and cause the colour of the solution to change to yellow. Using the VersaMax™ Tunable Microplate Reader (Molecular Devices, Wokingham, UK) the absorbance was read at 450 nm not later than 10 min after adding the stop solution.

2.8 Gene expression

2.8.1 RNA extraction

RNA isolation from a biological sample is the basis of several molecular biological techniques. A variety of methods exist to purify RNA from tissue samples or cells. The most common strategy is the guanidinium thiocyanate-phenol-chloroform extraction. The extraction of high-quality RNA is complicated by rapidly occurring RNA degradation because of the ubiquitous presence of RNases.

To perform total RNA extraction, the TRIzol-Reagent system (Sigma-Aldrich, Gillingham, UK) was used. Cell plates were taken from a -80°C freezer and left to thaw on ice. 500 µl of Tri-Reagent was added to each well. Subsequently, the adherent cells were harvested by scraping the surface of the well to detach the cells with the tip of a 1 ml pipette. Each well was transferred to a correspondingly labelled 1.5 ml Phasemaker™ Tube (Invitrogen, Paisley, UK). Samples were left standing for 5min at room temperature. 200 μl of chloroform per ml of TRI-Reagent was added and tubes were shaken for 15 seconds. Tubes were again left standing for 5 min at room temperature and afterwards centrifuged at 13200g for 15min at 4°C. Centrifugation results in 3 separated phases: a red organic phase and an interphase containing protein and DNA respectively plus an upper transparent aqueous phase containing RNA. The aqueous phase was transferred into a new tube and 500 μl of isopropanol per ml TRI-Reagent were added. To precipitate RNA in form of a pellet, tubes were centrifuged at 13200g for 10min at 4°C. Samples were then washed with 1 ml of 75% ethanol. After removal of 75% ethanol, the pellets were left to dry by air for 10min and then dissolved in 35 μl of nuclease-free water.

RNA concentration and purity was determined at OD260 using a NanoDrop® ND-1000 UV-Vis Spectrophotometer (Thermo Scientific, Hemel Hempstead, UK). Prior purification is important as all nucleotides including RNA, ssDNA and dsDNA have their maximal absorbance at wavelength 260 nm. The absorbance ratio 260/280 nm was used to evaluate purity and only samples with a ratio between 1.8 and 2.2 were further processed in experiments. Furthermore, absorbance of the 260/230 nm ratio was considered to assess proper wash out of contaminants such as phenol.

2.8.2 RNA sequencing

RNA sequencing is a powerful molecular biology technique used to analyze and quantify the presence and abundance of RNA molecules within a biological sample. It provides valuable insights into gene expression patterns, alternative splicing, RNA processing, and the discovery of noncoding RNA, such as microRNA and lncRNA. The RNA sequencing extracted RNA is either first filtered with poly(A)-tails to

only include coding regions or directly fragmented into smaller pieces to ensure that the complementary DNA (cDNA) fragments represent different regions of the original RNA and size selected to fit the sequencing machine. After reverse transcription, the first DNA strand is subjected to second strand synthesis resulting in double-stranded cDNA. This is followed by end repair of the doubled stranded cDNA to create blunt ends and adaptor ligation is used to ligate sequencing adapters to cDNA as recognition sites for subsequent amplification and sequencing steps. Afterwards the library amplification is performed to increase the amount of cDNA. The prepared sample is then subjected to high-throughput sequencing technologies in a flow cell. Once the sequencing is complete, the resulting data contains a vast number of short reads. These reads are then aligned or mapped to a reference genome. This allows to determine the origin of each read and to assemble them into complete transcripts or genes. By counting the number of reads that align to each transcript gene expression levels can be quantified.

The TRIzol-Reagent system (Sigma-Aldrich, Gillingham, UK) and 1.5 ml Phasemaker™ Tube (Invitrogen, Paisley, UK) were used as by manufacturer's instruction to extract total RNA. RNA concentration and purity were determined at OD260 using a NanoDropR ND-1000 UV-Vis Spectrophotometer (Thermo Scientific, Hemel Hempstead, UK). Quality control was performed with TapeStation 4150 (Agilent Technologies, Stockport, UK) and only samples with RIN values > 8 were used for library construction. The library was prepared by Poly-A enrichment after quality control assay. cDNA was generated from total RNA and second strand cDNA synthesis incorporated dUTP. The cDNA was end-repaired, A-tailed and adapter-ligated. Prior to amplification, samples underwent uridine digestion. The prepared libraries were size selected, multiplexed and quality controlled before paired end sequencing over two units of a NovaSeq6000 flow cell using NovaSeq 6000 Reagent Kits v1.5 (Illumina, Cambridge, United Kingdom). RNAseq read pairs were trimmed for Illumina adapters using skewer [229] before alignment to the GRGh37 reference genome using Hisat2 version-2.0.4 [230]. Gene annotation files were downloaded in GTF format from Ensembl [231]. Reads mapping to annotated exon features were

quantified with featureCounts [232], part of subread-v1.5.0 4 [233], using default parameters and keeping all aligned reads including potential duplicates. Quality metrics for aligned reads were estimated using CollectRnaSeqMetrics, implemented in Picard tools v1.92 (picard-tools https://broadinstitute.github.io/picard/, version at 10.01.2016). DeSeq2 was used for differential gene expression analysis [234]. Differentially expressed genes were reported for P value ≤ 0.05 and fold change of 1.5 and were considered statistically significant with a false discovery rate (Benjamini-Hochberg method) of adjusted P value ≤ 0.05. clusterProfiler was used for KEGG enrichment and gene ontology analysis [235].

2.8.3 Reverse Transcription Polymerase Chain Reaction

Reverse Transcription Polymerase Chain Reaction (RT-PCR) is a technique performed to look at mRNA expression by first converting single stranded RNA into cDNA and then amplifying specific DNA targets with polymerase chain reaction (PCR). Conversion is achieved by adding extracted RNA to a reaction mixture including reverse transcription. The reverse transcriptase will synthesize a complementary strand of DNA hybridised to the original mRNA strand. This is followed by the amplification process with cycling temperature levels. Temperature is first raised to denature RNA/DNA strands and then lowered for primers to anneal and polymerases to extend the new DNA strands.

Reverse transcription (RT) reaction was performed in 20 µL volumes. Reaction volume consisted of 1 µg sample RNA diluted in 10 µL nuclease-free water and 10 µL of 2X RT master mix using the Applied Biosystems Reverse Transcription Kit (Applied Biosystems, Warrington, UK). The 2X RT master mix was prepared by adding 2 µl of 10x RT buffer, 0.8 µl of 25x dNTPs mix (100mM), 2 µl of 10x RT Random primers, 1 µl of MultiScribe reverse transcriptase, 1 µl of RNase Inhibitor and 3.2 µl of nuclease-free water into a tube. Tube was vortexed and briefly centrifuged before adding the 2X master mix to the RNA solution. RT reaction was performed by incubating the RNA samples in MJ Research Thermal Cycler (Bio Rad, Watford, UK) for 10 min at 25°C to allow for optimal annealing

of the random hexamers, followed by 120 min at 37°C, the optimal temperature for the reverse transcriptase to polymerise the DNA and ending with 5 min at 85°C to inactivate the reverse transcriptase.

2.8.4 Quantitative Polymerase Chain Reaction

Quantitative PCR is a widely used technique in molecular biology to reliably quantify gene expression. It allows for real time measurement of amplification of a specific target DNA molecule whereas conventional PCR only allowed endpoint analysis. Amplification is achieved, as in conventional PCR, in a repeated cycle of three steps: denaturation of DNA by heat, annealing of primers to target sequence by cooling the samples and extension of primers through DNA polymerase. Real time analysis is made possible by monitoring increasing fluorescence during amplification. One way to evoke fluorescence is the use of TaqMan probes. TaqMan probe consist of a fluorophore on the 5' end and a quencher at the opposite 3' end, with a target specific minor groove binder (MGB) in the middle. The MGB will cause the TaqMan probe to bind its specific target at the time of primer annealing. Subsequently, during the synthesis of a new DNA strand Taq DNA polymerase cleaves the TaqMan probe through its endogenous 5' nuclease activity and thereby releases the fluorophore. Fluorescence emission, which has been absorbed so far by the quencher due to close proximity, can then be detected by the qPCR instrument.

To assess cDNA quality a standard curve was generated by a dilution series (1/10, 1/20, 1/40, 1/80, 1/160 and 1/320) in 10mM Tris-HCL using a pool containing 2 µl of each cDNA sample. 8 µl reaction were performed in triplicates for each dilution and tested against the housekeeping gene 18S rRNA. Therefore, 3.6 µl of cDNA, 4 µl KlearKall 2x Master Mix with standard ROX reference dye and 0.4 µl of 18S rRNA TaqMan probe (Applied Biosystems, Warrington, UK) were added to 0.1 ml Rotor-Gene® strip tubes. Samples were then analysed with the Rotor-Gene® 6000 real-time cycler (QIAgen, Manchester, UK) at the following conditions: 3 min at 95°C, followed by 40 cycles of 3 sec at 95°C and 20 sec at 60°C.

For qPCR analysis 6 µl reaction were executed in triplicates using a 384-well plate. The reaction consisted of 2.7 µl of cDNA, 3 µl KlearKall 2x Master Mix with standard ROX reference dye and 0.3 µl target specific TaqMan probes all provided by Applied Biosystems. QuantStudio 7 Flex real-time PCR system (Applied Biosystems, Warrington, UK) was used to measure fluorescence at the following conditions: 3 min at 95°C, followed by 40 cycles of 3 sec at 95°C and 20 sec at 60°C.

The Ct value of each sample was calculated using the following formula: ΔCt = E[min Ct-sample Ct], with E being the reaction efficiency determined from a standard curve. The standard curve was generated from a pool of all cDNAs as a calibrator and the relative expression ratio was determined using the equation: ratio = ΔCt[target]/ΔCt[ref]. Expression was normalised to the ΔCt value 18S rRNA. Statistical analysis was performed on the mean relative expression ratio values (ratio = ΔCt[target]/ΔCt).

2.9 Protein expression

2.9.1 Protein extraction

Protein extraction from cell culture requires the lysis of the external cell membrane. Different lysis buffers exist, with milder buffers having the benefit of less protein denaturation during the lysis process. The presence of proteinase needs to be considered as this may complicate the extraction. Sonification can be used to further break open cell membranes and homogenise the protein sample, followed by centrifugation to clear the sample from cell debris.

After removing the media HepG2 and Huh7 cells were washed twice with 500 µl 1x PBS. 200 μl of radioimmunoprecipitation assay (RIPA) buffer containing 50 mM NaCl, 1.0% IGEPAL® CA-630, 0.5% sodium deoxycholate, 0.1% SDS, 50mM Tris, pH 8.0 and additionally supplemented with 1:100 protease inhibitor and 1:100 phosphatase inhibitor was used to lyse the cells in each well (Sigma-Aldrich, Gillingham, UK). Subsequently, the adherent cells were harvested by scraping the surface of the well to detach the cells with the tip of a 1 ml pipette and were then transferred to a correspondingly label 1.5 ml Eppendorf tube. The lysate was

stored at -80°C and then thawed on ice before further processing. Sonification was performed using a Jencons sonicator at 40% power for 5 times 5 seconds. The lysate was then centrifuged for 10 min at 10000g and 4°C to clear the sample from cell debris and insoluble components. The supernatant was then transferred into a new 1.5 ml tube and used for quantification of protein concentration.

2.9.2 Protein quantification

Protein quantification was performed by using a detergent compatible (DC) protein assay (BioRad, Hertfordshire, UK). The colorimetric assay can determine protein concentration as a result of a twostep process. Protein and copper react at an alkaline pH which leads in a second step to the reduction of a Folin reagent mainly by oxygen atoms of amino acids tyrosine and tryptophan. The reduced Folin species have a characteristic colour and will cause the sample to turn blue. Absorbance can then be measured at 650 to 750 nm and quantified with a standard curve.

A standard curve was created with bovine serum albumin by serial dilution in lysis buffer ranging from 2, 1.5, 0.8, 0.4, 0.2, 0.1 to 0.0 mg/ml. 5 µl of standard curve or samples were then added to each well of a 96 well plate in duplicate. 24.5 µl of reagent A (copper tartrate solution) and 0.5 µl of reagent S (surfactant solution) was added to each sample. After adding 200 µl of reagent B (Folin reagent) to each well the plate is left to incubate away from light. Using the VersaMax™ Tunable Microplate Reader (Molecular Devices, Wokingham, UK) the absorbance was read at 650 nm 15 min after adding reagent B.

2.9.3 Western blotting

Western blotting is a widely used technique for the detection of specific proteins in molecular biology. With gel electrophoresis denatured proteins are separated by size or charge. Separated proteins are afterwards transferred from the gel onto a protein binding membrane, either nitrocellulose or polyvinylidene diflouride (PVDF) by electroblotting. Following the transfer, the membrane is blocked with a solution of protein, typically 3-5% bovine serum albumin (BSA) or milk to

prevent unspecific binding of antibodies. To detect the protein of interest the membrane is then incubated with a primary antibody followed by exposure to a secondary antibody which binds the primary and is linked to a reporter enzyme, such as alkaline phosphatase or horseradish peroxidase (HRP). HRP bound to the target protein can be used for detection as it cleaves a chemiluminescent substrate resulting in a proportional production of signal which can be detected by digital or film-based imaging.

10-20 µg of protein sample were prepared with the same amount of 2x Laemmli buffer and boiled at 70°C for 3 min. Samples were left to cool down at 4°C and quickly centrifuged before loading into TGX (Tris-Glycine eXtended) stain free criterion gels with 1x Tris/Glycine/SDS (TGS). The samples were then run for 5 min at 55V and for another 90 min at 108 V. The gels were imaged to control protein loading. The proteins were transferred onto a PVDF membrane using the transblot turbo system for 7 min, followed by imaging to check for successful transfer. Afterwards, the membranes were blocked with 20 ml of blocking buffer consisting of Tris-Buffered Saline (TBS) 0.1% Tween 5% milk powder for 1h on a rocking shaker. Membranes were then washed three times with washing buffer (TBS 0.1% Tween) before incubating with primary antibodies at 4°C overnight on the rocking shaker. After removing the primary antibodies, the membranes were washed three times for 15 min before adding the secondary antibody at a dilution of 1/1000 to incubate for 1 hour on a rocking shaker. This was followed by washing the membrane again three times for 15 min. 1 ml of peroxide reagent and 1 ml of Luminol/enhancer reagent were mixed to create 2 ml of chemiluminescent ECL substrate (BioRad, Hertfordshire, UK). This was then added onto the membranes and left for 5 min before imaging. The excess ECL substrate was shaken off, and the membranes transferred to cling film. The ChemiDocXS Touch Imaging System from BioRad was used to measure the signal and analysis was performed with ImageLab software from BioRad.

Table 2.1: Western blot anti-bodies

Protein Target	Antibody	Manufacturer	Dilution
AKR1C1	Rabbit polyclonal Anti-AKR1C1	Abcam plc, Cambridge, UK	1:500
POR	Rabbit monoclonal Anti-POR	Abcam plc, Cambridge, UK	1:1000
β-tubulin	Mouse monoclonal Anti-β-tubulin	Cell Signaling, Danvers, USA	1:1000
p-ACC	Rabbit monoclonal Anti-phospho-ACC	Cell Signaling, Danvers, USA	1:1000
Total ACC	Rabbit monoclonal Anti-ACC	Cell Signaling, Danvers, USA	1:1000
p-AMPKα	Rabbit monoclonal Anti-phospho-AMPKα	Cell Signaling, Danvers, USA	1:1000
Total AMPKα	Rabbit monoclonal Anti-AMPKα	Cell Signaling, Danvers, USA	1:1000
FASN	Rabbit monoclonal Anti-FASN	Cell Signaling, Danvers, USA	1:1000

2.10 Biochemical measurements

Glucose, triglycerides, non-esterified fatty acids (NEFA), cholesterol and 3-hydroxybutyrate (3-OHB) were analyzed using Instrumentation Laboratory kits (Instrumentation Laboratory, Milano, Italy) or Randox kits (Crumlin, County Antrim, UK) on an AU 480 Clinical Chemistry Analyzer (Beckman Coulter Ltd., High Wycombe, UK). Assays were carried out according to manufacturer's instructions and an appropriate calibrator or standard curve for quantification was used.

2.10.1 Sample preparation

Cells were cultured and treatments were carried out in 24-well plates. Cell media samples was collected, transferred into 1.5ml tubes and stored in -80°C. Cells were subsequently washed with 1x PBS before being lysed in 150µl 1% NP-40 lysis buffer (5M NaCl, 10% NP-40, 1M Tris-HCl, pH 8.0) followed by scraping and transfer into 1.5ml tube for storage at -80°C. For analysis, cell lysates were sonicated for 30 sec, then heated to 95°C for 30 min and spun at 12000 x g for

10 min, supernatant was removed for analysis. Cell lysate or media sample were used with the respective analysis kit as described below.

2.10.2 Glucose

Glucose of media samples was quantified using the glucose (Oxidase) Instrumentation Laboratory kit (Instrumentation Laboratory, Milano, Italy). The glucose (Oxidase) reagent contains the enzymes and substrates for the following reactions: oxidation of D-Glucose to Gluconic acid and hydrogen peroxide (H_2O_2) by glucose oxidase, followed by peroxidase catalyzing the reaction of H_2O_2 with phenol and 4-aminoantipyrine to produce red quinoneimine, leading to a purple colour which can be measured as absorbance at 540 nm.

2.10.3 TAG

The TAG assay kit (Instrumentation Laboratory, Milano, Italy) was used to determined TAG in cell and media samples. Before running samples, the iLab was calibrated using a range of glycerol standards at 50, 100, 200 and 1000µM. Sample was combined with triglycerides reagent containing enzymes and substrates for the following set of reactions: enzymatic hydrolysis of TAG by lipase to glycerol and NEFAs, before the formed glycerol is phosphorylated by glycerol kinase to glycerol-3-phosphate. Glycerol phosphate oxidase produces dihydroxyacetone phosphate and H_2O_2 through oxidation of glycerol-3-phosphate. H_2O_2 is then combined with 4-aminoantipyrine and 4-chlorophenol to produce red quinoneimine, measured as absorbance at 540 nm.

2.10.4 NEFA

NEFA was quantified with the NEFA assay kit by Randox (Crumlin, County Antrim, UK) containing enzymes and substrates necessary for the colourimetric determination of NEFA content. Acyl-CoA-synthetase converts NEFA, CoA to acyl-CoA using ATP. Acyl-CoA in turn is oxidised to 2,3,-trans-enoyl-CoA and H_2O_2

by acyl-CoA oxidase. When combining H_2O_2, 4-aminoantipyrine and N-ethyl-N-(2hydroxy-3-sulphopropyl) m-toluidine peroxidase produces a purple adduct which can be measure at absorbance 550 nm.

2.10.5 Cholesterol

Cholesterol was measured in cell lysate and media samples using the total cholesterol kit by Randox (Crumlin, County Antrim, UK). The reagent contains the enzymes and substrates for the following reactions: cholesterol esterase hydrolyses cholesterol esters from within the sample into cholesterol and free fatty acids, subsequently cholesterol oxidase oxidises cholesterol to produce cholest-4-en-3-one and H_2O_2. H_2O_2 is then combined with 4-aminoantipyrine and phenol to produce quinoneimine which can be measured as absorbance at 540 nm.

2.11 D-3-Hydroxybutyrate

For the quantitative in vitro determination of 3-OHB in media samples the RANBUT kit by Randox (Crumlin, County Antrim, UK) was used. This kit oxidises 3-OHB to acetoacetate with 3-OHB dehydrogenase. The concomitant reduction of the co-factor NAD+ to NADH and the associate change in absorbance can be directly correlated with the 3-OHB concentration, which is determined on an AU 480 clinical chemistry analyzer system measuring the absorbance at 505 nm. Prior to running samples, the iLAB was calibrated using 3 different concentrations (62.5, 125 and 500µmol/L) of the CAL standard supplied in the RANDBUT kit and reconstituted before each experiment. 100µl of samples were then transferred into a separate 3ml iLAB standard sample cup. Results were finally normalised against protein concentration.

2.12 Lipid measurements

2.12.1 Lipid extraction

Cells were collected in 1% NP-40 TAG lysis buffer and sonicated. Lipid was extracted according to the Folch method [236]. This method uses polarity differences between

chloroform and methanol, after the addition of water in the form of saline, to separate salts and hydrophilic cell components in the aqueous phase (approximate 3:48:47 (v/v/v) chloroform:methanol:water) and lipids in the largely non-polar, solvent phase (approximate 86:14:1 (v/v/v)). First, internal standards with known concentrations of glyceryl triheptadecanoate (15:0), heptade-canoic acid (17:0) and 1,2-diheptanoyl-sn-glycero-3-phosphocholine (17:0) were added to a glass tube. 500 µl of sample were added to each tube and mixed on the rotatory for 15 min with 5 ml 2:1 chloroform:methanol (v/v). 1 ml 1 M sodium chloride was added and samples were mixed again. Following centrifugation at 800 x g for 10 minutes at 14 °C, the aqueous phase was discarded and the solvent phase transferred to a new tube and then evaporated to dryness under nitrogen at 50°C in a Zymark TurboVap® LV (Biotage; Uppsala, Sweden). Samples were reconstituted with 1 ml chloroform and TAG, cholesterol ester (CE) and phospholipid (PL) fractions were separated using solid-phase extraction (SPE) as described previously [237]. SPE columns contain aminopropyl silica, which forms hydrogen bonds with lipids; in combination with specific solvents, different lipid classes can be isolated using selective extraction and elution. Columns had to be pre-washed with two times 1 ml acetone followed by two times 1 ml chloroform. The samples were then added on to the columns. To elute TAG and CE, which weakly bond to the silica, 1 ml chloroform was washed through. PLs were eluted with 2 ml mixture of chloroform and methanol (3:2 v/v). Fractions were captured in glass tubes and evaporated to dryness. TAG and CE, the non-polar lipid fraction, was then reconstituted in 1 ml hexane and fresh SPE columns were preconditioned with four times 1 ml hexane before the samples were added. Two times 1 ml Hexane was used to elute CE and 1 ml of chloroform and ethyl acetate (100:5:5 v/v/v) twice was used to elute TAG. Both fractions were evaporated to dryness. After, samples underwent methylation which reduces the polarity of FAs and allows accurate separation and measurement of FA species via gas chromatography (GC). 400 µl toluene and 800 µl sulphuric acid in methanol (1.5% v/v for TAG and 6% v/v for PLs) were added to samples and incubated in a water bath at 80°C (1 hour for TAG and NEFA and 2 hours for PLs) to achieve

transesterification. After cooling to room temperature, 2 ml of neutralising solution (25 mM potassium hydrogen carbonate and 25 mM potassium carbonate in water) and 2 ml cyclohexane were added to extract the fatty acid methyl esters (FAMEs). Samples were mixed on the rotatory and centrifuged at 800 x g for 10 minutes before the solvent phase was transferred to a new tube and evaporated to dryness under nitrogen. Fractions were finally reconstituted in 500 µl chloroform and transferred to a GC vial which contains 20 µl external standard (methyl tricosonate; 23:0).

2.12.2 Gas chromatography

GC vials were transferred to a 7890B GC System (Agilent Technologies; CA, USA). Gas chromatography allows the separation of components within a sample based on the time it takes for them to travel through a column and arrive at the detector. The retention time depends on the affinity of the component to remain in the liquid, stationary phase or move with the mobile, gas phase. Identification was based on retention time comparison against a standard containing 31 known fatty acids and quantified in micromolar based on the peak area and molecular weight. All was expressed relative to protein content of the respective sample. Each FA was represented as molar percentage (mol%) of total FA adjusted by protein. Enzyme activity estimates were made through product to precursor ratios from molar percentage values. SCD activity was estimated by the ratio of its products, palmitoleate and oleate (C16:1 and 18:1), to their precursors, palmitate and stearate (C16:0 and C18:0). Similarly, fatty acid elongase 6 (ELOVL6) activity was estimated by the ratio of stearate (C18:0) to palmitate (C16:0).

2.12.3 Gas chromatography-mass spectrometry

To determine stable isotope enrichment by GC-mass spectrometry (GC-MS), samples are first ionised, accelerated through a column and finally deflected by a magnetic field. The proportion of deflection allows a calculation of mass and the particle to be identified based on known masses. As mass is also affected by the charge of the particle, mass needs to be corrected for charge and is expressed as mass to

charge ratio (m/z). Intracellular DNL was determined based on the incorporation of deuterium from ^2H_2O in the media (Finnigan GasBench-II, ThermoFisher Scientific, UK) into [^{2}H]palmitate. [^{2}H]palmitate enrichments were measured by GC-MS using a 6890N GC System coupled to a 5973N MSD (Agilent Technologies; CA, USA). Ions with mass-to-charge ratios of 270 (M+0), 271 (M+1), 272 (M+2), 273 (M+3) and 274 (M+4) were assessed by selected ion monitoring. DNL was calculated based on the maximum number of deuterium molecules that can be incorporated into a newly synthesised palmitate (17 in vitro, 22 in vivo) (Lee et al., 1994a; Lee et al., 1994b) and the amount of deuterium enrichment (Semple et al., 2009).

2.13 Bile acids quantification

2.13.1 Total bile acid assay

Total BA content was measured using a fluorometric assay according to the manufacturer's protocol (Cell Biolabs Inc., San Diego, USA). Serum-free, phenol-red free cell media samples were collected after 24h of treatment. Standard curve was prepared and 50µl of each standard or sample was added in pairs into a 96- well microtiter black plate. Followed by adding 50µl of Assay reagent to one and NAD+ Reagent to the other well of the pairs. Afterwards 100µl of 1x Assay buffer was added to each well. The plate was incubated for 45-60min at room temperature, protected from light and read at an excitation wavelength of 560 nm and an emission wavelength of 590 nm with an FLUOstar® Omega multi-mode microplate reader (BMG LABTECH Ltd., Aylesbury Bucks, United Kingdom).

2.13.2 Liquid chromatography–mass spectrometry of bile acids

A mixture of standard substances containing the targeted BAs was dissolved in an internal standard (IS) solution of ursodeoxycholic acid-D4, with a concentration of 10 nmol/ml for each BA. This solution was further diluted step by step at a same dilution ratio of 1 to 4 (v/v) with the same solution to have 10-point calibration solutions. 10 µL of each solution was injected to run UPLC-(-)ESI-MS/MS with the

scheduled multiple-reaction monitoring. Linear-regression calibration curves were constructed with the analyte-to-internal standard peak area ratios (As/Ai) versus molar concentrations (nmol/ml). 50 µL of each medium sample was mixed with 100 µL of the ursodeoxycholic acid-D4 internal standard solution. After vortex-mixing, 250 µL of acetonitrile was added. The samples were vortexed for 1 min and then sonicated for 2 min in an ice-water bath, followed by centrifugation at 21,000 g and 10 °C for 10 min. The clear supernatant was collected and dried under a nitrogen gas flow at 30 °C. The residue was dissolved in 100 µL of 50% acetonitrile. 10-µL aliquots of the resultant solutions were injected into an Agilent 1290 Ultra High Performance Liquid Chromatography (UHPL) system coupled to a 6495B Agilent QQQ mass spectrometer (MS) (Agilent Technologies; CA, USA). The MS instrument was operated in the multiple-reaction monitoring mode with negative-ion (-) detection. A Waters BEH C18 column (2.1*150 mm, 1.7 µm) was used and the mobile phase was (A) 0.01% formic acid in water and (B) 0.01% formic acid in acetonitrile for binary-solvent gradient elution. Concentrations of detected BA were calculated by interpolating the internal standard- calibration, linear-regression calibration curves of individual BA prepared in 2.2, with the analyte-to-internal standard peak area ratios measured form injections of the sample solutions.

2.14 Statistical analysis

All data was analysed using the D'Agostino-Pearson normality test or Shapiro-Wilk-Test (if "n" too small for D'Agostino-Pearson) to check for normal distribution and outliers were identified and excluded from analysis using the ROUT method (Q = 1%). Human data is shown as mean ± standard deviation. Cellular expression data is shown as mean ± standard error. Normally distributed data was analysed using the Unpaired T test or One-way ANOVA with the Tukey test for multiple comparison. Non-parametric data was analysed using the Kruskal Wallis test with the Dunn's Test for multiple comparison. RNA sequencing analysis was performed using DESeq2 (applies Wald Test) for differential gene expression analysis. Results were considered statistically significant at P value ≤ 0.05 or adjusted P value (padj) ≤ 0.05 if not

otherwise specified. Significant P values or padj was specified using asterisk (* $\leq$ 0.05, ** $<$ 0.01, *** $<$ 0.001, **** $<$ 0.0001; unless otherwise specified). For analysis indicating significance all analysis was performed on raw data (even if graphs display fold change). Statistical analysis was performed in GraphPad Prism8 (Graphpad Software Inc., La Jolla, USA). RNA sequencing was analysed using R (R Core Team, 2020), RStudio (Rstudio Team, 2020). Kaplan Meier plots were created using KM plotter (kmplot.com) [238] and GEPIA (http://gepia.cancer-pku.cn/) [239].

2.15 Outsourced methods

All experimental work has been performed by myself unless declared otherwise in the following paragraphs. I extracted and quality checked RNA samples from cell culture. Afterwards, I sent samples of the AKR1C1 project for RNA sequencing to the Wellcome Centre for Human Genetics in Oxford (Nuffield Department of Medicine, Roosevelt Drive, Oxford OX3 7BN, UK). I performed all data processing from FASTQ and BAM format onwards including genome alignment and feature counter. Samples of the POR project were sent to Novogene (25 Science Park, Milton, Cambridge CB4 0FW, UK) and a full report including DESeq2, KEGG and DisGeNET were sent back. Pathview and Cnetplots were generated by me. The individual bile acids determined by UHPL was performed by an external service provider after extraction of media samples from my cell culture experiments. Media samples were sent to Creative Proteomics (Shirley, NY 11967, US) and data was processed by me upon receival. The clinical samples (RNA and urine steroid metabolites) were collected during prior clinical studies by Dr. Ahmad Moolla which included healthy individuals, patients with HCC and patients with NAFLD across all stages of disease. Datasets were processed and ratios were formed on my own to generate insights into AKR1C1 and POR activity. Mice husbandry and sample collection of RNA and protein were performed by other members within the group (Dr. Anastasia Arvaniti) and used for PCR and western blots done by myself.

3

Characterisation of AKR1C1 in humans

Contents

3.1 Introduction 62
3.1.1 AKR1C1 in cancer 62
3.1.2 AKR1C1 in NAFLD 63
3.1.3 AKR1C1 urinary steroid ratios 63
3.1.4 Hypothesis and aims 65
3.2 Methods 66
3.2.1 Data mining 66
3.2.2 Liver biopsies 66
3.2.3 Urine samples 67
3.3 *AKR1C1* expression in HCC 69
3.4 *AKR1C1* expression in NAFLD 71
3.5 Functional AKR1C1 activity in humans 74
3.6 Discussion 77

3.1 Introduction

3.1.1 AKR1C1 in cancer

AKR1C1 has been found to be differentially expressed and/or associated with aggressive growth and chemo resistance in a range of cancers, including breast, prostate, bladder, lung and head and neck tumours [170–174]. Even though AKR1C1 is most highly expressed in the liver (see Chapter 1.6.3), research looking into its role in HCC is lacking. Data are now emerging to suggest that it might have a role in the pathogenesis and natural history of HCC [136, 240–242].

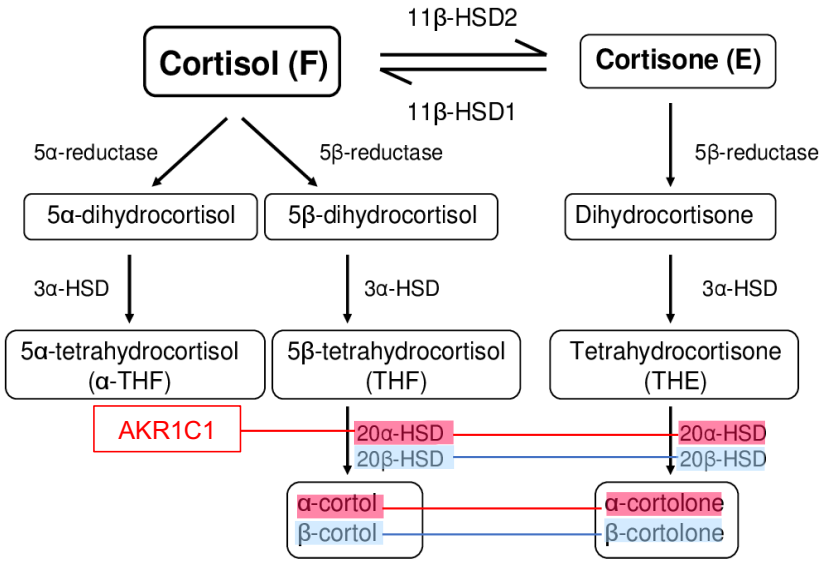


Figure 3.1: Urinary glucocorticoid metabolites can be used to calculate substrate to product ratios as a proxy for enzyme activity. AKR1C1 activity, 20α-HSD, can be estimated via α-cortol/5β-tetrahydrocortisol and α-cortolone/tetrahydrocortisone. 20β-HSD activity is estimated via β-cortol/5β-tetrahydrocortisol and β-cortolone/tetrahydrocortisone.

3.1.2 AKR1C1 in NAFLD

Steroid hormones play a crucial role in maintaining lipid homeostasis by regulating the expression of genes involved in lipid synthesis, export, and metabolism as stated in Chapter 1.4.2. Research within our group has provided the first evidence of the involvement of AKR1 family member AKR1D1 in NAFLD. Patients suffering from NAFLD showed lower AKR1D1 expression and silencing of AKR1D1 drove steatosis and inflammation in hepatoma cell model [243]. However, the association of other AKR1 enzymes expression and activity, including AKR1C1, in the liver with NAFLD still remains unexplored. Research is needed to look at AKR1C1 expression in NAFLD and generate an understanding of a potential involvement of AKR1C1 in the pathogenesis and/or progression of NAFLD.

3.1.3 AKR1C1 urinary steroid ratios

Urinary steroid metabolites can be used as a reflection of specific enzyme activity, in particular the 20α-HSD reaction carried out by AKR1C1. Multiple ratios can be formed to estimate AKR1C1s functional activity *in vivo*. α-cortol

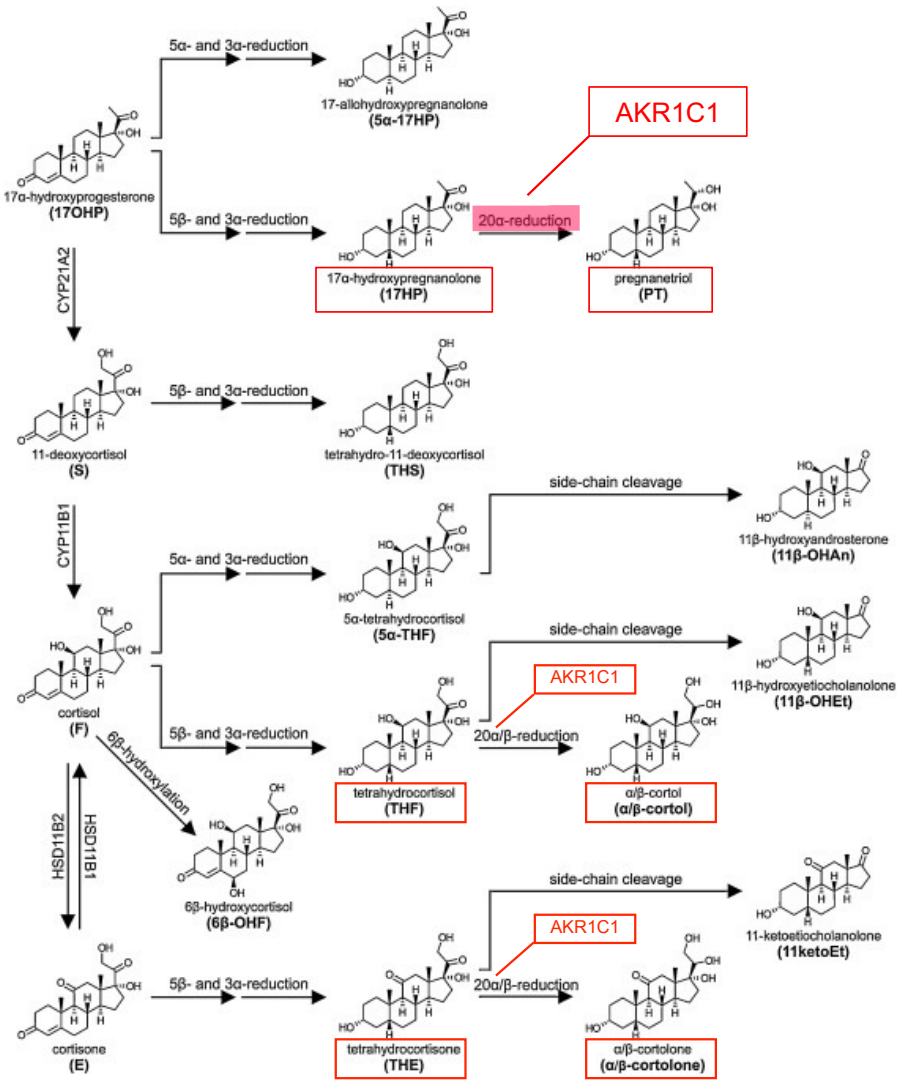


Figure 3.2: The urinary pregnanelone metabolite ratio, pregnanetriol/17α-hydroxypregnanolone, can be used to estimate AKR1C1 activity as 17α-hydroxypregnanolone is converted to pregnanetriol via 20α-HSD reduction. CAVE: 11β-OHAn and 11β-OHEt also originate form androstenedione and testosterone. Figure adapted from Schiffer et al., 2019[244].

Table 3.1: Urinary product-substrate ratios of steroid hormones

Enzyme Activity	Steroid Group	Product-Substrate Ratio
20α-HSD (AKR1C1)	Glucocorticoids	α-cortol/5β-tetrahydrocortisol
		α-cortolone/tetrahydrocortisone
	Progesterones	Pregnanetriol/
		17α-hydroxypragnanolone
20β-HSD	Glucocorticoids	β-cortol/5β-tetrahydrocortisol
		β-cortolone/tetrahydrocortisone

and α-cortolone are both inactive metabolites of cortisol and cortisone and are produced through the 20α-HSD reaction from 5β-tetrahydrocortisol and tetrahydrocortisone, respectively. Therefore, the ratios α-cortol/5β-tetrahydrocortisol and α-cortolone/tetrahydrocortisone are a reflection of AKR1C1 activity (Figure 3.1). Furthermore, the 20α-HSD reaction reducing 17α-hydroxypragnanolone to pregnanetriol can be used as another indicator in the form of a pregnanetriol/17α-hydroxypregnanolone ratio to estimate AKR1C1 activity 3.2.

3.1.4 Hypothesis and aims

Based on existing AKR1C1 research in cancers and high expression of AKR1C1 in the liver, I hypothesised that I will identify changes of AKR1C1 expression and activity in patients with HCC compared to matched controls. Further, I wanted to investigate whether there is any, as yet unexplored, association between AKR1C1 and NAFLD in humans.

I set out to undertake data mining studies using publicly available resources and use in-house gene expression and mass spectrometry data to analyse AKR1C1 expression in liver biopsies and AKR1C1 activity via urinary steroid metabolites. The data was collected during prior clinical studies by Dr. Ahmad Moolla which included healthy individuals, patients with HCC and patients with NAFLD across all stages of disease.

3.2 Methods

3.2.1 Data mining

RNA expression data from HCC individuals compared to control and within HCC stages I-IV was performed using the Gene Expression Profiling Interactive Analysis (GEPIA), an interactive web server offering the possibility to analyse RNA sequencing expression data from 9,736 tumors and 8,587 normal samples of TCGA and GTEx projects, using a standard processing pipeline. GEPIA provides customisable functions such as tumor/normal differential expression analysis, profiling according to cancer types or pathological stages and patient survival analysis. This tool was developed by Zefang Tang, Chenwei Li and Boxi Kang of Zhang Lab, Peking University [239] and is available at http://gepia.cancer-pku.cn/. Analysis of AKR1C1's transcriptional prognostic significance in HCC patients and HCC patients with late stage treatment was performed using the Kaplan-Meier Plotter (KM plotter) at http://kmplot.com/ [245]. The KM plotter is based on sources such as GEO, EGA, and TCGA and is capable of assessing the correlation between the expression of all genes (mRNA, miRNA, protein) and survival in >30k samples from 21 tumor types including breast, ovarian, lung, gastric cancer and liver cancer. Primary purpose of the tool is a meta-analysis-based discovery and validation of survival markers for cancer research. RNA seq based liver cancer database was used to explore AKR1C1 [238].

3.2.2 Liver biopsies

RNA was collected through liver biopsies from obese individuals subject to their full informed consent. Male (n = 7) and female (n = 27), undergoing primary bariatric surgery (laparoscopic sleeve gastrectomy or Roux-en-Y gastric bypass) were eligible to be recruited into a dedicated bariatric surgery biobank study (Ref: 16/YH/0247) run by our group. Detailed clinical data (including weight, height, medical history, medications, family history and alcohol intake) was recorded for all participants prior to surgery. As control, liver biopsies of lean individuals (n = 8) with phenotypically

healthy livers according to a consultant liver histopathologist were used, with limited knowledge of their medical history. Intraoperatively, a wedge biopsy was taken from the anatomical left lobe of the liver after pneumoperitoneum was established. Half of the tissue was stored in formalin prior to histological analysis by a consultant liver histopathologist according to Kleiner's NAFLD Activity Score (NAS) and fibrosis staging classification [246]; F0 represents the absence of fibrosis, F1 portal or peri-sinusoidal fibrosis, F2 portal/peri-portal and peri-sinusoidal fibrosis, F3 septal or bridging fibrosis and F4 cirrhosis. The remainder of the tissue was washed in 0.9% NaCl then stored in RNAlater stabilization solution at -80 °C until RNA extraction.

3.2.3 Urine samples

A total of 275 subjects; 169 patients with established liver disease (NAFLD n = 121; alcohol n = 48) and 106 controls without known liver disease were recruited with full written informed consent and national research ethical committee approval (refs. 09/H0403/1, 12/WM/0288, 07/H1211/168, 09/H604/20, and 10/H0402/23). Control status was determined by the review of medical history and the absence of risk factors for any known liver disease. Subjects with abnormal liver chemistry or with elevated tests for liver disease severity were excluded from the analysis as control. From each subject clinical data (including weight, height, medical history, medications, family history and alcohol intake) and spot urine samples were collected from a single void of urine and stored at -80 °C. Urinary steroid metabolites measurements were undertaken using GC-MS.

1 ml of urine was used to extract free and conjugated steroids via a 5-step solid-phase extraction method as described previously [247]. Solid-phase extraction of free and conjugated steroids was performed, followed by enzymatic hydrolysis of steroid conjugates, solid-phase re-extraction of steroids, chemical derivatisation to form ethers and finally liquid-liquid extraction. GC/MS was carried out on an Agilent 5973 MSD single-quadrupole gas chromatography mass spectrometer (Agilent) instrument allowing quantification of up to 32 steroid metabolites, with representation of major steroids and their metabolites from all the adrenal-derived

steroid hormone classes (androgens, glucocorticoids and mineralocorticoids). SIM (single ion monitoring) mode was used to identify and quantify steroids relative to authentic reference standards. All precursors and end products of the major steroid hormone classes (androgens, glucocorticoids and mineralocorticoids) were included in the multi-steroid profiling. Urine samples were corrected by creatinine trying to adjust for differing times and durations of collection. The measurement of individual concentrations of steroid hormones and their metabolites allowed the assessment analysis specific enzymatic activity through product-substrate metabolite ratios.

3.3 *AKR1C1* expression in HCC

Data mining studies within our group and recently by other groups [248] have uncovered that cancer tissue from patients with HCC has higher expression of *AKR1C1* compared to healthy individuals (Figure 3.3A) but when looking at liver cancer stages I to IV there was no difference in *AKR1C1* expression between early and progressed stages of cancer (Figure 3.3B). Interestingly, high *AKR1C1* expression within the HCC patient population appears to be associated with lower overall survival as shown in Figure 3.3C and 3.3D. The treatment of HCC is currently still very limited, especially at a progressed stage. One of the only options is the chemotherapeutic agent sorafenib, a multi kinase inhibitor and first line treatment in advanced HCC. The pattern of higher *AKR1C1* expression going hand in hand with lower survival in HCC patients was also reflected in late stage HCC patients treated with sorafenib. This raises the question as to whether AKR1C1 may govern aspects of chemo resistance in patients with HCC (Figure 3.3E).

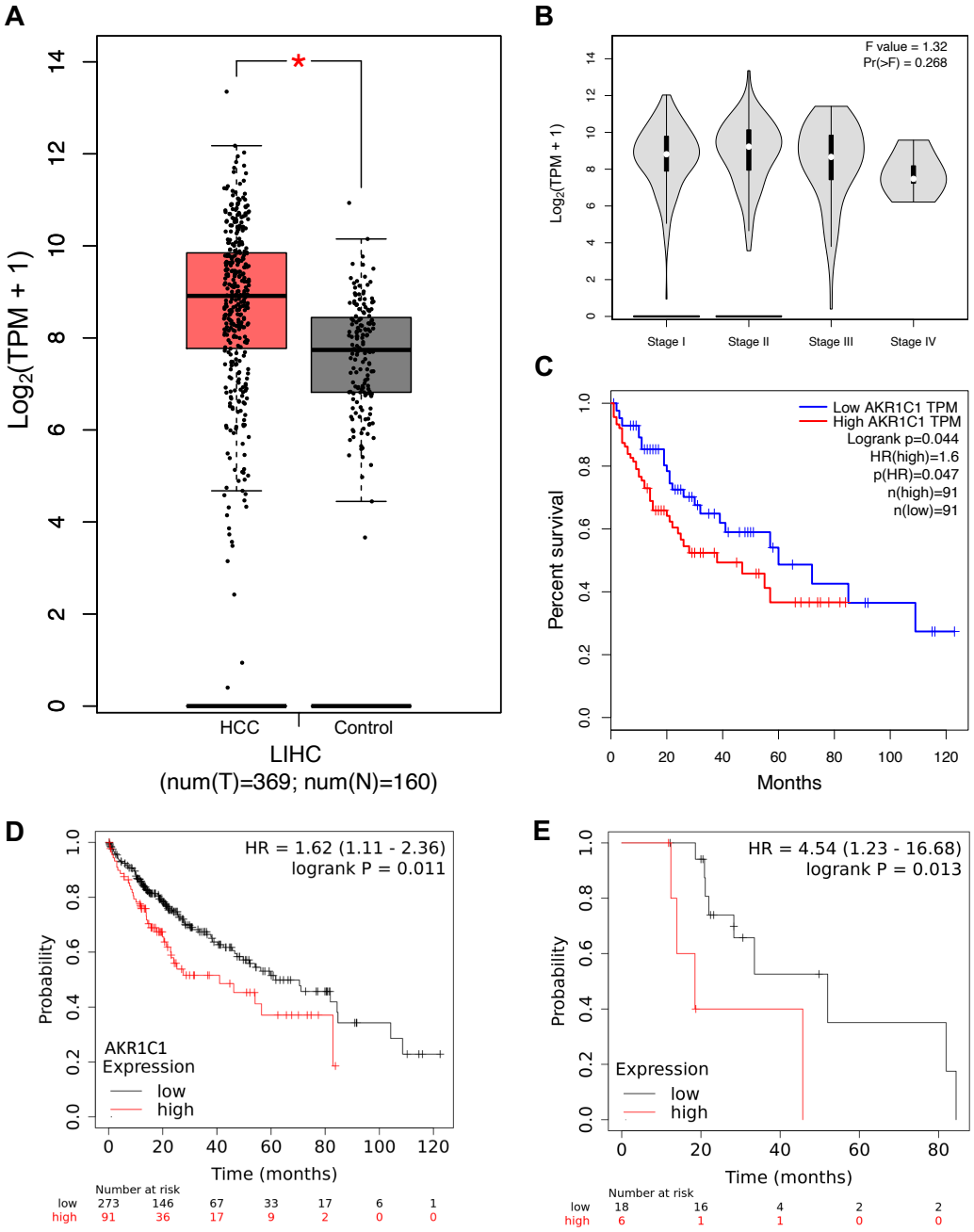


Figure 3.3: Expression of AKR1C1 is higher in biopsies of HCC compared to the liver of healthy individuals A) but there is no difference in between stages I to IV B). We applied an ANOVA to calculate differential gene expression and used the Benjamini-Hochberg false discovery rate (FDR) method to adjust the p-value to the multiple testing adjusted q-value (considered significant < 0.01; * < 0.01) displaying it as a boxplot. In two different datasets, higher expression of AKR1C1 (we selected top 25% *vs.* lower 75% due to large overlap with healthy individuals) seems to be associated with lower over survival in the general HCC population (C-D) and a sub-population treated with late stage chemotherapeutic sorafenib E). For survival analysis the Log Rank test was performed and considered significant for $p < 0.05$ Source: (A-C) Tang, Z. et al. (2017) GEPIA: a web server for cancer and normal gene expression profiling and interactive analyses. Nucleic Acids Res, 10.1093/nar/gkx247.; (D-E) RNAseq and survival data on KM Plotter (https://kmplot.com/analysis/)

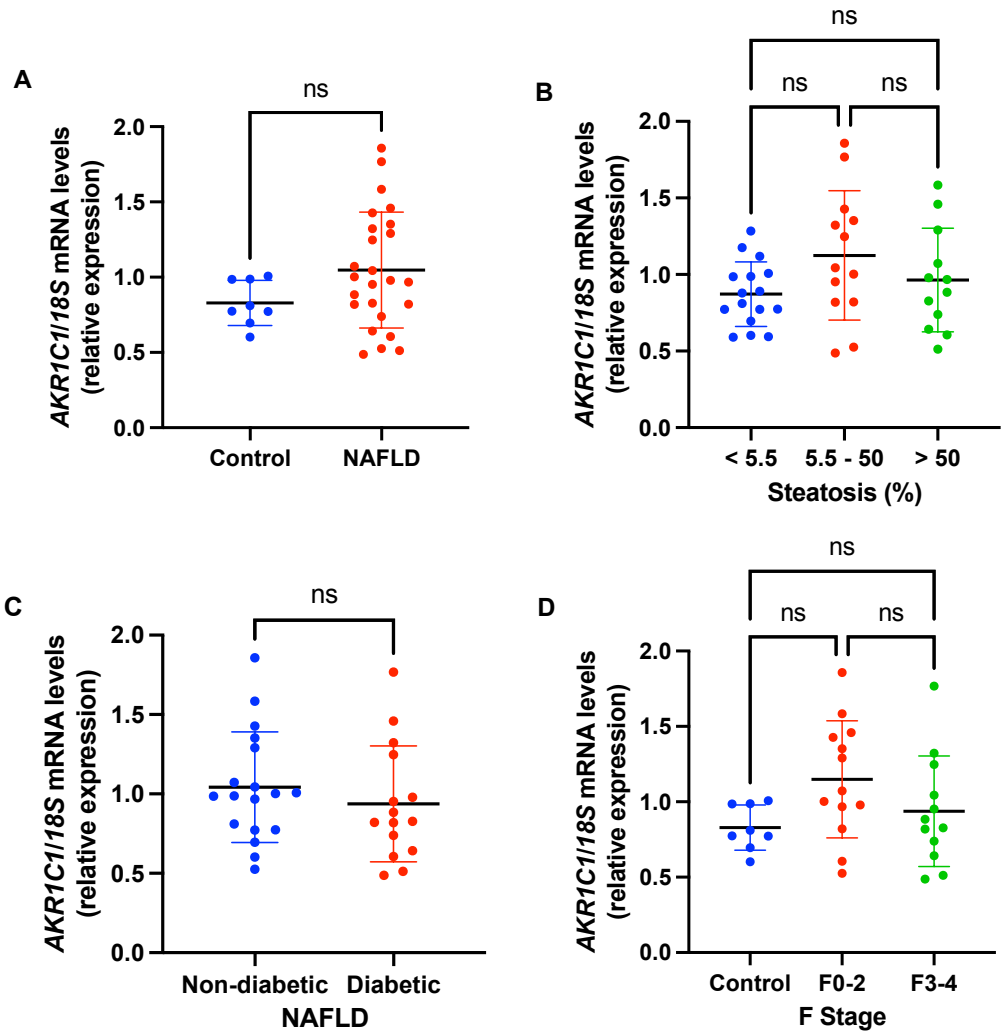


Figure 3.4: Expression of *AKR1C1* mRNA in liver biopsies is A) similar in healthy, lean individuals and patients with NAFLD (Unpaired T Test). When looking at the impact of B) the degree of steatosis (One-way ANOVA, Tukey test for multiple comparison), C) diabetes status (Unpaired T Test) and D) individuals grouped depending on their F stage (One-way ANOVA, Tukey test for multiple comparison), we show that *AKR1C1* mRNA expression does not significantly change in any of the groups, showing that expression does not change depending on severity of NAFLD.

3.4 *AKR1C1* expression in NAFLD

Healthy, lean individuals and patients with NAFLD had similar levels of hepatic *AKR1C1* mRNA expression (Figure 3.4A). When further examining the patient data, there was no notable variation in hepatic *AKR1C1* mRNA expression based

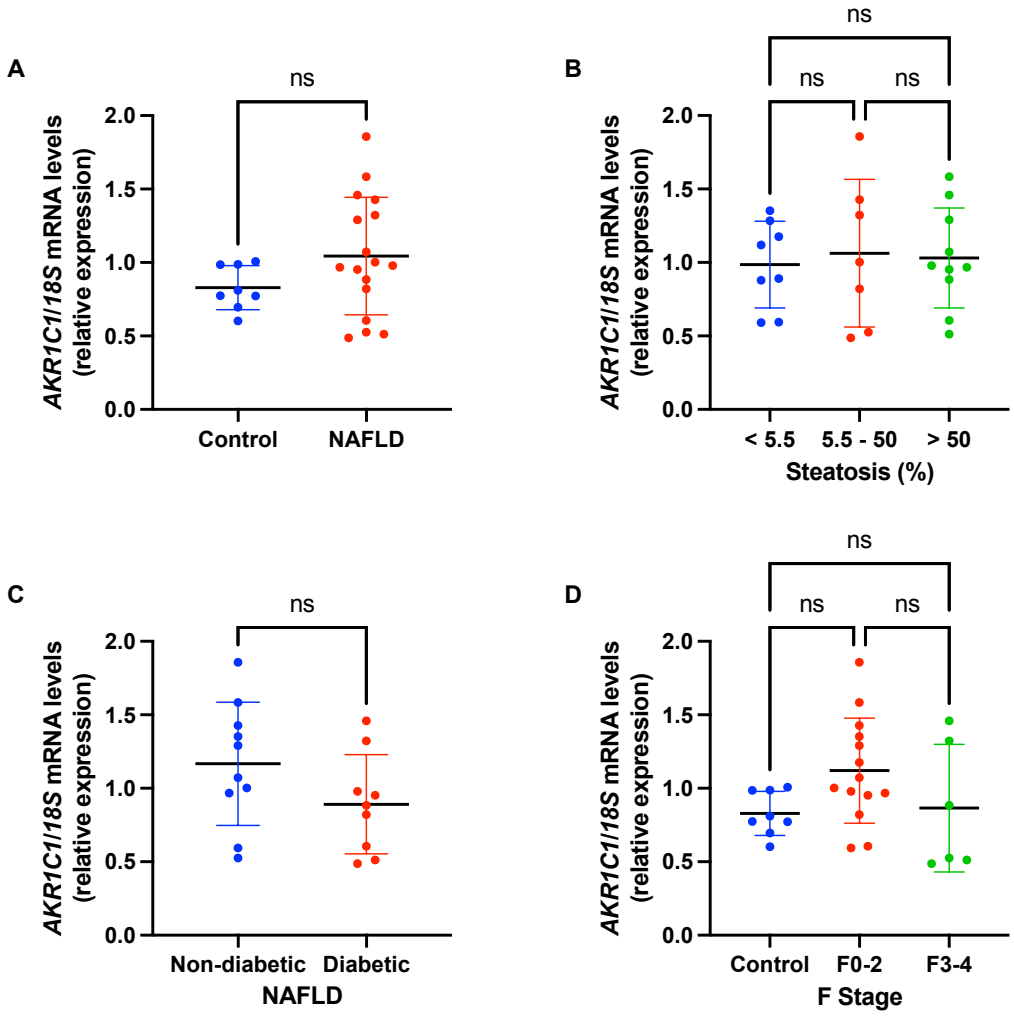


Figure 3.5: Liver expression of *AKR1C1* mRNA in female is A) similar in healthy, lean individuals and patients with NAFLD (Unpaired T Test). When looking at the impact of B) the degree of steatosis (One-way ANOVA), C) diabetes status (Unpaired T Test) and D) individuals grouped depending on their F stage (One-way ANOVA), we show that *AKR1C1* mRNA expression does not significantly change in any of the groups. Indicating no sex dependent effect of *AKR1C1* on NAFLD and progression of disease.

on the extent of liver steatosis (Figure 3.4B). Additionally, diabetic status (Figure 3.4C) and liver inflammation or fibrosis according to F stage (Figure 3.4D) showed no impact on mRNA expression level in the liver. All these results indicate that the level of *AKR1C1* mRNA expression has no impact on the extent of disease and thereby progression within NAFLD stages.

Analysis was repeated dividing subjects by sex to see if there are any sex-

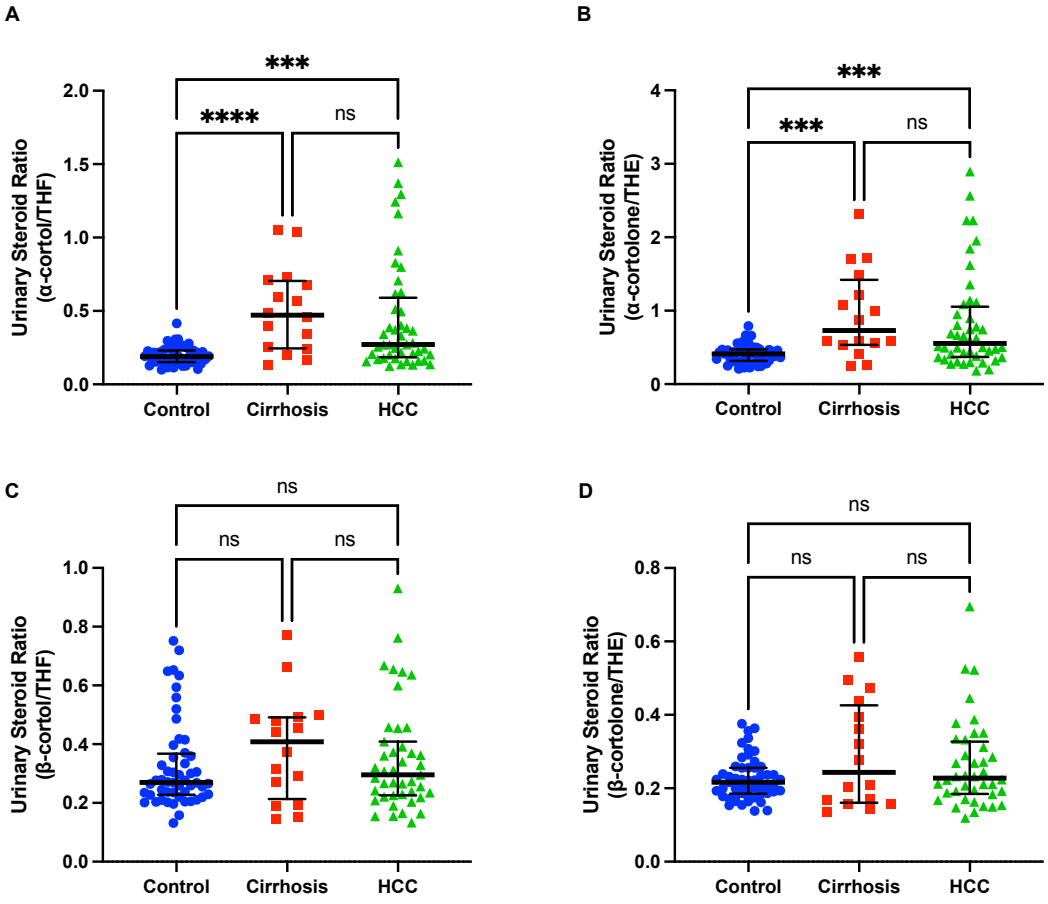


Figure 3.6: The urinary steroid metabolites in patients with cirrhosis and HCC have increased AKR1C1 activity (20α-HSD) as measured by ratio of A) α-cortol/5β-tetrahydrocortisol and B) α-cortolone/Tetrahydrocortisone. 20β-HSD activity is similar between controls, and patients with cirrhosis and HCC as shown by C) β-cortol/5β-tetrahydrocortisol and D) β-cortolone/tetrahydrocortisone ratios. Statistics were calculated using an One-way ANOVA and Tukey test for multiple comparison.

specific differences due to AKR1C1's role in steroid hormones. Consistent with the previous data, we did not show any difference in *AKR1C1* mRNA expression between female healthy, lean individuals and female patients with NAFLD (Figure 3.5A). Furthermore, the female only cohort also showed no difference in *AKR1C1* mRNA expression depending on extent of steatosis, diabetic status or severity of NAFLD (Figure 3.5B, C and D).

3.5 Functional AKR1C1 activity in humans

Whilst we were unable to demonstrate changes in *AKR1C1* mRNA expression across the spectrum of NAFLD severity, we have identified functional changes in AKR1C1 activity as reflected by changes in urinary steroid metabolites in NAFLD, cirrhosis and HCC patients. We observed an increased ratio of α-cortol/5β-tetrahydrocortisol and α-cortolone/tetrahydrocortisone, inactive metabolites of cortisol and cortisone, in patients with both cirrhosis and HCC compared to healthy individuals. These findings are indicative of an increased 20α-HSD conversion of 5β-tetrahydrocortisol and tetrahydrocortisone to their metabolites α-cortol and α-cortolone respectively (Figure 3.6A and 3.6B) by AKR1C1. No change has been observed in patients with cirrhosis and HCC in β-cortol/5β-tetrahydrocortisol (Figure 3.6C) and β-cortolone/tetrahydrocortisone (Figure 3.6D) ratios reflecting a selective higher 20α-HSD activity with no change in 20β-HSD activity. This selective increase of 20α-HSD is further illustrated by the ratio formed of the sum of α-cortol and α-cortolone divided by the sum of β-cortol and β-cortolone in Figure 3.8A.

When comparing healthy individuals to patients with NAFLD, we observed increased 20α-HSD activity (α-cortol/5β-tetrahydrocortisol (Figure 3.7A) and α-cortolone/tetrahydrocortisone (Figure 3.7B) ratios) only in patients with advanced NAFLD disease stages (F3 and F4). Whilst the magnitude of the effect was greatest for the AKR1C1 mediated 20α-HSD reaction, we also observed changes in the 20β-HSD reaction as measured with an increased β-cortol/5β-tetrahydrocortisol ratio in patients with advance disease stages (Figure 3.7C) and a lower β-cortolone/tetrahydrocortisone ratio in early disease stages (Figure 3.7D) ratios. This was suggestive of a more general increase or disturbance of 20-HSD activity and is reflected in Figure 3.8B. No clear trend is visible between α-cortol/-cortolone and β-cortol/-cortolone ratios that could be indicative of relative change in 20α-HSD *vs.* 20β-HSD in NAFLD patients.

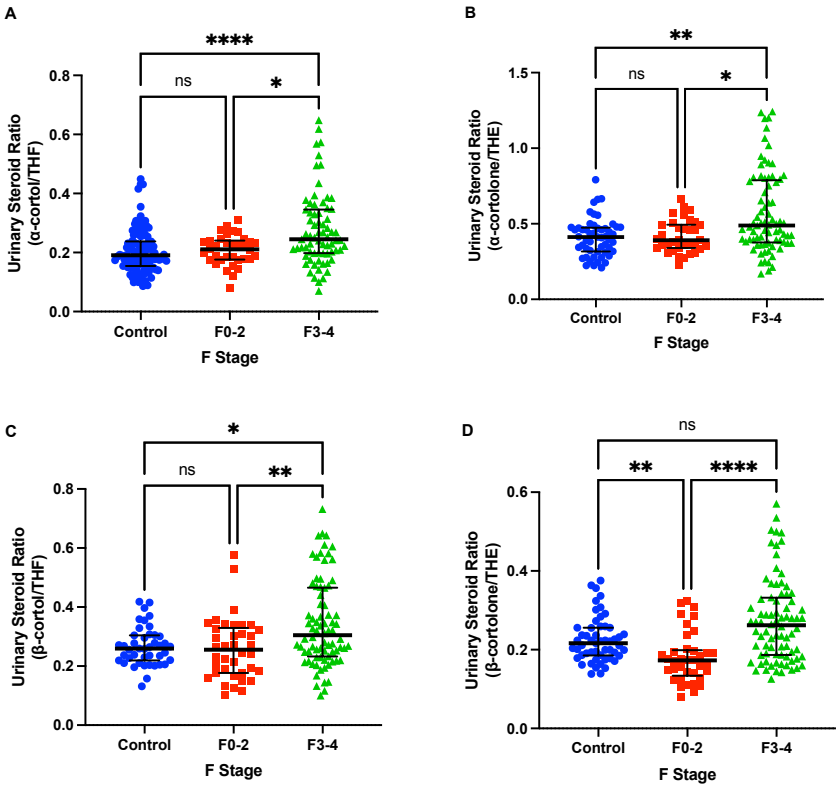


Figure 3.7: The urinary steroid metabolites in NAFLD show elevated AKR1C1 activity in the advanced stages of disease. Increased AKR1C1 activity (20α-HSD) is shown through ratios of A) α-cortol/5β-tetrahydrocortisol and B) α-cortolone/Tetrahydrocortisone. Increased 20β-HSD activity is demonstrated with C) β-cortol/5β-tetrahydrocortisol and D) β-cortolone/tetrahydrocortisone ratios (data from Tomlinson group, unpublished). Statistics were calculated using an One-way ANOVA and Tukey test for multiple comparison.

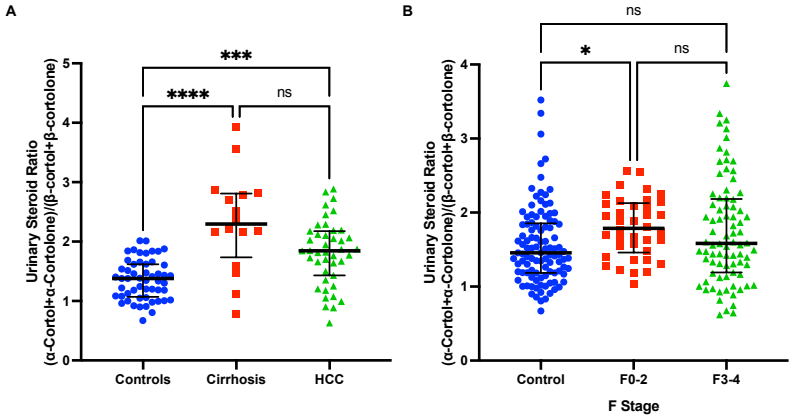


Figure 3.8: Specific increase of AKR1C1's 20α-HSD activity in A) cirrhosis and HCC as shown through an increase in the ratio formed of the sum of α-cortol and α-cortolone divided by the sum of β-cortol and β-cortolone. In NAFLD, there is a small significant differences which is explained general increase of both 20α-HSD and 20β-HSD in NAFLD B) with no significant changes in α/β-cortol and cortolone ratio. Statistics were calculated using an One-way ANOVA and Tukey test for multiple comparison.

3.6 Discussion

In this chapter we have presented evidence from gene expression analysis alongside functional activity from urine steroid metabolites to show that expression and activity of AKR1C1 are higher in patients with HCC compared to healthy individuals. However, this increased expression does not appear to be associated with early or progressed stages of cancer, and is instead associated with a lower overall survival in patients with HCC suggesting that it could have a prognostic function. Our findings also indicate that healthy individuals and patients with NAFLD have similar levels of *AKR1C1* mRNA expression across the disease spectrum, but that AKR1C1 activity seemed to increase specifically in the most advanced NAFLD stages, including cirrhosis. The selective changes in 20α-HSD as seen in cirrhosis and HCC, may indicate that AKR1C1 plays a specific role in the development and progression of disease. In this case, the increased activity of AKR1C1 may be utilised as a marker of the disease and or the activity may contribute to specific pathological changes associated with cirrhosis or HCC. In contrast, the changes in multiple enzymes, such as 20α-HSD and 20β-HSD as observed in NAFLD patients, might indicate a more general response to injury or stress in the liver. It could be the result of a disturbance or a compensatory mechanism where the body is trying to increase the activity of multiple enzymes in order to maintain normal physiological function. This might explain why shifts are mainly observed in later stages of NAFLD, where liver injury is more severe and sustained. It is also possible that the increase in 20α-HSD and 20β-HSD activity in NAFLD is not specific to these enzymes but rather a result of a general increase in the activity of enzymes involved in steroid metabolism in response to the inflammation and injury at stages F3-4. The statistical significance of our findings on both mRNA and urinary derived AKR1C1 activity underscore AKR1C1 deregulation during cirrhosis and HCC. However, the substantial overlap of data points in both the expression (Figure 3.3) and the activity data (Figure 3.6), even though significant, raises concerns about the generalisability of the results and make it unlikely that AKR1C1 on its own can serve a prognostic function. The statistical results are likely driven by a

small subset of individuals which suggests a need for caution in interpreting these findings. In general, there is difficulty in identifying specific mechanism of disease and diagnostic targets for HCC due to the heterogeneity of the disease and limited concordance between studies. The genetic heterogeneity of HCC might be explained by the variety of underlying liver diseases. Therefore, we speculate that the key to understanding the differences in *AKR1C1* expression might also lie in understanding the underlying disease aetiology of HCC. Looking at the ratio formed of the sum of α-cortol and α-cortolone divided by the sum of β-cortol and β-cortolone in patients with alcoholic cirrhosis we see a significant up-regulation indicating specifically higher 20α-HSD (AKR1C1) activity (data not shown). Considering that our HCC cohort had, in large, a background in alcoholic cirrhosis this could explain observed differences compared to NAFLD stage F3-4. This hypothesis is further supported by data looking at differentially expressed genes from control, hepatitis B, hepatitis C and haemochromatosis. There is an *AKR1C1* mRNA up-regulation specific to the HCC's disease aetiology in heamochromatosis [136]. While our data underlines the importance of researching the impact of AKR1C1 on HCC, it does not necessarily imply causation. Without additional data from animal models or cell studies, it is difficult to determine whether AKR1C1 plays a causal role in the development and/or progression of HCC. At present, no such animal model has been established and very limited cell data is available. The AKR superfamily is highly conserved across different species but the AKR1C family shows important differences between rodents and humans making the model development extremely difficult. In rodents the AKR1C family includes AKR1C6, -1C12, -1C13, -1C14, -1C18, -1C19, -1C20 and -1C21 and there are significant phylogenetic and functional dissimilarities between murine AKR1C family members and their human counterpart [249]. In cellular experiments, multiple potential candidates for HCC treatment seem to affect *AKR1C1* expression. ZnS, a saponin from Dioscorea zingiberensis, demonstrated inhibitory effects on the malignant progression of HCC through the suppression of autophagy and inhibition of the AKR1C1-mediated JAK2/STAT3 signaling pathway. Interestingly, overexpression of AKR1C1 weakened the inhibitory effect

of ZnS [240]. Another study exploring the cellular and molecular mechanisms of gamma-linolenic acid (GLA) exposure of human HCC cell line Huh7 showed an induction of *AKR1C1* expression believed to play a cancer protective role in this context [242]. This underlines the need for a cellular model to explore AKR1C1 in a HCC cell model. Furthermore, no research has been conducted looking at the effects of AKR1C1 on sorafenib. Sorafenib, a multi kinase inhibitor, targets several different signaling pathways that are dysregulated in cancer cells, including the RAF/MEK/ERK pathway and the VEGF receptor pathway. While the exact mechanism of sorafenib is not fully understood, it is thought to induce cell cycle arrest and apoptosis in cancer cells, as well as inhibit angiogenesis and tumor growth [250–252]. It is possible that AKR1C1 could metabolize sorafenib or one of its metabolites, potentially altering its pharmacokinetics and/or pharmacodynamics leading to lower survival in patients treated with sorafenib as observed in our data mining studies. Overall, our results highlight the complex role of AKR1C1 in liver disease and suggest that changes in *AKR1C1* expression and activity may be important in the development and progression of HCC and NAFLD. The increase of *AKR1C1* expression as seen in HCC and cirrhosis, the impact on overall survival of HCC patients, as well as the observed changes of AKR1C1 activity during liver injury underline the need for further exploration of AKR1C1 in a human hepatoma cell model. Based on our results we want to specifically look into the impact of AKR1C1 activity through genetic and pharmacological manipulation of activity and expression on HCC pathogenesis and progression in Huh7 and HepG2 cell lines.

4

AKR1C1 in hepatocellular model

Contents

4.1 Introduction 81
4.1.1 AKR1C1 in liver cancer 81
4.1.2 Hypothesis and aim 82
4.2 Methods 83
4.2.1 Cell culture 83
4.2.2 Pharmacological AKR1C1 inhibition 83
4.2.3 Pregnanediol-3-Glucuronide Competitive ELISA 83
4.2.4 Transient knockdown 85
4.2.5 CRISPR/Cas9 86
4.2.6 Overexpression 86
4.2.7 MTS cell proliferation and viability assays 86
4.2.8 Chemotoxicity assays 87
4.2.9 Wound healing assay 87
4.3 AKR1C1 expression in hepatoma cell lines 88
4.4 Pharmacological inhibition 88
4.5 Transient knockdown 89
4.5.1 siRNA variants 89
4.5.2 Dose optimisation 89
4.6 Stable knockdown 90
4.7 Overexpression 92
4.8 RNA sequencing 94
4.9 Proliferation and chemo resistance 98
4.10 Motility 102
4.11 Discussion 104

4.1 Introduction

4.1.1 AKR1C1 in liver cancer

Our data presented in chapter 3 have shown increased *AKR1C1* expression and specific changes in activity that were observed in patients with HCC, as well as associations between lower survival and higher *AKR1C1* expression. Furthermore, a study, specifically classifying HCC by underlying liver diseases aetiology, observed that HCC arising from hereditary haemochromatosis had increased *AKR1C1* expression. The liver damage caused by hereditary haemochromatosis is mainly based on an oxidative stress mechanisms leading to oxidised cellular proteins, lipids and DNA bases compared to HCV and HBV, which are mainly driven by inflammation and viral DNA integration [136]. This increase in oxidative stress in HCC could be an important driver of increased *AKR1C1* expression at a molecular level. *AKR1C1* increased during oxidative stress, exposure to ROS, and appears to be up-regulated by exposure to HNE, a product of lipid peroxidation through oxidative stress [157, 177]. NRF2 appears to regulate *AKR1C1* expression [178, 179]. Therefore, the up-regulation of *AKR1C1* expression could be explained by NRF2 overexpression in HCC, which correlated with differentiation, metastasis and tumour size [180]. Overexpression of NRF2 has been shown to increase transcriptional activity of genes containing the ARE in their promotor, one of these being AKR1C1. This has further been confirmed in HepG2 cells where the ARE has been identified in the proximal promotor of *AKR1C1* [181]. up-regulation of *AKR1C1* as an antioxidative response gene is further supported by its potential to reduce HNE [157]. Interestingly, it is possible that HCC may develop a mechanism to evade apoptosis or ferroptosis via a decrease in oxidised cardiolipin and its oxidation product HNE which can trigger intrinsic cell death [182]. Ferroptosis, a type of programmed cell death, is characterized by the accumulation of lipid peroxides and iron-dependent ROS in cells. It is distinct from other forms of cell death, such as apoptosis and necrosis and the current evidence suggest targeting ferroptosis might be a promising strategy for cancer therapy [253]. Consistent with this idea, NRF2

activation and high expression of *AKR1C1* is associated with resistance to ferroptosis induced by HCC first line chemotherapeutic treatment sorafenib [183, 184].

4.1.2 Hypothesis and aim

To date, cellular models to explore and establish the effects of AKR1C1 on HCC have not been developed. We believe that a hepatocellular model with manipulated AKR1C1 activity and/or expression is of importance based upon the changes in *AKR1C1* expression, activity and substrate preference in HCC as described in Chapter 3.3 and 3.5. Therefore, I set out the establish a cellular model and test how AKR1C1 impacts metabolism, cellular proliferation, chemo-resistance and cell motility.

4.2 Methods

4.2.1 Cell culture

For all experiments with AKR1C1 manipulation cell lines HepG2 and Huh7 were used. Cell lines were cultured as described in Chapter 2.2.

4.2.2 Pharmacological AKR1C1 inhibition

Pharmacological AKR1C1 inhibition was measured by determining PDG, a downstream metabolite of progesterone reduction by AKR1C1 (Figure 4.1). The AKR1C1 inhibitor 3-Bromo-5-phenylsalicylic acid (5-PBSA) (Sigma-Aldrich, Gillingham, UK) was tested in doses of 1, 10 or 100 µM. Doses were chosen based on dose-response experiments in bovine aortic endothelial cells by El-Kabbani et al. (Figure 4.2) and the AKR1C1-specificity of 5-PBSA [254]. Cells were left for 48h after seeding. After removal of media, cells were treated for 24h with phenol red-free DMEM supplemented with 1% non-essential amino acids, 1% sodium pyruvate and 1% L-glutamine, which additionally contained either 200 nM progesterone (as an AKR1C1 substrate) or progesterone supplemented with 5-PBSA. Successful functional inhibition was established as lower levels or missing of PDG in the collected cell media.

4.2.3 Pregnanediol-3-Glucuronide Competitive ELISA

Enzyme-linked immunosorbent assays are commonly used to identify antibodies, antigens, proteins, peptides and hormones in a variety of biological samples. These samples are added to a specially absorbent plate which binds the target. The immobilized target can then be complexed with a detection antibody linked to an enzyme. This allows the quantification of a target via an enzymatic activity measurement. This general principle does not directly translate to all different forms of ELISAs that exist (direct, indirect, sandwich, reverse and competitive (inhibition)). The competitive ELISA e.g. measures lower enzymatic activity the higher the substrate concentrations are because substrate and detection enzyme compete to bind the same antibody binding site.

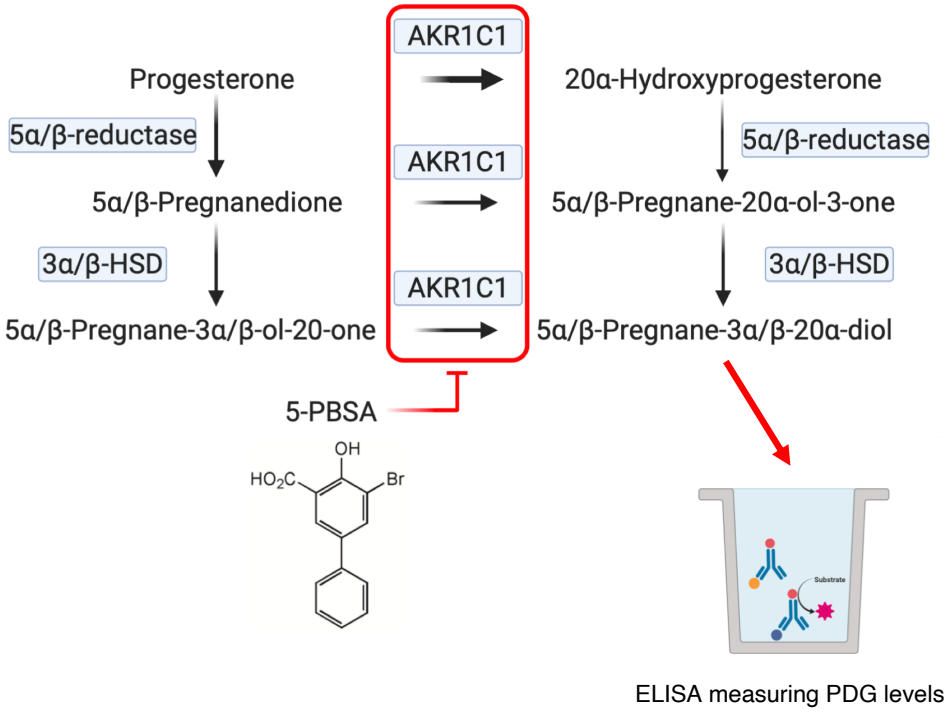


Figure 4.1: Inhibiting the formation of Pregnanedio-3-glucuronide (PDG) by interrupting progesterone metabolism via 5-PBSA induced AKR1C1 inhibition. PDG levels were measured in cell media using an ELISA. Created with BioRender.com.

To measure AKR1C1 activity we used a commercial solid-phase Pregnanediol-3-Glucuronide (PDG) Competitive ELISA kit (Invitrogen, Paisley, UK) which was cell media compatible. First, a standard curve was created by serial dilution from 50 ng/ml to 0.781 ng/ml PDG. 50 μl of standard curve, negative control or samples were added into wells. Then PDG conjugate and PDG Antibodies were added to each well and the plate left to incubate for 2 hours at room temperature with shaking. The ELISA plate was thoroughly washed with 1X wash buffer before 100 μl of the chromogen TMB substrate was added to each well which caused the substrate solution to turn blue. After 30min incubation at room temperature without shaking, 50 μl of stop solution was added to terminate the enzymatic reaction and cause the colour of the solution to change to yellow. Using the VersaMax™ Tunable Microplate Reader (Molecular Devices, Wokingham, UK) the absorbance was read at 450 nm not later than 10 min after adding the stop solution.

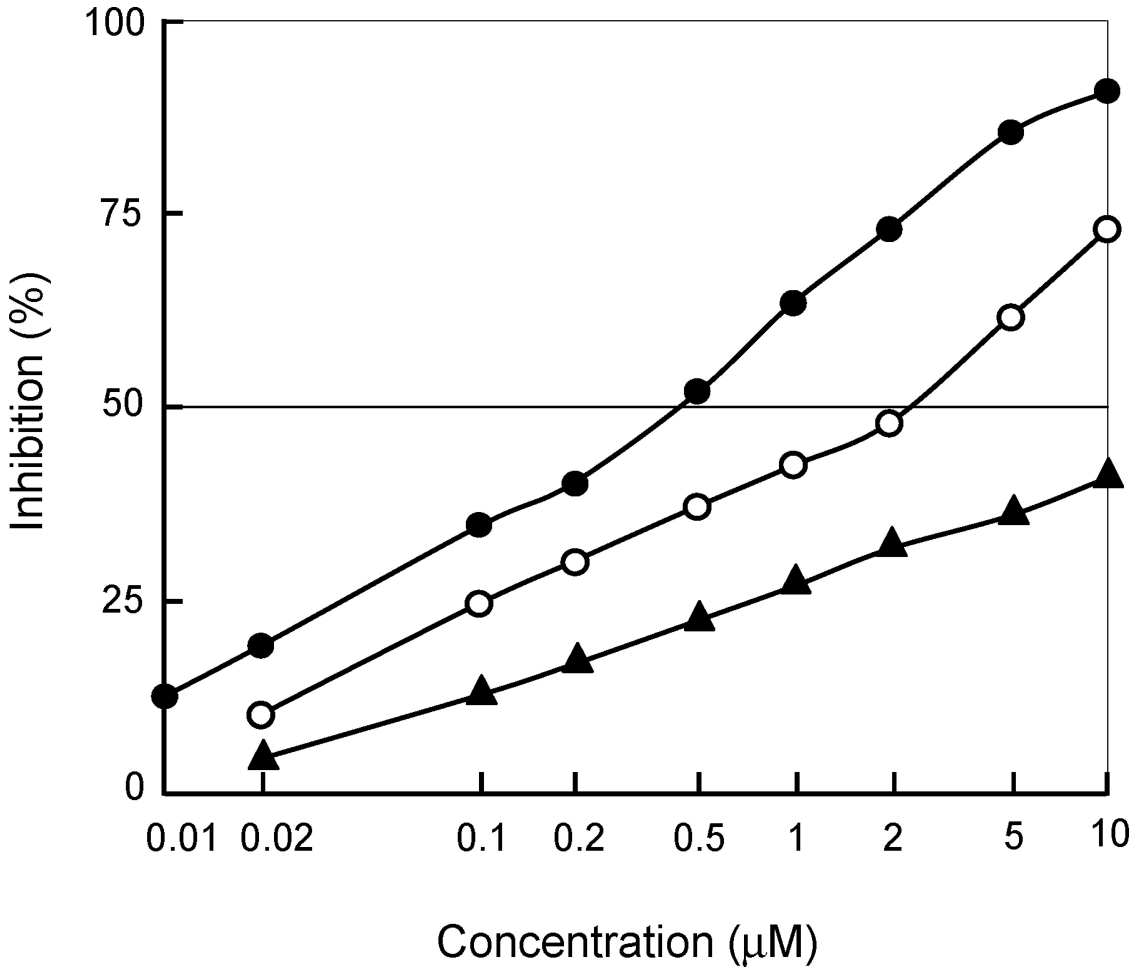


Figure 4.2: Three different compounds have been tested by El Kabbani et al. [254] in regards to their potential to inhibit AKR1C1 activity. Inhibition was measured in terms of decreased PDG generation from progesterone compared to vehicle control. 5-PBSA (▲) is the most AKR1C1-selective of the three tested compounds and doses 1, 10 and 100 µM were selected for testing in hepatoma cells based on this data. 3,5-dibromosalicylic (○) and an undisclosed compound (●) were more potent inhibitors already at lower doses but were not as specific to AKR1C1 as they cross reacted with other AKR1C family members to a higher degree. Figure taken from El Kabbani et al. [254]

4.2.4 Transient knockdown

Transient knockdown was achieved transfecting siRNA at a 40 nM and 10 nM concentration in HepG2 and Huh7, respectively. For *AKR1C1* siRNA optimisation silencer select (Invitrogen, Paisley, UK) siRNA1 (id: s56843) and siRNA2 (id: s56844) were used. For *AKR1C1* siRNA knockdown siRNA1 (id: s56843) was used. Detailed methods are described in Chapter 2.6.1.

4.2.5 CRISPR/Cas9

The principle as described in Chapter 2.6.2. Briefly, cells were seeded in a 6-well plate at 1.6 x 10^5/ml and 1.4 x 10^5/ml for HepG2 and Huh7 respectively for 24h before transfection. Media was changed to 2.5 ml DMEM supplemented with 1-10% FBS and 1% non-essential amino acids. 2.5 µg of CRISPR plasmid was gently mixed with 7.5 µl TransIT-LT1 reagent (Cambridge Bioscience, Cambridge, UK) in 250 µl Opti-MEM, left to incubate for 20min at room temperature and then added dropwise to each well. 48h after transfection, cells were selected for another 48h with complete growth media substituted with 5 µg/ml Puromycin. The selected, successfully transfected, cells were then grown out in T25 and T75 flasks. No colony selection was performed. Plasmids with three different guide RNAs targeting *AKR1C1* and a control plasmid were tested.

Table 4.1: Three different guide RNAs tested for stable knockdown of *AKR1C1*. For highest binding efficiency an extra Guanine (g) will be added as first base if not already present.

gRNA 1	gCTACCTATGGTTACTCCCCC
gRNA 2	GATCCCACCGAGAAGAACCA
gRNA 3	GCCAGCTTCAATTGCCAATT

4.2.6 Overexpression

500 ng/well of an GFP tagged AKR1C1 or empty vector DNA plasmid was introduced via lipofection into HepG2 as *AKR1C1* overexpression or control model. Methods in more detail have previously been described in Chapter 2.6.3.

4.2.7 MTS cell proliferation and viability assays

Cell proliferation and cell viability was measured in a 96-well plate format using the CellTiter 96® AQueous One Solution Cell Proliferation Assay (MTS) by Promega Corp., Madison, USA. Media was changed to phenol red free DMEM supplemented with 1% non-essential amino acids, 1% sodium pyruvate and 1% GlutaMAX. 24 hours after media change 20 µL of assay was added to each well and left to incubate

for 1-4 hours as per the manufacturers protocol. Absorbance was measured at 490 nm with the VersaMax™ Tunable Microplate Reader (Molecular Devices, CA, USA).

4.2.8 Chemotoxicity assays

Chemotoxicity was measured in a 96-well plate to the above mentioned CellTiter 96® AQueous One Solution Cell Proliferation Assay with the addition of Sorafenib (Sigma-Aldrich, Gillingham, UK), a protein kinase inhibitor and fist line chemotherapy of advanced HCC. Doses ranging from 100 nM up to 50 µM were made up in DMSO and used to test a dose response curve in cells which were *AKR1C1* siRNA transfected as to the protocol described in Chapter 2.6.1. Sorafenib was added to the cells in a phenol red free DMEM supplemented with 1% non-essential amino acids, 1% sodium pyruvate and 1% GlutaMAX and left for 24h before adding MTS. Furthermore, doses ranging from 1 μM to 50 μM were tested in pharmacologically AKR1C1 inhibited cells. The addition of Sorafenib and MTS was performed as described above.

4.2.9 Wound healing assay

Commercial 96-well plates, Oris™ Migration Assays by Platypus Technologies (AMS Biotechnology, Milton Abingdon, UK), with collagen and fibronecting coatings were used. Cells were seeded, left to grow to confluency for 24h. According to protocol, silicon inserts were removed at that point and pictures were taken with a light microscope at time points 0, 24 and 48h at a 10x magnification. ImageJ and the MRI wound healing tool was used to calculate percentage of area covered by cells.

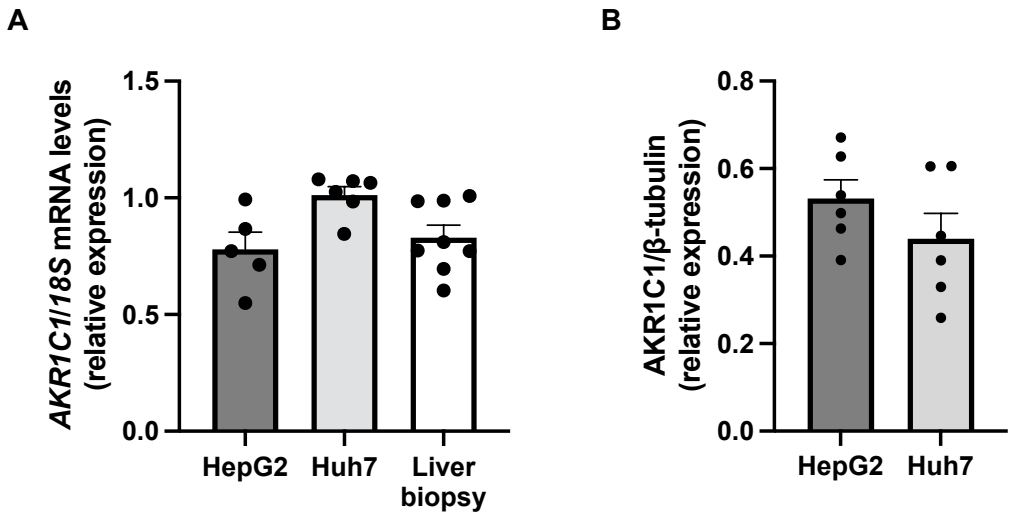


Figure 4.3: AKR1C1 has similar levels of A) mRNA expression in HepG2 cells, Huh7 cells and liver biopsies. Protein levels of AKR1C1, B), is similar in cell lines HepG2 and Huh7. These results suggest HepG2 cells and Huh7 cells are suitable cell lines for model development.

4.3 AKR1C1 expression in hepatoma cell lines

To create a cellular model mRNA and protein expression of AKR1C1 in two HCC appropriate cells lines, HepG2 and Huh7, were measured and compared to the AKR1C1 mRNA expression of liver biopsies to assure their suitability to explore AKR1C1's effect on HCC. Both cell lines express AKR1C1 mRNA and protein as measured by qPCR and western blot. AKR1C1 mRNA expression levels are on similar levels as in human liver biopsy samples and the cell lines were therefore deemed suitable and taken forward for further model development (figure4.3).

4.4 Pharmacological inhibition

Three doses of 5-PBSA were chosen to inhibit AKR1C1 activity; 1, 10 and 100 µM. Treatments with 5-PBSA (10 μM and 100 μM) significantly reduced PDG levels in HepG2 and showed a clear trend in Huh7 cells consistent with inhibition of AKR1C1 activity. Due to the low sample size and slightly lower overall PDG levels, treatment in Huh7 resulted in not being statistically significant even though no

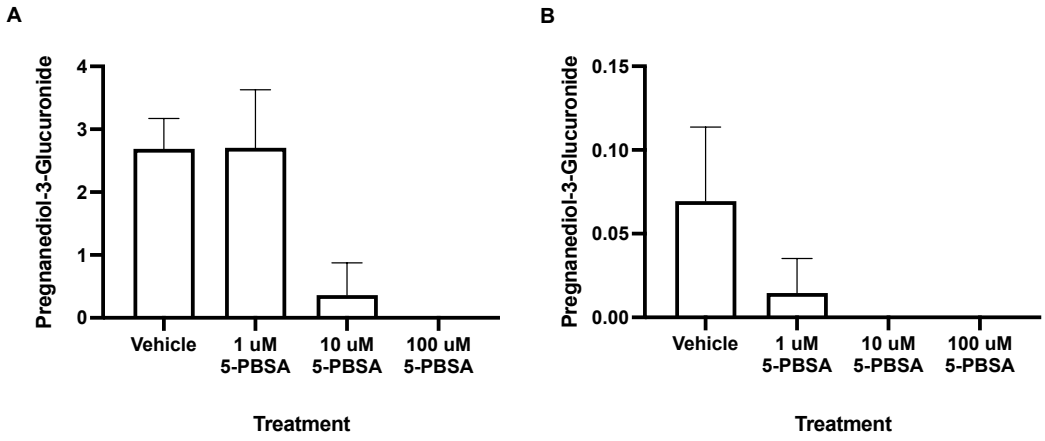


Figure 4.4: Decreased Pregnandiol-3-Glucuronide (PDG) generation after pharmacological AKR1C1 inhibition with 5-PBSA in A) HepG2 and B) Huh7 cells (n = 2; mean with SD).

measurable PDG concentration was found in the cell media. Treatment with 1 µM 5-PBSA showed no difference between intervention and control in HepG2, although a trend of inhibition of AKR1C1 activity was observed in Huh7 cells (Figure 4.4).

4.5 Transient knockdown

To explore the AKR1C1 knockdown efficiency we used two different AKR1C1-targeted siRNAs in a dose-dependent manner (10, 20 and 40 nM), in both Huh7 and HepG2 cells.

4.5.1 siRNA variants

AKR1C1 siRNA1 (id: s56843) and siRNA2 (id: s56844) both achieved a reduction of AKR1C1 mRNA and protein levels compared to scrambled control, with siRNA1 having the greatest effect in both cell lines with up to 50% knockdown. Therefore, all further studies were undertaken using siRNA1(Figure 4.5).

4.5.2 Dose optimisation

Transfection concentrations of 10, 20 and 40 nM of siRNA resulted in a divergence in knockdown efficiency in between cell lines. In Huh7 cells, mRNA and protein

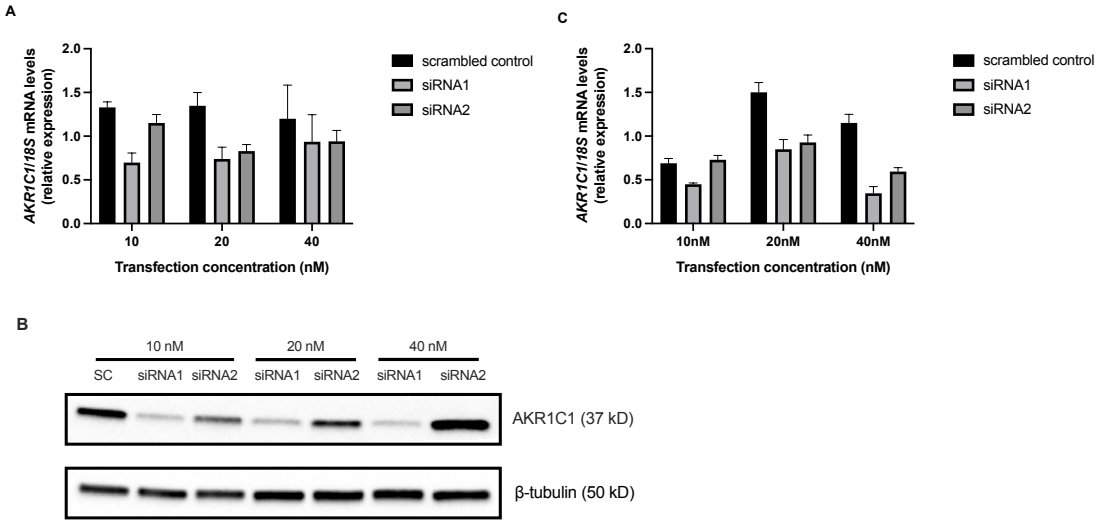


Figure 4.5: Optimisation of different doses and siRNA variants for transient *AKR1C1* KD on A) mRNA (n = 3) and B) protein level in Huh7 as well as C) mRNA (n = 3) in HepG2 cells. (SC; scrambled control, siRNA1; siRNA variant 1, siRNA2; siRNA variant 2)

expression were not significantly different across different concentrations of siRNA. In contrast, mRNA of HepG2 cells showed a clear dose respondent effect with the highest knockdown efficiency in 40 nM siRNA1-transfected cells (Figure 4.5). The dose respondent effect in HepG2 was further confirmed in HepG2 cells on mRNA and protein level (Figure 4.6). In experiments going forward concentrations of siRNA were therefore used at 10 nM and 40 nM, respectively for Huh7 and HepG2. This model achieved an average *AKR1C1* knockdown effect in mRNA and protein of 58.6% and 79.2% in Huh7 and 52.7% and 65.4% in HepG2 (Figure 4.6).

4.6 Stable knockdown

Three different AKR1C1 CRISPR/Cas9 stable knockdown cell lines and a control were generated in HepG2 and Huh7 cells. After puromycin selection, the highest efficiency for AKR1C1 knockdown was shown within gRNA2-plasmid, followed by gRNA1-plasmid-transfected cell lines as seen in western blot (Figure 4.7). Based on these results gRNA1 and gRNA2 manipulated cell lines were selected for further validation of stable knockdown. Stable knockdown showed a reduction of 35% and 89% in*AKR1C1*mRNA levels for gRNA1- and gRNA2-transfected HepG2 cells,

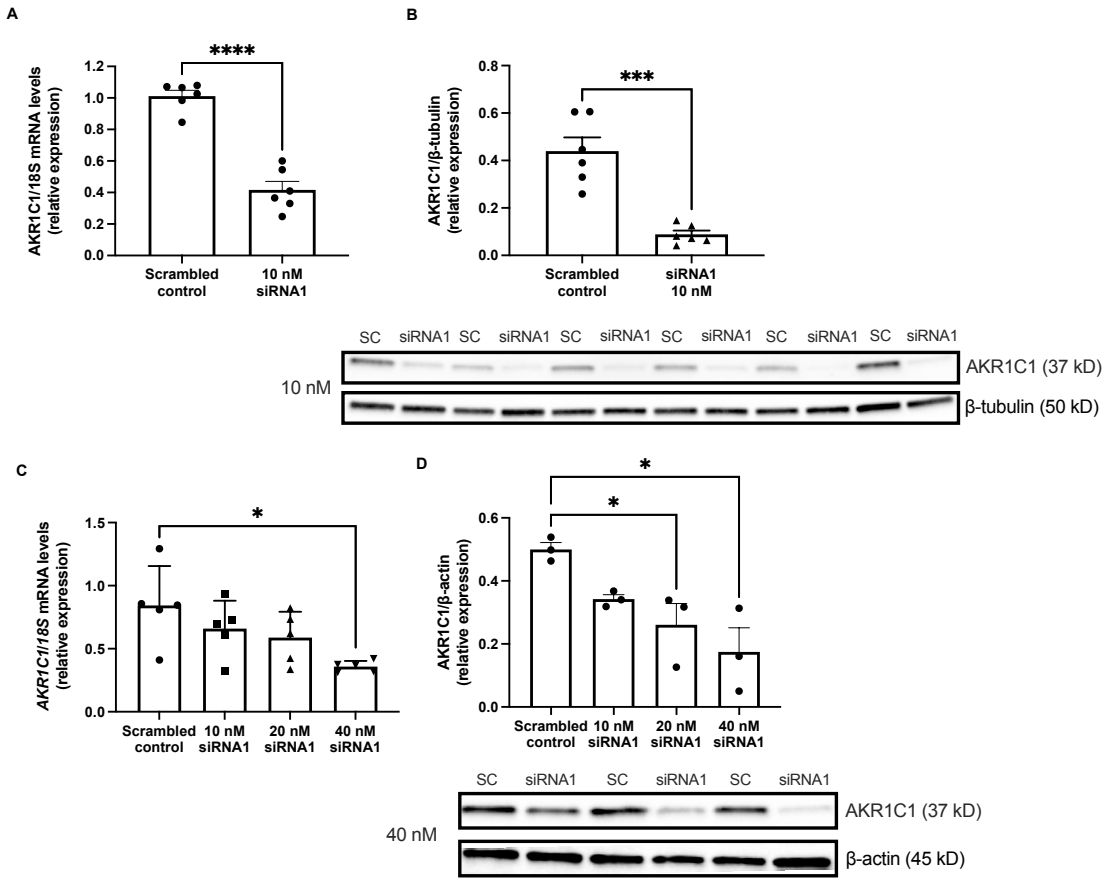


Figure 4.6: Established model for transient siRNA knockdown of *AKR1C1* in Huh7 as shown in A) mRNA and B) protein with 10 nM siRNA. In HepG2, a dose dependent effect was observed with a significant reduction of both C) mRNA and D) protein at transfection concentration of 40 nM. Unpaired T Test was used. (SC; scrambled control)

respectively. Controlling for effects on *AKR1C3* and *AKR1C4*, mRNA levels showed a non-significant increase in *AKR1C4* and a small but significant ($p < 0.01$) down-regulation in *AKR1C3*. These changes are most likely due to compensation rather than CRISPR/Cas9 off target effects as the proportional decrease in *AKR1C1* was matched with an increase in *AKR1C4* and decrease in *AKR1C3* of similar magnitude when comparing control, gRNA1 and gRNA2 (Figure 4.8A). Consistent with the mRNA data a decrease of 49% and 93% in AKR1C1 protein levels can be shown in gRNA1- and gRNA2-transfected HepG2 cell lines compared to control (Figure 4.8B).

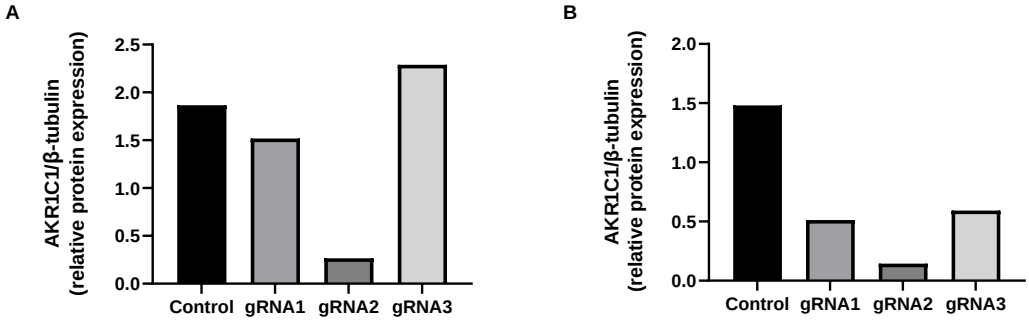


Figure 4.7: Stable *AKR1C1* knockdown generation via CRISPR/Cas9 in HepG2 and Huh7 using three different gRNAs (n = 1).

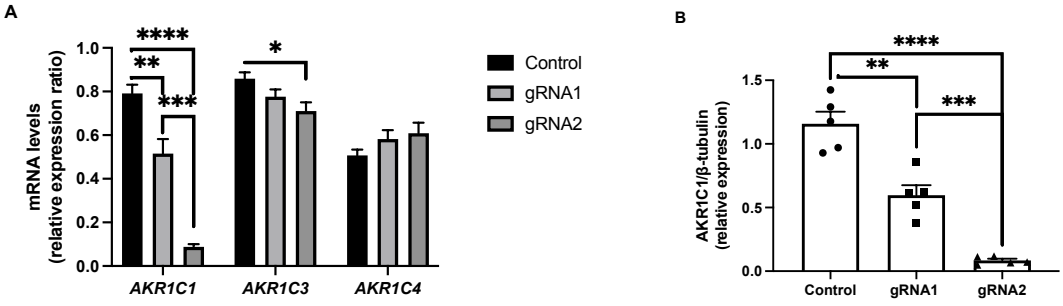


Figure 4.8: AKR1C1 mRNA is significantly reduced in HepG2, n = 5. *AKR1C3* mRNA shows significant reduction and *AKR1C4* a trend to higher levels A). AKR1C1 protein is significantly down-regulated by both gRNA1 and gRNA2 in n = 5 B). Unpaired T Test was used.

4.7 Overexpression

An *AKR1C1* overexpression model in HepG2 cell line was established. *AKR1C1* was successfully overexpressed with the addition of 500 ng of *AKR1C1* plasmid DNA as measured by western blot when compared to empty vector. An AKR1C1 protein increase of 25% was observed in transcfected HepG2 cells (Figure 4.9). Transiently overexpressed GFP-AKR1C1 can be identified at 65 kD on western blot as the molecular weight of AKR1C1, 37 kD, increased by 28kD due to tagging with GFP.

Green fluorescence was detected under fluorescence microscopy in both cells transfected with empty vector or *AKR1C1* clone plasmid, further confirming successful transfection. This underlines that observed differences in protein are

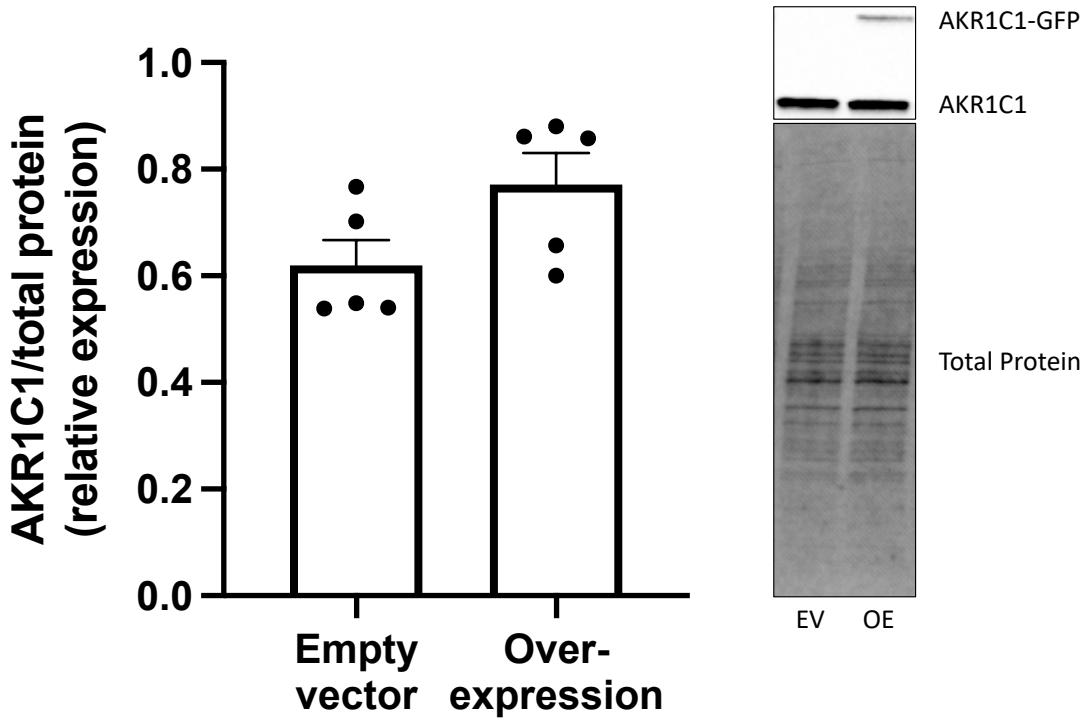


Figure 4.9: AKR1C1 overexpression of GFP-tagged protein in HepG2, normalised to total protein in n = 5. AKR1C1-GFP is visible at 65 kD and native AKR1C1 at 37 kD. (EV; empty vector, OE; overexpression)

due to the introduced plasmid (Figure 4.10).

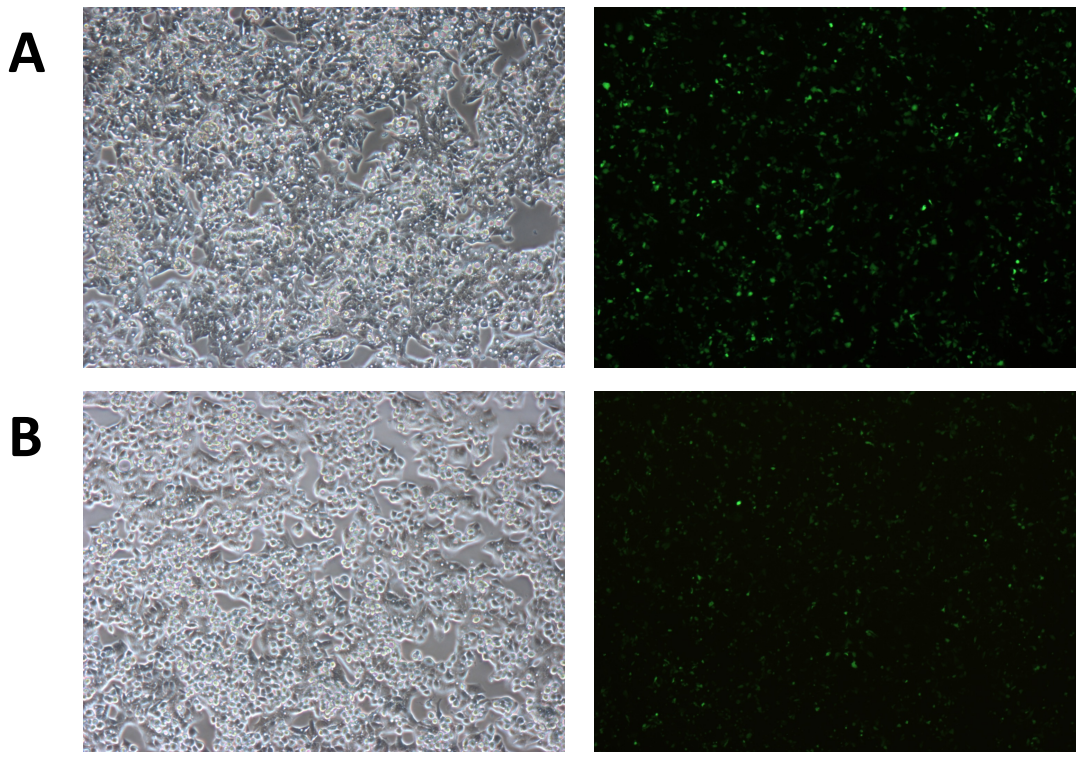


Figure 4.10: Fluorescence is visible in both empty vector A) and *AKR1C1* vector B) transfected cells, indicating successful transfection in both groups.

4.8 RNA sequencing

RNA sequencing was performed in *AKR1C1* siRNA-transfected and scrambled control siRNA-transfected HepG2 cells. Principal component analysis, comparing mRNA expression, shows strongly overlapping clusters indicative of variance not being attributable to a specific difference between groups. Principal component 1 and 2 are very small with 22.2 % and 17.6 % respectively 4.11.

Using DESeq2 we identified 20 differentially expressed genes from *AKR1C1* siRNA-transfected cells with a multiple testing adjusted p-value ≤ 0.05; 18 genes were up-regulated and 2 were down-regulated (Figure 4.12A) indicating small differences between scrambled control and *AKR1C1* siRNA-transfected cells (Figure 4.12B). Successful AKR1C1-transfection was confirmed by RNA sequencing results and validated via qPCR (Figure 4.12C). Selected gene expression changes including those in *ESAM*, AKAP12 and RAB3B results where validated with qPCR (Figure

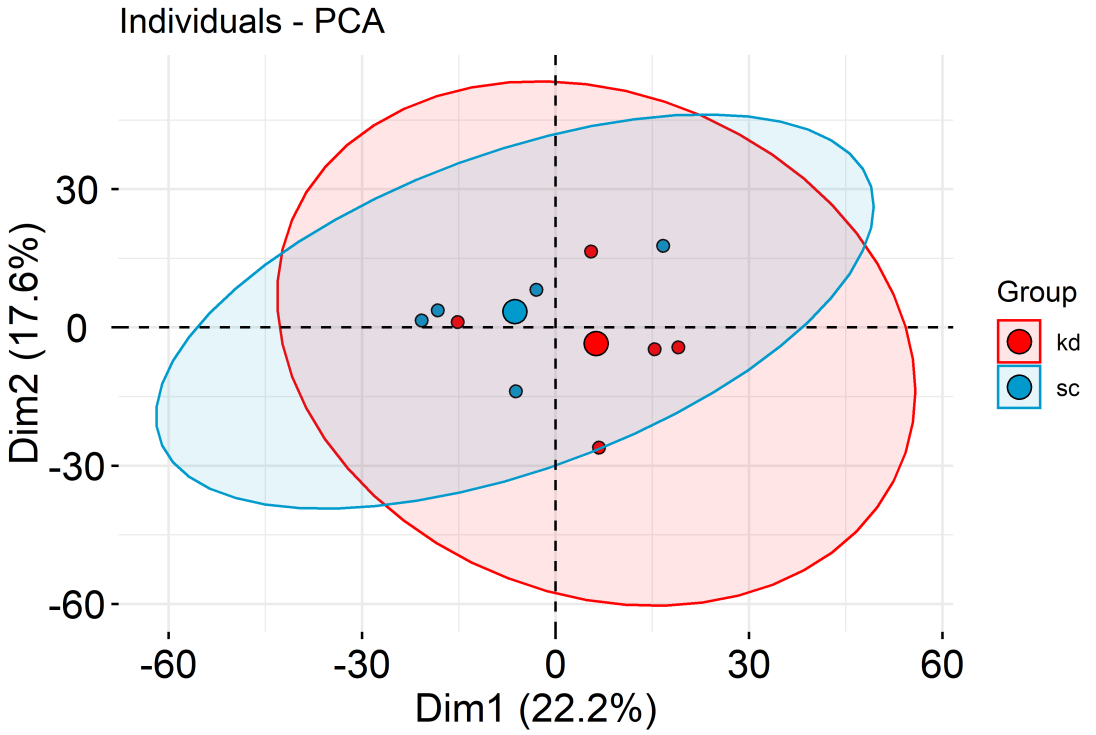


Figure 4.11: Principal component analysis shows strongly overlapping clusters of *AKR1C1* siRNA- and scrambled control-transfected cells. (Dim1; Principal component 1, Dim2; Principal component 2)

4.12D). Due to up-regulation of CDK2NA, the mRNA expression of additional cell cycle genes was examined in HepG2. No additional evidence of differentially expressed cell cycle genes were found that could have been missed due to lack of sensitivity in RNA sequencing (Figure 4.13) To validate our results in an additional cell line (*AKR1C1* siRNA-transfected Huh7 cells) and in the pharmacological AKR1C1 inhibition model (HepG2 treated with 5-PBSA) selected cell cycle gene expression was measured (Figure 4.14A and B). Based on this approach we were unable to detect any other changes in mRNA expression of cell cycle genes in *AKR1C1* knockdown or pharmacological inhibition of hepatoma cell lines.

Gene functional enrichment analysis of siRNA transfected HepG2 was not able to highlight any deregulated pathway or disease with only *AKR1C1* and *AKR1C2* downregulated.

RNA-sequencing results of CRISPR/Cas9 *AKR1C1* knockdown model reproduced similar results with strong overlapping clusters in the principal component

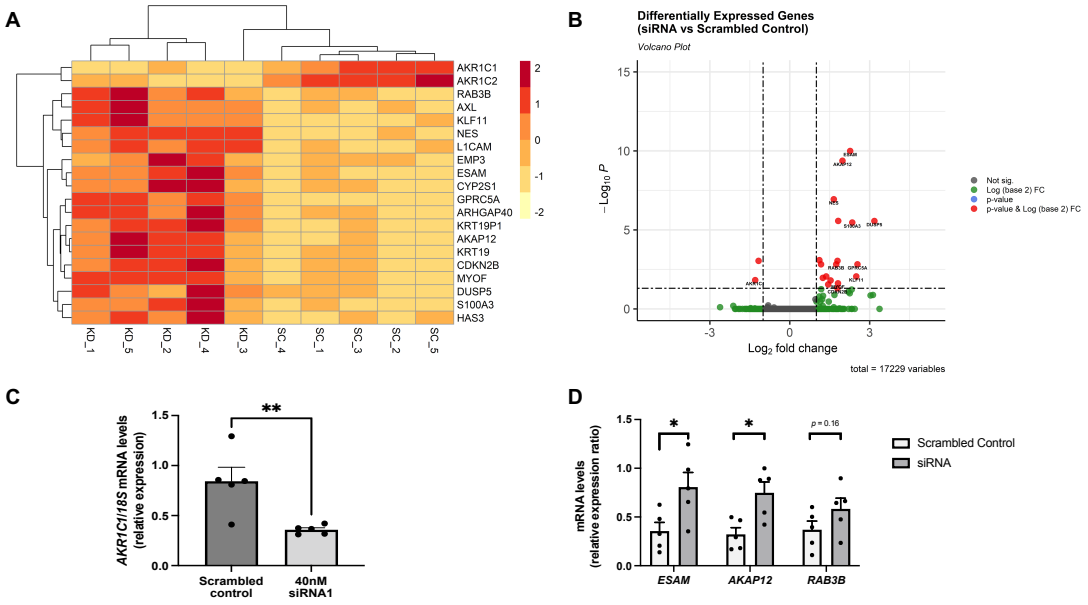


Figure 4.12: Differential gene expression analysis comparing *AKR1C1* siRNA-transfected with control. The heatmap A) illustrates all 20 significantly deregulated genes: *AKR1C1* and AKR1C2 were down-regulated, all other genes were up-regulated. Volcano plot B) shows that very few genes are in fact deregulated and differences between *AKR1C1* knockdown and control cells are minimal. down-regulation of *AKR1C1* C) and up-regulation observed in *ESAM* and *AKAP12* D) was validated using qPCR. DESeq2 (Wald Test) and unpaired T Test for qPCR were used as statistical methods.

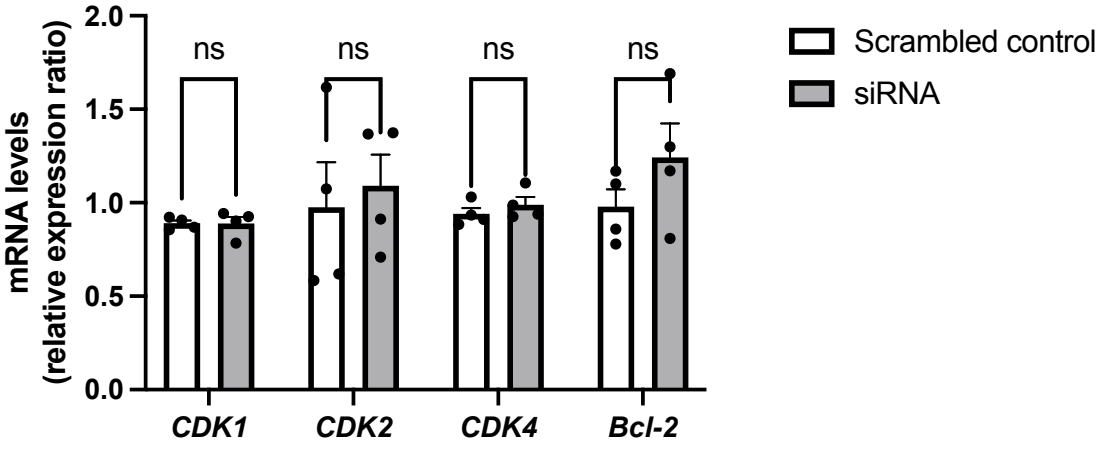


Figure 4.13: No change of cell cycle and apoptosis regulator genes observed in *AKR1C1* siRNA-transfected HepG2 cells (Unpaired T Test).

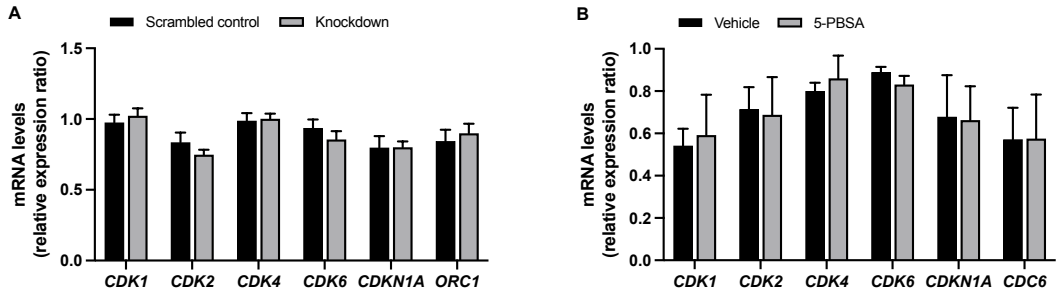


Figure 4.14: No change of cell cycle regulators observed in A) *AKR1C1* siRNA-transfected Huh7 cells and B) 5-PBSA treated HepG2 cells compared to scrambled control or vehicle (Unpaired T Test).

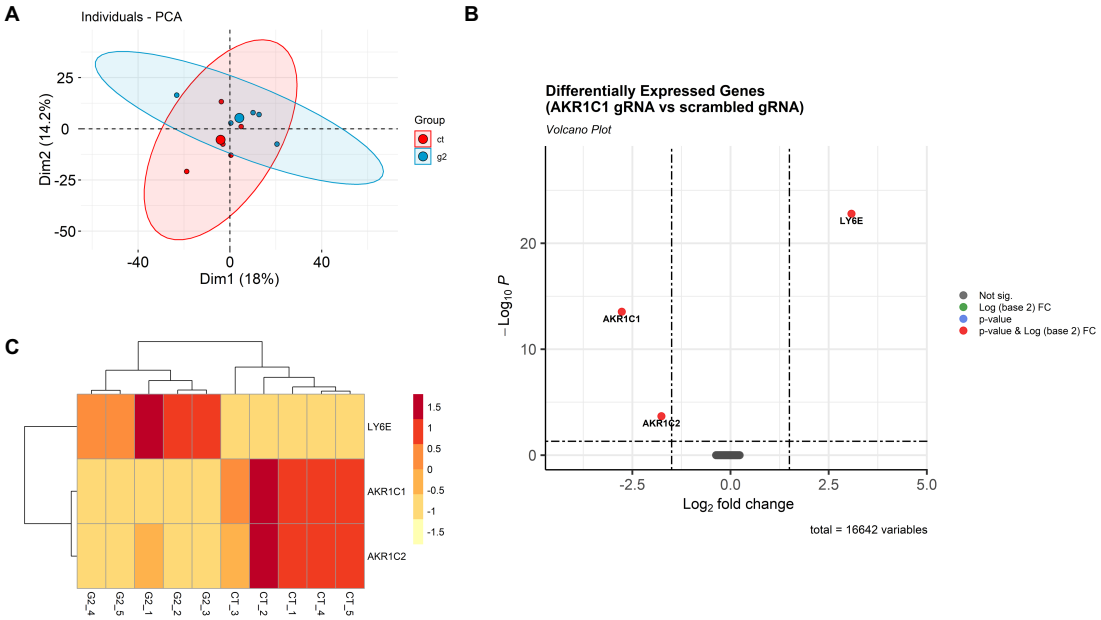


Figure 4.15: Principal component analysis A) shows strongly overlapping clusters with small components indicating very little difference between *AKR1C1* stable knockdown and control. Volcano plot B) illustrates that only 3 genes are in fact deregulated and there is almost no difference between *AKR1C1* knockdown and control cells. AKR1C1, AKR1C2 are down-regulated and LY6E is up-regulated as illustrated in the heatmap C). (CT; control vector, G2; guide RNA 2)

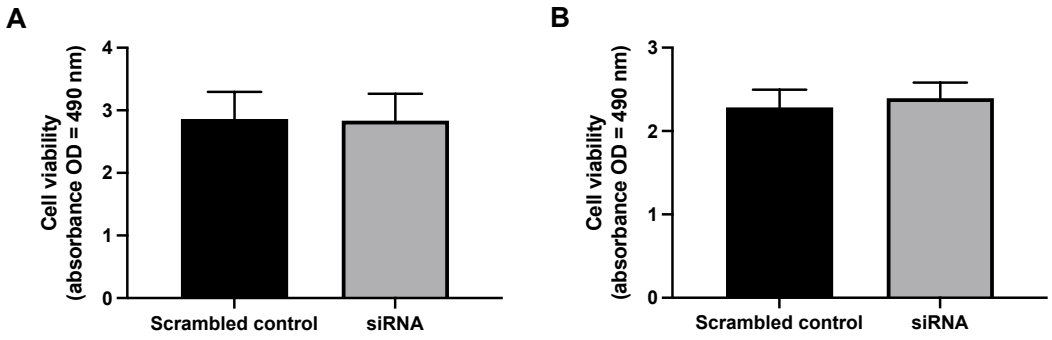


Figure 4.16: HepG2 A) and Huh7 B) proliferated at the same rate when comparing scrambled control and *AKR1C1* siRNA knockdown (Unpaired T Test).

analysis, with principal components again very small in the range of 14.2 % and 18 % (Figure 4.15). The differential gene expression analysis with DESeq2 highlights only 3 genes as deregulated: *AKR1C1* and *AKR1C2* are down-regulated and *LY6E* is up-regulated (Figure 4.15). No further comparative gene expression analysis was possible due to the limited effect of the *AKR1C1* stable knockdown.

After having demonstrated a very limited effect of *AKR1C1* siRNA-transfection or CRISPR/Cas9 *AKR1C1* knockdown on differential gene expression levels, we believed it was important to consider post-transcriptional effects. The clinical data that we have described in Chapter 3 encouraged us to perform functional experiments exploring proliferation, chemo resistance and cellular motility.

4.9 Proliferation and chemo resistance

No difference in the rate of cellular proliferation and viability over a period of 5 days were observed comparing scrambled control and *AKR1C1* siRNA-transfected HepG2 and Huh7 cells as illustrated by Figure 4.16.

Similar observations were made in both cell lines using the MTS assay after selective pharmacological AKR1C1 inhibition with 5-PBSA at doses 1 and 10 µM; there were no differences in cell proliferation and viability compared to control after 5 days (Figure 4.17).

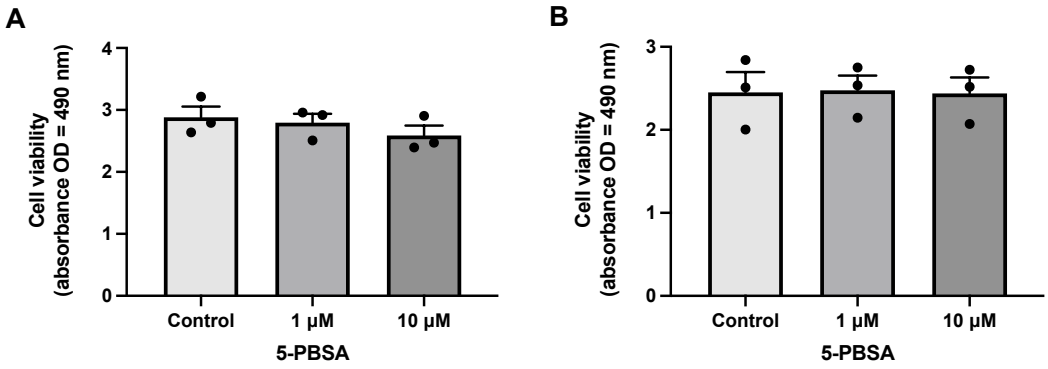


Figure 4.17: AKR1C1 inhibition by 5-PBSA does not influence proliferation rate of HepG2 A) or Huh7 B) cells at 1 µM or 10 µM (One-way ANOVA, Tukey test for multiple comparison).

Having established that AKR1C1 *in vitro* manipulation does not impact proliferation in our models, we further explored how differential expression of *AKR1C1* regulates chemotherapeutic treatment response, based upon the clinical outcome data. Chemotherapeutic sorafenib caused a dose dependent decrease in cell viability in both HepG2 and Huh7 at concentrations >1 μM. The manipulation of *AKR1C1* though mRNA knockdown did not affect the potency of Sorafenib treatment in HepG2 and Huh7 cells, indicating that AKR1C1 does not seem to impact the metabolism or mechanism of action of Sorafenib *in vitro* (Figure 4.18). Further, pharmacological AKR1C1 inhibition did not influence Sorafenib efficacy in HepG2 and Huh7, thereby recapitulating observations made in the transient knockdown model, see Figure 4.18.

To determine whether other members of the AKR1C family could potentially compensate for the lack of AKR1C1 activity in our cell models following *AKR1C1* knockdown, additional knockdown experiments were performed using a non-specific *AKR1C* siRNA variant in Huh7 cells which also targets *AKR1C3* and *AKR1C4*. Huh7 cells do not express *AKR1C2* (data not shown). The specific *AKR1C1* siRNA variant had no significant impact on *AKR1C3* and *AKR1C4* mRNA expression (Figure 4.19A). Following transfection of the non-specific *AKR1C* siRNA, successful knockdown of AKR1C1, *AKR1C3* and *AKR1C4* was confirmed by qPCR (Figure 4.19B). The specific *AKR1C1* siRNA variant as well as the non-specific siRNA

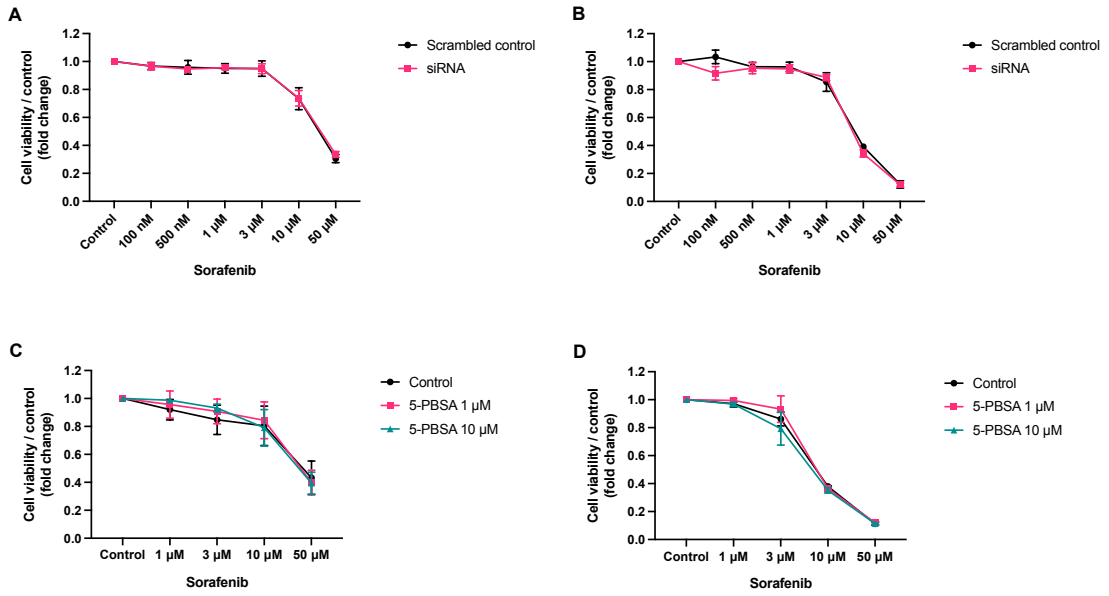


Figure 4.18: *AKR1C1* siRNA knockdown in HepG2 A) and Huh7 B) shows no effect on chemo sensitivity after Sorafenib treatment at doses ranging from 100 nM to 50 µM. Pharmacological AKR1C1 inhibition did not impact Sorafenib efficacy at doses 1 µM to 50 µM in HepG2 C) and Huh7 D) cells. All graphs display fold change of absorbance after Sorafenib treatment compared to control (Two-way ANOVA).

resulted in similar decreases in AKR1C1 protein levels (Figure 4.19C). On its own the non-specific *AKR1C* knockdown did not affect cell viability and despite the significant reduction in the expression of all AKR1Cs following non-specific siRNA transfection did not impact cellular response to sorafenib. 24h Sorafenib treatment did not show any differences in Sorafenib chemo sensitivity between non-specific or specific siRNA, compared to scrambled control-transfected Huh7 cells (Figure 4.19D). This highlights that AKR1C1 most likely does not impact Sorafenib response in hepatoma cells.

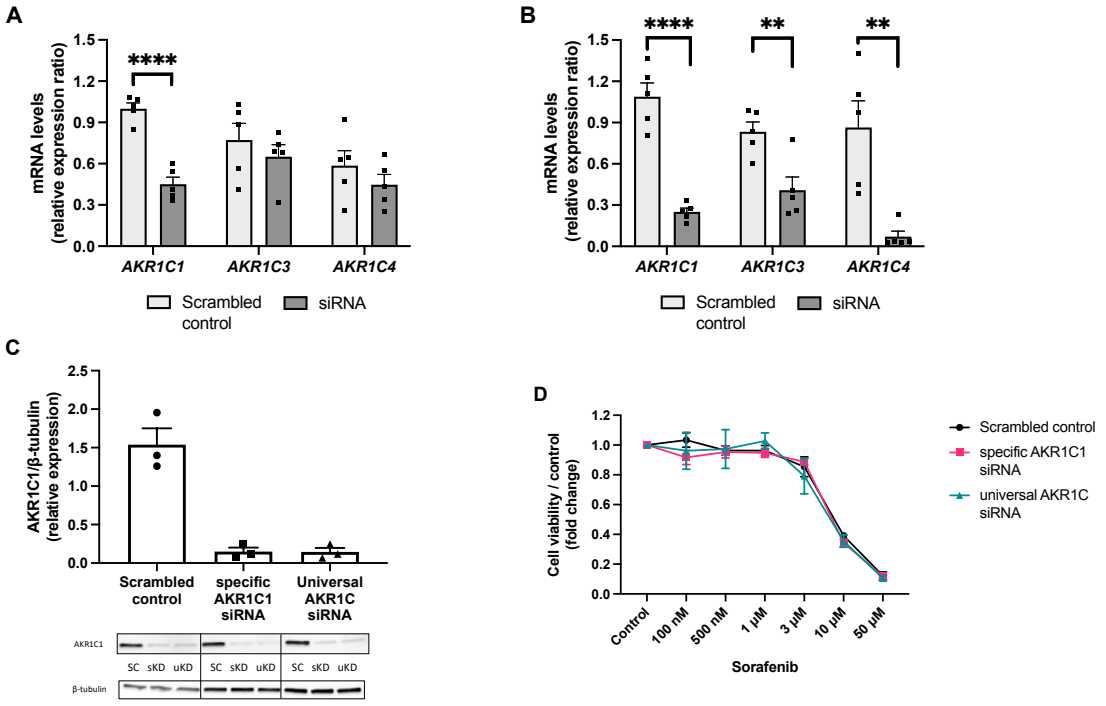


Figure 4.19: Specific *AKR1C1* siRNA knockdown A) achieved a significant reduction in *AKR1C1* mRNA levels whereas *AKR1C3* and *AKR1C4* are not significantly affected. Using an *AKR1C* universal siRNA variant B), *AKR1C1*, *AKR1C3* and *AKR1C4* were all significantly down-regulated. Protein levels of AKR1C1 were diminished by the same extent by both specific *AKR1C1* and non-specific (universal) *AKR1C* siRNA knockdown C). The comparison during Sorafenib treatment indicates that the absence of an effect of *AKR1C1* knockdown is not to be explained through AKR1C family members compensating but more likely due to truly having no influence on Sorafenib efficacy. Unpaired T Test was used for statistical analysis and a Two-way ANOVA to see differences in Sorafenib efficacy. (SC; scrambled control, sKD; specific siRNA knockdown, uKD; universal siRNA knockdown)

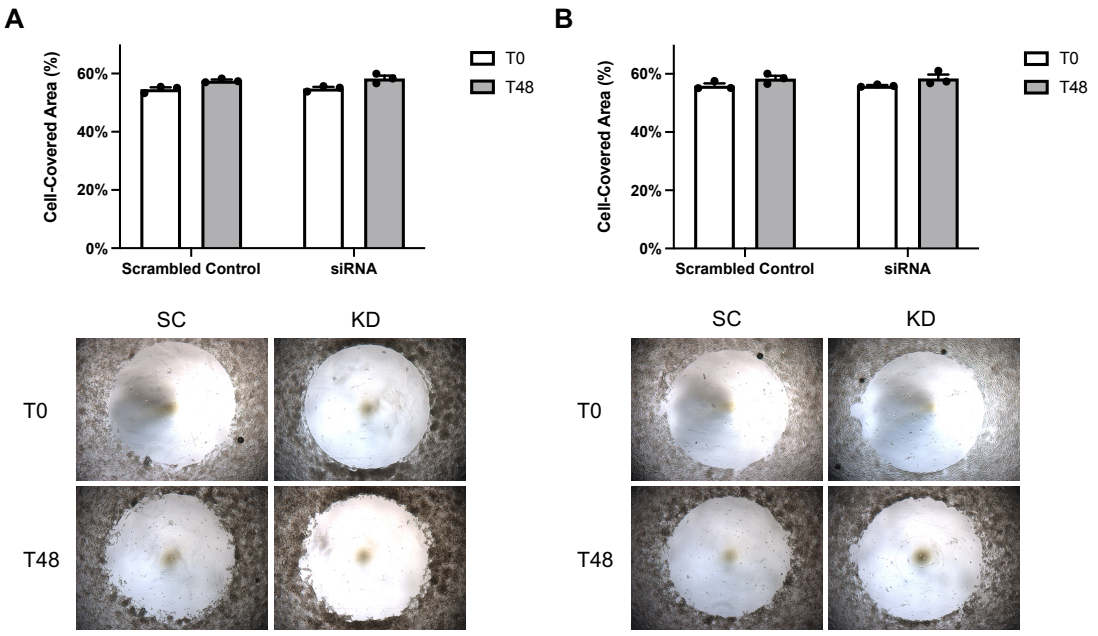


Figure 4.20: Cellular motility did not change after *AKR1C1* siRNA knockdown on both collagen A) and fibronectin B) well coatings after 48h (Unpaired T Test). (SC; scrambled control, KD; siRNA knockdown)

4.10 Motility

A commercial wound healing assay was used to explore the effect of AKR1C1 manipulation on cellular motility and metastatic potential. 2D Motility was not affected by *AKR1C1* siRNA transfection on both collagen or fibronectin coated wells 48 h after removal of silicon inserts(Figure 4.20).

Observations made in the siRNA knockdown model were endorsed with results from both well surface coatings using cells from the CRISPR/Cas9 *AKR1C1* knockdown model and comparing them to control cells (Figure 4.21). These results suggest that differential *AKR1C1* expression does most likely not alter the invasive and metastatic potential of hepatoma cells.

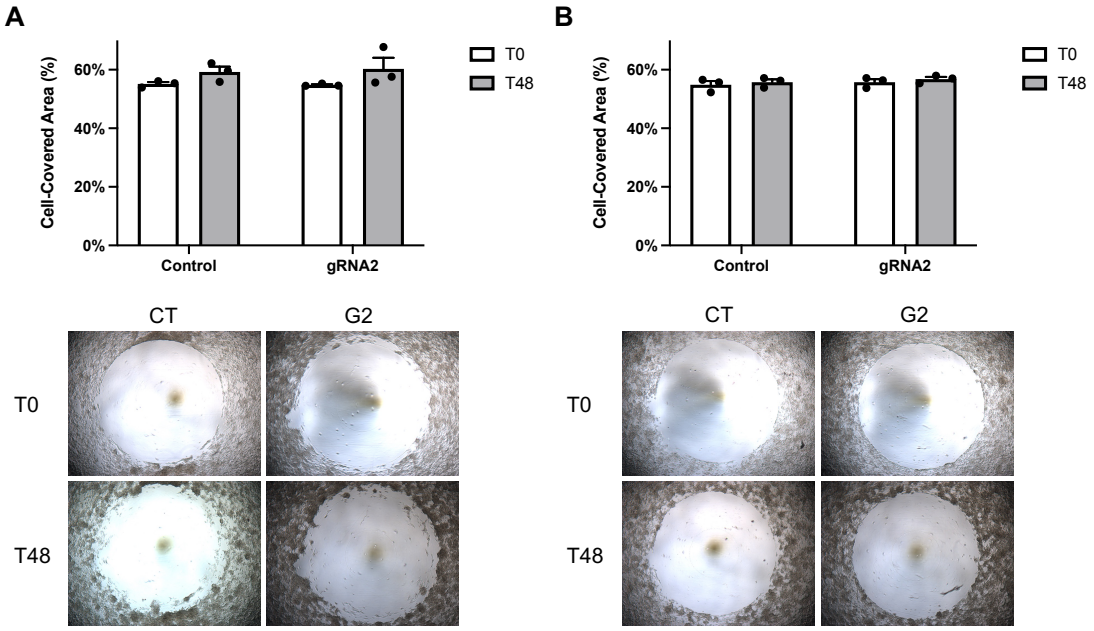


Figure 4.21: Cellular motility was unchanged 48h after removal of inserts in HepG2 cell line with *AKR1C1* CRISPR/Cas knockdown on both collagen A) and fibronectin B) coated well surfaces (Unpaired T Test). (CT; control, G2; guide RNA 2)

4.11 Discussion

AKR1C1 plays an important role in steroid hormone, lipid aldehyde, prostaglandin and retinol metabolism and has its highest expression in liver and adipose tissue [41, 152, 153, 157, 160]. Both steroid hormones and lipid aldehydes are implicated in metabolic liver disease and the progression to HCC [255–259]. However, AKR1C1s influence remained almost entirely unexplored in that context. For the first time, we have shown that AKR1C1 manipulation has very little effect on hepatoma cell lines as measured through differential gene expression and further does not cause any changes in proliferation and cell motility in an *in vitro* liver cancer model. The conclusion from these data is that AKR1C1 is rather unlikely to play a role in the development or progression of HCC. This is in contrast to what has been described in other cancer forms such as cervical, NSCLC and bladder cancer [171, 172, 260] as well as the potential role AKR1C1 has been hypothesised to play in breast cancer [261].

There are a number of reasons that may account for this lack of an effect and the most likely being enzyme redundancy. In our experiments, even a 93 % reduction in AKR1C1 protein levels did not significantly alter gene expression profiles, suggesting that the specific enzymatic AKR1C1 activity in an *in vitro* cell model is expendable. With the liver being a highly active metabolic tissue, it is possible that other enzymes could substitute for the missing AKR1C1 activity. At a functional level, with respect to chemotherapy resistance, we explored the role of other AKR1C family members and excluded their roles as potential substitutes for specific AKR1C1 activity. The possibility that AKR1C3 or AKR1C4 could compensate for other unexplored functions of AKR1C1 remains unknown, and further gene expression analysis using non-specific *AKR1C* siRNA may be illuminating. Another point to consider is that our model did not include AKR1C1 substrates such as progesterone or glucocorticoids and these may be critical in unmasking the impact of decreasing *AKR1C1* expression or activity. A limitation of this experimental design is that we are not able to assess how a lower or higher *AKR1C1* expression affects progesterone or glucocorticoids and thereby the effects of hormones further downstream on hepatoma cell lines.

Previous studies have shown non-enzymatic effects on Jak/STAT pathway in both NSCLC cells and head and neck tumours. They have shown that NSCLC cells with higher levels of AKR1C1 have enhanced invasive ability *in vitro* and increased metastatic foci in vivo. In turn, the depletion of AKR1C1 was able to prevent *in vitro* invasion and ameliorate *in vivo* metastasis. Following AKR1C1 depletion, STAT3 was found to be among the most significantly down-regulated transcription factors, suggesting its involvement in AKR1C1-mediated NSCLC metastasis [171]. In head and neck tumours the study finds that AKR1C1 contributes to cis-platin resistance and cancer stemness phenotype by activating STAT signalling pathways [174]. However, we were not able to endorse these findings in our studies and have shown no non-enzymatic effects on pathways such as STAT3 as described in above mentioned studies. In particular, the motility experiments with HepG2 in both *AKR1C1* siRNA and CRISPR/Cas9 knockdown were in agreement with the RNA sequencing results, that failed to show significant disruption of any major metabolic or proliferative pathways. Our data failed to recapitulate observations demonstrating more invasive cells and activation of metastasis associated genes shown in other forms of cancer [171, 172]. A limitation of these results is the fact that we did not perform a clonal expansion of our CRISPR/Cas9 model due to a very high efficiency of our gRNA. We refrained from establishing a complete knockout and analysed bulk HepG2 cell mass containing a low number of cells fully expressing AKR1C1. The up-regulation of cell cycle inhibitor CDKN2A, seen in RNA sequencing after transient *AKR1C1* knockdown, could support the idea of a more rapid cell cycle and quicker proliferation in case of high *AKR1C1* expression. RNA sequencing and qPCR results from the CRISPR/Cas9 model show unchanged cell cycle genes in both HepG2 and Huh7 cell lines quite clearly indicating no effect of AKR1C1 on the proliferative phenotype of cells. This is further reinforced by results from functional experiments showing unchanged proliferation in a MTS assay after AKR1C1 manipulation on mRNA and pharmacological level. Interestingly, proliferation was also not affected when treating AKR1C1 manipulated hepatoma cells with Sorafenib. This clearly indicates that in contrast to other chemotherapeutic agents, such as cisplatin, used

in a wide variety of cancers, Sorafenib does not seem to be affected by AKR1C1 in both its metabolism and in its mode of action [174, 262]. Taken together, our data would suggest that AKR1C1 is not playing a critical role in determining the sensitivity of HCC to sorafenib chemotherapy.

Up-regulation of endothelial cell adhesion molecule (*ESAM*) and L1 cell adhesion molecule (*L1CAM*) gene expression after *AKR1C1* siRNA-transfection was particularly interesting because they are involved in cell motility, adhesion and implicated in cancer progression. *ESAM* has been implicated to regulate tumour microvasculatur and endothelial cell migration in melanoma [263], whereas mutations or overexpression of *L1CAM* are associated with aggressive tumour growth and poor survival in patients, as well as promoting increased cell proliferation and migration in multiple cancers including gastric, breast cancer and endometrial cancer [264–267]. Importantly, it seems not only of prognostic significance but could present to be an attractive therapeutic target for cancers [268]. Higher expression of RAB3B, a member of the RAS oncogene family, as found in our transient *AKR1C1* knockdown has been associated with higher metastatic potential and chemoresistance of hepatoma cells after injection into the spleen of mice [269]. All these results would indicate lower *AKR1C1* expression to be detrimental for liver cancer patients and are contrary to current literature of AKR1C1's influence on other forms of cancer and also our HCC data mining studies. The same logic would apply to higher LY6E expression in the stable knockdown model. Clinical trials have associated up-regulation of LY6E in cancer tissue with poor prognosis in multiple malignancies [270]. In breast cancer specifically it has been implicated in immune evasion and drug resistance [271].

Overall the effects of AKR1C1 manipulation are modest and have shed disappointingly few insights into the pathogenesis, metastatic potential or chemoresistance of HCC. There is clearly a disconnect between the clinical data (Chapter 3) and the *in vitro* data presented in this chapter and much may relate to cause and effect in that the clinical observations may be a reflection of the cancer itself rather than being a primary pathogenic driver. With no relevant rodent models available due to

challenges in finding human *vs.* mouse homologues, differing localisation, substrate preferences and functionalities it will pose a challenge to elucidate the relationship of AKR1C1 and HCC in an *in vivo* model. Therefore, future experiments and further exploration of the impact of AKR1C1 on HCC would have to be conducted in the context of human primary hepatocytes or iPSCs. *AKR1C1* CRISPR/Cas9 knock out in iPSCs could allow more fundamental studies into the question of cause or consequence when cells have not yet differentiated.

5

Characterisation of POR in human and rodent NAFLD model

Contents

5.1 Introduction 108
5.1.1 POR deficiency 108
5.1.2 POR in NAFLD 109
5.1.3 POR urinary steroid ratio 110
5.1.4 Hypothesis and aims 110
5.2 Methods 111
5.2.1 Liver biopsies 111
5.2.2 Urine samples 112
5.2.3 Mouse husbandry and experimental design 113
5.2.4 Mouse tissue collection 114
5.2.5 Cell culture 115
5.2.6 OPLA2 lipid loading 115
5.3 POR in patients with NAFLD 116
5.3.1 *POR* mRNA expression 116
5.3.2 POR activity 118
5.3.3 CYP mRNA expression 119
5.4 POR in rodent NALFD model 121
5.5 POR in fat loaded cell model 121
5.5.1 Optimisation of lipid loading 121
5.5.2 POR mRNA and protein expression after lipid loading . 121
5.6 Discussion 124

5.1 Introduction

5.1.1 POR deficiency

The congenital disorder cytochrome P450 oxidoreductase deficiency (PORD) is a rare disease which is caused by reduced POR activity and leads to disruption of

the electron transfer from NADPH to type 2 CYPs [272–274]. This can cause a wide range of symptoms depending on the extent of PORD. In severe cases PORD can lead to congenital adrenal hyperplasia (CAH), cortisol deficiency, ambiguous genitalia likely due to the disturbance of CYP17A1, CYP19A1 and CYP21A2 as well as Antley-Bixler syndrome due to PORD's impact on CYP51A1 and CYP26B1. Missing electron transfer to CYP51A1, limiting CYP51A1 enzyme activity, impairs cholesterol synthesis and hedgehog protein signaling which is believed to lead to skeletal abnormalities [275, 276]. Another factor could be retinol metabolism disturbance due to missing CYP26B1 activity [272, 277–279]. Complete deletion of POR is very likely non-compatible with life in humans. Prior studies in mice have shown POR deletion to be lethal at embryonic stage [189, 211].

5.1.2 POR in NAFLD

Drug metabolism studies of liver-specific POR knockout mice implicate POR as a potential important regulator in NAFLD. Incidental findings during post-mortem analysis revealed that hepatic Por-null mice show hepatomegaly as well as microvesicular and macrovesicular lipid changes compared to wild type animals. Furthermore, the studies detected hepatic hyperlipidaemia, lower circulating levels of cholesterol, lower circulating triglycerides and an increase in serum ALT in hepatic knock out mice *vs.* wild type animals [190, 221, 280]. The impact of POR knock out on these molecules are in agreement with POR's significant role in enabling CYP metabolism which in turn is essential for the conversion of lanosterol to cholesterol, the clearance of cholesterol and the biosynthesis of BA. Studies were also able to show that an inducible hepatic or hepatic and gastrointestinal POR deletion mouse model initially develops normally, but upon induction of POR suppression shows the same pattern with enlarged liver and lower circulating triglycerides and cholesterol as seen in the hepatic Por-null mice [281].

5.1.3 POR urinary steroid ratio

Urinary steroid metabolites can be used as a reflection of specific enzyme activity *in vivo* and help discern underlying disease mechanisms. In humans, deficiency of POR which leads to combined CAH due to deficiencies in 17α-hydroxylase and 21-hydroxylase can be discovered non-invasively through GC/MS of urine steroid metabolites and the specific changes thereof [282, 283]. One of the most holistic ratios uses total pregnanediol (total PD), the main metabolite of progesterone which is higher during POR deficiency, divided by the sum of tetrahydrocortisol (THF), 5α-tetrahydrocortisol (5αTHF) and tetrahydrocortisone (THE), cortisol and cortisone metabolites downstream of 17α-hydroxylase and 21-hydroxylase (Figure 5.1). This inverse POR activity ratio (total PD / (THF + 5αTHF + THE)) indicates lower POR activity the higher the ratio [273, 284].

5.1.4 Hypothesis and aims

Based on above presented research in rodents, I hypothesised that we might identify lower *POR* mRNA expression and POR activity in patients suffering from NAFLD compared to healthy individuals. Further, I wanted to investigate if a NAFLD inducing diet in mice or hepatoma cells induced to become steatotic have the potential to cause changes in POR mRNA and protein expression when compared to mice with a normal diet or cells in normal medium.

I set out to perform gene expression, protein expression and mass spectrometry studies to analyse *POR* expression in liver biopsies from humans, mice and cells as well as POR activity in human via urinary steroid metabolites.

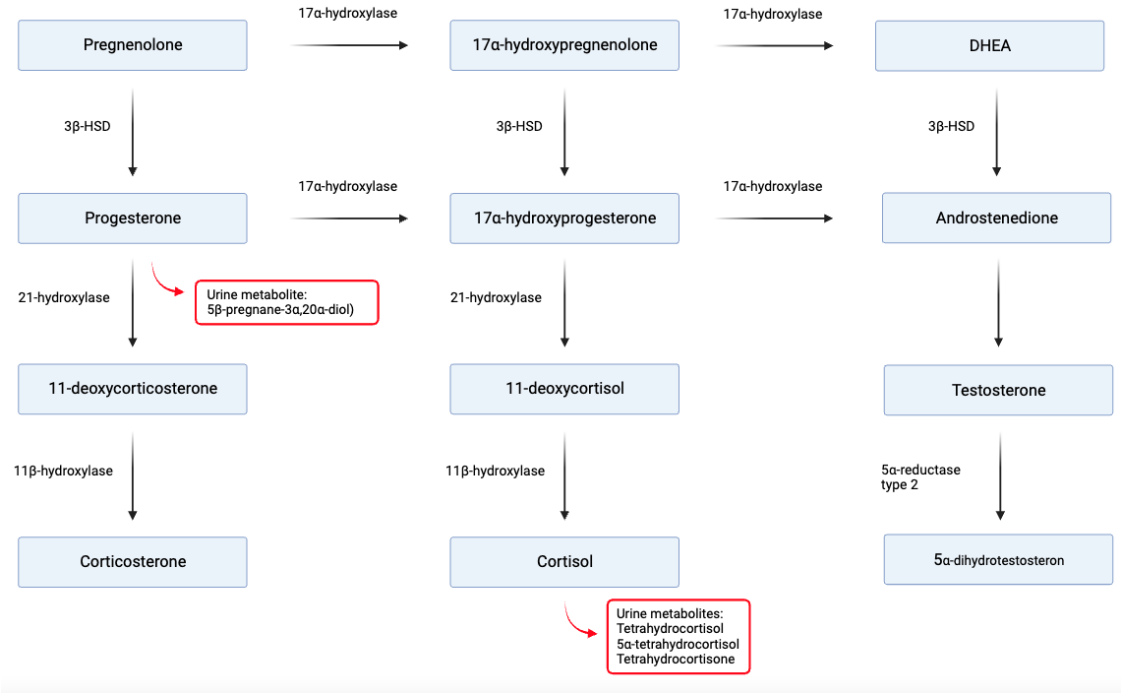


Figure 5.1: Physiological function of 17α-hydroxylase and 21-hydroxylase in steroid metabolism and biosynthesis is dependent on POR electron transfer. Measured urinary metabolites are highlighted: 5β-pregnane-3α,20α-diol / Pregnanediol (PD), a progesterone metabolite, upstream of 17α-hydroxylase and 21-hydroxylase and cortisol and cortisone metabolites tetrahydrocortisol (THF), 5α-tetrahydrocortisol (5αTHF) and tetrahydrocortisone (THE) downstream of both of 17α-hydroxylase and 21-hydroxylase. Created with BioRender.com.

5.2 Methods

5.2.1 Liver biopsies

RNA was collected through liver biopsies from obese individuals subject to their full informed consent. Male (n = 7) and female (n = 27), undergoing primary bariatric surgery (laparoscopic sleeve gastrectomy or Roux-en-Y gastric bypass) were eligible to be recruited into a dedicated bariatric surgery biobank study (Ref: 16/YH/0247) run by our group. Detailed clinical data (including weight, height, medical history, medications, family history and alcohol intake) was recorded for all participants prior to surgery. As control, liver biopsies of lean individuals (n = 8) with phenotypically healthy livers according to a consultant liver histopathologist were used, with limited knowledge of their medical history. Intraoperatively, a wedge biopsy was taken from the anatomical left lobe of the liver after pneumoperitoneum

was established. Half of the tissue was stored in formalin prior to histological analysis by a consultant liver histopathologist according to Kleiner's NAS and fibrosis staging classification [246]; F0 represents the absence of fibrosis, F1 portal or perisinusoidal fibrosis, F2 portal/periportal and perisinusoidal fibrosis, F3 septal or bridging fibrosis and F4 cirrhosis. The remainder of the tissue was washed in 0.9% NaCl then stored in RNA later stabilization solution at -80 °C until RNA extraction.

5.2.2 Urine samples

A total of 275 subjects; 169 patients with established liver disease (NAFLD n = 121; alcohol n = 48) and 106 controls without known liver disease were recruited with full written informed consent and national research ethical committee approval (refs. 09/H0403/1, 12/WM/0288, 07/H1211/168, 09/H604/20, and 10/H0402/23). Control status was determined by the review of medical history and the absence of risk factors for any known liver disease. Subjects with abnormal liver chemistry or with elevated tests for liver disease severity were excluded from the analysis as control. From each subject clinical data (including weight, height, medical history, medications, family history and alcohol intake) and spot urine samples were collected from a single void of urine were and stored at -80 °C. Urinary steroid metabolites measurements were undertaken using GC-MS.

1 ml of urine was used to extract free and conjugated steroids via a 5-step solid-phase extraction method as described previously [247]. Solid-phase extraction of free and conjugated steroids was performed, followed by enzymatic hydrolysis of steroid conjugates, solid-phase re-extraction of steroids, chemical derivatisation to form ethers and finally liquid-liquid extraction. GC/MS was carried out on an Agilent 5973 MSD single-quadrupole gas chromatography mass spectrometer (Agilent) instrument allowing quantification of up to 32 steroid metabolites, with representation of major steroids and their metabolites from all the adrenal-derived steroid hormone classes (androgens, glucocorticoids and mineralocorticoids). SIM (single ion monitoring) mode was used to identify and quantify steroids relative to authentic reference standards. All precursors and end products of the major steroid

hormone classes (androgens, glucocorticoids and mineralocorticoids) were included in the multi-steroid profiling. Urine samples were corrected by creatinine trying to adjust for differing times and durations of collection. The measurement of individual concentrations of steroid hormones and their metabolites allowed the assessment analysis specific enzymatic activity through product-substrate metabolite ratios.

5.2.3 Mouse husbandry and experimental design

Male and female C57BL/6NTac mice were housed and studied according to United Kingdom Home Office legislation and local ethical guidelines outlined by the Medical Research Council (Responsibility in the Use of Animals in Medical Research, July 1993; Home Office licence 30/3146). The procedures used were in compliance with the Animals (Scientific Procedures) Act 1986 Amendment Regulations 2012 (SI 4 2012/3039). The mice were kept under a controlled environment of light (light 7 AM to 7 PM, dark 7 PM to 7 AM), temperature (21 ± 2°C), and humidity (55 ± 10%) with ad libitum access to water containing 9–13 ppm chlorine and a commercial diet (SDS Rat and Mouse No.3 Breeding diet, RM3; Special Diet Services, Witham, Essex, United Kingdom) until they reached 10 weeks of age. After 10 weeks, the mice were transferred to either a control diet (NC; SDS Rat and Mouse No.3 Breeding diet, RM3) or an American lifestyle-induced obesity syndrome (ALIOS) diet (D06031302, Research Diets; and TD.06415 with hydrogenated vegetable fats, Envigo [45% fat, of which 30% is trans-fat] with 55% fructose-45% glucose in drinking water) for a further 52 weeks. Cohorts of male and female mice were bred for phenotyping. They were housed in single-sex groups across multiple litters and were not randomised into groups. Animal identifiers (IDs) and diets were recorded on the cages and operators were not blinded. Sample size estimates were based on previous experience with mouse models in which hepatic inflammation was measured ([285]), the sample sizes were n = 17 NC males, n = 12 ALIOS males, n = 15 NC females, and n = 15 ALIOS females. After 52 weeks on either NC or ALIOS, mice were culled by cervical dislocation.

5.2.4 Mouse tissue collection

After euthanasia, the right lateral lobe of the liver was fixed in 4% (vol/vol) buffered formaldehyde and the remaining liver tissue was snap frozen in liquid nitrogen.

Protein extraction and western blotting

Total liver protein was homogenised in 500 µl of RIPA buffer (Sigma-Aldrich, UK) supplemented with protease and phosphatase inhibitors. Tissue homogenate was incubated at 4°C for 18 hours before sonication at 40% speed for 30 seconds with a Jencons sonicator and a final centrifugation at 4°C and 13,000 g for 10 minutes to remove tissue debris. The supernatant was aliquoted and stored at -80°C. Protein concentration was measured using a commercially available assay (Bio-Rad, Hemel Hempstead, UK). Protein was run on an 18-well Criterion TGX Stain-Free Precast Gels and total protein visualised using the ChemiDoc MP Imaging System (Bio-Rad, Watford, UK). Primary anti-POR (Table 2.1) and secondary antibodies from Dako (Agilent Technologies, Santa Clara, USA) were used at a dilution of 1/1000. Bands were visualised with Bio-Rad Clarity Western ECL (Watford, Hertfordshire, UK) on a ChemiDocXS imager (Bio-Rad, Watford, UK), quantified by densitometry and normalised to total protein from the same gel using ImageJ (National Institutes of Health). Quantifications are based on n = 16 mice (n = 8 NC, n = 8 ALIOS).

RNA extraction, reverse transcription and qPCR

Total RNA was extracted from snap-frozen liver using Tri-Reagent (Sigma-Aldrich) and concentration was determined at OD260 on a Nanodrop spectrophotometer (Thermo Scientific). Reverse transcription and qPCR were conducted according to same protocol as described in Chapter 2.8.3 and 2.8.4. The Ct value of each sample was calculated using the following formula (where E is the reaction efficiency determined from a standard curve): ΔCt = E[min Ct-sample Ct] using the 1/40 dilution from a standard curve that was generated from a pool of all cDNAs as a calibrator and the relative expression ratio was determined using the equation: ratio = ΔCt[target]/ΔCt[ref]. Expression was normalised to the geometric mean

of 18S rRNA and hypoxanthine-guanine phosphoribosyltransferase (HPRT) for the liver RNA. Statistical analysis was performed on the mean relative expression ratio values (ratio = ΔCt[target]/ΔCt).

5.2.5 Cell culture

For experiments to explore to impact of fat on POR expression the HepG2 cell line was used. HepG2 cells were cultured as described in Chapter 2.2.

5.2.6 OPLA2 lipid loading

The impact of lipid loading on POR expression in HepG2 cells was determined by fat loading cells with different doses of OPLA2 fatty acid treatment composed of oleate, palmitate, linoleate and α-linolenate and comparing them against standard culture media. Cells were seeded in Costar® 24 well plate (Corning, Flintshire, UK) at 1.6 x 10^5/ml in 500 µl culture media. Cells were left for 24h after seeding, then media was changed to culture media alone or culture media with OPLA2 at doses of 200 μM (100 μM oleate, 70 μM palmitate, 28 μM linoleate, 2 μM α-linolenate) or 800 μM (400 μM oleate, 280 μM palmitate, 112 μM linoleate, 8 μM α-linolenate). This change of media was repeated after 48h and again after a subsequent 48h post media change, totaling up to an OPLA2 treatment duration of 144h (6 days). Afterwards, media was collected and frozen for later analysis. Cells were washed twice with PBS and frozen at -80°C for later RNA, protein and lipid extraction.

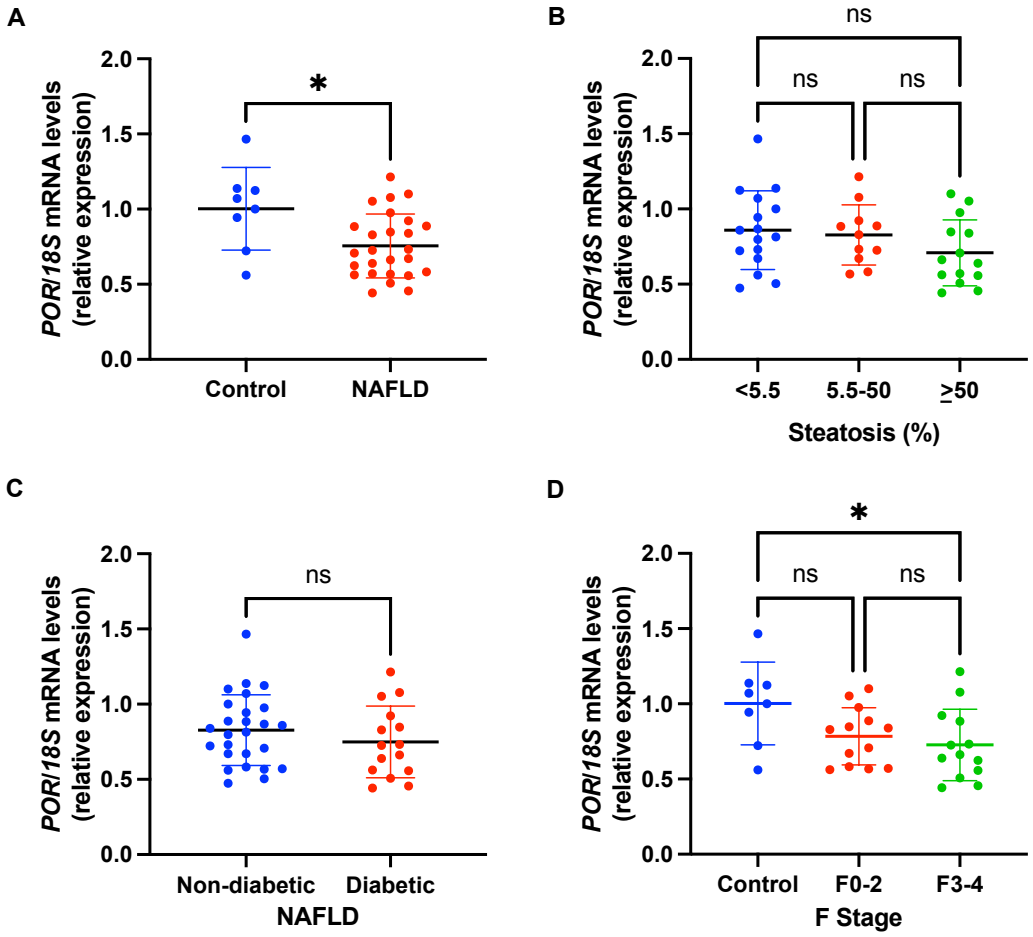


Figure 5.2: Expression of *POR* mRNA in liver biopsies is A) significantly attenuated in patients with NAFLD compared to healthy control (Unpaired T Test). When looking at subgroups within the NAFLD cohort there is no difference comparing *POR* expression based on B) their degree of steatosis (One-way ANOVA, Tukey test for multiple comparison) or C) their diabetes status (Unpaired T Test). Grouping patients depending on their F stage, we show significant down-regulation of *POR* mRNA expression when comparing healthy individuals with patients at stage F3-F4 but no significant difference between patients at stages F0-F2, even though there seems to be a trend towards similar levels as observed in patients with NAFLD F stage F3-4 (One-way ANOVA, Tukey test for multiple comparison).

5.3 POR in patients with NAFLD

5.3.1 *POR* mRNA expression

Patients with NAFLD *vs.* control showed significantly decreased mRNA expression of POR in liver biopsies (Figure 5.2A). Analysing this patient cohort based on their extent of steatosis (Figure 5.2B) and diabetes status (Figure 5.2C) we observed

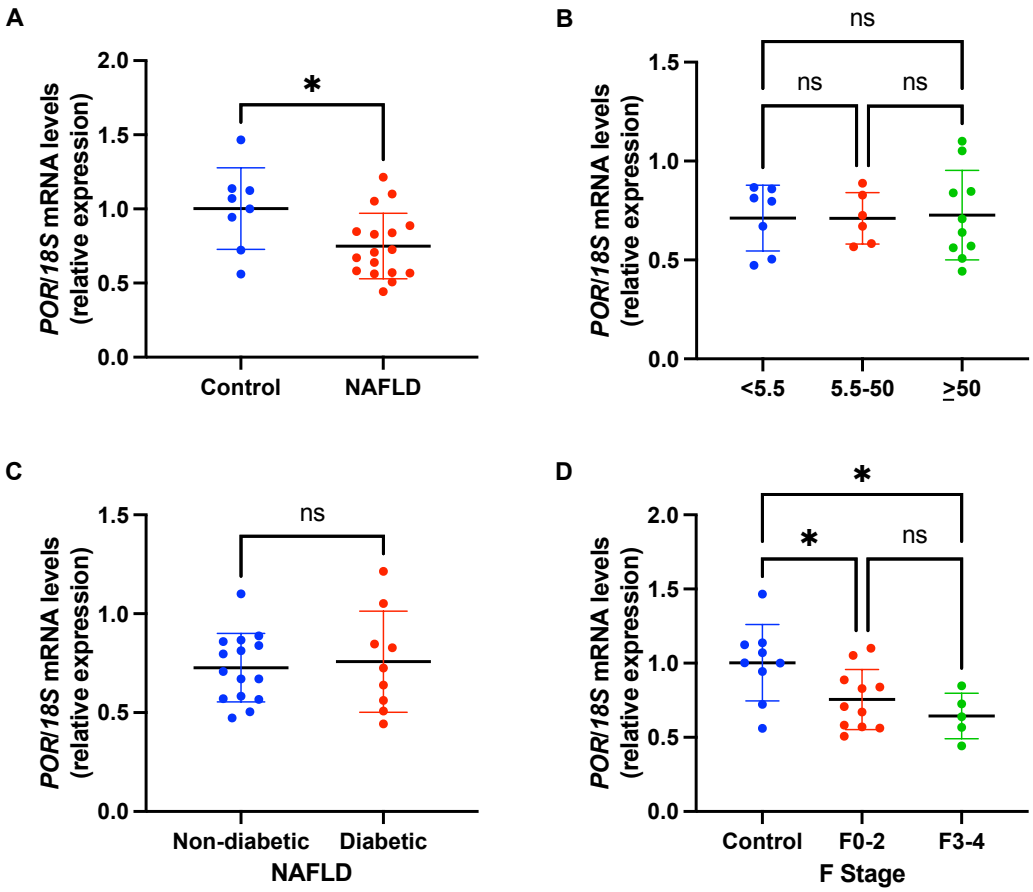


Figure 5.3: Expression of *POR* mRNA in liver biopsies is A) significantly attenuated in female patients with NAFLD compared to healthy control (Unpaired T Test). When looking at subgroups within the female NAFLD cohort there is no difference comparing *POR* expression based on B) their degree of steatosis (One-way ANOVA, Tukey test for multiple comparison) or C) their diabetes status (Unpaired T Test). Female patients with NAFLD F0-2 and F3-4 both show a significant reduction of *POR* mRNA expression compared to healthy control (One-way ANOVA, Tukey test for multiple comparison).

no significant change of *POR* mRNA expression. However, comparing control vs patients with F stage F0-2 and F3-4 a significant down-regulation at the later stages and only a trend towards lower expression at F0-2 is observed, indicating that *POR* mRNA expression falls with disease progression (Figure 5.2D). Looking at a female only cohort, checking for sex specific differences, we see similar results as in the overall cohort with a significant difference between control and patients with NAFLD at early and late stages (Figure 5.3).

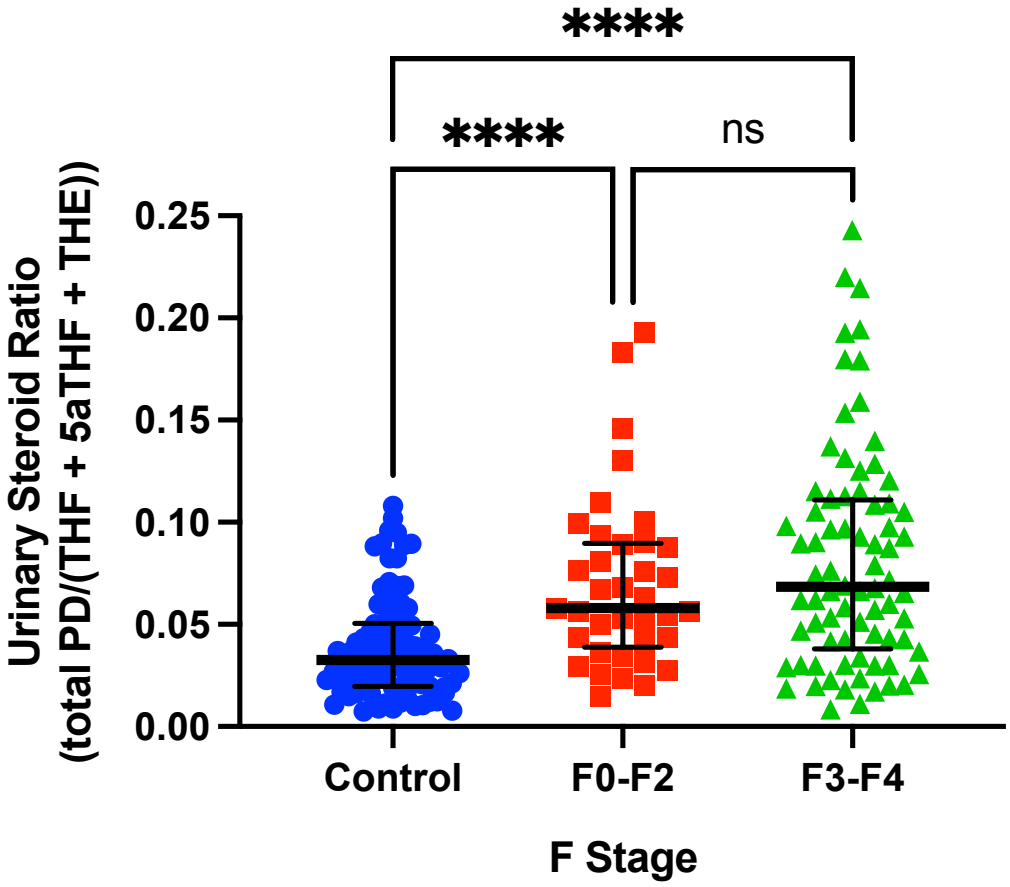


Figure 5.4: Urinary metabolites pregnanediol (total PD), the main metabolite of progesterone, divided by the sum of tetrahydrocortisol (THF), 5α-tetrahydrocortisol (5αTHF) and tetrahydrocortisone (THE) were used to form the inverse POR activity ratio. POR activity is significantly lower in healthy controls compared to patients with NAFLD F0-2 and F3-4 (One-way ANOVA, Tukey test for multiple comparison).

5.3.2 POR activity

Urinary metabolites forming the inverse POR activity ratio show a significant decrease in POR activity in patients with NAFLD compared to healthy individuals as indicated by a higher ratio of total PD divided by the sum of THF, 5αTHF and THE (Figure 5.4). The increase is present in both early and later stages of disease compared to control with the highest expression measured in patients with NAFLD F3-4 but there is no significant difference depending on F stage of

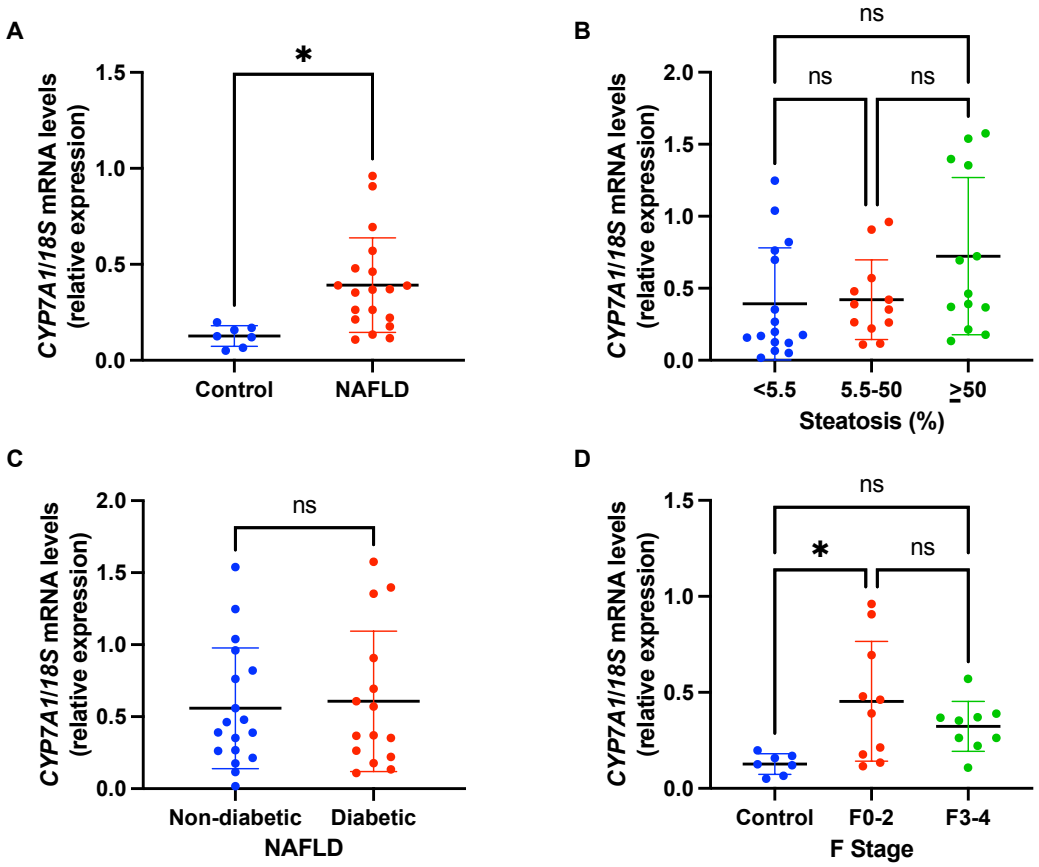


Figure 5.5: *CYP7A1* mRNA expression in liver biopsies is A) significantly increased in patients with NAFLD compared to healthy control (Unpaired T Test). When looking at subgroups within the NAFLD cohort there is no difference comparing *CYP7A1* expression based on B) their degree of steatosis (One-way ANOVA, Tukey test for multiple comparison) or C) their diabetes status (Unpaired T Test). Grouping patients depending on their F stage, we show significant up-regulation of *CYP7A1* mRNA expression when comparing healthy individuals *vs.* patients with NAFLD F0-F2 and there seems to be a trend to higher levels in patients with NAFLD F3-4 (One-way ANOVA, Tukey test for multiple comparison).

NAFLD. These results are aligned with the observed trend to lower *POR* mRNA expression seen in patients with NAFLD F0-2 and the significant decrease of *POR* mRNA expression in later stages.

5.3.3 CYP mRNA expression

CYP7A1 and *CYP7B1* mRNA expression were measured to explore the hypothesis that the extent of reduction in *POR* mRNA expression and activity as described above, would translate into compensatory up-regulation of CYP mRNA expression

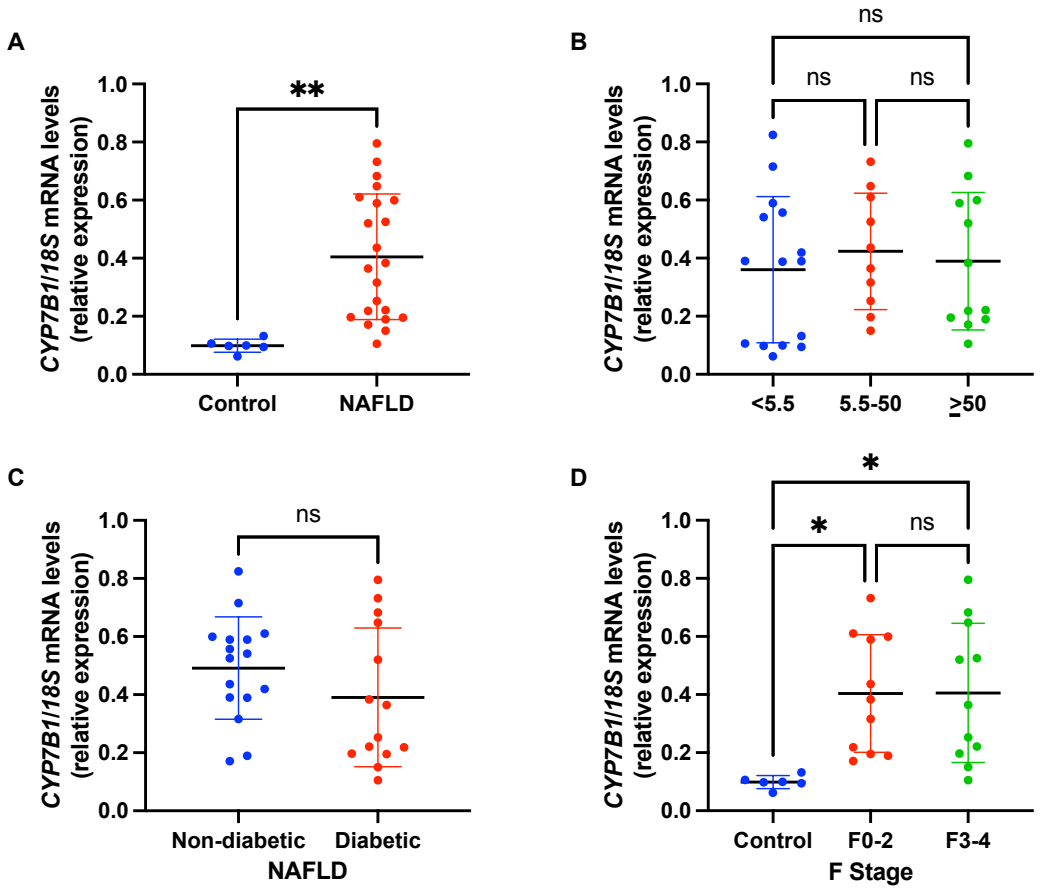


Figure 5.6: *CYP7B1* mRNA expression in liver biopsies is A) significantly increased in patients with NAFLD compared to healthy control (Unpaired T Test). When looking at subgroups within the NAFLD cohort there is no difference comparing *CYP7A1* expression based on B) their degree of steatosis (One-way ANOVA, Tukey test for multiple comparison) or C) their diabetes status (Unpaired T Test) but D) *CYP7B1* shows significant difference between both NAFLD F0-2 and F3-4 compared to healthy individuals (One-way ANOVA, Tukey test for multiple comparison).

as a result of impaired CYP activity. Our results comparing *POR* mRNA expression in liver from healthy, lean individuals *vs.* patients with NAFLD seem to corroborate such findings with significant up-regulation in both *CYP7A1* (Figure 5.5A) and *CYP7B1* (Figure 5.6A) in patients with NAFLD compared to healthy individuals. Furthermore, the analysis of patients by extent of steatosis, diabetes status and F stage seem to further underline this hypothesis with no significant changes seen dependent on level of steatosis (Figure 5.5B and 5.6B) and diabetes status (Figure 5.5C and 5.6C) but significant up-regulation in patients with NAFLD F0-2 and F3-4

compared to control (Figure 5.5D and 5.6D) in *CYP7A1* and *CYP7B1*, respectively.

5.4 POR in rodent NALFD model

A rodent NAFLD model was explored due to the underlying literature of liver steatosis in hepatic Por-null mice and the results from our human trial data. *Por* mRNA expression was significantly down-regulated in mice fed the ALIOS diet compared to normal chow (Figure 5.7A) and confirmed results shown with our human data. No sex specific changes of female (Figure 5.7B) and male (Figure 5.7C) *Por* mRNA expression and female (Figure 5.7D) and male (Figure 5.7E) protein expression were found with both female and male mRNA and protein expression significantly down-regulated. Interestingly, although male and female mice had similar *Por* mRNA levels the overall Por protein expression relative to β-actin seemed to be higher in male animals.

5.5 POR in fat loaded cell model

5.5.1 Optimisation of lipid loading

We established a lipid loading model in HepG2 cells to test our hypothesis, based on the results observed in human and rodent *in vivo* data, that lipid loading can decrease POR expression in HepG2 cells. Significantly more lipids, approximately 3 times the amount per gram of protein, were found in HepG2 cells after 800 μM OPLA2 treatment compared to vehicle and 200 μM OPLA2 and no significant difference between treatment with vehicle and 200 μM OPLA2 (Figure 5.8). For all further experiments looking at the impact of lipid loading on POR expression within HepG2 cells we used 800 μM OPLA2.

5.5.2 POR mRNA and protein expression after lipid loading

HepG2 cells had significantly lower *POR* mRNA expression and POR protein expression after lipid loading with an average decrease of around 10% and 17% in mRNA and protein, respectively (Figure 5.9), endorsing our *in vivo* data.

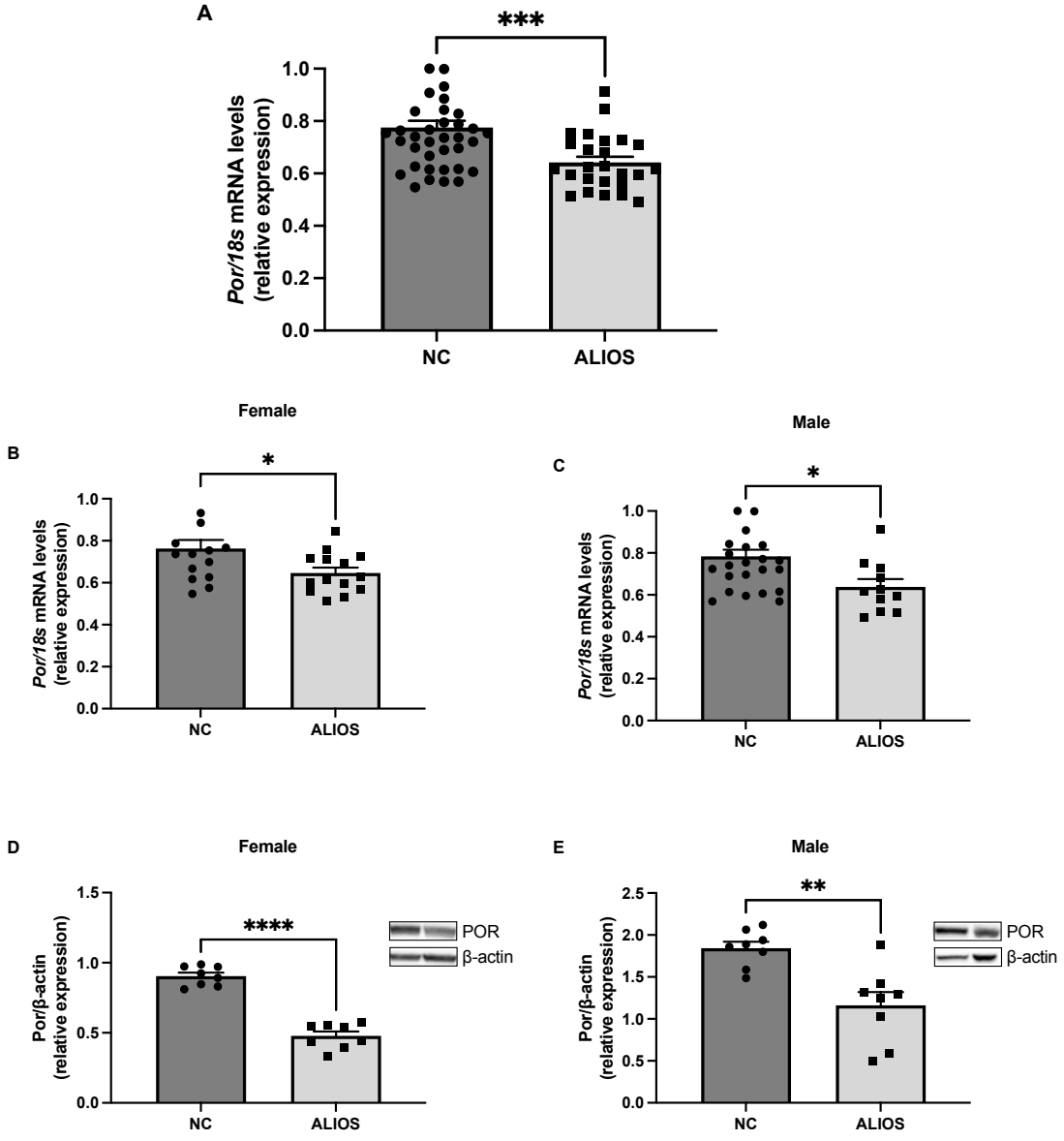


Figure 5.7: *Por* mRNA expression in the liver was measured of normal chow compared to ALIOS diet fed mice. A) Overall, *Por* mRNA expression is significantly down-regulated in ALIOS fed mice. Furthermore, mice were analysed by sex with B) female and C) male mice showing a sex independent down-regulation of *Por* mRNA expression. This was further confirmed in Por protein levels of D) female and E) male mice. Unpaired T Test was used for statistical analysis.

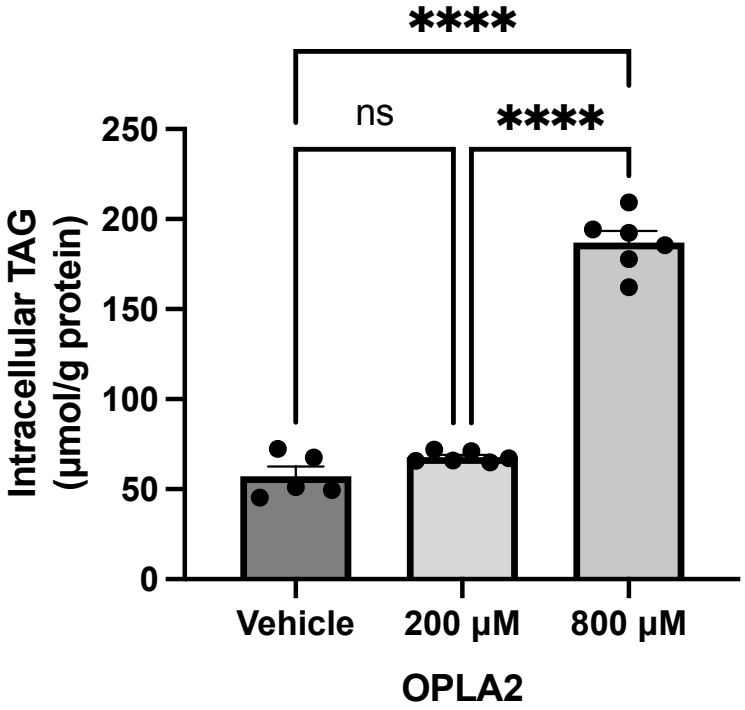


Figure 5.8: Lipid loading of HepG2 cells with vehicle or OPLA2 at 200 and 800μM. Significant difference between 800 μM OPLA2 compared to vehicle and 200 μM OPLA2 treatment (One-way ANOVA, Tukey test for multiple comparison).

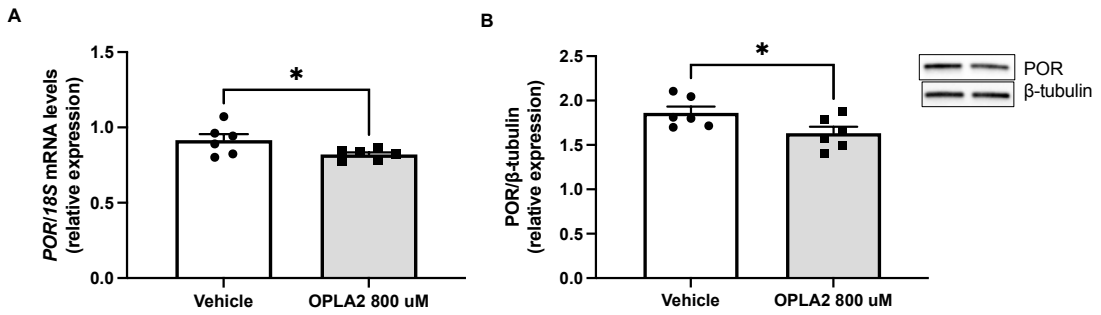


Figure 5.9: mRNA and protein of POR in HepG2 cells was analysed after 800 μM OPLA2 lipid loading. Both A) *POR* mRNA expression and B) POR protein expression was significantly down-regulated (Unpaired T Test).

5.6 Discussion

In this chapter we presented robust evidence showing lower POR expression and activity in human, rodent and cellular NAFLD models compared to control. We provided mRNA and protein expression analysis alongside functional activity from urine steroid metabolites to show that expression and activity of *POR* was down-regulated in patients with NAFLD compared to healthy individuals. These results were endorsed by a comparison of rodent *in vivo* NAFLD models to healthy animals presenting the same changes in expression data. Furthermore, we have shown that the down-regulation in POR mRNA and protein expression can be replicated in a cellular model through lipid loading HepG2 cells over 7 days. According to all of this data there does seem to be a clear association of lower *POR* expression in patients with NAFLD and NAFLD disease models. The prognostic value of POR in the context of NAFLD is still insufficiently clear. Current data from GWAS studies have not flagged *POR* [286], even though it is a very polymorphic gene, which would suggest our results in humans to be more a consequence and not necessarily a driver of disease. Still, based on prior research in mice and our results we hypothesised that the decreased POR activity in NAFLD patients may contribute to the development and progression of the disease by promoting the metabolism of lipids and unbalancing BA metabolism in ways that lead to further liver damage. Our *Por*/*POR* mRNA expression results showing *Por* and *POR* reduction most likely due to hepatocellular lipid load in both rodent model and cellular data would support such a hypothesis. Additionally, previous research in rodents having shown liver specific Por knockout to cause liver lipidosis compared to control mice [221, 281] suggests that missing enzymatic activity of Por does in fact drive fat accumulation in the liver. We therefore hypothesise that a vicious cycle of lower POR activity upon initial liver damage leads to disease progression which in turn leads to even lower *POR* mRNA expression, resulting again in even lower POR activity as observed in both human and mice data. So far it has not been determined what causes the described liver lipidosis but disruption of cholesterol de novo synthesis and degradation due to CYP disturbances could be one of the

potential causes. POR dependent CYPs such as CYP51 and CYP7A1 play a key role in cholesterol and BA biosynthesis, respectively and have been shown in mice knockout studies to be essential for normal liver function and BA composition [287, 288]. The question remains as to if impaired POR activity in NAFLD is sufficient to translate into impaired CYP activity that could have downstream phenotypic effects. This hypothesis may be supported by studies observing lower levels of circulating cholesterol and significantly reduced BA levels in hepatic Por-null mice [221, 281]. Furthermore, we now present human expression data of patients with NAFLD that have significantly up-regulated CYP mRNA expression which we argue to be a compensatory mechanism for attenuated CYP activity due to significantly lower POR activity in this patient group. The overall difficulty in understanding the pathogenesis of NAFLD is impacted significantly by the multifactorial nature of the disease. This limitation clearly needs to be considered when interpreting our results as we focused solely on POR and its downstream effects. Additionally, our human *in vivo* data analysis is a retrospective analysis and can therefore only establish association and no causation. Individuals included in the study were also not tested for specific polymorphisms that could affect CYP activity levels and potentially explain some of the variability in the clinical data. Different POR and CYP polymorphisms are population specific and show clear ethnic differences with our results mostly representing Caucasian individuals. So far Furthermore, the urinary steroid metabolite ratio we used to determine POR activity, is well suited to diagnose POR deficiency but there might be limitations to transfer its use to quantify POR activity in NAFLD. Even though the liver has the highest *POR* mRNA expression, it is closely followed by expression of the adrenal and gonads which are likely to influence the applied ratio [289]. Especially as the metabolites used within the ratio (total PD, THF, 5αTHF and THE) are mainly originating from given location. Therefore, specific hepatic POR activity needs to be explored in future research. A further limitation to total PD/(THF + 5αTHF + THE) ratio is the potential of other enzymes such as 5α-reductase, 5β-reductase and AKR1C1 to influence urinary steroid metabolites. Their activity, converting glucocorticoids

to there less active form of dihydro-metabolites or THF and THE to α-cortol and α-cortolone, respectively, has also been shown to increase in NAFLD and could therefore impact the results we present for POR [290, 291]. In NAFLD, adrenal deregulation could further play a part as chronic subclinical hypercortisolism and adrenal androgen abnormalities have been observed [292]. Overall, in the context of our NAFLD research it would be particularly interesting to have specific insights into hepatic POR activity, which the above used ratio does not provide. At present, direct POR modification has only been explored in rodent *in vivo* models or in rat hepatocytes but not yet in human hepatocytes or hepatoma cell lines.

In conclusion, our results show that POR is altered in NAFLD and suggest that changes observed in human, mouse and cell model may be important in the development and progression of NAFLD. The reduction of *POR* expression and activity we observed in humans with NAFLD emphasise the need for further exploration of POR in a human hepatoma cell model, especially in the context of prior research showing POR reduction to cause liver lipidosis. The very consistent changes seen in multiple models further underline the urgency to better understand the downstream effects of POR deactivation in a liver cell model. Based on our results we want to explore the specific effects of genetic manipulation of *POR* expression and activity on NAFLD pathogenesis, fatty acid and BA metabolism in HepG2 cell line.

6

Actions of POR on metabolic pathways

Contents

6.1 Introduction 127
6.1.1 Hypothesis and aims 129
6.2 Methods 130
6.2.1 Cell culture 130
6.2.2 Transient knockdown 130
6.2.3 Overexpression 130
6.2.4 Biochemical measurements 130
6.2.5 Lipid measurements 131
6.2.6 AdipoRed assay 131
6.2.7 Bile acid quantification 131
6.2.8 Proliferation assay 131
6.3 POR expression in HepG2 cell line 133
6.4 Transient knockdown 133
6.5 Overexpression 134
6.6 RNA sequencing 135
6.7 Lipid metabolism 140
6.7.1 Triacylglycerol 142
6.7.2 Cholesterol 146
6.8 Bile acid metabolism 149
6.9 Glucose metabolism 154
6.10 Discussion 157

6.1 Introduction

In the previous Chapter 5 we have presented first-time evidence in human, mice and cell data showing that NAFLD and a NAFLD inducing diet or cell culture conditions lead to an attenuation of POR expression on gene and protein levels as well as POR activity measurements. Considering our results and the previous

research in hepatic Por-null mice showing enlarged and fatty livers [190, 221, 280], it is still unclear if in the context of fatty liver diseases, POR expression and activity is attributable as cause or consequence. POR deficiency or knockout models have previously been looked at to understand the underlying mechanism in the context of drug, BA and cholesterol metabolism [293–295]. In vivo, results showed that POR deficiency impacts drug and steroid metabolism with impaired CYP function even though the enzymes are genotypically up-regulated [217]. The specific impact on the liver has so far been unexplored. In addition, POR attenuation in a human hepatocellular model and the effect on TAG and lipid composition have never been described. In 2021, Heintze et al. published a POR CRISPR knockdown liver cell model with very limited exploration of NALFD and its underlying mechanisms. They showed increased levels of cholesterol precursor lanosterol and the BA CDCA as well as a decrease in CA. Interestingly, they observed a transcriptional decrease of CYP enzymes which seems counterintuitive and goes against what has been shown in *in vivo* measurements [217, 296]. Finally, research showing that exogenous flavin supplementation can restore defective POR activity underlines the importance to better understand POR and its impact on NAFLD as there is a potential to directly influence outcome [297].

6.1.1 Hypothesis and aims

In this chapter I set out to explore the impact of POR manipulation on hepatocellular metabolism to better understand the mechanism that could contribute to the development of NAFLD. Based on prior results in hepatic Por-null mice I hypothesised that POR attenuation in human hepatoma cell line HepG2 will show changes in genes and proteins involved in lipid metabolism, increased TAG content and altered lipid composition. Further, I wanted to explore and validate the influence on cholesterol and BA biosynthesis. Therefore, I began establishing a cellular POR manipulation model and test how POR influences metabolism and what consequences this carries for hepatocellular phenotype.

6.2 Methods

6.2.1 Cell culture

For all experiments with POR manipulation the HepG2 cell line was used. HepG2 cells were cultured as described in Chapter 2.2.

6.2.2 Transient knockdown

Transient knockdown of *POR* was achieved transfecting HepG2 cells with *POR* siRNA at a 10 nM concentration. For *POR* siRNA optimisation silencer select (Invitrogen, Paisley, UK) siRNA1 (id: PORHSS108263), siRNA2 (id: PORHSS108264) and siRNA3 (id: PORHSS182524) were used. For *POR* siRNA knockdown experiments siRNA2 (id: PORHSS108264) was used. Detailed methods are described in Chapter 2.6.1.

6.2.3 Overexpression

Untagged *POR* or empty vector DNA plasmid at a concentration of 500 ng DNA/well was introduced via lipofection into HepG2 as POR overexpression or control model. Methods in more detail have previously been described in Chapter 2.6.3.

6.2.4 Biochemical measurements

To determine glucose, TAG, NEFA, cholesterol and 3-OHB, Instrumentation Laboratory kits (Instrumentation Laboratory, Milano, Italy) or Randox kits (Crumlin, County Antrim, UK) were used on an AU 480 Clinical Chemistry Analyzer (Beckman Coulter Ltd., High Wycombe, UK). All, assays were carried out as to manufacturer's instructions and have been described in more detail in Chapter 2.10.

Sample preparation

Cells were cultured and treated in 24-well plates. Cell lysate and cell media samples were collected, transferred into 1.5ml tubes and stored in -80°C. Samples were then used with the respective analysis kit as described in the respective subsection of Chapter 2.10.

6.2.5 Lipid measurements

Total lipid were extracted according to the method of Folch [236] and TAG, CE and PL fractions were separated using SPE as previously described by Burdge et al. 2000 [237]. Detailed extraction methods are described in Chapter 2.12.1. Quantification was performed using a 7890B GC System (Agilent Technologies; CA, USA) as described in Chapter 2.12.2. DNL was measured by GC-MS *via* [^{2}H]palmitate enrichments from ^2H_2O in the culture media using a 6890N GC System coupled to a 5973N MSD (Agilent Technologies; CA, USA). GC-MS methods in more detail can be found in Chapter 2.12.3.

6.2.6 AdipoRed assay

Intracellular lipid droplets were measured with the AdipoRed assay (Lonza, Walkersville, USA) enabling quantification of droplets in a high throughput manner. 5 µl of AdipoRed reagent were added to each well in a 96-well plate, mixed thoroughly and incubated at 37°C for 15 min. Afterwards, wells were washed with 200 µl of PBS and fluorescence with excitation at 485 nm and emission at 572 nm measured with a FLUOstar® Omega multi-mode microplate reader (BMG LABTECH Ltd., Aylesbury Bucks, United Kingdom).

6.2.7 Bile acid quantification

Total BA were first quantified with a fluorometric assay according to the manufacturer's protocol (Cell Biolabs Inc., San Diego, USA). Individual BA and specific fractions were afterwards determined with liquid chromatography–mass spectrometry as described in Chapter 2.13.

6.2.8 Proliferation assay

Proliferation was measured with a CyQUANT Direct cell proliferation assay (Invitrogen, Paisley, UK). 11.7 ml PBS, 48 µl CyQUANT Direct nucleic acid stain and 240 µl CyQUANT Direct background suppressor were combined, mixed well and kept at room temperature until use. 100 µl CyQUANT Direct 2X

detection reagent was added to each well in a 96-well plate and incubated for 60 min at 37°C. Afterwards, the FLUOstar® Omega multi-mode microplate reader (BMG LABTECH Ltd., Aylesbury Bucks, United Kingdom) was used to measure fluorescence at 508/527 nm. A standard curve of fluorescence vs. cell number was plotted to generate quantitative results.

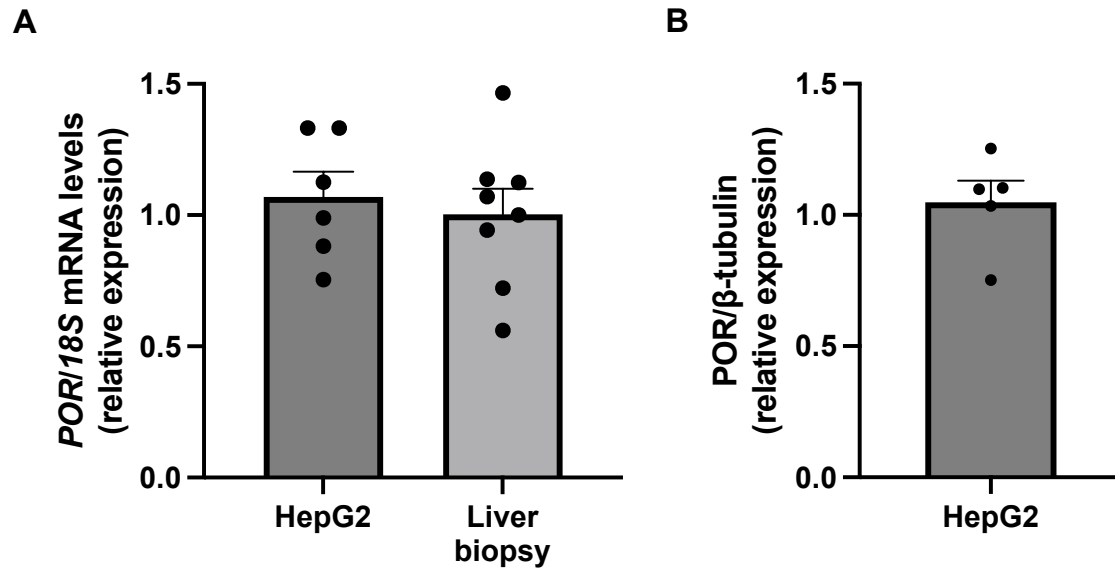


Figure 6.1: A) *POR* mRNA expression in HepG2 cells is on a comparable level as in human liver biopsies. B) POR protein is highly expressed in HepG2 cells.

6.3 POR expression in HepG2 cell line

For the creation of a cellular model, mRNA and protein expression of POR was measured in an appropriate cells line, HepG2, and *POR* mRNA compared to the mRNA expression of liver biopsies to assure their suitability to explore POR's effect on NAFLD. HepG2 cells express POR mRNA and protein as measured by qPCR and western blot. *POR* mRNA expression levels in HepG2 cells and human liver biopsy samples are on similar levels and the cell line was therefore deemed suitable and taken forward for further model development (Figure 6.1).

6.4 Transient knockdown

A POR specific transient knockdown model was established in HepG2 cells using siRNA. To explore optimal POR knockdown efficiency, we used three different POR-targeted siRNAs in a 10nM dose in HepG2 cells. *POR* siRNA1 (id: PORHSS108263), siRNA2 (id: PORHSS108264) and siRNA3 (id: PORHSS182524) achieved a reduction of *POR* mRNA 78.2%, 90.5% and 78.2% and POR protein 82.5%, 90.2% and 70.9%, respectively, compared to scrambled control. With *POR* siRNA2 showing

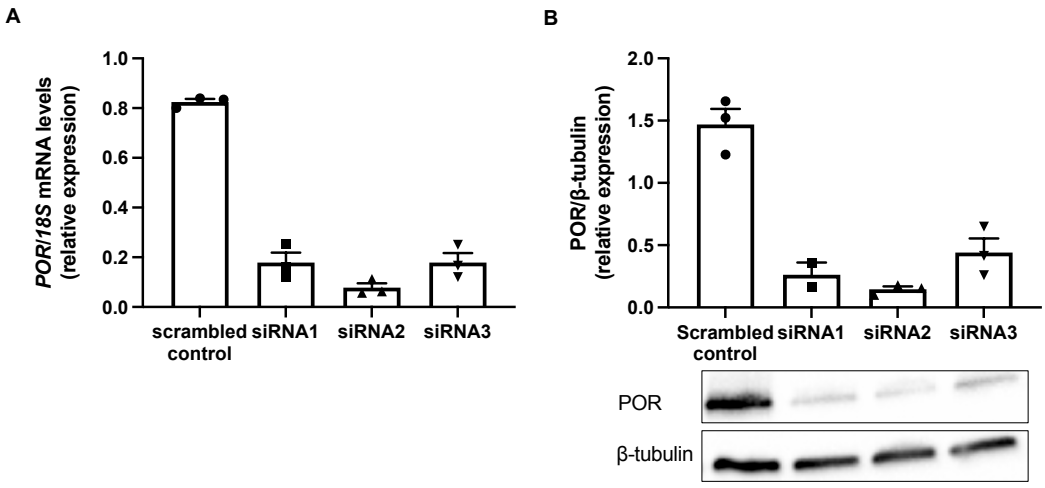


Figure 6.2: Transient knockdown optimisation of three different siRNA variants in HepG2 has been performed with siRNA2 showing the highest efficiency in both POR A) mRNA and B) protein expression.

the greatest and the most consistent effect on POR mRNA and protein expression, all further studies were undertaken using siRNA2 (Figure 6.2).

6.5 Overexpression

A POR overexpression model was established in HepG2 cells using a DNA plasmid. POR was successfully overexpressed with the addition of 500ng POR plasmid DNA as measured on mRNA and protein level. *POR* mRNA levels were elevated 60X compared to empty vector transfected cells as measured with qPCR (Figure 6.3A). POR protein expression increased by a factor 4.4 in POR plasmid transfected HepG2 cells compared to empty vector as measured with western blot (Figure 6.3B).

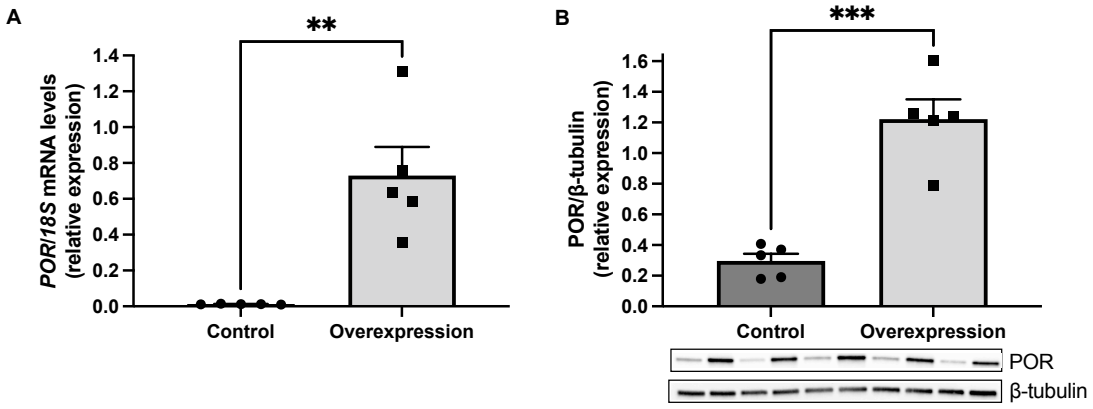


Figure 6.3: Overexpression was achieved in HepG2 cells for A) *POR* mRNA and B) POR protein with 500ng of POR DNA plasmid (Unpaired T Test).

6.6 RNA sequencing

To gain broad insight into the impact of POR reduction in hepatoma cells a transcriptome analysis was performed with RNA sequencing in *POR* siRNA-transfected and scrambled control siRNA-transfected HepG2 cells. In total, 11933 genes were found to be expressed with 11315 being expressed by both POR and scrambled control siRNA-transfected HepG2 cells. 349 sequenced transcripts, including many lncRNA and miRNA, where only found in the *POR* siRNA transfected and 269 only in the scrambled control (Figure 6.4A) group. Principal component analysis, comparing transcript expression, shows clearly separated data points for *POR* and scrambled control siRNA-transfected cells, indicative of variance being attributable to a specific difference between groups. Interestingly, principal component 1 and 2 are rather small with 23.2 % and 14.9 % respectively (Figure 6.4B) but it seems that POR and scrambled-siRNA transfection have a high impact on principal component 1 and variance in between biological replicates on principal component 2.

DESeq2 analysis identified 100 genes which are significantly differentially expressed with a multiple testing adjusted p-value ≤ 0.05 and fold change ≥ 2 as a function of *POR* siRNA knockdown compared to scrambled control. Of these

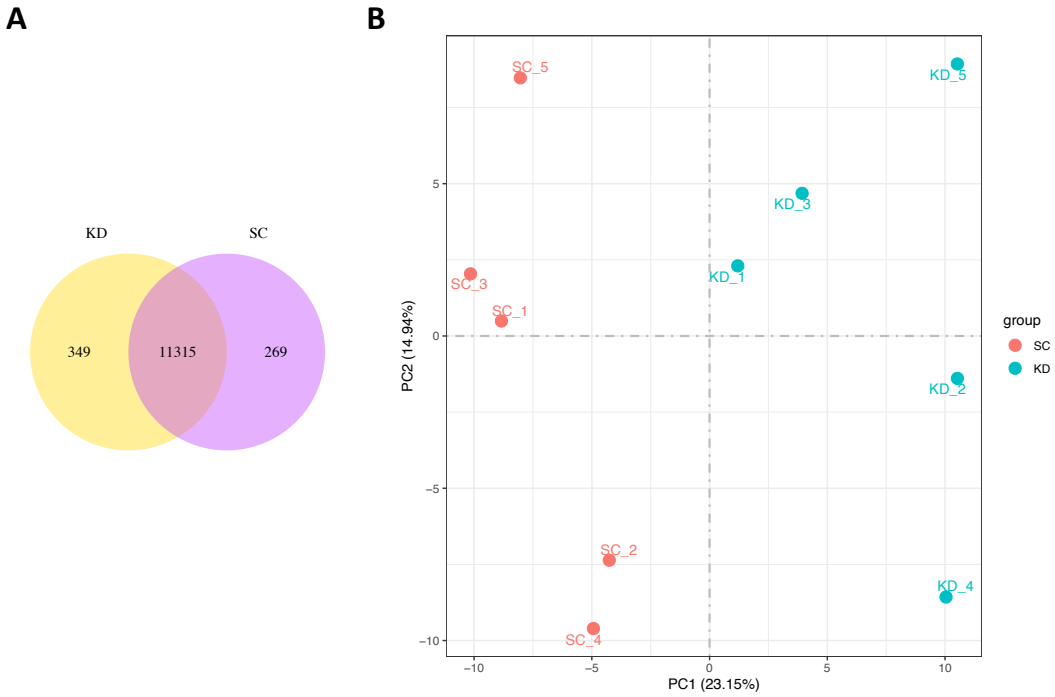


Figure 6.4: Overall, the HepG2 cells expressed A) 11933 genes with expression differences in *POR* siRNA and scrambled control transfected cells. Looking at the B) principal component analysis, the amount of variance seems to be distinctive but not overly high. On the other hand, we observed a clear separation in clusters of knockdown and control HepG2 cells, showcasing that the two treatment groups explain a big part of the genetic variance between the samples. (kd; knockdown, sc; scrambled control)

100 genes, 83 are up- and 17 are down-regulated (Figure 6.5), with the top 30 most differentially expressed genes listed in Table 6.1. For wider exploration of the impact of *POR* knockdown on the molecular processes in HepG2 several different gene functional enrichment analyses were performed. This included Gene Ontology (GO), Kyoto Encyclopedia of Genes and Genomes (KEGG) pathway analysis and DisGeNET mapping, a discovery platform containing one of the largest publicly available collections of genes and variants associated to human diseases. KEGG analysis shows significant changes in many expected pathways which should be affected by CYP impairment such as steroid hormone biosynthesis, retinol and primary BA biosynthesis. Further, genes of pathways involved in fatty acid metabolism were also identified such as PPAR signaling pathway and synthesis as well as degradation of ketone bodies (Figure 6.5C. The DisGeNET mapping interestingly revealed fatty acid, hypercholesterolaemia and steatohepatitis, next

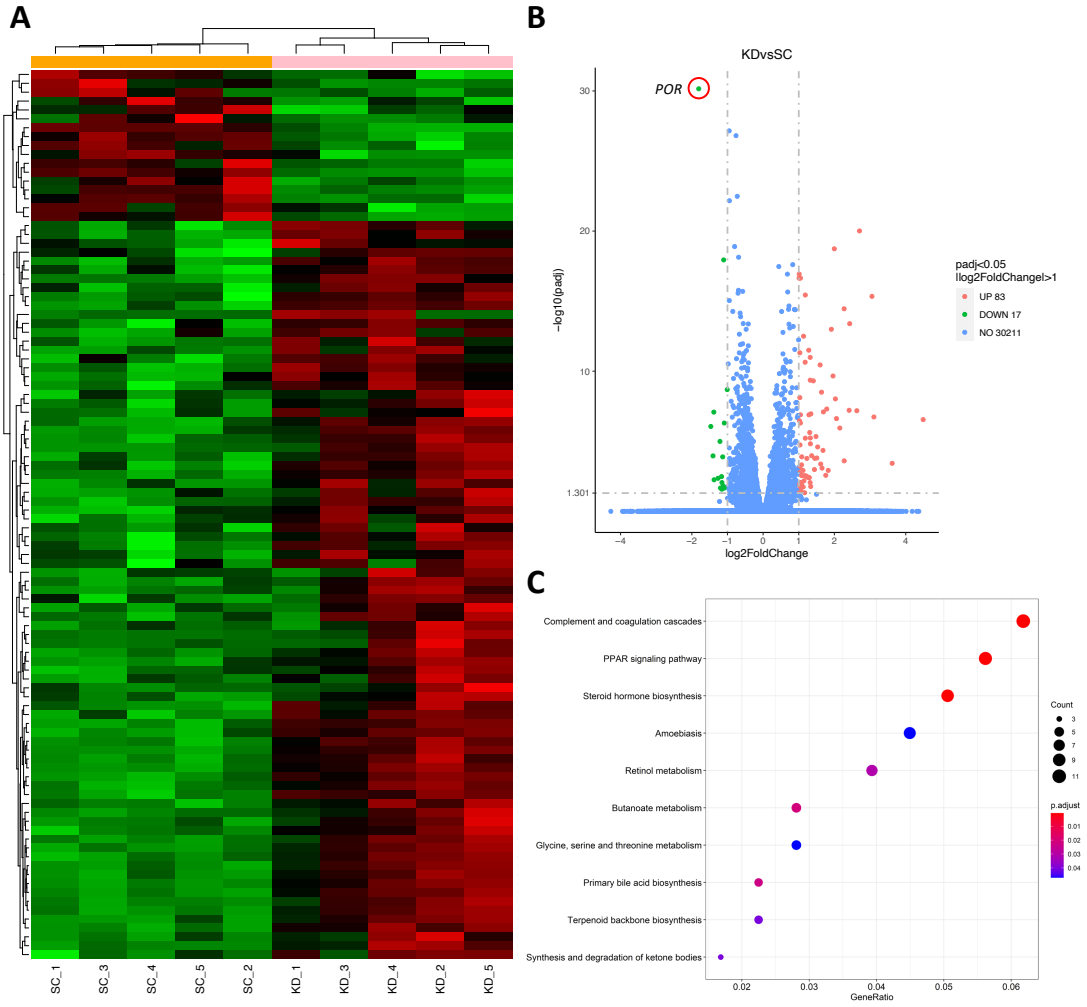


Figure 6.5: Differential expression analysis of *POR* vs scrambled control siRNA-transfected HepG2 cells shows 100 significantly up or down-regulated genes at adjusted p-value ≤ 0.05 and fold change ≥ 2. Cluster analysis was performed and displayed as a A) heat map of the expression changes (normalised counts per million) with bright red colour and bright green indicating higher and lower expression, respectively. Genes are illustrated in a B) volcano plot illustrating fold-change in expression (log2FC) against statistical significance (–log10 adjusted p-values). C) KEGG pathway analysis illustrated as a function of the ratio of differentially expressed genes to all genes contributing to each annotated KEGG pathway. The colour gradient of the dot plot is defined by the statistical significance of pathway enrichment and the size of the individual dot represents the number of genes contributing to each annotated pathway. DESeq2 (Wald Test) was used for differential gene expression analysis.

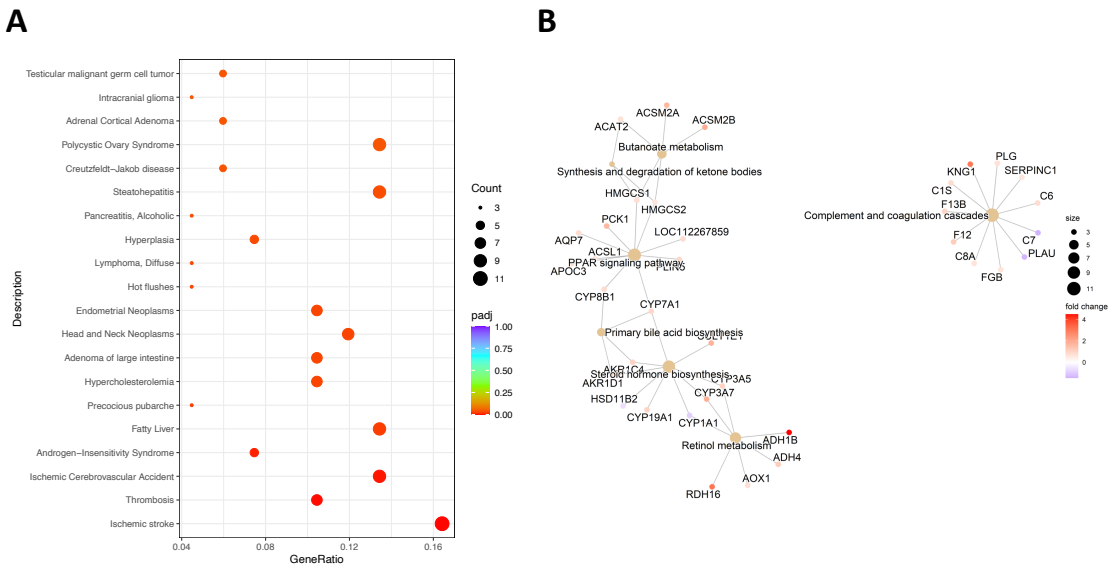


Figure 6.6: Transcriptomic profile of *POR* knockdown HepG2 cells associated with steatohepatitis and fatty liver disease according to the A) DysGeNET database mapping. B) CNET plot based on the top KEGG pathways indicates to two major groups with one being mostly CYP involved pathways.

to vascular-metabolic diseases such as stroke, to be the most strongly associated diseases with such a transcriptomics profile (Figure 6.6A). Depicting the KEGG pathway network through a CNET plot "complement and coagulation cascades", and CYP associated groups "PPAR, retinoids and bile acids" are flagged (Figure 6.6B). These two groups are again in line with the most prominent groups in the DysGeNET analysis. Overall, having shown broad deregulation in *POR* siRNA-transfected HepG2 cells we decided to further explore the lipid metabolism and content, BA composition and glucose metabolism.

Table 6.1: Top 40 expressed CYP genes in HepG2 *POR* siRNA knockdown

Gene ID	Gene name	padj	log2FoldChange
ENSG00000127948	POR	5.05E-35	-1.806198652
ENSG00000137869	CYP19A1	1.18E-17	1.011412213
ENSG00000186529	CYP4F3	3.18E-13	1.134353698
ENSG00000186115	CYP4F2	4.34E-10	1.321524062
ENSG00000021461	CYP3A43	9.44E-09	2.027441886
ENSG00000186204	CYP4F12	5.60E-08	0.664371272
ENSG00000106258	CYP3A5	3.49E-07	1.022976034
ENSG00000180432	CYP8B1	6.10E-07	0.850628135
ENSG00000171903	CYP4F11	0.000251774	0.421558561
ENSG00000073067	CYP2W1	0.000867514	-0.310795317
ENSG00000160870	CYP3A7	0.001193048	1.826984507
ENSG00000167910	CYP7A1	0.00140995	0.914316804
ENSG00000140465	CYP1A1	0.009095717	-0.917622555
ENSG00000001630	CYP51A1	0.019006368	0.341999811
ENSG00000134716	CYP2J2	0.030377029	0.489600165
ENSG00000100197	CYP2D6	0.152388585	0.520147442
ENSG00000233588	CYP51A1P2	0.174402693	0.737839205
ENSG00000241095	CYP51A1P1	1	1.183134563
ENSG00000140459	CYP11A1	0.210390014	0.436682158
ENSG00000108242	CYP2C18	1	3.273546074
ENSG00000255974	CYP2A6	1	-2.257163828
ENSG00000155016	CYP2U1	0.360665194	0.206263336
ENSG00000248313	CYP4F27P	1	-2.470762848
ENSG00000269516	CYP4F23P	1	0.727045037
ENSG00000268529	CYP2T3P	1	2.797081964
ENSG00000138061	CYP1B1	1	1.534358199
ENSG00000130649	CYP2E1	1	-0.737497387
ENSG00000233622	CYP2T1P	1	0.745322851
ENSG00000186104	CYP2R1	0.518265519	0.221703947
ENSG00000215223	CYP51A1P3	1	-2.153232847
ENSG00000160868	CYP3A4	1	-0.637471532
ENSG00000188693	CYP51A1-AS1	1	0.628556168
ENSG00000036530	CYP46A1	1	1.850730848
ENSG00000146233	CYP39A1	1	1.136484862
ENSG00000186377	CYP4X1	1	2.181840259
ENSG00000167600	CYP2S1	0.64730485	-0.393061695
ENSG00000148795	CYP17A1	1	0.56323692
ENSG00000095596	CYP26A1	1	2.092105296
ENSG00000138109	CYP2C9	1	1.217868328
ENSG00000003137	CYP26B1	1	-0.328183095

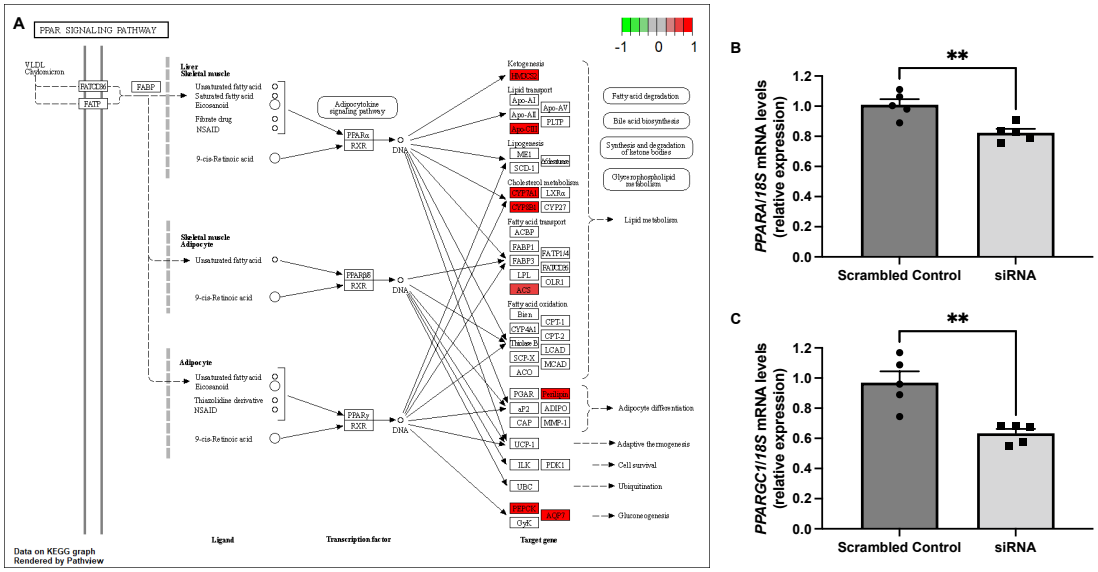


Figure 6.7: Pathway analysis of *PPARA*, *PPARD* and *PPARG* shows significant up-regulation of multiple downstream enzymes which lead us to validate *PPARA* and *PGC-1α* with qPCR. Both show a significant down regulation in *POR* siRNA-transfected cells compared to scrambled control (Unpaired T Test).

6.7 Lipid metabolism

Based on the KEGG results, showing broad up-regulation of genes downstream in the PPAR pathway (Figure 6.7A), *PPARA*, an important lipid metabolism regulator, and Peroxisome proliferator-activated receptor gamma coactivator 1α (*PGC-1α*), involved in regulation of energy metabolism, mitochondrial biogenesis and gluconeogenesis, were looked at in more detail using qPCR analysis. We were able to show a significant down-regulation of *PPARA* and *PGC-1α* in the *POR* siRNA-transfected cells compared to scrambled control.

Furthermore, we looked at AMPK, another important regulator of lipid metabolism in the liver, and one of its target enzyme ACC. Upon phosphorylation, AMPK phosphorylates and thereby inactivates ACC limiting the malonyl CoA production and DNL. As a result of lower malonyl CoA production *CPT1A* is up-regulated, an enzyme controlling a rate limiting step in β-oxidation. Our results show no difference in RNA sequencing (not shown) and in total protein expression of both AMPK and ACC but a significant increase of phosphorylated AMPK and

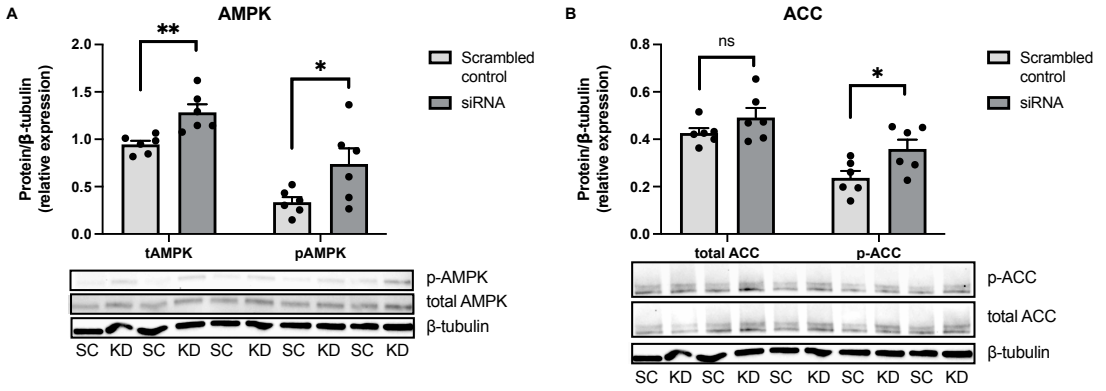


Figure 6.8: AMPK and its downstream target ACC did not show changes in transcriptomics analysis. Total protein expression of A) AMPK is increased and B) ACC is unchanged in *POR* siRNA-transfected compared to scrambled control siRNA-transfected HepG2 cells but both A) phosphorylated AMPK (p-AMPK) and B) phosphorylated ACC (p-ACC) are significantly up-regulated. Unpaired T Test was used for statistical analysis.

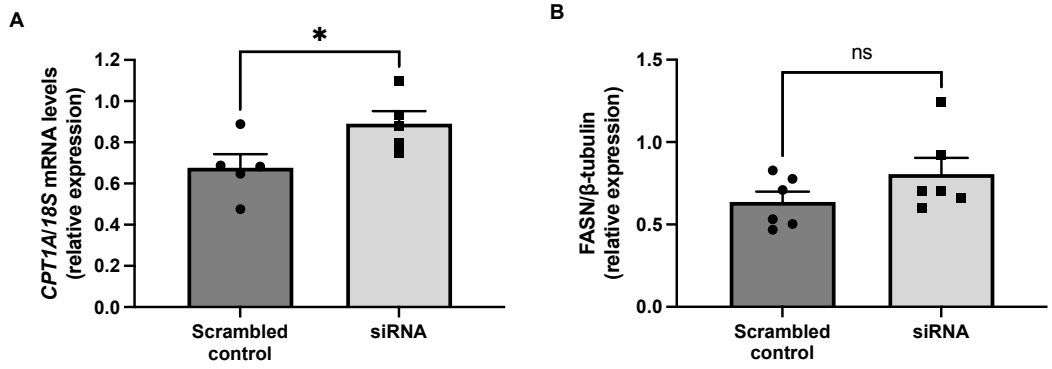


Figure 6.9: Marker for β-oxidation, A) *CPT1A*, is significantly up-regulated in POR vs scrambled control siRNA-transfected HepG2 cells, whereas DNL marker B) FASN showed no significant difference (Unpaired T Test).

its downstream product phosphorylated ACC in *POR* siRNA-transfected cells compared to control (Figure 6.8).

In line with these results, we observed increased *CPT1A* mRNA expression which indicates higher β-oxidation (Figure 6.9A). We further explored FASN, a marker of DNL, which remained unchanged after *POR* siRNA tranfection of HepG2 cells (Figure 6.9B). These results show that lipid metabolism is impacted on multiple critical levels upon POR reduction by siRNA transfection and experiments to determine cellular lipid content seemed justified. siRNA-transfected HepG2 cells impacts

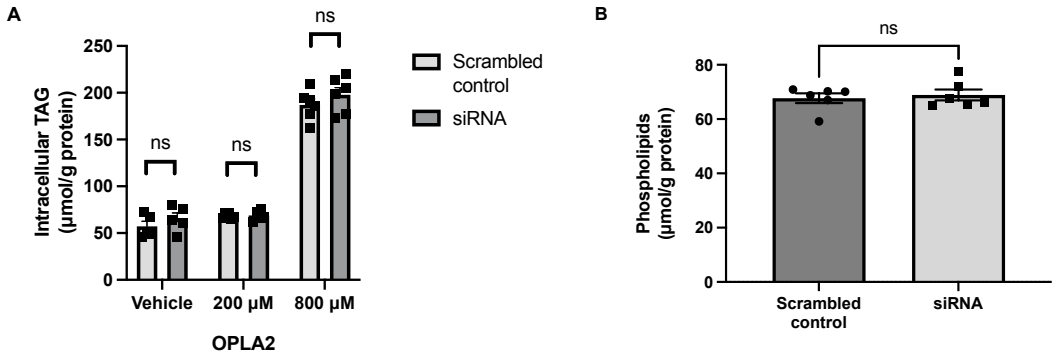


Figure 6.10: Lipid measurements of A) TAG and B) phospholipids with GC showed no difference between POR and scrambled control siRNA-transfected HepG2 cells (Unpaired T Test). Multiple culturing conditions with different levels of OPLA2 and without any lipids were tested but showed no significant impact on TAG.

6.7.1 Triacylglycerol

Having clearly established deregulated lipid metabolism pathways we measured intracellular TAG and phospholipids via GC in *POR* siRNA transfected HepG2 cells to understand the impact on the lipid phenotype of HepG2 cells. *POR* siRNA-transfection did not alter the TAG lipid content adjusted for protein of HepG2 cells compared to scrambled control siRNA-transfected cells while being treated with standard culture media (SC vs KD; 57.2 vs 65.3 μmol/g) or culture media with OPLA2 at doses of 200 μM (SC vs KD; 67.8 vs 68.9 μmol/g) or 800 μM (SC vs KD; 186.9 vs 197.7 μmol/g) (Figure 6.10A). PL (SC vs KD; 67.7 vs 68.8 μmol/g) were also not impacted by *POR* siRNA knockdown when culturing HepG2 in standard culture media supplemented with 200 μM OPLA2 (Figure 6.10B).

Seeing no difference in GC lipid analysis, cellular lipid content was validated with a second method. Using an AdipoRed assay intracellular lipid droplets of HepG2 cells cultured with 200 μM OPLA2 supplemented into standard culture media were successfully stained. No difference of lipid droplets quantity during visual inspection and fluorescence-based quantification using a plate reader was observed between HepG2 cells transfected with POR or scrambled control siRNA in line with results from GC analysis (Figure 6.11).

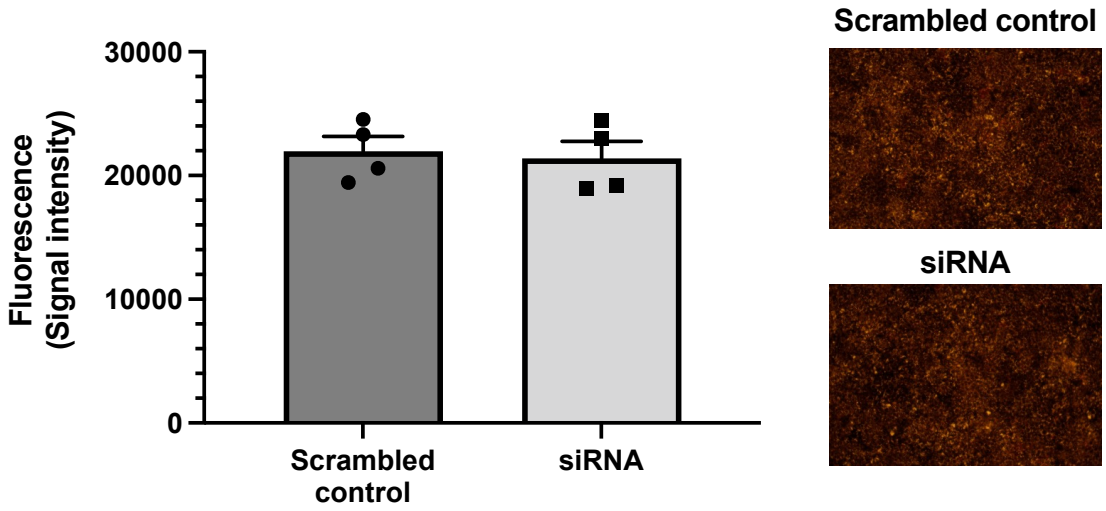


Figure 6.11: AdipoRed assay successfully stained intracellular lipid droplets. No difference was observed between *POR* siRNA and scrambled control siRNA-transfected HepG2 cells (Unpaired T Test).

De novo lipogenesis

Having shown a reduction of *PPARA* and higher expression levels of p-AMPK, p-ACC and *CPT1A* but no difference in cellular lipid content emphasised the need to better understand DNL. [2H]palmitate enrichments were measured by GC-MS in HepG2 cells with deuterium containing media to calculate deuterium inclusion into palmitate. HepG2 cells which were cultured with standard culture media or culture media containing 200 μM or 800 μM OPLA2 showed clear suppression of DNL in a dose dependent manner dependent on fatty acid content (F value; vehicle: 0.87, OPLA2 200 μM: 0.56, OPLA2 800 μM: 0.19). Transfection of *POR* siRNA compared to scrambled control siRNA showed a small but significant difference of DNL when cultured without fatty acids (SC vs KD; 0.87 vs 0.85 F value). When cultured with fatty acids at concentrations 200 μM OPLA2 (SC vs KD; 0.56 vs 0.59 F value) or 800 μM OPLA2 (SC vs KD; 0.19 vs 0.18 F value) no difference in DNL was measured in *POR* siRNA knockdown compared to scrambled control (Figure 6.12).

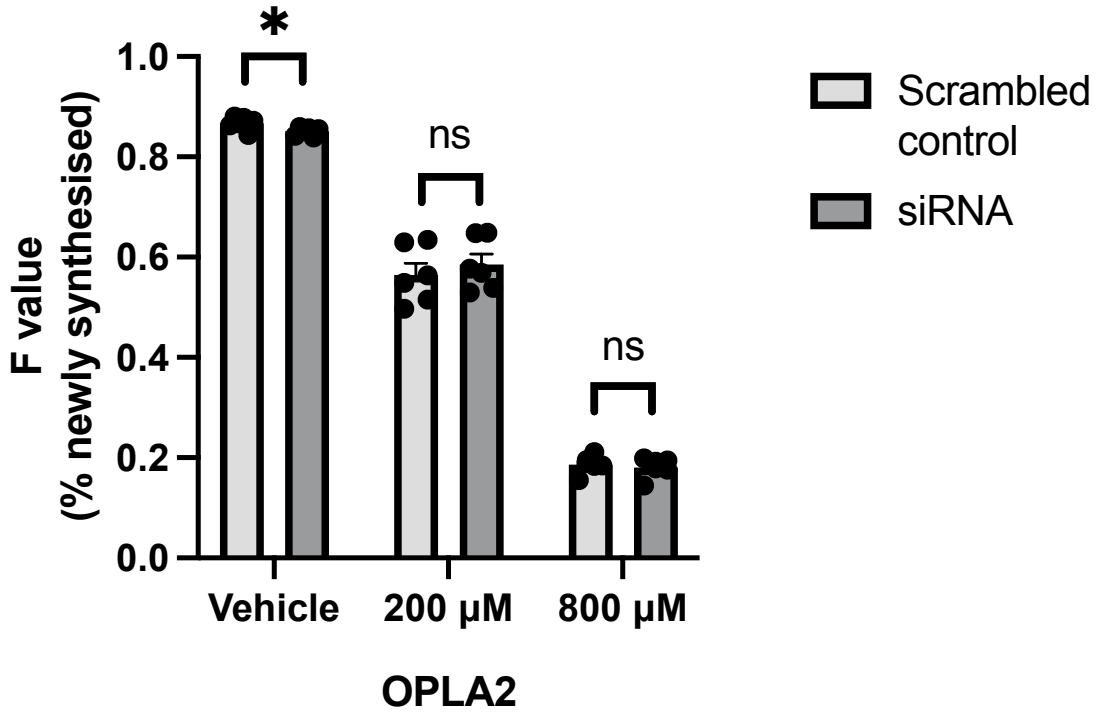


Figure 6.12: DNL is displayed as F value (% newly synthesised palmitate) showing a clear dose dependent DNL suppression based on fatty acid concentration in culture media. POR vs scrambled control siRNA-transfection shows a small significant ($p = 0.03$) down-regulation in HepG2 cells cultured without OPLA2 in media, in others DNL was unchanged (Unpaired T Test).

Cellular lipid secretion, uptake and β-oxidation

Corresponding media samples of prior lipid content and DNL experiments show significantly increased free TAG concentrations (SC vs KD; 13.5 vs 17.9 μM/mg), higher NEFA (SC vs KD; 4.5 vs 7.2 μM/mg) and 3-OHB (SC vs KD; 2.5 vs 4.7 μM/mg) of HepG2 cells cultured with 200 μM OPLA2 when transfected with *POR* siRNA compared to scrambled control siRNA (Figure 6.13). These results indicate an increased TAG secretion and reduced fatty acid uptake of HepG2 upon POR knockdown as NEFA is not secreted by hepatocytes and TAG has not been supplemented but both are found in higher concentration in the media. In addition, elevated 3-OHB indicates increased β-oxidation in line with increased p-AMPK, p-ACC and *CPT1A* (Figures 6.8 and 6.9).

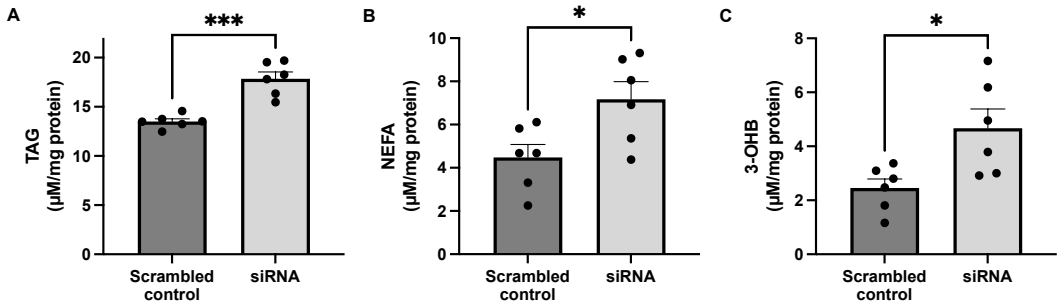


Figure 6.13: Significant increases in POR vs scrambled control siRNA-transfected cells of A) TAG, B) NEFA and C) 3-OHB were observed in samples from cell culture media initially substituted with 200 μM OPLA2. This indicates lower uptake of lipids as well as increased β-oxidation. Unpaired T Test was performed for statistical analysis between scrambled control and *POR* siRNA transfection.

TAG composition

Having determined that there is no difference in cellular TAG and PL lipid content but a differentially regulated lipid metabolism with slight suppression of DNL (in cells fed no OPLA2 in media) and an increase in β-oxidation we further screened the RNA sequencing data for significantly differentially expressed genes which have an impact on lipid composition known to impact NAFLD. Elovl6, the enzyme controlling the rate limiting step of C12-C16 fatty acid elongation by C2, showed an mRNA expression increase by factor 1.44 with an adjusted p-value < 0.0001 (Figure 6.14A). Investigating the C16 and C18 fatty acids we observed no difference in composition in *POR* siRNA knockdown to scrambled control cells (Figure 6.14B). In general, there is no observable change in TAG and PL composition (data not shown).

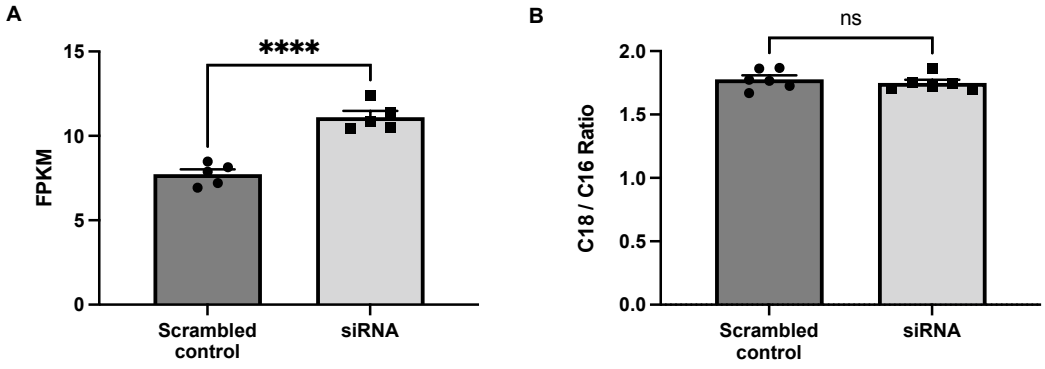


Figure 6.14: TAG composition is unaffected by a significant increase of A) *ELOVL6* as shown by C18/C16 ratio formed by the sum of C18:0 and C18:1 divided by the sum of C16:0 and C16:1 (Unpaired T Test).

6.7.2 Cholesterol

RNA sequencing clearly shows multiple key elements of cholesterol biosynthesis as well as apolipoproteins that are significantly up-regulated (circled red in Figure 6.15A) and receptors responsible for cholesterol up take into hepatocytes that are down-regulated (circled green in Figure 6.15A) in cells which were transfected with *POR* siRNA knockdown when compared to scrambled control transfected cells.

HMGCR (fold change (fc) 1.45, adjusted p value (padj) < 0.0001), the gene of the first rate-limiting enzyme of cholesterol synthesis, *FDFT1* (fc 1.35, padj $<$ 0.0001), the gene coding for the cholesterol biosynthesis enzyme forming squalene, and *SQLE* (fc 1.17, padj = 0.008), the gene for the second rate-limiting enzyme in cholesterol synthesis, providing evidence for disturbed cholesterol biosynthesis (Figure 6.15B). For SQLE to function, it obtains an electron from POR but SQLE is believed to be able switch at least partially to cytochrome b5 as an electron donor [197]. Interestingly, we also observed significant down-regulation of *LRP1* (fc 0.66, padj < 0.0001) and trends towards lower expression in both *LDLR* and *SCARB1* which would indicate lower cholesterol uptake (Figure 6.15B). Validating selected genes with qPCR, we were able to confirm results from RNA sequencing with

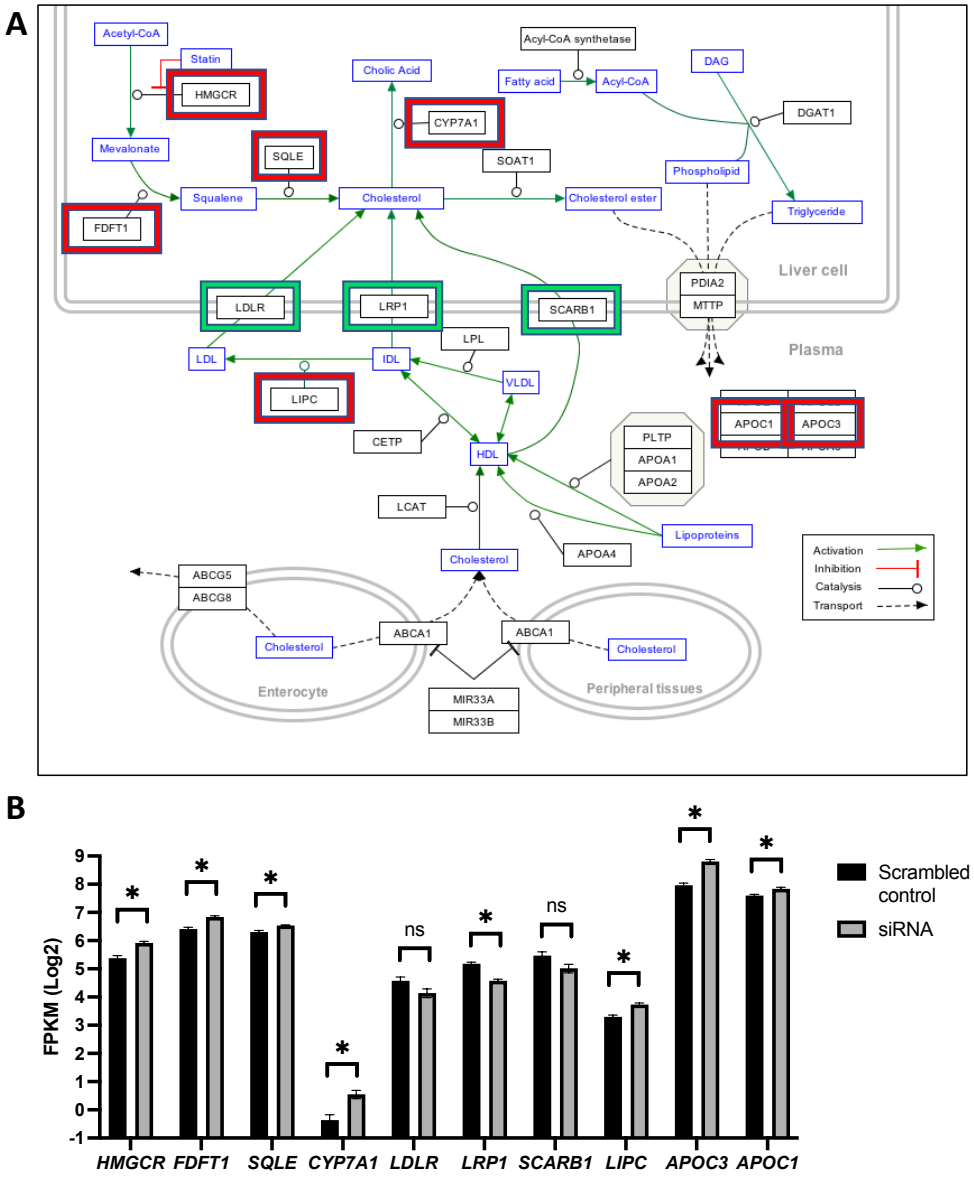


Figure 6.15: A) Gene overview of cholesterol biosynthesis, transport and utilisation. Up and down-regulated genes are circled red and green, respectively. Figure adapted from WikiPathways Statin inhibition of cholesterol production (WP430). B) RNA sequencing results presented as Fragments Per Kilobase of transcript per Million mapped reads (FPKM) and deemed significant if p-value corrected for multiple testing (padj) ≤ 0.05.

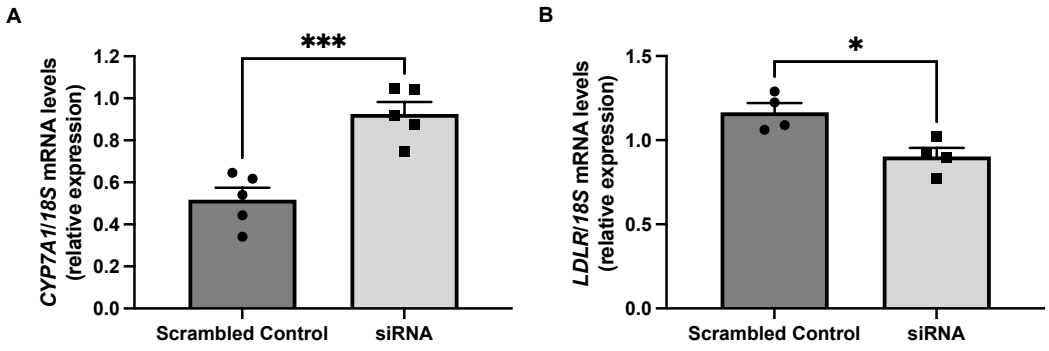


Figure 6.16: Expression of A) *CYP7A1* was significantly up-regulated and B) *LDLR* significantly down-regulated as measured by qPCR and confirms results observed in RNA sequencing (Unpaired T Test).

significant up-regulation of *CYP7A1* (Figure 6.16A) and significant down-regulation in *LDLR* (Figure 6.16B) in *POR* siRNA knockdown cells.

The gene changes described indicate an increase in cholesterol biosynthesis or compensatory up-regulation due to impaired cholesterol synthesis and down-regulation of cholesterol uptake underpinning the importance to determine cholesterol concentrations within our experiments. Using an ILab 650 Clinical Chemistry analyzer and a GC analyzer, total cellular cholesterol, cholesterol ester and cholesterol in cell media were measured. We observed a significant increase in the culture media of *POR* siRNA-transfected HepG2 cells but no change in total cholesterol and cholesterol ester (Figure 6.17). These results underpin the expression results obtained for *LRP1*, *LDLR* and *SCARB1*.

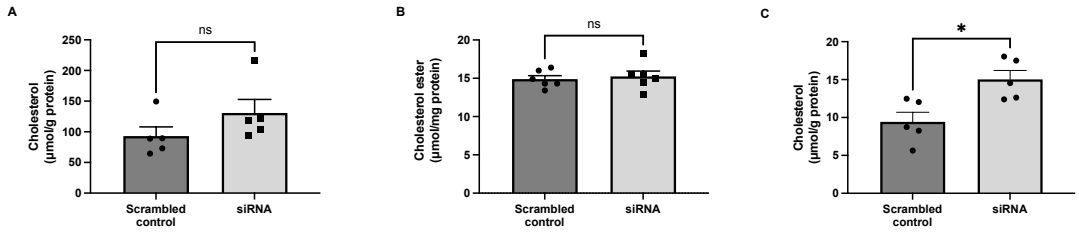


Figure 6.17: Cholesterol was measured as A) total cellular cholesterol (p-value = 0.19), B) cholesterol ester (p-value = 0.61) and C) the cholesterol in the cell culture media (p-value = 0.01). None of the cellular cholesterol was significantly different between the two treatment groups but a significant increase in media cholesterol was shown (Unpaired T Test).

6.8 Bile acid metabolism

CYPs are essential in the metabolism of BA and their disruption upon POR suppression has been observed in humans [272, 277–279]. Therefore, our results showing significantly higher expression of the rate limiting enzyme *CYP7A1* and other critical enzymes such as *CYP8B1*, *AKR1D1* and *AKR1C4* in the BA biosynthesis pathway is in line with compensatory up-regulation due to impaired enzyme function (Figure 6.18).

Validation with qPCR reaffirmed above observations with significant mRNA up-regulation of *CYP7A1* (fc 1.79, $p < 0.001$), *AKR1D1* (fc 1.38, $p = 0.02$) and *AKR1C4* (fc 2.09, $p < 0.001$) expression (Figure 6.19). Furthermore, expression of *NR1H4* (fc 1.28, $p = 0.04$), the gene coding for FXR, is also significantly increased (Figure 6.19). Looking at FXR downstream targets such as SHP, MRP2, MDR3, UGT2B4, BAT or BACS no activation can be observed (data not shown).

Due to prior literature reporting changes in BA composition and the deregulation of BA metabolism as measured above, we determined BA concentration in cell culture media and showed a significant up-regulation of total BA. When separating total BA into unconjugated and conjugated BA, no difference in conjugated but a significant increase in unconjugated BA is observed (Figure 6.20).

Further segmenting into individual BA shows a significant 1.92-fold increase of CDCA ($p = 0.002$) in *POR* siRNA-transfected cells compared to scrambled

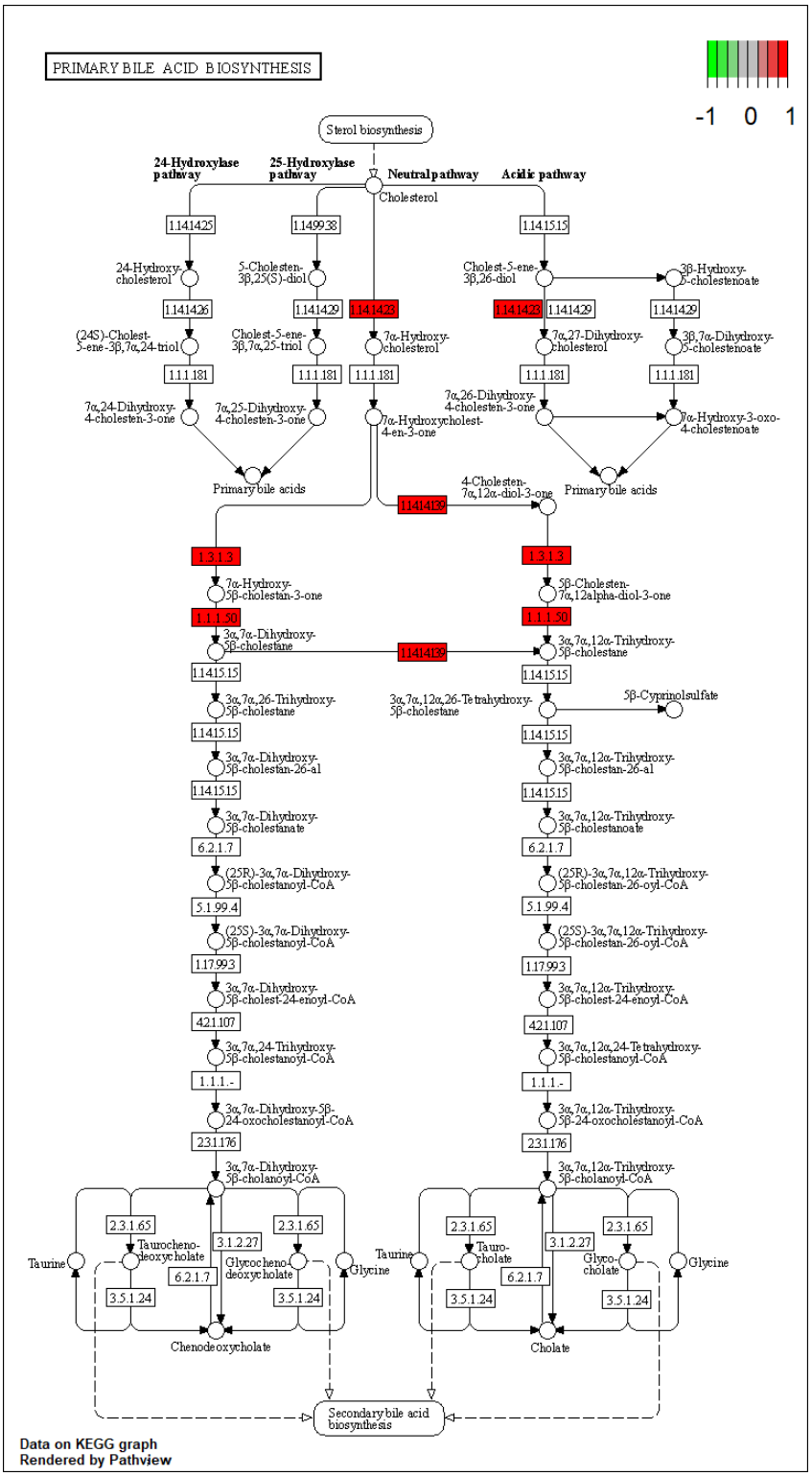


Figure 6.18: Bile acid biosynthesis KEGG pathway. CYP7A1 (1.14.14.23), CYP8B1 (1.14.14.139), AKR1D1 (1.3.1.3) and AKR1C4 (1.1.1.50) have a significantly higher expression in HepG2 cells with *POR* siRNA knockdown compared to scrambled control.

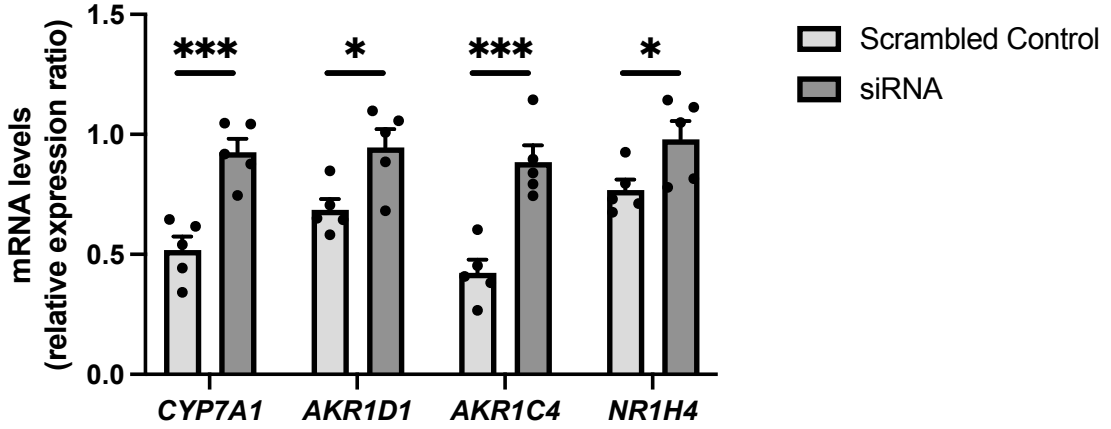


Figure 6.19: Significant increase of bile acid biosynthesis gene expression in qPCR: *CYP7A1* (fc 1.79, $p = 0.01$), *AKR1D1* (fc 1.38, $p = 0.01$) and *AKR1C4* (fc 2.09, $p < 0.01$). The gene coding for FXR, a negative regulator of CYP7A1, *NR1H4* showed increased expression (fc 1.28, $p = 0.01$). Unpaired T Test was used for statistical analysis.

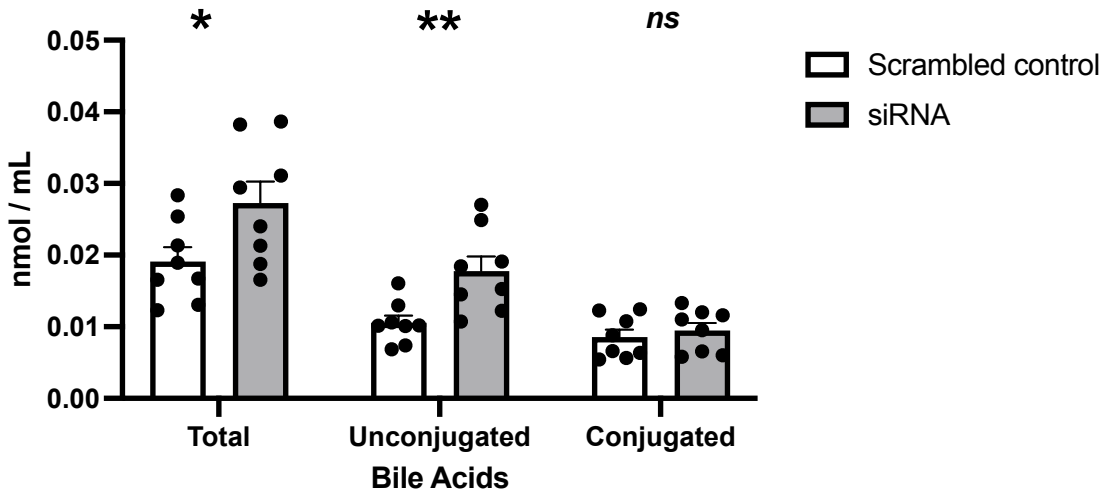


Figure 6.20: Significant increase in total bile acid concentration. Subdividing bile acids into conjugated and unconjugated shows that the increase in total bile acids stems from significantly higher levels of unconjugated bile acids (Unpaired T Test).

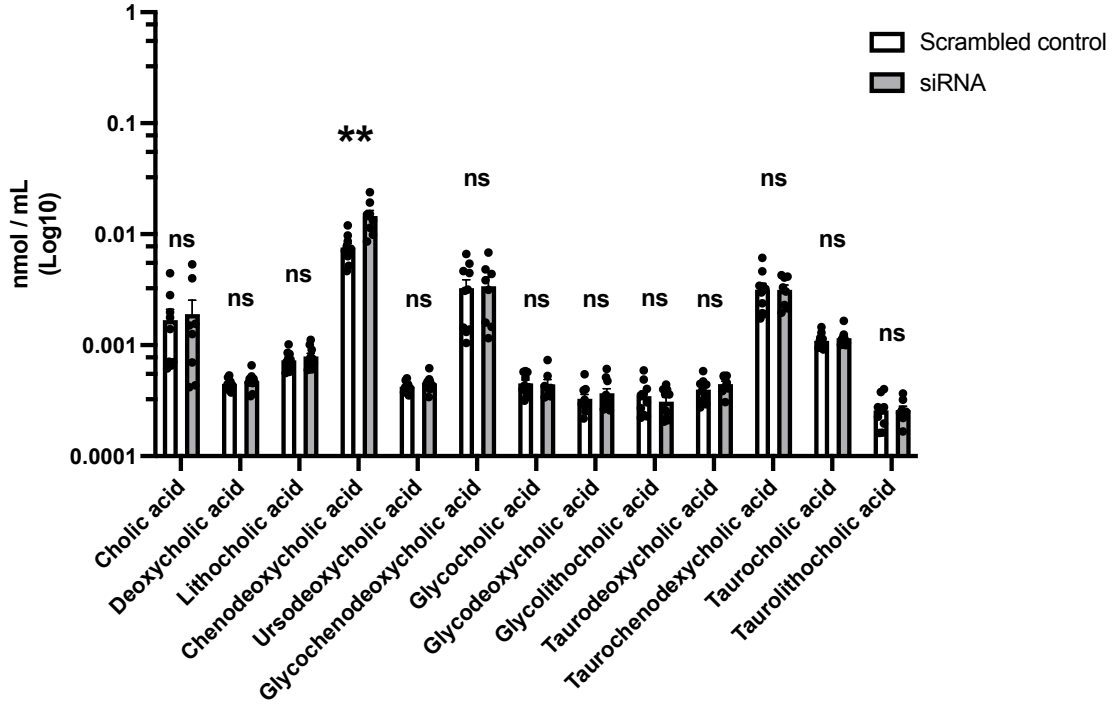


Figure 6.21: Using liquid chromatography–mass spectrometry individual bile acids were measured, showing a significant increase of chenodeoxycholic acid (fc 1.92, $p = 0.002$). Other bile acids were unchanged after *POR* siRNA-transfection compared to scrambled control siRNA-transfected HepG2 cells. Statistical analysis was performed using a Two-way ANOVA with a Šídák's multiple comparisons test (chenodeoxycholic acid $p < 0.0001$) and was also significant when using an Unpaired T Test (chenodeoxycholic acid $p = 0.001$).

control. All other BA are unchanged in cell media. As shown above (Figure 6.18) CYP8B1 is up-regulated. Therefore, we investigated S12α-hydroxylated and non-12α-hydroxylated BA, showing a significant increase of non-12α-hydroxylated BA (Figure 6.22 and a significantly lower 12α-hydroxylated to non-12α-hydroxylated BA ratio (Figure 6.22B).

In a POR overexpression model, no differences in total, conjugated or unconjugated BA were observed between POR overexpressed HepG2 cells and empty vector transfected cells (Figure 6.23A). Looking specifically at CDCA, which showed a significant increase in *POR* siRNA knockdown, we observed a significant attenuation of CDCA levels in the POR overexpression model (Figure 6.23), underlining the

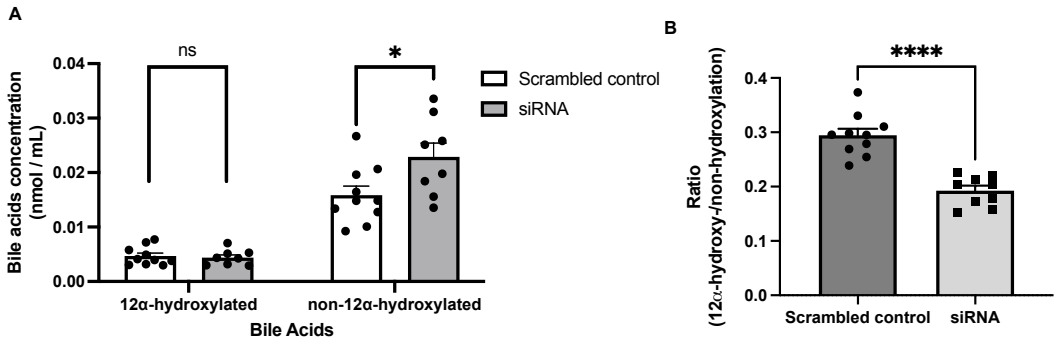


Figure 6.22: Non-12α-hydroxylated bile acids showed a significant increase while 12α-hydroxylated bile acids were on similar levels and in *POR* siRNA-transfected HepG2 cells compared to scrambled control, see A) (Unpaired T Test). This was also reflected in a significant decrease of B) the 12α-hydroxylated / non-12α-hydroxylated bile acids ratio, reflective of impaired CYP8B1 activity (Unpaired T Test).

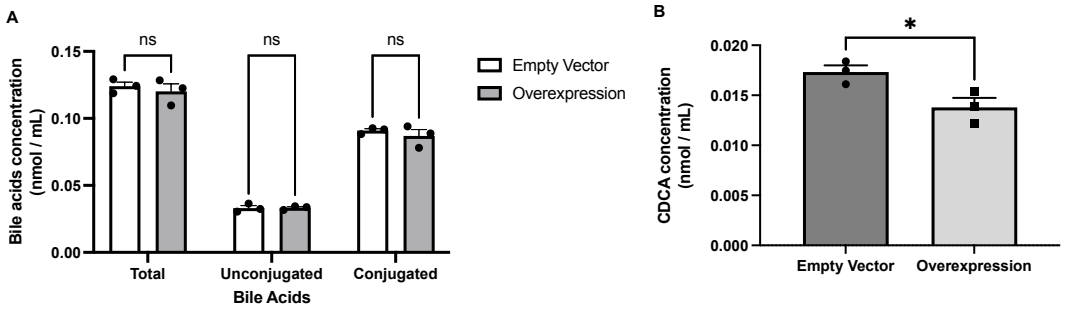


Figure 6.23: A) total bile acids, as well as the composition of total bile acids, conjugated and unconjugated bile acids, were unchanged in POR overexpressed HepG2 cells. B) CDCA is significantly lower in POR overexpressed HepG2 cells compared to empty vector transfected controls (Unpaired T Test).

direct impact of POR activity on CDCA levels in hepatoma cells.

The POR overexpression model did not show significant differences in 12α-hydroxylated and non-12α-hydroxylated BA (Figure 6.24A) but there seems to be a trend to a higher 12α-hydroxylated to non-12α-hydroxylated BA ratio (Figure 6.24B). This trend in the overexpression model showing exactly the opposite than the knockdown model does fit with our results and indicates that POR availability has a direct impact on BA composition via regulation of CYP8B1 enzyme activity.

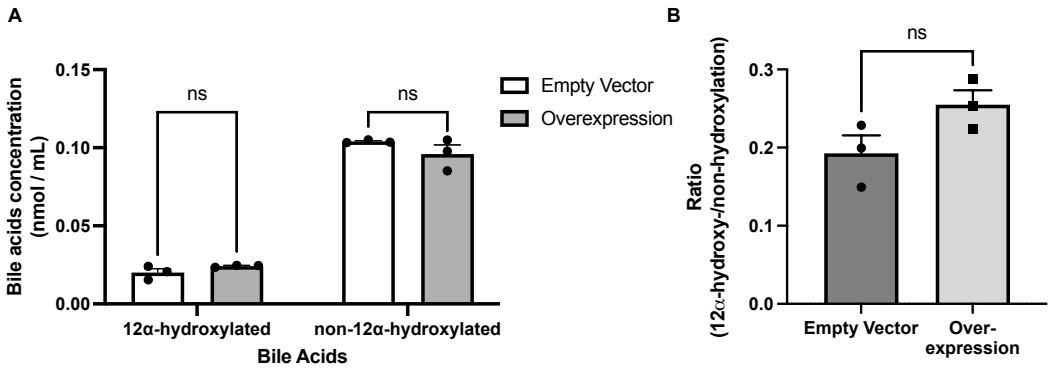


Figure 6.24: A) 12α-hydroxylated and non-12α-hydroxylated bile acids are not significantly different in POR overexpressed HepG2 cells compared to empty vector transfected cells (Unpaired T Test). The ratio of 12α-hydroxylated and non-12α-hydroxylated bile acids shows a trend but more replicates would have been necessary for a conclusive analysis (Unpaired T Test).

6.9 Glucose metabolism

POR siRNA knockdown in HepG2 leads to a broad deregulation of energy metabolism as seen with the PPAR pathway, in which phosphoenolpyruvate carboxykinase (PEPCK) a key regulator in glucose metabolism was flagged (Figure 6.7A). Therefore, using qPCR we explored key genes of glucose metabolism and demonstrated increased expression of phosphoenolpyruvate carboxykinase 1 (*PCK1*) (fc 2.76; $p = 0.002$), the cytosolic isozyme of PEPCK which is mainly expressed in liver and kidney, and *GLUT2* (fc 1.32, $p = 0.006$), the major glucose transporter in liver in HepG2 with *POR* siRNA knockdown (Figure 6.25A and B). Furthermore, glycogen synthase 1 (*GYS1*) (fc 0.86, $p = 0.02$), a key enzyme in glycogenesis, and glycogen phosphorylase L (*PYGL*) (fc 0.82, $p = 0.02$), regulating the release of glucose 1-phosphate from glycogen stores, were both significantly attenuated in *POR* siRNA transfected cells compared to scrambled control (Figure 6.25C and D).

Measuring glucose in media of HepG2 cells, we were not able to show a significant difference in glucose levels in cell culture media of cells transfected with *POR* siRNA compared to scrambled control transfected cells (Figure 6.26).

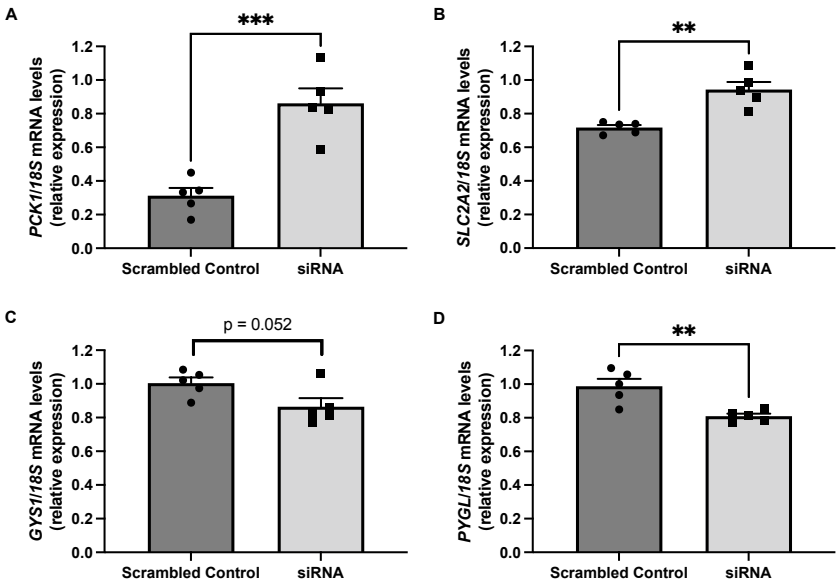


Figure 6.25: *POR* siRNA-transfected HepG2 cells impacts glucose metabolism with significant up-regulation of mRNA expression of A) *PCK1* and B) *GLUT2* as well as significant attenuation of D) *PYGL* expression. C) *GYS1* shows a similar trend to *PYGL*. Unpaired T Test was used for statistical analysis.

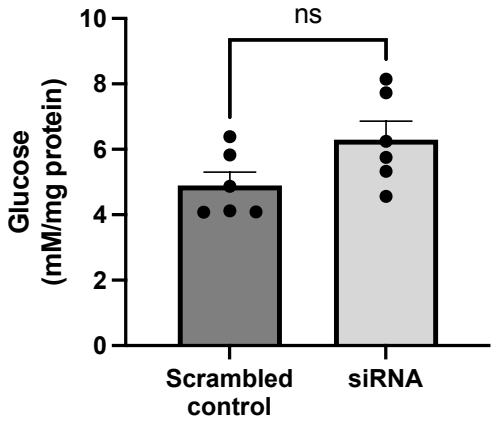


Figure 6.26: Glucose concentration is not significantly different in culture media of *POR* siRNA-transfected HepG2 cells compared to scrambled control ($p = 0.07$, Unpaired T Test).

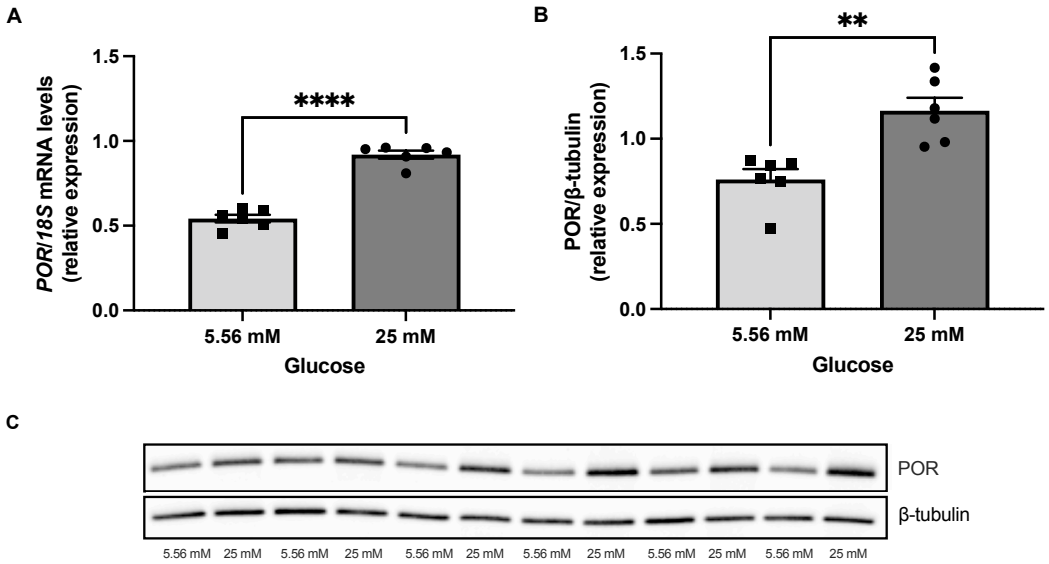


Figure 6.27: POR expression was significantly increased in A) mRNA and B) protein quantified in HepG2 cells cultured in 25 mM glucose media compared to 5.56 mM glucose media (Unpaired T Test). C) Protein gel underlying protein quantification analysis in B).

To better understand the impact of glucose on POR we cultured HepG2 cells with a low (5.56 mM) and high (25 mM) glucose culture media and measured mRNA and protein expression using qPCR and western blotting. Both mRNA expression and protein expression of POR was significantly increased in HepG2 cells cultured under high glucose compared to low glucose culture media (Figure 6.27).

6.10 Discussion

POR has been shown to be an important regulator of steroid hormone, BA and retinol metabolism [272, 277–279] and has been implicated in NAFLD due to liver lipidosis in hepatic Por-null mice [190, 221, 280]. In this chapter, we present the first evidence of a human hepatocellular model of *POR* siRNA knockdown and its wide-ranging impact on lipid, BA and glucose metabolism. Our data shows clear changes in energy homeostasis through deregulation of key genes and proteins of TAG, cholesterol, BA and glucose metabolism. Furthermore, the fundamental impact of POR on a broad spectrum of metabolic pathways is underlined by differences in BA availability, changes in cellular secretion as well as uptake of lipids and glucose, and an increase in β-oxidation markers.

Based on our results in *POR* siRNA knockdown HepG2 cells, we hypothesise that POR might serve cells as an indirect way to steer lipid metabolism and potentially more generally energy homeostasis. mRNA and protein expression of AMPK and further downstream ACC and *CPT1* suggest increased β-oxidation. This β-oxidation increase observed on transcriptional and protein level is further supported by bio-marker measurements showing a significant increase of 3OHB in culture media. Our data further suggests that *POR* siRNA-transfected HepG2 cells have a slight suppression of DNL (cells cultured without OPLA2) as measured by GCMS and increased media lipid levels with a higher proportion of TAG and higher levels of NEFA indicating lower fatty acid uptake from the culture media and higher secretion of TAG. Overall, these results indicate that *POR* siRNA transfected HepG2 cells have increased lipid catabolism and limited uptake compared to scrambled control transfected cells. POR might be directly involved in a protective mechanism of cells against lipid overloading or cells increase NADH concentrations *via* β-oxidation trying to yield higher rates of electron transfer to CYP. Our results from human cellular experiments are in contrast with a hepatic POR-null mouse model and a *POR* siRNA knockdown rat hepatoma cell model, which clearly showed liver lipidosis and lower TAG in serum [190, 221, 280], and lipid accumulation in cells [298], respectively. Furthermore, we present the first evidence in a human cellular

model showing that not only the TAG content of cells is unchanged but that the fatty acid composition of TAG is also unchanged in a *POR* siRNA knockdown model. This is of particular interest as we also show that POR knockdown leads to an increase of *Elovl6*, which regulates fatty acid composition and has been implicated to play a role in NASH [299–301].

With regards to cholesterol synthesis and metabolism, data seems to be more similar between human and mouse cell models with significant accumulation of lanesterol, a cholesterol precursor, in cellular POR knockdown models of both species [296, 298]. Our experiments on cholesterol were limited by the inability to differentiate between cholesterol, lathosterol and lanosterol. We therefore only present overall cholesterol and cholesterol ester in *POR* siRNA knockdown of HepG2 cells and were not able to show differences, even though we show a clear increase of mRNA expression of key enzymes in the cholesterol biosynthesis pathway, including lanosterol 14α-demethylase (*CYP51A1*) 6.28. This is believed to be mostly compensatory due to impaired CYP and epoxidase functions which require POR's electron transfer activity. The *in vivo* data from mice showing lower circulating cholesterol in plasma would further support the hypothesis of impaired sterol metabolism [190, 221]. Although we did not see differences in cellular cholesterol, we found a significant difference in media cholesterol, indicating that HepG2 cells secret cholesterol or more likely cholesterol precursor to keep cellular cholesterol levels stable.

Looking at the impact of POR on BA synthesis, we observe an overall increase in BA production due to an increase in CDCA upon *POR* silencing and were able to show that a POR overexpression model is able to significantly decrease CDCA levels, establishing that POR based CYP acitvity can determine CA and CDCA ratios in hepatocytes. This is in accordance with prior literature reporting an increase in CDCA and reduction of CA in *POR* CRISPR/Cas9 model [296]. The deregulation of the classic or neutral biosynthesis pathway as detected in RNA sequencing and qPCR is most likely to represent a compensatory increase in transcription in both *CYP7A1* and *CYP8B1* due to missing electron transfer

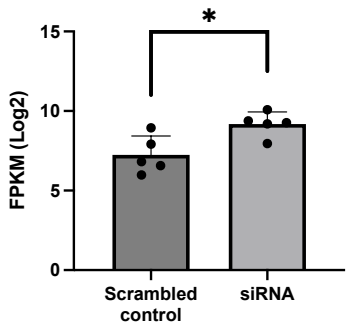


Figure 6.28: *CYP51A1* mRNA expression is significantly higher in *POR* siRNA transfected HepG2 cells compared to wild type HepG2 cells. DESeq2 analysis (Wald test): fc 1.27, padj = 0.019.

by POR. Our interpretation is that POR deficiency, and thereby impaired CYP activity, leads to a broad transcriptional increase of type 2 CYPs *via* feedback loop due to limitation in CYP activity. The broad CYP gene down-regulation after *POR* CRSIPR/Cas9 knockdown as observed by Heintze et al. stands in contrast to such theory but we have shown very consistently within multiple models, including cellular experiments as well as human data presented in Chapter 5, that POR activity attenuation leads to broad CYP up-regulation [296]. This compensatory up-regulation in transcription is further supported by the BA composition data showing higher levels of CDCA and a lower fraction of 12α-hydroxylated BA indicating lower CYP8B1 activity and increased BA production *via* the alternative biosynthesis pathway. Overall, based on increased CDCA concentration, unchanged expression of CYP27A1, CYP7B1 and presumably compensatory high levels of expression of *CYP7A1* and *CYP8B1* our results suggest that *POR* siRNA knockdown drives a shift to the alternative BA biosynthesis pathway. This is fully coherent with the fact that CYP27A1 is unaffected by POR as a type 1 CYP but dependent on ferredoxin reductase and ferredoxin [188]. Interestingly, there is an established link between BA biosynthesis and lipogenesis with increased CYP7A1 expression leading to increased transcription of genes regulated by SREBP [302]. This could be one of the explanations connecting POR reduction with lipid metabolism in our studies.

Finally, for the first time we show findings regarding the regulation of POR based on glucose exposure. The treatment of HepG2 cells with higher levels of glucose led to an up-regulation of POR expression on both mRNA and protein levels. In Chapter 5, we have shown that when HepG2 cells are exposed to lipids, we observe a down-regulation of POR mRNA and protein expression. These results suggest a dynamic regulatory mechanism of POR expression in response to different nutritional stimuli. High glucose and insulin levels are known to increase HMG-CoA [303] and sterol biosynthesis which the induction of POR expression could be a part of. Attenuation of POR expression upon high fat could implicate a regulatory feedback loop to decrease bile acid secretion to reduce fat uptake. Considering our results, POR attenuation could further drive β-oxidation and gluconeogenesis (upregulation of *PCK1*) expression (fc 2.76; $p = 0.002$)). These results imply that suppression of POR during NAFLD could lead to further metabolic downstream consequences and different diets might help to normalise and mitigate the impact of POR in NAFLD. Further exploration of the underlying signaling pathways and transcriptional regulators of POR could lead to valuable insight.

Several limitations should be considered when interpreting the results from our study of *POR* siRNA-transfected HepG2 cells. A single cell line has been used which may impact the interpretation and generalisability of these findings. POR has been shown to function as an oxidoreductase in HeLa cells and HepG2 cells show no private protein-altering single nucleotide variant or insertion/deletion polymorphism for POR compared to the 1000 Genomes Project and the Exome Sequencing Project [304] but the expression of POR and a big variety of CYP is lower in HepG2 compared to hepatocytes and HepaRG as determined via RNA sequencing [305, 306]. The inducibility of the CYP enzymes was also limited compared to hepatocytes or the HepaRG cell line, which is more closesly related to hepatocytes and might represent a better model for studies looking at CYP enzymes and lipid metabolism [307–309]. Further, to better understand the impact of *POR* siRNA knockdown a more realistic physiological context would be required such as liver organoids or co-culturing with stellate cells enabling cell-cell interaction.

In addition, the *in vitro* nature of our experiments clearly limits the exploration of POR as it fails to represent the actual tissue organisation and zonation along the lobules present in the liver. This is particularly important as POR, as well as many other CYPs (e.g. CYP7A1), are located pericentrally wereas HMGCR, important in cholesterol synthesis, is located periportally [162, 163, 302].

Overall, POR manipulation showed a broad deregulation of energy homeostasis in-line with lipid catabolism, disturbed cholesterol synthesis and a shift of BA production to higher levels of CDCA via the alternative BA biosynthesis pathway. With clear differences in mouse and human cellular models, it is unlikely that we can extrapolate the *in vivo* results from mice models to human physiology. Therefore, there is need for further research validating these results in a second hepatoma cell line or for this research to be complemented by future research within primary hepatocytes. Additional research will need to explore intracellular oxysterol and the impact of POR on FXR, retinol metabolism and RXR signalling. Furthermore, clinical studies should be run with POR deficient patients looking at BA and metabolomics.

7 Discussion

Contents

7.1 Conclusion and discussion 162
7.2 Future experiments and directions 167
7.2.1 AKR1C1 in HCC and as prognostic marker 167
7.2.2 POR and fibrosis 168
7.2.3 POR and bile acids 169
7.2.4 POR and nuclear receptor activation 169
7.2.5 POR activity for clinical diagnostics 169

7.1 Conclusion and discussion

The focus of this thesis was to investigate the role of AKR1C1 and POR in NAFLD and HCC. In the first two chapters, the expression and activity of AKR1C1 were examined in patients with NAFLD and HCC and multiple hepatocellular models were established to explore pharmacological inhibition, siRNA and CRISPR knockdown of AKR1C1, as well as overexpression. The results showed no change in expression but increased AKR1C1 activity in patients with NAFLD in advanced stages, including cirrhosis. In patients with HCC, higher AKR1C1 expression and activity were observed and lower overall survival within HCC patients with higher AKR1C1 expression, independent of cancer stage, suggests a potential prognostic function. The observed overlap makes it likely that such AKR1C1 changes are limited to a small subset of individuals with HCC. When AKR1C1 was manipulated in hepatoma cell lines, there was little effect on gene expression, proliferation,

or cell motility, indicating that AKR1C1 might not play a significant role in the development or progression of HCC.

Although AKR1C1 is found most highly expressed in the liver and has been implicated in multiple forms of cancers including cervical, bladder cancer and NSCLC, we have comprehensively shown that in multiple hepatocellular models we were not able to replicate effects on proliferative and metastatic potential or chemoresistance which seem to be tissue specific and limited to chemotherapy agents not routinely used in HCC therapy [171, 172, 260]. Therefore, for the first time we have shown that AKR1C1 is unlikely to play a direct role in pathogenesis, progression and chemoresistance of HCC, but changes in expression are more likely to represent a consequence of disease. One possible explanation being the overexpression of NRF2 and the overactivation of a wide range of NRF2 target genes coincidentally including *AKR1C1* [180, 181, 310]. The impact of AKR1C1 on ROS, lipid aldehydes and ferroptosis therefore seem negligible in the context of HCC and are likely compensated for by other similar enzymes in our knockdown experiments. The presence of such a complex intracellular system for steroid hormone metabolism, oxidative stress and lipid aldehydes and the lack of an appropriate animal model make it difficult for AKR1C1's impact to be elucidated in more detail. Human primary hepatocytes or iPSC could be used to further explore how AKR1C1 impacts on a more natural liver phenotype or affects the differentiation of iPSC to liver cells.

The third and fourth chapter explored POR expression, activity and the underlying mechanisms in patients with NAFLD, in mouse and different cellular models. For the first time, we showed a consistent down-regulation of POR expression and activity in a variety of cellular, rodent and human models, clearly linking the expression of POR in the liver to a metabolic phenotype. The human data demonstrated lower hepatic POR expression and lower POR activity in patients with NAFLD compared to healthy individuals underlined by compensatory CYP mRNA up-regulation. These findings were supported by NAFLD inducing experiments in mouse and cellular models, both showing down-regulation of POR and substantiating the association of lower POR expression with NAFLD. These

results are somewhat contrary to GWAS studies of NAFLD patients. Even though POR is a very polymorphic gene no association with NAFLD has been found. Therefore the prognostic value of POR in NAFLD remained unclear, but based on the results and prior research, we hypothesized that decreased POR activity might contribute to the development and progression of NAFLD by affecting lipid and BA metabolism, leading to liver damage. Using a hepatocellular model of POR knockdown, a significant impact on lipid, BA, and glucose metabolism were revealed.

Even though we were able to show clear deregulation of lipid metabolism, our results stand in contrast with studies of hepatic Por-null mice which showed clear evidence of increased hepatic lipid content [190, 221]. Our results showed no change of TAG concentration and TAG composition. One explanation in our cellular model could be the observed increase of FAO on transcriptional, protein and biomarker level. Furthermore, patients with NAFLD did not show a difference in POR expression or activity when stratified by different levels of steatosis suggesting that POR activity might have different consequences on lipid metabolism in human compared to rodent models. With regards to cholesterol, human and mouse metabolism seem to be more similar as in both species POR knockdown cell models revealed a significant accumulation of the cholesterol precursor lanesterol [296, 298]. Complementary to this data, we showed up-regulation of multiple type 2 CYP enzymes upon POR knockdown which are involved in cholesterol synthesis, indicating compensatory up-regulation due to impaired cholesterol production. Type 1 CYP, CYP27A1, was found unaffected by POR and is fully aligned with prior literature [188]. The most convincing effect of POR knockdown and overexpression was centered around BA biosynthesis with a clear increase and decrease of CDCA upon knockdown and overexpression, respectively. This is relevant as CDCA is the more potent FXR agonist compared to CA which only leads to a partial effect on FXR [64]. We believe our results indicate an increased bile acid production *via* the alternative BA synthesis pathway as its rate limiting step is a type 1 CYP which is non-POR dependent but depends on ferrodoxin reductase and ferrodoxin for the electron transfer. This underlines the importance of POR's impact on BA composition as

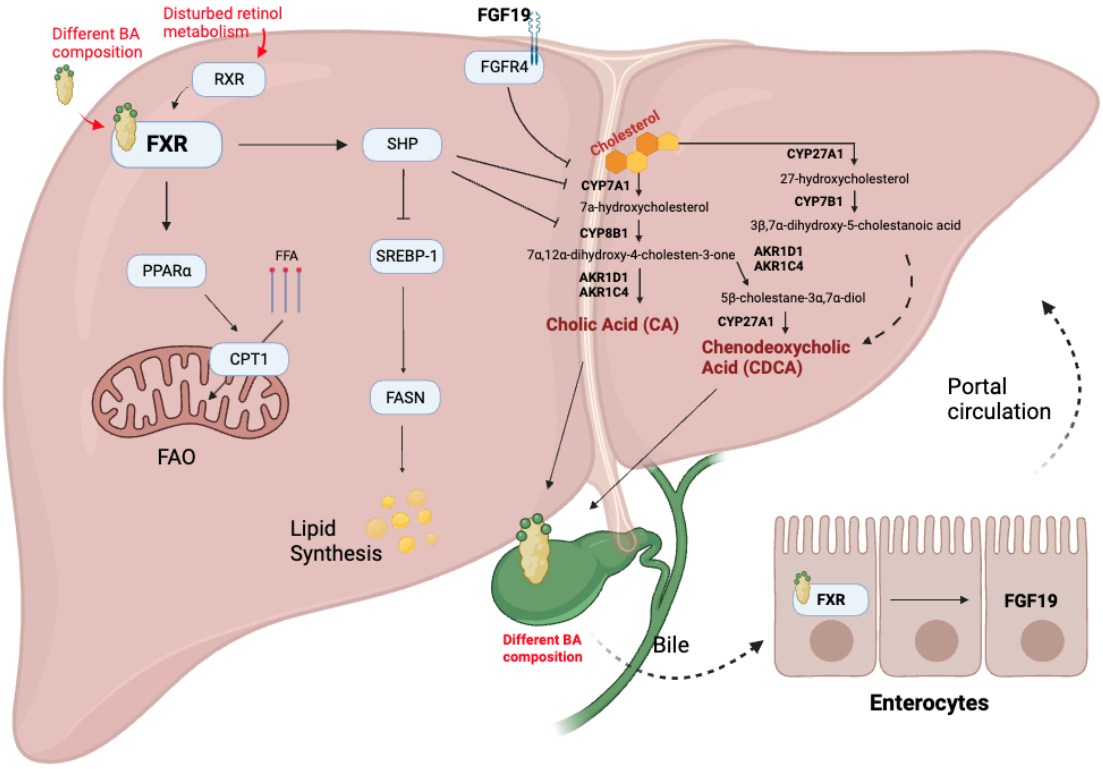


Figure 7.1: POR's impact on bile acid composition and retinol metabolism could potentially cause a disturbed FXR pathway. Created with BioRender.com.

well as activation of BA receptors such as FXR. This is particularly interesting as changes in BA composition and lower FXR activation have been implicated in the pathogenesis of NAFLD [85]. Considering the FXR feedback loop (Figure 7.1) our results with higher *NR1H4* expression, pAMPK, pACC and *CPT1A* might indicate that POR attenuation serves as a way to increase CDCA and thereby higher FXR activation. Furthermore, one could speculate that POR attenuation drives FXR activity due to its impact on retinol metabolism: impaired CYP26B1 leads to an increase in all-trans-retinoic acid and consequently increased RXR binding. Such a hypothesis would see POR more as a consequence or protective mechanism but the body of evidence presented in this thesis on POR's impact on cholesterol and BA synthesis suggests that there is a high likelihood of broad oxysterol deregulation upon POR attenuation, which in turn is highly relevant as driver for NAFLD progression as oxysterols have been linked to metabolic and inflammatory disease [311].

One could further speculate that POR down regulation after OPLA2 treatment

in our cellular experiments could be a potential feedback loop mechanism upon high fat load within the cells to decrease bile acid secretion and limit fat uptake as observed with FXR agonists [312]. Our results showing POR being induced by glucose and down regulated by fat in cell media supports such speculation as increased cholesterol synthesis during times of high glucose [303] could cause an increase in POR and in contrast lower need for POR activity during times of high fat/cholesterol uptake. In the context of NAFLD, hepatic steatosis causing lower POR activity could as an effect lead to impaired glucose to cholesterol utilisation as hypothesised above and further aggravate lipid accumulation in the form of cholesterol precursors. This emphasises the need for continued research into POR's influence on sterol metabolism, BAs and metabolic health. At present the observed changes in our POR knockdown models are unclear and further exploration in combination with FXR might be highly relevant for NAFLD.

The impact on our cellular models was, as expected, greater when manipulating POR, as it regulates a host of enzymes including type 2 CYP and HO, but manipulation of both AKR1C1 and POR expression have the potential to impact metabolic phenotype. In the clinical context of NAFLD, measuring POR activity might have the potential to serve as a non-invasive clinical tool that indicates disturbed metabolic function but at present further clinical research into hepato-specific POR activity is necessary to substantiate such a hypothesis.

Furthermore, considering that POR polymorphisms and expression have been suggested to influence HCC prognosis, POR down-regulation during NAFLD could have a consequence on HCC development and outcome. The impact of POR on HCC needs to be further explored; there is a need to examine the underlying liver disease aetiology as POR may be differentially regulated and this could influence clinical outcome. Additionally, POR might be more relevant to the treatment of HCC than AKR1C1 as it affects CYP3A4 activity which oxidises Sorafenib. Patients with polymorphisms K49N, A115V and G413S, presenting with higher CYP3A4 activity [214], could potentially fail treatment due to fast Sorafenib metabolism or

the more widely observed down regulation of POR in liver disease could lead to a drug toxicity effect as CYP3A4 does not clear Sorafenib sufficiently [313, 314].

With regards to AKR1C1, our cellular data suggested no mechanistic link to NAFLD or HCC and its urinary steroid metabolites are not a sufficiently accurate marker to discern between patients with or without HCC. The significant overlap of AKR1C1 expression further limits its potential as a prognostic marker. Nonetheless, it is possible that a panel of multiple enzyme activity ratios derived from the urine steroid metabolome such as the proxy measures of POR and AKR1C1 presented within the thesis could offer more accurate diagnostic solutions for NAFLD and HCC where we currently only have insufficient or invasive solutions.

In summary, this thesis provides comprehensive insights into the roles of AKR1C1 and POR in NAFLD and HCC. While AKR1C1 seems to have a limited impact on HCC progression, it may hold potential as a prognostic marker for a subgroup of HCC patients or as a part of a larger panel. On the other hand, POR appears to be significantly associated with NAFLD development, impacting various metabolic pathways. The role POR might play in NAFLD pathogenesis remains unclear. These findings contribute to our understanding of liver diseases and may have implications for future diagnostic and therapeutic strategies targeting AKR1C1 and POR pathways. However, further research is warranted to fully elucidate the mechanisms underlying their functions in such multifactorial diseases.

7.2 Future experiments and directions

7.2.1 AKR1C1 in HCC and as prognostic marker

AKR1C1 has been extensively explored in hepatoma cell lines throughout this thesis. To validate our findings, research in primary hepatocytes or iPSC could serve as a more physiological approach and shed new light on the impact of AKR1C1 during the development of new hepatocytes. More importantly, the clinical data we presented warrants further exploration of downstream products of AKR1C1 in a larger steroid metabolome panel as non-invasive prognostic tool for HCC. The longitudinal analysis of measurements of the Steroids & HCC study run by our

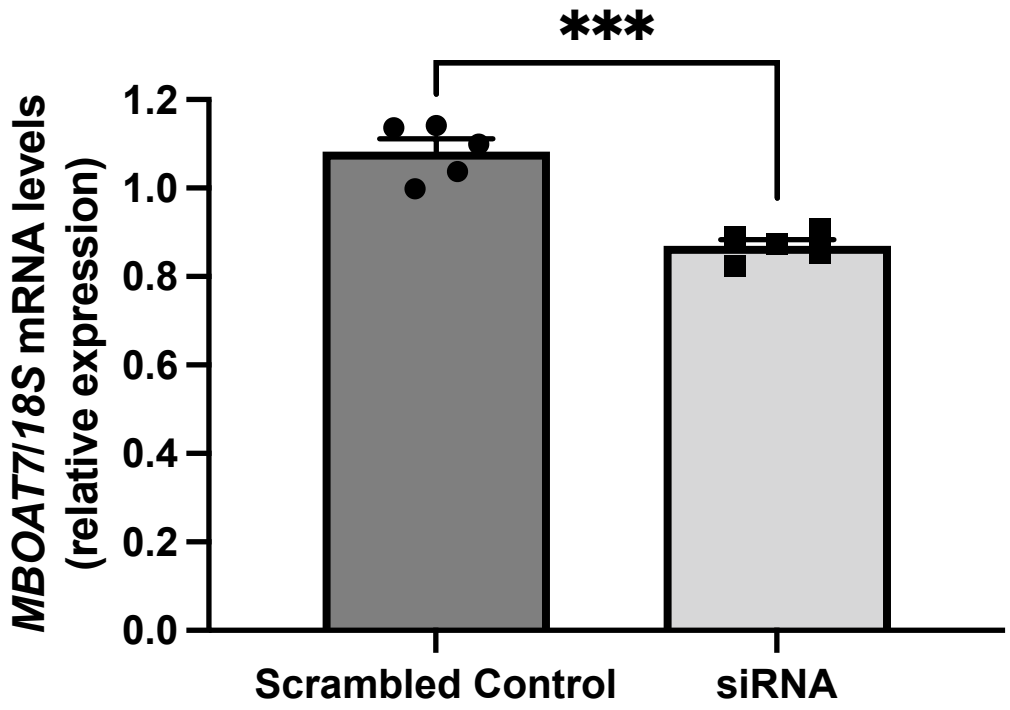


Figure 7.2: *MBOAT7* expression is significantly downregulated in *POR* siRNA transfected HepG2 cells (Unpaired T Test).

group would allow to perform such validation of a combination of steroid metabolites with a prognostic function for HCC in clinical practice.

7.2.2 POR and fibrosis

Having focused mostly on metabolism in this thesis, future experiments should look at the connection of fibrosis and POR activity in more detail. We uncovered significant down-regulation of *MBOAT7* after *POR* siRNA knockdown (Figure 7.2), which has been associated with liver fibrosis, increased risk of advanced disease and HCC development in patients with NAFLD [315–318]. For this reason, experiments co-culturing hepatocellular cell lines with HSC could grant deeper insight if impaired POR activity drives a profibrotic environment as suggested by the down-regulation of *MBOAT7*.

7.2.3 POR and bile acids

In Chapter 6, we present robust evidence of deregulation of BA synthesis and changes in composition. POR knockdown caused CDCA up-regulation in the cell culture media. These changes will need to be explored in more detail and a profile of BA and oxysterols present within hepatocellular cell lines should be established. This would allow to gain a better understanding of which receptors are activated by metabolites created through POR deficiency. Furthermore, it would allow to test whether these changes in BA composition impact on primary hepatocyte function and see if they are a major driver of the metabolic changes described in this thesis, potentially *via* FXR activation, or if they have a key role to play in driving inflammation and fibrosis.

7.2.4 POR and nuclear receptor activation

POR deficiency in humans has been shown to cause a major deregulation in retinol metabolism probably *via* CYP26 deficiency leading to retinoic acid excess [277]. It is still not clear as to exactly how attenuation of POR activity impacts retinoid signalling. Retinoid acids are normally stored in HSC and are typically released upon liver damage. They influence both hepatocyte proliferation and HSC activation [319]. A reduction in signalling has been suggested to influence numerous liver diseases including NAFLD and HCC [320]. Furthermore, the effect of POR attenuation on FXR in NAFLD models needs to be explored. Therefore, experiments to better understand the downstream consequences of POR knockdown on retinol content by measuring retinoic acid and testing RAR, RXR as well as FXR activation using e.g. luciferase receptor assays systems, could be highly informative providing a better understanding of NAFLD and potential new therapeutic approaches.

7.2.5 POR activity for clinical diagnostics

POR activity should be measured in future clinical studies using the Karolisnka or Inje cocktail as this would allow to differentiate between hepato specific and general POR activity *in vivo* and might therefore allow for better conclusions and

closer association with NAFLD that might be clinically relevant. The Karolinska cocktail is a mix of caffeine, losartan, omeprazole, debrisoquin and quinine, that can be utilised to phenotype CYP1A2, CYP2C9, CYP2C19, CYP2D6, and CYP3A4 activity via blood and urine samples to serve as a proxy for hepatic POR activity [321]. The Inje cocktail is also used to phenotype the *in vivo* enzyme activities of CYP1A2, CYP2C9, CYP2C19, CYP2D6, and CYP3A in blood samples after 4 h and 8h urine collection but is using a slightly adjusted drug cocktail of caffeine, losartan, omeprazole, dextromethorphan and midazolam [322]. The longitudinal analysis of such CYP activities as POR proxy measurement should be used to gain further insights on POR activity and might be highly relevant in NAFLD and HCC.

Appendices

References

[1] D. Kimberley Molina and Vincent J.M. DiMaio. "Normal organ weights in men: Part II - The Brain, Lungs, Liver, Spleen, and Kidneys". *American Journal of Forensic Medicine and Pathology* 33.4 (2012), pp. 368–72.

[2] D. Kimberley Molina and Vincent J.M. DiMaio. "Normal organ weights in women: Part II - The Brain, Lungs, Liver, Spleen, and Kidneys". *American Journal of Forensic Medicine and Pathology* 36.3 (2015), pp. 182–7.

[3] Francis Sutherland and Julie Harris. "Claude Couinaud: a passion for the liver." *Archives of surgery (Chicago, Ill. : 1960)* 137.11 (2002), pp. 1305–1310.

[4] Harold Ellis. "Anatomy of the liver". *Surgery* (2011).

[5] Vishy Mahadevan. "Anatomy of the liver". *Surgery* (2014).

[6] American Joint Committee on Cancer. *AJCC Cancer Staging Manual*. 8th edition. Springer, 2017.

[7] T. Ricken et al. "Modeling function–perfusion behavior in liver lobules including tissue, blood, glucose, lactate and glycogen by use of a coupled two-scale PDE–ODE approach". *Biomechanics and Modeling in Mechanobiology* 14.3 (2015), pp. 515–36.

[8] Z Kmieć. "Cooperation of liver cells in health and disease." *Advances in anatomy, embryology, and cell biology* 161 (2001), pp. 1–151.

[9] Harvey Lodish. *Molecular Cell Biology*. 8th edition. W.H. Freeman, 2016.

[10] Frank A. Anania and Joel P. Wedd. "Liver Anatomy and Histopathology". *Sitaraman and Friedman's Essentials of Gastroenterology*. 2017.

[11] Francis J. Eng and Scott L. Friedman. "Fibrogenesis. I. New insights into hepatic stellate cell activation: The simple becomes complex". *American Journal of Physiology - Gastrointestinal and Liver Physiology* 279.1 (2000), G7–G11.

[12] A. Geerts. "History, heterogeneity, developmental biology, and functions of quiescent hepatic stellate cells". *Seminars in Liver Disease* 21.3 (2001), pp. 311–35.

[13] Florian Winau et al. "Ito Cells Are Liver-Resident Antigen-Presenting Cells for Activating T Cell Responses". *Immunity* 26.1 (2007), pp. 117–29.

[14] Murli Krishna. "Microscopic anatomy of the liver". *Clinical Liver Disease* 2.Suppl 1 (2013), pp. 4–7.

[15] Zhutian Zeng et al. "CRIg Functions as a Macrophage Pattern Recognition Receptor to Directly Bind and Capture Blood-Borne Gram-Positive Bacteria". *Cell Host and Microbe* 20.1 (2016), pp. 99–106.

[16] Laura J. Dixon et al. "Kupffer cells in the liver". *Comprehensive Physiology* 3.2 (2013), pp. 785–97.

[17] A. M. Rappaport. "Hepatic blood flow: morphologic aspects and physiologic regulation." *International review of physiology* 21 (1980), pp. 1–63.

[18] Stuart Smith and Shiou Chuan Tsai. "The type I fatty acid and polyketide synthases: A tale of two megasynthases". *Natural Product Reports* 24.5 (2007), pp. 1041–72.

[19] Fatima Ameer et al. "De novo lipogenesis in health and disease". *Metabolism: Clinical and Experimental* 63.7 (2014), pp. 895–902.

[20] Yu Wang et al. "Acetyl-CoA Carboxylases and Diseases". *Frontiers in Oncology* 12 (2022), pp. 836–58.

[21] Neil B. Ruderman, Asish K. Saha, and Edward W. Kraegen. "Minireview: Malonyl CoA, AMP-Activated Protein Kinase, and Adiposity". *Endocrinology* 144.12 (2003), pp. 5166–71.

[22] Daniel W. Foster. "Malonyl-CoA: The regulator of fatty acid synthesis and oxidation". *Journal of Clinical Investigation* 122.6 (2012), pp. 1958–9.

[23] Takayuki Sassa and Akio Kihara. "Metabolism of very long-chain fatty acids: Genes and pathophysiology". *Biomolecules and Therapeutics* 22.2 (2014), pp. 83–92.

[24] Leanne Hodson and Pippa J. Gunn. "The regulation of hepatic fatty acid synthesis and partitioning: the effect of nutritional state". *Nature Reviews Endocrinology* 15.12 (2019), pp. 689–700.

[25] Charlotte J. Green and Leanne Hodson. "The influence of dietary fat on liver fat accumulation". *Nutrients* 6.11 (2014), pp. 5018–33.

[26] Bertrand Perret et al. "Hepatic lipase: Structure/function relationship, synthesis, and regulation". *Journal of Lipid Research* 43.8 (2002), pp. 1163–9.

[27] Marian C. Cheung et al. "Lipoprotein lipase and hepatic lipase: Their relationship with HDL subspecies Lp(A-I) and Lp(A-I,A-II)". *Journal of Lipid Research* 44.8 (2003), pp. 1552–8.

[28] Liangyou Rui. "Energy metabolism in the liver". *Comprehensive Physiology* 4.1 (2014).

[29] Sander Kersten. "Integrated physiology and systems biology of PPARα". *Molecular Metabolism* 3.4 (2014), pp. 354–71.

[30] Cristina Mascaró et al. "Control of human muscle-type carnitine palmitoyltransferase I gene transcription by peroxisome proliferator-activated receptor". *Journal of Biological Chemistry* 273.15 (1998), pp. 8560–3.

[31] L. Hagenfeldt et al. "Uptake of individual free fatty acids by skeletal muscle and liver in man." *The Journal of clinical investigation* 51.9 (1972), pp. 2324–30.

[32] David W. Russell. "The enzymes, regulation, and genetics of bile acid synthesis". *Annual Review of Biochemistry*. Vol. 72. 2003, pp. 137–74.

[33] M. Sawkat Anwer. "Cellular Regulation of Hepatic Bile Acid Transport in Health and Cholestasis". *Hepatology* 39.3 (2004), pp. 581–90.

[34] Sander M. Houten, Mitsuhiro Watanabe, and Johan Auwerx. "Endocrine functions of bile acids". *EMBO Journal* 25.7 (2006), pp. 1419–25.

[35] John Y.L. Chiang. "Bile acids: Regulation of synthesis". *Journal of Lipid Research* 50.10 (2009), pp. 1955–66.

[36] John Y.L. Chiang. "Bile Acid Metabolism and Signaling". *Comprehensive Physiology* 3.3 (2013), p. 1191.

[37] John Y.L. Chiang and Jessica M. Ferrell. "Bile acid receptors FXR and TGR5 signaling in fatty liver diseases and therapy". *American Journal of Physiology - Gastrointestinal and Liver Physiology* 318.3 (2020), G554–G573.

[38] Irina A. Pikuleva. "Cytochrome P450s and cholesterol homeostasis". *Pharmacology and Therapeutics* 112.3 (2006), pp. 761–73.

[39] Yi Jin et al. "Metabolism of the synthetic progestogen norethynodrel by human ketosteroid reductases of the aldo-keto reductase superfamily". *Journal of Steroid Biochemistry and Molecular Biology* 129.3-5 (Apr. 2012), pp. 139–144.

[40] Yi Jin et al. "Human cytosolic hydroxysteroid dehydrogenases of the aldo-ketoreductase superfamily catalyze reduction of conjugated steroids: Implications for phase I and phase II steroid hormone metabolism". *Journal of Biological Chemistry* 284.15 (Apr. 2009), pp. 10013–10022.

[41] Stephan Steckelbroeck et al. "Human cytosolic 3α-hydroxysteroid dehydrogenases of the aldo-keto reductase superfamily display significant 3β-hydroxysteroid dehydrogenase activity: Implications for steroid hormone metabolism and action". *Journal of Biological Chemistry* 279.11 (Mar. 2004), pp. 10784–10795.

[42] Stephan Steckelbroeck et al. "Tibolone metabolism in human liver is catalyzed by 3a/3b- hydroxysteroid dehydrogenase activities of the four isoforms of the aldo-keto reductase (AKR)1C subfamily". *Journal of Pharmacology and Experimental Therapeutics* 316.3 (Mar. 2006), pp. 1300–1309.

[43] Dario Mizrachi and Richard J. Auchus. "Androgens, estrogens, and hydroxysteroid dehydrogenases". *Molecular and Cellular Endocrinology* 301.1-2 (Mar. 2009), pp. 37–42.

[44] Catherine Mazza et al. "Unusual charge stabilization of NADP+ in 17b-hydroxysteroid dehydrogenase". *Journal of Biological Chemistry* 273.14 (Apr. 1998), pp. 8145–8152.

[45] Alan F. Hofmann, Lee R. Hagey, and Matthew D. Krasowski. "Bile salts of vertebrates: Structural variation and possible evolutionary signifi cance". *Journal of Lipid Research* 51.2 (2010), pp. 226–46.

[46] Martin C. Carey and Donald M. Small. "Micelle Formation by Bile Salts: Physical-Chemical and Thermodynamic Considerations". *Archives of Internal Medicine* 130.4 (1972), pp. 506–27.

[47] Antonio Molinaro, Annika Wahlström, and Hanns Ulrich Marschall. "Role of Bile Acids in Metabolic Control". *Trends in Endocrinology and Metabolism* 29.1 (2018), pp. 31–41.

[48] Rumei Li et al. "Gut microbiome and bile acids in obesity-related diseases". *Best Practice and Research: Clinical Endocrinology and Metabolism* 35.3 (2021), p. 101493.

[49] Laura P. Smith et al. "The bile acid synthesis pathway is present and functional in the human ovary". *PLoS ONE* 4.10 (2009), p. 7333.

[50] H. M.G. Princen et al. "Cyclosporin A blocks bile acid synthesis in cultured hepatocytes by specific inhibition of chenodeoxycholic acid synthesis". *Biochemical Journal* 275.2 (1991), pp. 501–5.

[51] Z. R. Vlahcevic et al. "Quantitative estimations of the contribution of different bile acid pathways to total bile acid synthesis in the rat". *Gastroenterology* 113.6 (1997), pp. 1949–57.

[52] Amir Babiker et al. "Elimination of cholesterol in macrophages and endothelial cells by the sterol 27-hydroxylase mechanism. Comparison with high density lipoprotein- mediated reverse cholesterol transport". *Journal of Biological Chemistry* 272.42 (1997), pp. 26253–61.

[53] K. I. Okuda. "Liver mitochondrial P450 involved in cholesterol catabolism and vitamin D activation". *Journal of Lipid Research* 35.3 (1994), pp. 361–72.

[54] A. F. Hofmann and D. M. Small. "Detergent properties of bile salts: correlation with physiological function." *Annual review of medicine* 18 (1967), pp. 333–76.

[55] R. E. Roberts et al. "The relationship between postprandial bile acid concentration, GLP-1, PYY and ghrelin". *Clinical Endocrinology* 74.1 (2011), pp. 67–72.

[56] Dennis Stamp and Gareth Jenkins. "An overview of bile-acid synthesis, chemistry and function". *Issues in Toxicology* (2008).

[57] AF Hofmann. "The Function Of Bile Salts In Fat Absorption. The Solvent Properties Of Dilute Micellar Solutions Of Conjugated Bile Salts". *Biochemical Journal* 89.1 (1963), pp. 57–68.

[58] Douglas V. Guzior and Robert A. Quinn. "Review: microbial transformations of human bile acids". *Microbiome* 9.1 (2021), p. 140.

[59] Thippeswamy H. Sannasiddappa, Peter A. Lund, and Simon R. Clarke. "In vitro antibacterial activity of unconjugated and conjugated bile salts on Staphylococcus aureus". *Frontiers in Microbiology* 8.Aug. (2017), p. 1581.

[60] Peter Kurdi et al. "Mechanism of growth inhibition by free bile acids in lactobacilli and bifidobacteria". *Journal of Bacteriology* 188.5 (2006), pp. 1979–86.

[61] Robert A. Quinn et al. "Global chemical effects of the microbiome include new bile-acid conjugations". *Nature* 579.7797 (2020), pp. 123–129.

[62] Hong Lin et al. "Alterations of Bile Acids and Gut Microbiota in Obesity Induced by High Fat Diet in Rat Model". *Journal of Agricultural and Food Chemistry* 67.13 (2019).

[63] Masayuki Nagahashi et al. "The roles of bile acids and sphingosine-1-phosphate signaling in the hepatobiliary diseases". *Journal of Lipid Research* 57.9 (2016), pp. 1636–43.

[64] Jane L. Lew et al. "The Farnesoid X Receptor Controls Gene Expression in a Ligand- and Promoter-selective Fashion". *Journal of Biological Chemistry* 279.10 (2004), pp. 8856–61.

[65] Inés Pineda Torra et al. "Bile acids induce the expression of the human peroxisome proliferator-activated receptor α gene via activation of the farnesoid X receptor". *Molecular Endocrinology* 17.2 (2003), pp. 259–72.

[66] Yang Jiao, Yan Lu, and Xiao Ying Li. "Farnesoid X receptor: A master regulator of hepatic triglyceride and glucose homeostasis". *Acta Pharmacologica Sinica* 36.1 (2015), pp. 44–50.

[67] Li Wang et al. “Redundant pathways for negative feedback regulation of bile acid production”. *Developmental Cell* 2.6 (2002), pp. 721–31.

[68] Jason A. Holt et al. “Definition of a novel growth factor-dependent signal cascade for the suppression of bile acid biosynthesis”. *Genes and Development* 17.13 (2003), pp. 1581–91.

[69] Bryan Goodwin et al. “A regulatory cascade of the nuclear receptors FXR, SHP-1, and LRH-1 represses bile acid biosynthesis”. *Molecular Cell* 6.3 (2000), pp. 517–26.

[70] Timothy T. Lu et al. “Molecular basis for feedback regulation of bile acid synthesis by nuclear receptos”. *Molecular Cell* 6.3 (2000), pp. 507–15.

[71] Insook Kim et al. “Differential regulation of bile acid homeostasis by the farnesoid X receptor in liver and intestine”. *Journal of Lipid Research* 48.12 (2007), pp. 2664–72.

[72] Tsutomu Matsubara, Fei Li, and Frank J. Gonzalez. “FXR signaling in the enterohepatic system”. *Molecular and Cellular Endocrinology* 368.1-2 (2013), pp. 17–29.

[73] Xiao Jun Wang et al. “Nrf2 enhances resistance of cancer cells to chemotherapeutic drugs, the dark side of Nrf2”. *Carcinogenesis* 29.6 (2008), pp. 1235–43.

[74] Takeshi Inagaki et al. “Regulation of antibacterial defense in the small intestine by the nuclear bile acid receptor”. *Proceedings of the National Academy of Sciences of the United States of America* 103.10 (2006), pp. 3920–5.

[75] Da Gang Zhang et al. “Obeticholic acid protects against carbon tetrachloride-induced acute liver injury and inflammation”. *Toxicology and Applied Pharmacology* 314 (2017), pp. 39–47.

[76] Zobair M. Younossi et al. “Epidemiology of Nonalcoholic Fatty Liver Disease and Nonalcoholic Steatohepatitis: Implications for Liver Transplantation”. *Transplantation* 103.1 (2019), pp. 22–27.

[77] A. F. Hofmann and L. R. Hagey. “Bile acids: Chemistry, pathochemistry, biology, pathobiology, and therapeutics”. *Cellular and Molecular Life Sciences* 65.16 (2008), pp. 2461–83.

[78] James E. Heubi, Kenneth D.R. Setchell, and Kevin E. Bove. “Inborn Errors of Bile Acid Metabolism”. *Clinics in Liver Disease* 22.4 (2018), pp. 671–87.

[79] Kenneth D.R. Setchell et al. “Genetic defects in bile acid conjugation cause fat-soluble vitamin deficiency”. *Gastroenterology* 144.5 (2013), pp. 945–55.

[80] Shikha S. Sundaram et al. “Mechanisms of disease: Inborn errors of bile acid synthesis”. *Nature Clinical Practice Gastroenterology and Hepatology* 5.8 (2008), pp. 456–468.

[81] Jason M. Ridlon, Dae Joong Kang, and Phillip B. Hylemon. “Bile salt biotransformations by human intestinal bacteria”. *Journal of Lipid Research* 47.2 (2006), pp. 241–59.

[82] John P. Thomas et al. “The Emerging Role of Bile Acids in the Pathogenesis of Inflammatory Bowel Disease”. *Frontiers in Immunology* 13.3 (2022), p. 829525.

[83] Nathan Calzadilla et al. "Bile acids as inflammatory mediators and modulators of intestinal permeability". *Frontiers in Immunology* 13 (2022), p. 1021924.

[84] Benthe van der Lugt et al. "The effects of sulfated secondary bile acids on intestinal barrier function and immune response in an inflammatory in vitro human intestinal model". *Heliyon* 8.2 (2022), p. 08883.

[85] Na Jiao et al. "Suppressed hepatic bile acid signalling despite elevated production of primary and secondary bile acids in NAFLD". *Gut* 67.10 (2018), pp. 1881–91.

[86] Annette Hammes et al. "Role of endocytosis in cellular uptake of sex steroids". *Cell* 122.5 (Sept. 2005), pp. 751–762.

[87] Nancy H. Ing. "Steroid Hormones Regulate Gene Expression Posttranscriptionally by Altering the Stabilities of Messenger RNAs". *Biology of Reproduction* 72.6 (June 2005), pp. 1290–1296.

[88] Chen Wang, Yi Liu, and Ji Min Cao. "G Protein-Coupled Receptors: Extranuclear Mediators for the Non-Genomic Actions of Steroids". *International Journal of Molecular Sciences* 15.9 (Sept. 2014), p. 15412.

[89] Manpreet S. Mundi et al. "Evolution of NAFLD and Its Management". *Nutrition in Clinical Practice* 35.1 (2020), pp. 72–84.

[90] Mary E. Rinella et al. "A multi-society Delphi consensus statement on new fatty liver disease nomenclature". *Journal of Hepatology* Online.ahead of print (June 2023).

[91] Mattias Ekstedt et al. "Fibrosis stage is the strongest predictor for disease-specific mortality in NAFLD after up to 33 years of follow-up". *Hepatology* 61.5 (May 2015), pp. 1547–1554.

[92] Patrizia Burra, Chiara Becchetti, and Giacomo Germani. "NAFLD and liver transplantation: Disease burden, current management and future challenges". *JHEP Reports* 2.6 (Dec. 2020), p. 100192.

[93] Elena Buzzetti, Massimo Pinzani, and Emmanuel A. Tsochatzis. "The multiple-hit pathogenesis of non-alcoholic fatty liver disease (NAFLD)". *Metabolism: Clinical and Experimental* 65.8 (2016), pp. 1038–48.

[94] J. K. Dowman, J. W. Tomlinson, and P. N. Newsome. "Pathogenesis of non-alcoholic fatty liver disease". *QJM* 103.2 (Nov. 2009), pp. 71–83.

[95] J. M. Lavoie and M. S. Gauthier. "Regulation of fat metabolism in the liver: Link to non-alcoholic hepatic steatosis and impact of physical exercise". *Cellular and Molecular Life Sciences* 63.12 (2006), pp. 1393–409.

[96] Quentin M. Anstee, Giovanni Targher, and Christopher P. Day. "Progression of NAFLD to diabetes mellitus, cardiovascular disease or cirrhosis". *Nature Reviews Gastroenterology and Hepatology* 10.6 (2013), pp. 330–44.

[97] Varman T. Samuel and Gerald I. Shulman. "The pathogenesis of insulin resistance: Integrating signaling pathways and substrate flux". *Journal of Clinical Investigation* 126.1 (2016), pp. 12–22.

[98] María Eugenia Miquilena-Colina et al. "Hepatic fatty acid translocase CD36 upregulation is associated with insulin resistance, hyperinsulinaemia and increased steatosis in non-alcoholic steatohepatitis and chronic hepatitis C". *Gut* 60.10 (2011), pp. 1394–402.

[99] Francesco M. Perla et al. "The role of lipid and lipoprotein metabolism in non-alcoholic fatty liver disease". *Children* 4.6 (2017), p. 46.

[100] Alexander R. Moschen et al. "Adipose and liver expression of interleukin (IL)-1 family members in morbid obesity and effects of weight loss". *Molecular Medicine* 17.7-8 (2011), pp. 840–845.

[101] Yehuda Kamari et al. "Lack of interleukin-1α or interleukin-1β inhibits transformation of steatosis to steatohepatitis and liver fibrosis in hypercholesterolemic mice". *Journal of Hepatology* 55.5 (2011), pp. 1086–94.

[102] Jennifer E. Lambert et al. "Increased de novo lipogenesis is a distinct characteristic of individuals with nonalcoholic fatty liver disease". *Gastroenterology* 146.3 (2014), pp. 726–35.

[103] Kerry L. Donnelly et al. "Sources of fatty acids stored in liver and secreted via lipoproteins in patients with nonalcoholic fatty liver disease". *Journal of Clinical Investigation* 115.5 (2005), pp. 1343–51.

[104] Nobito Higuchi et al. "Liver X receptor in cooperation with SREBP-1c is a major lipid synthesis regulator in nonalcoholic fatty liver disease". *Hepatology Research* 38.11 (2008), pp. 1122–9.

[105] Elena Lima-Cabello et al. "Enhanced expression of pro-inflammatory mediators and liver X-receptor-regulated lipogenic genes in non-alcoholic fatty liver disease and hepatitis C". *Clinical Science* 120.6 (2011), pp. 239–50.

[106] Jose A. Chavez and Scott A. Summers. "A ceramide-centric view of insulin resistance". *Cell Metabolism* 15.5 (2012), pp. 585–94.

[107] Michael Schrader et al. "Peroxisome-mitochondria interplay and disease". *Journal of Inherited Metabolic Disease* 38.4 (2015), pp. 681–702.

[108] Geoffrey C. Farrell et al. "NASH is an inflammatory disorder: Pathogenic, prognostic and therapeutic implications". *Gut and Liver* 6.2 (2012), pp. 149–71.

[109] Gardar Sveinbjornsson et al. "Multiomics study of nonalcoholic fatty liver disease". *Nature Genetics* 54.11 (2022), pp. 1652–1663.

[110] Meng Yang, Feng Ma, and Min Guan. "Role of steroid hormones in the pathogenesis of nonalcoholic fatty liver disease". *Metabolites* 11.5 (2021), p. 320.

[111] Jonathan M. Hazlehurst and Jeremy W. Tomlinson. "Mechanisms in endocrinology: Non-alcoholic fatty liver disease in common endocrine disorders". *European Journal of Endocrinology* 169.2 (Aug. 2013), pp. 27–37.

[112] International Agency for Research on Cancer. *World Health Organization*. 2020. URL: `https://gco.iarc.fr/today/home`.

[113] Centers for Disease Control and Prevention. *United States Cancer Statistics (USCS)*. 2020.

[114] Cancer Research UK. *Cancer Research UK (Liver Cancer Statistic and Cancer Stages)*. 2020. URL: `https://www.cancerresearchuk.org`.

[115] Ahmedin Jemal et al. "Annual Report to the Nation on the Status of Cancer, 1975-2014, Featuring Survival". *Journal of the National Cancer Institute* 109.9 (2017), p. 30.

[116] Patricia C. Valery et al. “Projections of primary liver cancer to 2030 in 30 countries worldwide”. *Hepatology* 67.2 (2018), pp. 600–611.

[117] Office for National Statistics. “Cancer survival in England: adult, stage at diagnosis and childhood - patients followed up to 2018”. *Office for National Statistics* August (2019), pp. 1–37.

[118] World Health Organization: World Cancer Report. *World Cancer Report 2014*. Tech. rep. World Health Organization, 2014, Chapter 5.6.

[119] S. C. Larsson and A. Wolk. “Overweight, obesity and risk of liver cancer: A meta-analysis of cohort studies”. *British Journal of Cancer* 97.7 (2007), pp. 1005–1008.

[120] Zobair Younossi et al. “Nonalcoholic Steatohepatitis Is the Fastest Growing Cause of Hepatocellular Carcinoma in Liver Transplant Candidates”. *Clinical Gastroenterology and Hepatology* 17.4 (2019), pp. 748–755.

[121] Véronique Grando-Lemaire et al. “Hepatocellular carcinoma without cirrhosis in the West: epidemiological factors and histopathology of the non-tumorous liver”. *Journal of Hepatology* 31.3 (1999), pp. 508–513.

[122] Sara Torrecilla et al. “Trunk mutational events present minimal intra- and inter-tumoral heterogeneity in hepatocellular carcinoma”. *Journal of Hepatology* 67.6 (2017), pp. 1222–1231.

[123] M. J. Ferber et al. “Integrations of the hepatitis B virus (HBV) and human papillomavirus (HPV) into the human telomerase reverse transcriptase (hTERT) gene in liver and cervical cancers”. *Oncogene* 22.24 (2003), pp. 3813–20.

[124] Izumi Horikawa and J. Carl Barrett. “cis-activation of the human telomerase gene (hTERT) by the hepatitis B virus genome”. *Journal of the National Cancer Institute* 93.15 (2001), pp. 1171–3.

[125] Y. Murakami et al. “Large scaled analysis of hepatitis B virus (HBV) DNA integration in HBV related hepatocellular carcinomas”. *Gut* 54.8 (2005), pp. 1162–8.

[126] Akihiro Tamori et al. “Alteration of gene expression in human hepatocellular carcinoma with integrated hepatitis B virus DNA”. *Clinical Cancer Research* 11.16 (2005), pp. 5821–6.

[127] T Tokino et al. “Chromosomal translocation and inverted duplication associated with integrated hepatitis B virus in hepatocellular carcinomas.” *Journal of Virology* 61.12 (1987), pp. 3848–54.

[128] Ming Geng et al. “Molecular mechanism of hepatitis B virus X protein function in hepatocarcinogenesis”. *World Journal of Gastroenterology* 21.38 (2015), pp. 10732–38.

[129] Christine Neuveut, Yu Wei, and Marie Annick Buendia. “Mechanisms of HBV-related hepatocarcinogenesis”. *Journal of Hepatology* 52.4 (2010), pp. 594–604.

[130] Jan H.M.B. Stoot et al. “Malignant transformation of hepatocellular adenomas into hepatocellular carcinomas: a systematic review including more than 1600 adenoma cases.” *HPB : the official journal of the International Hepato Pancreato Biliary Association* 12.8 (2010), pp. 509–22.

[131] Xiao Xiao Ding et al. "Precision medicine for hepatocellular carcinoma: Driver mutations and targeted therapy". *Oncotarget* 8.33 (2017), pp. 55715–30.

[132] Derek Y. Chiang et al. "Focal gains of VEGFA and molecular classification of hepatocellular carcinoma". *Cancer Research* 68.16 (2008), pp. 6779–88.

[133] Eric T. Sawey et al. "Identification of a Therapeutic Strategy Targeting Amplified FGF19 in Liver Cancer by Oncogenomic Screening". *Cancer Cell* 19.3 (2011), pp. 347–58.

[134] Tatsuhiro Shibata and Hiroyuki Aburatani. "Exploration of liver cancer genomes". *Nature Reviews Gastroenterology and Hepatology* 11.6 (2014), pp. 340–9.

[135] Ruidong Xue et al. "Variable Intra-Tumor Genomic Heterogeneity of Multiple Lesions in Patients with Hepatocellular Carcinoma". *Gastroenterology* 150.4 (2016), pp. 998–1008.

[136] Aileen Marshall et al. "Global Gene Expression Profiling Reveals SPINK1 as a Potential Hepatocellular Carcinoma Marker". *PLoS ONE* 8.3 (Mar. 2013), p. 59459.

[137] Daniel Q. Huang, Hashem B. El-Serag, and Rohit Loomba. "Global epidemiology of NAFLD-related HCC: trends, predictions, risk factors and prevention". *Nature Reviews Gastroenterology and Hepatology* 18.4 (2021), pp. 223–238.

[138] George N. Ioannou. "Epidemiology and risk-stratification of NAFLD-associated HCC". *Journal of Hepatology* 75.6 (2021), pp. 1476–84.

[139] Friedrich Foerster et al. "NAFLD-driven HCC: Safety and efficacy of current and emerging treatment options". *Journal of Hepatology* 76.2 (2022), pp. 446–57.

[140] Rohit Loomba, Scott L. Friedman, and Gerald I. Shulman. "Mechanisms and disease consequences of nonalcoholic fatty liver disease". *Cell* 184.10 (May 2021), pp. 2537–2564. URL: `http://www.cell.com/article/S0092867421004943/fulltext%20http://www.cell.com/article/S0092867421004943/abstract%20https://www.cell.com/cell/abstract/S0092-8674(21)00494-3`.

[141] Chi Ma et al. "NAFLD causes selective CD4(+) T lymphocyte loss and promotes hepatocarcinogenesis". *Nature* 531.7593 (Mar. 2016), pp. 253–257.

[142] Shabnam Shalapour et al. "Inflammation-induced IgA+ cells dismantle anti-liver cancer immunity". *Nature* 551.7680 (2017), pp. 340–45.

[143] Kanokwan Pinyopornpanish et al. "Hepatocellular carcinoma in nonalcoholic fatty liver disease with or without cirrhosis: a population-based study". *BMC Gastroenterology* 21.1 (2021), p. 394.

[144] Fasiha Kanwal et al. "Risk of Hepatocellular Cancer in Patients With Non-Alcoholic Fatty Liver Disease". *Gastroenterology* 155.6 (2018), pp. 1828–37.

[145] F. J. Vizoso et al. "Liver expression of steroid hormones and Apolipoprotein D receptors in hepatocellular carcinoma". *World Journal of Gastroenterology* 13.23 (2007), pp. 3221–7.

[146] Zeni Wu et al. "Endogenous sex steroid hormones and risk of liver cancer among US men: Results from the Liver Cancer Pooling Project". *JHEP Reports* 5.7 (July 2023), p. 100742.

[147] Yalan Xu and Jie Qiao. *Association of Insulin Resistance and Elevated Androgen Levels with Polycystic Ovarian Syndrome (PCOS): A Review of Literature*. 2022.

[148] Dalia Walzer et al. "Excess 11-Oxygenated Androgens in Women With Severe Insulin Resistance Are Mediated by Adrenal Insulin Receptor Signaling". *Journal of Clinical Endocrinology and Metabolism* 107.9 (2022).

[149] Trevor M. Penning and Jason E. Drury. "Human aldo-keto reductases: Function, gene regulation, and single nucleotide polymorphisms". *Archives of Biochemistry and Biophysics* 464.2 (Aug. 2007), pp. 241–250.

[150] T. M. Penning et al. "Structure-function of human 3α-hydroxysteroid dehydrogenases: Genes and proteins". *Molecular and Cellular Endocrinology* 215.1-2 (2004), pp. 63–72.

[151] Mikio Nishizawa et al. "Close kinship of human 20alpha-hydroxysteroid dehydrogenase gene with three aldo-keto reductase genes". *Genes to Cells* 5.2 (Feb. 2000), pp. 111–125.

[152] T. M. Penning et al. "Human 3α-hydroxysteroid dehydrogenase isoforms (AKR1C1-AKR1C4) of the aldo-keto reductase superfamily: Functional plasticity and tissue distribution reveals roles in the inactivation and formation of male and female sex hormones". *Biochemical Journal* 351.1 (Oct. 2000), pp. 67–77.

[153] Linn Fagerberg et al. "Analysis of the human tissue-specific expression by genome-wide integration of transcriptomics and antibody-based proteomics". *Molecular and Cellular Proteomics* 13.2 (2014), pp. 397–406.

[154] N. Beranič, S. Gobec, and T. Lanišnik Rižner. "Progestins as inhibitors of the human 20-ketosteroid reductases, AKR1C1 and AKR1C3". *Chemico-Biological Interactions* 191.1-3 (2011), pp. 227–33.

[155] Kamalesh K. Sharma et al. "Deoxycorticosterone inactivation by AKR1C3 in human mineralocorticoid target tissues". *Molecular and Cellular Endocrinology* 248.1-2 (2006), pp. 79–86.

[156] Yu Higaki et al. "Selective and potent inhibitors of human 20α-hydroxysteroid dehydrogenase (AKR1C1) that metabolizes neurosteroids derived from progesterone". *Chemico-Biological Interactions* 143-144 (2003), pp. 503–13.

[157] Michael E. Burczynski et al. "The Reactive Oxygen Species- and Michael Acceptor-inducible Human Aldo-Keto Reductase AKR1C1 Reduces the α,β-Unsaturated Aldehyde 4-Hydroxy-2-nonenal to 1,4-Dihydroxy-2-nonene". *Journal of Biological Chemistry* 276.4 (Jan. 2001), pp. 2890–2897.

[158] Kazuya Matsuura et al. "Identification of amino acid residues responsible for differences in substrate specificity and inhibitor sensitivity between two human liver dihydrodiol dehydrogenase isoenzymes by site-directed mutagenesis". *Biochemical Journal* 323.1 (Apr. 1997), pp. 61–64.

[159] F. Xavier Ruiz et al. "Retinaldehyde is a substrate for human aldo-keto reductases of the 1C subfamily". *Biochemical Journal* 440.3 (2011), pp. 335–44.

[160] Hermann Esterbauer, Rudolf Jörg Schaur, and Helmward Zollner. "Chemistry and biochemistry of 4-hydroxynonenal, malonaldehyde and related aldehydes". *Free Radical Biology and Medicine* 11.1 (1991), pp. 81–128.

[161] Sandro Michelini et al. "Aldo-Keto Reductase 1C1 (AKR1C1) as the First Mutated Gene in a Family with Nonsyndromic Primary Lipedema". *International Journal of Molecular Sciences 2020* 21.17 (Aug. 2020), p. 6264.

[162] Shani Ben-Moshe and Shalev Itzkovitz. "Spatial heterogeneity in the mammalian liver". *Nature Reviews Gastroenterology & Hepatology* 16.7 (Apr. 2019), pp. 395–410.

[163] Shani Ben-Moshe et al. "Spatial sorting enables comprehensive characterization of liver zonation". *Nature Metabolism* 1.9 (Sept. 2019), pp. 899–911.

[164] I Dufort et al. "Molecular cloning of human type 3 3 alpha-hydroxysteroid dehydrogenase that differs from 20 alpha-hydroxysteroid dehydrogenase by seven amino acids." *Biochemical and biophysical research communications* 228.2 (Nov. 1996), pp. 474–9.

[165] Isabelle Dufort, Fernand Labrie, and Van Luu-The. "Human Types 1 and 3 3α-Hydroxysteroid Dehydrogenases: Differential Lability and Tissue Distribution". *The Journal of Clinical Endocrinology & Metabolism* 86.2 (Feb. 2001), pp. 841–846.

[166] I Dufort et al. "Characteristics of a highly labile human type 5 17beta-hydroxysteroid dehydrogenase." *Endocrinology* 140.2 (Feb. 1999), pp. 568–74.

[167] Ossama El-Kabbani et al. "Probing the inhibitor selectivity pocket of human 20α-hydroxysteroid dehydrogenase (AKR1C1) with X-ray crystallography and site-directed mutagenesis". *Bioorganic and Medicinal Chemistry Letters* 21.8 (2011), pp. 2564–7.

[168] Andrew D. Yates et al. "Ensembl 2020". *Nucleic Acids Research* 48.D1 (2020), pp. 682–88.

[169] Alex Bateman. "UniProt: A worldwide hub of protein knowledge". *Nucleic Acids Research* 47.D1 (2019), pp. 506–15.

[170] Qing Ji et al. "Impaired dihydrotestosterone catabolism in human prostate cancer: Critical role of AKR1C2 as a pre-receptor regulator of androgen receptor signaling". *Cancer Research* 63.3 (2007), pp. 1361–9.

[171] Hong Zhu et al. "AKR1C1 activates STAT3 to promote the metastasis of non-small cell lung cancer". *Theranostics* 8.3 (2018), pp. 676–692.

[172] Ryuji Matsumoto et al. "Aldo-keto reductase 1C1 induced by interleukin-1β mediates the invasive potential and drug resistance of metastatic bladder cancer cells". *Scientific Reports* 6.1 (Dec. 2016), p. 34625.

[173] Qing Ji et al. "Selective loss of AKR1C1 and AKR1C2 in breast cancer and their potential effect on progesterone signaling". *Cancer Research* 64.20 (2004), pp. 7610–7617.

[174] Wei Min Chang et al. "AKR1C1 controls cisplatin-resistance in head and neck squamous cell carcinoma through cross-talk with the STAT1/3 signaling pathway". *Journal of Experimental and Clinical Cancer Research* 38.1 (2019), pp. 1–14.

[175] Lisha Mou et al. "Construction of a lipid metabolism-related risk model for hepatocellular carcinoma by single cell and machine learning analysis". *Frontiers in Immunology* 14 (Mar. 2023), p. 1036562.

[176] Olivier Govaere et al. "A proteo-transcriptomic map of non-alcoholic fatty liver disease signatures". *Nature Metabolism* 5.4 (Apr. 2023), pp. 572–578.

[177] Michael E. Burczynski, Hseuh Kung Lin, and Trevor M. Penning. "Isoform-specific induction of a human aldo-keto reductase by polycyclic aromatic hydrocarbons (PAHs), electrophiles, and oxidative stress: Implications for the alternative pathway of PAH activation catalyzed by human dihydrodiol dehydrogenase". *Cancer Research* 59.3 (1999), pp. 607–614.

[178] Kyeong Ah Jung et al. "Identification of aldo-keto reductases as NRF2-target marker genes in human cells". *Toxicology Letters* 218.1 (2013), pp. 39–49.

[179] Trevor M. Penning. "Aldo-keto reductase regulation by the Nrf2 system: Implications for stress response, chemotherapy drug resistance, and carcinogenesis". *Chemical Research in Toxicology* 30.1 (2017), pp. 162–76.

[180] Mingxin Zhang et al. "Nrf2 is a potential prognostic marker and promotes proliferation and invasion in human hepatocellular carcinoma". *BMC Cancer* 15 (2015), p. 531.

[181] Huan Lou et al. "Induction of AKR1C2 by phase II inducers: Identification of a distal consensus antioxidant response element regulated by NRF2". *Molecular Pharmacology* 69.5 (2006), pp. 1662–72.

[182] Huiyong Yin. "The role of lipid peroxidation during the progression of human hepatocellular carcinoma (HCC)". *Free Radical Biology and Medicine* 124 (2018), pp. 563–564.

[183] Scott J. Dixon et al. "Pharmacological inhibition of cystine-glutamate exchange induces endoplasmic reticulum stress and ferroptosis". *eLife* 3 (2014), p. 2523.

[184] Xiaofang Sun et al. "Activation of the p62-Keap1-NRF2 pathway protects against ferroptosis in hepatocellular carcinoma cells". *Hepatology* 63.1 (2016), pp. 173–84.

[185] Mitsuru Haniu et al. "Structural and Functional Analysis of NADPH-Cytochrome P-450 Reductase from Human Liver: Complete Sequence of Human Enzyme and NADPH-Binding Sites". *Biochemistry* 28.21 (1989), pp. 8639–8645.

[186] *NADPH–cytochrome P450 reductase isoform 1 [Homo sapiens] - Protein - NCBI*. URL: `https://www.ncbi.nlm.nih.gov/protein/NP_001382342`.

[187] Rachel R. Scott et al. "Apparent manifesting heterozygosity in P450 oxidoreductase deficiency and its effect on coexisting 21-hydroxylase deficiency". *Journal of Clinical Endocrinology and Metabolism* 92.6 (2007), pp. 2318–22.

[188] Walter L. Miller. *Steroidogenic electron-transfer factors and their diseases*. 2021.

[189] Anna L. Shen, Kathleen A. O'Leary, and Charles B. Kasper. "Association of multiple developmental defects and embryonic lethality with loss of microsomal NADPH-cytochrome P450 oxidoreductase". *Journal of Biological Chemistry* 277.8 (2002), pp. 6536–41.

[190] Jun Gu et al. "Liver-specific Deletion of the NADPH-Cytochrome P450 Reductase Gene". *Journal of Biological Chemistry* 278.28 (2003), pp. 25895–901.

[191] Emmanuel Lesuisse, Monique Casteras-Simon, and Pierre Labbe. "Cytochrome P-450 reductase is responsible for the ferrireductase activity associated with isolated plasma membranes of Saccharomyces cerevisiae". *FEMS Microbiology Letters* 156.1 (1997), pp. 147–52.

[192] B. A. Schacter et al. "Immunochemical evidence for an association of heme oxygenase with the microsomal electron transport system." *Journal of Biological Chemistry* 247.11 (1972), pp. 3601–7.

[193] H. G. Enoch and P. Strittmatter. "Cytochrome b5 reduction by NADPH-cytochrome P-450 reductase." *Journal of Biological Chemistry* 254.18 (1979), pp. 8976–81.

[194] Todd D. Porter. "The roles of cytochrome b5 in cytochrome P450 reactions". *Journal of Biochemical and Molecular Toxicology* 16.6 (2002), pp. 311–6.

[195] T. Ono and K. Bloch. "Solubilization and partial characterization of rat liver squalene epoxidase". *Journal of Biological Chemistry* 250.4 (1975), pp. 1571–9.

[196] Z. Ilan, R. Ilan, and D. L. Cinti. "Evidence for a new physiological role of hepatic NADPH:ferricytochrome (P-450) oxidoreductase. Direct electron input to the microsomal fatty acid chain elongation system." *Journal of Biological Chemistry* 256.19 (1981), pp. 10066–72.

[197] Todd D. Porter. "New insights into the role of cytochrome P450 reductase (POR) in microsomal redox biology". *Acta Pharmaceutica Sinica B* 2.2 (Apr. 2012), pp. 102–106.

[198] Takashi Iyanagi, Chuanwu Xia, and Jung Ja P. Kim. "NADPH-cytochrome P450 oxidoreductase: prototypic member of the diflavin reductase family". *Archives of biochemistry and biophysics* 528.1 (Dec. 2012), pp. 72–89.

[199] A. W. Munro et al. "Determination of the Redox Properties of Human NADPH-Cytochrome P450 Reductase". *Biochemistry* 40.7 (Feb. 2001), pp. 1956–1963.

[200] J. L. Vermilion and M. J. Coon. "Identification of the high and low potential flavins of liver microsomal NADPH-cytochrome P-450 reductase." *Journal of Biological Chemistry* 253.24 (Dec. 1978), pp. 8812–8819.

[201] Svetlana Simtchouk et al. "Kinetic analysis of cytochrome P450 reductase from Artemisia annua reveals accelerated rates of NADPH-dependent flavin reduction". *The FEBS Journal* 280.24 (Dec. 2013), pp. 6627–6642.

[202] Ana C. Ebrecht et al. "Biochemical and structural insights into the cytochrome P450 reductase from Candida tropicalis". *Scientific Reports 2019 9:1* 9.1 (Dec. 2019), pp. 1–11.

[203] Martin Šrejber et al. "Membrane-attached mammalian cytochromes P450: An overview of the membrane's effects on structure, drug binding, and interactions with redox partners". *Journal of Inorganic Biochemistry* 183 (2018), pp. 117–136.

[204] Ming Wang et al. "Three-dimensional structure of NADPH-cytochrome P450 reductase: Prototype for FMN- and FAD-containing enzymes". *Proceedings of the National Academy of Sciences of the United States of America* 94.16 (1997), pp. 8411–6.

[205] Chuanwu Xia et al. "Structural basis for human NADPH-cytochrome P450 oxidoreductase deficiency". *Proceedings of the National Academy of Sciences of the United States of America* 108.33 (Aug. 2011), pp. 13486–13491.

[206] Walter L. Miller et al. "Consequences of POR mutations and polymorphisms". *Molecular and Cellular Endocrinology* 336.1-2 (2011), pp. 174–9.

[207] Christa E. Flück, Catherine Nicolo, and Amit V. Pandey. "Clinical, structural and functional implications of mutations and polymorphisms in human NADPH P450 oxidoreductase". *Fundamental and Clinical Pharmacology* 21.4 (2007), pp. 399–410.

[208] Yang Bai, Jinhui Li, and Xiaoli Wang. "Cytochrome P450 oxidoreductase deficiency caused by R457H mutation in POR gene in Chinese: Case report and literature review". *Journal of Ovarian Research* 10.1 (2017), p. 16.

[209] Claudia Boettcher and Christa E. Flück. "Rare forms of genetic steroidogenic defects affecting the gonads and adrenals". *Best Practice and Research: Clinical Endocrinology and Metabolism* 36.1 (2022), p. 101593.

[210] Christopher C. Marohnic et al. "Diminished FAD binding in the Y459H and V492E Antley-Bixler syndrome mutants of human cytochrome P450 reductase". *Journal of Biological Chemistry* 281.47 (2006).

[211] Diana M. E. Otto et al. "Identification of Novel Roles of the Cytochrome P450 System in Early Embryogenesis: Effects on Vasculogenesis and Retinoic Acid Homeostasis". *Molecular and Cellular Biology* 23.17 (2003), pp. 6103–16.

[212] Liang Gong et al. *Polymorphisms in cytochrome P450 oxidoreductase and its effect on drug metabolism and efficacy*. 2017.

[213] Christa E. Flück, Primus E. Mullis, and A. V. Pandey. "Reduction in hepatic drug metabolizing CYP3A4 activities caused by P450 oxidoreductase mutations identified in patients with disordered steroid metabolism". *Biochemical and Biophysical Research Communications* 401.1 (2010).

[214] Xuan Chen et al. "Influence of various polymorphic variants of Cytochrome P450 Oxidoreductase (POR) on drug metabolic activity of CYP3A4 and CYP2B6". *PLoS ONE* 7.6 (2012).

[215] Duanpen Sandee et al. "Effects of genetic variants of human P450 oxidoreductase on catalysis by CYP2D6 in vitro". *Pharmacogenetics and Genomics* 20.11 (2010).

[216] Murali Subramanian et al. "Effect of P450 oxidoreductase variants on the metabolism of model substrates mediated by CYP2C9.1, CYP2C9.2, and CYP2C9.3". *Pharmacogenetics and Genomics* 22.8 (2012).

[217] Dorota Tomalik-Scharte et al. "Impaired hepatic drug and steroid metabolism in congenital adrenal hyperplasia due to P450 oxidoreductase deficiency". *European Journal of Endocrinology* 163.6 (2010), pp. 919–24.

[218] Fei Cao, Anguo Luo, and Chaowen Yang. "G6PD inhibits ferroptosis in hepatocellular carcinoma by targeting cytochrome P450 oxidoreductase". *Cellular Signalling* 87 (2021), p. 110098.

[219] Yan Fang et al. "The POR rs10954732 polymorphism decreases susceptibility to hepatocellular carcinoma and hepsin as a prognostic biomarker correlated with immune infiltration based on proteomics". *Journal of Translational Medicine* 20.1 (2022), p. 88.

[220] Ketuan Huang et al. "Genetic variants and expression of cytochrome p450 oxidoreductase predict postoperative survival in patients with hepatitis B virus-related hepatocellular carcinoma". *Journal of Cancer* 10.6 (2019), pp. 1453–1465.

[221] Colin J. Henderson et al. "Inactivation of the hepatic cytochrome P450 system by conditional deletion of hepatic cytochrome P450 reductase". *Journal of Biological Chemistry* 278.15 (2003), pp. 13480–6.

[222] Mercedes Barzi et al. "A novel humanized mouse lacking murine P450 oxidoreductase for studying human drug metabolism". *Nature Communications* 8.1 (2017), p. 39.

[223] David P. Aden et al. "Controlled synthesis of HBsAg in a differentiated human liver carcinoma-derived cell line". *Nature* 282.5739 (1979), pp. 615–616.

[224] Hidekazu Nakabayashi et al. "Growth of human hepatoma cell lines with differentiated functions in chemically defined medium". *Cancer Research* 42.9 (1982), pp. 3858–63.

[225] Brigitte Bressac et al. "Abnormal structure and expression of p53 gene in human hepatocellular carcinoma". *Proceedings of the National Academy of Sciences of the United States of America* 87.5 (1990), pp. 1973–1977.

[226] Kin Tak Chan and Maria Li Lung. "Mutant p53 expression enhances drug resistance in a hepatocellular carcinoma cell line". *Cancer Chemotherapy and Pharmacology* 53.6 (June 2004), pp. 519–526.

[227] M Reiser et al. "Induction of cell proliferation arrest and apoptosis in hepatoma cells through adenoviral-mediated transfer of p53 gene." *Journal of hepatology* 32.5 (May 2000), pp. 771–82.

[228] Bruno Sainz, Naina Barretto, and Susan L. Uprichard. "Hepatitis C virus infection in phenotypically distinct Huh7 cell lines". *PLoS ONE* 4.8 (Aug. 2009), p. 6561.

[229] Hongshan Jiang et al. "Skewer: a fast and accurate adapter trimmer for next-generation sequencing paired-end reads". *BMC Bioinformatics* 15.1 (June 2014), pp. 1–12.

[230] Daehwan Kim, Ben Langmead, and Steven L Salzberg. "HISAT: a fast spliced aligner with low memory requirements". *Nature methods* 12.4 (Mar. 2015), p. 357.

[231] Fiona Cunningham et al. "Ensembl 2015". *Nucleic Acids Research* 43.D1 (Jan. 2015), pp. D662–D669.

[232] Liao Y, Smyth GK, and Shi W. "featureCounts: an efficient general purpose program for assigning sequence reads to genomic features". *Bioinformatics (Oxford, England)* 30.7 (Apr. 2014), pp. 923–930.

[233] Yang Liao, Gordon K. Smyth, and Wei Shi. "The Subread aligner: fast, accurate and scalable read mapping by seed-and-vote". *Nucleic Acids Research* 41.10 (May 2013), e108.

[234] Michael I Love, Wolfgang Huber, and Simon Anders. "Moderated estimation of fold change and dispersion for RNA-seq data with DESeq2". *Genome Biology* 15.12 (Dec. 2014), pp. 1–21.

[235] Guangchuang Yu et al. "clusterProfiler: an R Package for Comparing Biological Themes Among Gene Clusters". *https://home.liebertpub.com/omi* 16.5 (May 2012), pp. 284–287.

[236] Jordi Folch, M Lees, and G H Sloane. "A Simple Method For The Isolation And Purification Of Total Lipides From Animal Tissues". *Journal of Biological Chemistry* 226 (1957), pp. 497–509.

[237] G. C. Burdge et al. "A method for separation of phosphatidylcholine, triacylglycerol, non-esterified fatty acids and cholesterol esters from plasma by solid-phase extraction*". *British Journal of Nutrition* 84.5 (2000), pp. 781–787.

[238] Otília Menyhárt, Ádám Nagy, and Balázs Győrffy. "Determining consistent prognostic biomarkers of overall survival and vascular invasion in hepatocellular carcinoma". *Royal Society Open Science* 5.12 (2018), p. 181006.

[239] Zefang Tang et al. "GEPIA: A web server for cancer and normal gene expression profiling and interactive analyses". *Nucleic Acids Research* 45.W1 (2017), pp. 98–102.

[240] Keqing He et al. "Zingiberensis Newsaponin Inhibits the Malignant Progression of Hepatocellular Carcinoma via Suppressing Autophagy Moderated by the AKR1C1-Mediated JAK2/STAT3 Pathway". *Evidence-based Complementary and Alternative Medicine* 2021 (2021), p. 4055209.

[241] Kai Li et al. "Hepatitis B virus X protein up-regulates AKR1C1 expression through nuclear factor-Y in human hepatocarcinoma cells". *Hepatitis Monthly* 13.5 (2013), pp. 1–9.

[242] Shinji Itoh et al. "Antineoplastic effects of gamma linolenic acid on hepatocellular carcinoma cell lines". *Journal of Clinical Biochemistry and Nutrition* 47.1 (2010), pp. 81–90.

[243] Nikolaos Nikolaou et al. "AKR1D1 is a novel regulator of metabolic phenotype in human hepatocytes and is dysregulated in non-alcoholic fatty liver disease". *Metabolism: Clinical and Experimental* 99 (2019), pp. 67–80.

[244] Lina Schiffer et al. *Human steroid biosynthesis, metabolism and excretion are differentially reflected by serum and urine steroid metabolomes: A comprehensive review.* 2019.

[245] András Lánczky and Balázs Győrffy. "Web-based survival analysis tool tailored for medical research (KMplot): Development and implementation". *Journal of Medical Internet Research* 23.7 (2021), e27633.

[246] David E. Kleiner et al. "Design and validation of a histological scoring system for nonalcoholic fatty liver disease". *Hepatology* 41.6 (2005), pp. 1313–21.

[247] Cedric H.L. Shackleton. "Mass spectrometry in the diagnosis of steroid-related disorders and in hypertension research". *Journal of Steroid Biochemistry and Molecular Biology* 45.1-3 (1993), pp. 127–40.

[248] Shou-Feng Zhao et al. "AKR1C1-3, notably AKR1C3, are distinct biomarkers for liver cancer diagnosis and prognosis: Database mining in malignancies". *Oncology Letters* 18.5 (Sept. 2019), pp. 4515–4522.

[249] Pedro Veliça et al. "Lack of functional and expression homology between human and mouse aldo-keto reductase 1C enzymes: Implications for modelling human cancers". *Molecular Cancer* 8 (2009), p. 121.

[250] Scott M. Wilhelm et al. "BAY 43-9006 exhibits broad spectrum oral antitumor activity and targets the RAF/MEK/ERK pathway and receptor tyrosine kinases involved in tumor progression and angiogenesis". *Cancer Research* 64.19 (2004), pp. 7099–109.

[251] Yong S. Chang et al. "Sorafenib (BAY 43-9006) inhibits tumor growth and vascularization and induces tumor apoptosis and hypoxia in RCC xenograft models". *Cancer Chemotherapy and Pharmacology* 59.5 (2007), pp. 561–74.

[252] Josep M. Llovet et al. "Sorafenib in advanced hepatocellular carcinoma". *New England Journal of Medicine* 359.4 (2008), pp. 378–90.

[253] Sheng xian Yuan et al. "Long noncoding RNA DANCR increases stemness features of hepatocellular carcinoma by derepression of CTNNB1". *Hepatology* 63.2 (2016), pp. 499–511.

[254] Ossama El-Kabbani et al. "Structure-guided design, synthesis, and evaluation of salicylic acid-based inhibitors targeting a selectivity pocket in the active site of human 20α-hydroxysteroid dehydrogenase (AKR1C1)". *Journal of Medicinal Chemistry* 52.10 (2009), pp. 3259–64.

[255] Patricia K. Eagon et al. "Quantitation of estrogen and androgen receptors in hepatocellular carcinoma and adjacent normal human liver". *Digestive Diseases and Sciences* 36.9 (1991), pp. 1303–8.

[256] M. Barone et al. "Role of sex steroid hormones on hepatocellular carcinoma (HCC) development in HBV transgenic mice". *Digestive and Liver Disease* 39.A3 (2007).

[257] Francesco Bellanti et al. "Lipid oxidation products in the pathogenesis of non-alcoholic steatohepatitis". *Free Radical Biology and Medicine* 111 (2017), pp. 173–185.

[258] Hadi Ali et al. "Lipid peroxidation derived reactive aldehydes in alcoholic liver disease". *Current Opinion in Toxicology* 13 (2019), pp. 110–7.

[259] Liang Shi et al. *Role of estrogen in hepatocellular carcinoma: Is inflammation the key?* 2014.

[260] Xing Wei et al. "AKR1C1 Contributes to Cervical Cancer Progression via Regulating TWIST1 Expression". *Biochemical Genetics* 59.2 (2021), pp. 516–530.

[261] Natascia Marino et al. "Upregulation of lipid metabolism genes in the breast prior to cancer diagnosis". *npj Breast Cancer* 6 (2020), p. 50.

[262] Toshiyuki Matsunaga et al. "Pathophysiological roles of aldo-keto reductases (AKR1C1 and AKR1C3) in development of cisplatin resistance in human colon cancers". *Chemico-Biological Interactions* 202.1-3 (2013), pp. 234–42.

[263] Husni M. Cangara et al. "Role of endothelial cell-selective adhesion molecule in hematogeneous metastasis". *Microvascular Research* 80.1 (2010), pp. 133–41.

[264] Dong Liang Chen et al. "L1cam promotes tumor progression and metastasis and is an independent unfavorable prognostic factor in gastric cancer". *Journal of Hematology and Oncology* 6.1 (June 2013), pp. 1–14.

[265] Monica Huszar et al. "Up-regulation of LICAM is linked to loss of hormone receptors and E-cadherin in aggressive subtypes of endometrial carcinomas". *Journal of Pathology* 220.5 (2010), pp. 551–61.

[266] Louis J.M. Van Der Putten et al. "L1CAM expression in endometrial carcinomas: An ENITEC collaboration study". *British Journal of Cancer* 115.6 (2016), pp. 716–24.

[267] Kai Doberstein et al. "L1CAM is expressed in triple-negative breast cancers and is inversely correlated with Androgen receptor". *BMC Cancer* 14.1 (2014), p. 958.

[268] Alain G. Zeimet et al. "L1CAM in early-stage type i endometrial cancer: Results of a large multicenter evaluation". *Journal of the National Cancer Institute* 105.15 (2013), pp. 1142–50.

[269] Ryouichi Tsunedomi et al. "Elevated expression of RAB3B plays important roles in chemoresistance and metastatic potential of hepatoma cells". *BMC Cancer* 22.1 (2022), p. 260.

[270] Linlin Luo et al. "Distinct lymphocyte antigens 6 (Ly6) family members Ly6D, Ly6E, Ly6K and Ly6H drive tumorigenesis and clinical outcome". *Oncotarget* 7.10 (2016), pp. 11165–11193.

[271] Midrar Alhossiny et al. "Ly6E/K signaling to TGFβ promotes breast cancer progression, immune escape, and drug resistance". *Cancer Research* 76.11 (2016), pp. 3376–86.

[272] Wiebke Arlt et al. "Congenital adrenal hyperplasia caused by mutant P450 oxidoreductase and human androgen synthesis: Analytical study". *Lancet* 363.9427 (2004), pp. 2128–35.

[273] Nils Krone et al. *Congenital adrenal hyperplasia and P450 oxidoreductase deficiency*. Feb. 2007.

[274] Christa E. Flück and Amit V. Pandey. "Human P450 oxidoreductase deficiency". *Encyclopedia of Endocrine Diseases*. 2nd edition. Academic Press, 2018.

[275] Nils Krone et al. "Genotype-Phenotype Analysis in Congenital Adrenal Hyperplasia due to P450 Oxidoreductase Deficiency". *Journal of Clinical Endocrinology and Metabolism* 97.2 (2012).

[276] Françoise Gofflot et al. "Molecular mechanisms underlying limb anomalies associated with cholesterol deficiency during gestation: Implications of Hedgehog signaling". *Human Molecular Genetics* 12.10 (2003).

[277] Mark Sperling. *Pediatric Endocrinology: Fourth Edition*. Saunders, 2014.

[278] Nicole Reisch et al. "Alternative pathway androgen biosynthesis and human fetal female virilization". *Proceedings of the National Academy of Sciences of the United States of America* 116.44 (2019), pp. 22294–22299.

[279] Shaheena Parween et al. "Molecular basis of CYP19A1 deficiency in a 46,XX patient with R550W mutation in POR: Expanding the PORD phenotype". *Journal of Clinical Endocrinology and Metabolism* 105.4 (2020), p. 76.

[280] Monika Gonzalez et al. "Defining a relationship between dietary fatty acids and the cytochrome P450 system in a mouse model of fatty liver disease". *Physiological Genomics* 43.3 (2011), pp. 121–35.

[281] Robert D. Finn et al. "Conditional Deletion of Cytochrome P450 Oxidoreductase in the Liver and Gastrointestinal Tract: A New Model for Studying the Functions of the P450 System". *Journal of Pharmacology and Experimental Therapeutics* 322.1 (July 2007), pp. 40–47.

[282] Michael P. Caulfield et al. "The diagnosis of congenital adrenal hyperplasia in the newborn by gas chromatography/mass spectrometry analysis of random urine specimens". *Journal of Clinical Endocrinology and Metabolism* 87.8 (2002), pp. 3682–90.

[283] Cedric Shackleton et al. "Prenatal diagnosis of P450 oxidoreductase deficiency (ORD): A disorder causing low pregnancy estriol, maternal and fetal virilization, and the Antley-Bixler syndrome phenotype". *American Journal of Medical Genetics* 129.2 (2004), pp. 105–12.

[284] Nils Krone et al. *Gas chromatography/mass spectrometry (GC/MS) remains a pre-eminent discovery tool in clinical steroid investigations even in the era of fast liquid chromatography tandem mass spectrometry (LC/MS/MS)*. 2010.

[285] Joanna K. Dowman et al. "Loss of 5α-Reductase Type 1 accelerates the development of hepatic steatosis but protects against hepatocellular carcinoma in male mice". *Endocrinology* 154.12 (2013), pp. 4536–47.

[286] Yanhua Chen et al. "Genome-wide association meta-analysis identifies 17 loci associated with nonalcoholic fatty liver disease". *Nature Genetics* 55.10 (2023).

[287] Žiga Urlep et al. "Disrupting hepatocyte Cyp51 from cholesterol synthesis leads to progressive liver injury in the developing mouse and decreases RORC signalling". *Scientific Reports* 7 (2017), p. 40775.

[288] Jessica M. Ferrell et al. "Cholesterol 7α-hydroxylase-deficient mice are protected from high-fat/high-cholesterol diet-induced metabolic disorders". *Journal of Lipid Research* 57.7 (2016), pp. 1144–54.

[289] Mathias Uhlén et al. "Tissue-based map of the human proteome". *Science* 347.6220 (2015).

[290] René Baudrand et al. "Overexpression of hepatic 5α-reductase and 11β-hydroxysteroid dehydrogenase type 1 in visceral adipose tissue is associated with hyperinsulinemia in morbidly obese patients". *Metabolism: Clinical and Experimental* 60.12 (2011).

[291] Sarah Konopelska et al. "Hepatic 11beta-HSD1 mRNA expression in fatty liver and nonalcoholic steatohepatitis". *Clinical Endocrinology* 70.4 (2009).

[292] Labrini Papanastasiou, Stelios Fountoulakis, and Ioannis Anastasios Vatalas. *Adrenal disorders and non-alcoholic fatty liver disease*. 2017.

[293] Colin J. Henderson, Georgia J. Pass, and C. Roland Wolf. "The hepatic cytochrome P450 reductase null mouse as a tool to identify a successful candidate entity". *Toxicology Letters* 162.1 (2006), pp. 111–7.

[294] Amit V. Pandey and Patrick Sproll. "Pharmacogenomics of human P450 oxidoreductase". *Frontiers in Pharmacology* 5 (2014), p. 103.

[295] Gregor Lorbek, Monika Lewinska, and Damjana Rozman. "Cytochrome P450s in the synthesis of cholesterol and bile acids – from mouse models to human diseases". *The FEBS Journal* 279.9 (May 2012), pp. 1516–1533.

[296] Tamara Heintze et al. "Effects of Diminished NADPH:cytochrome P450 Reductase in Human Hepatocytes on Lipid and Bile Acid Homeostasis". *Frontiers in Pharmacology* 12 (Nov. 2021), p. 2959.

[297] Catherine Nicolo et al. "Restoration of mutant cytochrome P450 reductase activity by external flavin". *Molecular and Cellular Endocrinology* 321.2 (2010), pp. 245–52.

[298] Todd D. Porter et al. "Suppression of cytochrome P450 reductase (POR) expression in hepatoma cells replicates the hepatic lipidosis observed in hepatic POR-null mice". *Drug Metabolism and Disposition* 39.6 (2011), pp. 966–73.

[299] Donald B. Jump. "Mammalian Fatty Acid Elongases". *Methods in molecular biology (Clifton, N.J.)* 579 (2009), p. 375.

[300] Takashi Matsuzaka et al. "Elovl6 promotes nonalcoholic steatohepatitis". *Hepatology (Baltimore, Md.)* 56.6 (Dec. 2012), pp. 2199–2208.

[301] Sonja M. Kessler et al. "Fatty acid elongation in non-alcoholic steatohepatitis and hepatocellular carcinoma". *International Journal of Molecular Sciences* 15.4 (2014), pp. 5762–73.

[302] Sohye Kang and Roger A. Davis. "Cholesterol and hepatic lipoprotein assembly and secretion". *Biochimica et Biophysica Acta (BBA) - Molecular and Cell Biology of Lipids* 1529.1-3 (Dec. 2000), pp. 223–230.

[303] Gene C. Ness, Zhihong Zhao, and Linda Wiggins. "Insulin and glucagon modulate hepatic 3-hydroxy-3-methylglutaryl-coenzyme A reductase activity by affecting immunoreactive protein levels". *Journal of Biological Chemistry* 269.46 (1994).

[304] Bo Zhou et al. "Haplotype-resolved and integrated genome analysis of the cancer cell line HepG2". *Nucleic Acids Research* 47.8 (2019).

[305] Alexander V. Tyakht et al. "RNA-Seq gene expression profiling of HepG2 cells: The influence of experimental factors and comparison with liver tissue". *BMC Genomics* 15.1 (2014).

[306] Viktoriia Arzumanian, Mikhail Pyatnitskiy, and Ekaterina Poverennaya. "Comparative Transcriptomic Analysis of Three Common Liver Cell Lines". *International Journal of Molecular Sciences* 24.10 (2023).

[307] H. H.J. Gerets et al. "Characterization of primary human hepatocytes, HepG2 cells, and HepaRG cells at the mRNA level and CYP activity in response to inducers and their predictivity for the detection of human hepatotoxins". *Cell Biology and Toxicology* 28.2 (2012).

[308] Danyel G.J. Jennen et al. "Comparison of HepG2 and HepaRG by whole-genome gene expression analysis for the purpose of chemical hazard identification". *Toxicological Sciences* 115.1 (2010).

[309] Benjamin Berger et al. "Comparison of Liver Cell Models Using the Basel Phenotyping Cocktail". *Frontiers in Pharmacology* 7.NOV (2016).

[310] Effi Haque et al. "Molecular mechanisms underlying hepatocellular carcinoma induction by aberrant nrf2 activation-mediated transcription networks: Interaction of nrf2-keap1 controls the fate of hepatocarcinogenesis". *International Journal of Molecular Sciences* 21.15 (2020), p. 5378.

[311] Charlotte Lefort and Patrice D. Cani. "The liver under the spotlight: Bile acids and oxysterols as pivotal actors controlling metabolism". *Cells* 10.2 (2021), p. 400.

[312] Bethan L. Clifford et al. "FXR activation protects against NAFLD via bile-acid-dependent reductions in lipid absorption". *Cell Metabolism* 33.8 (2021).

[313] Ling Ye et al. “Sorafenib metabolism is significantly altered in the liver tumor tissue of hepatocellular carcinoma patient”. *PLoS ONE* 9.5 (2014).

[314] Renuka Iyer et al. *Sorafenib: A clinical and pharmacologic review.* 2010.

[315] Veera Raghavan Thangapandi et al. “Loss of hepatic Mboat7 leads to liver fibrosis”. *Gut* 70.5 (2021), pp. 940–50.

[316] Miriam Longo et al. “TM6SF2/PNPLA3/MBOAT7 loss-of function genetic variants impact on NAFLD development and progression both in patients and in in vitro models”. *Cellular and Molecular Gastroenterology and Hepatology* 13.3 (2022), pp. 759–788.

[317] Rosellina Margherita Mancina et al. “The MBOAT7-TMC4 Variant rs641738 Increases Risk of Nonalcoholic Fatty Liver Disease in Individuals of European Descent”. *Gastroenterology* 150.5 (2016), pp. 1219–1230.

[318] Jawaher Alharthi et al. “A metabolic associated fatty liver disease risk variant in MBOAT7 regulates toll like receptor induced outcomes”. *Nature Communications* 13.1 (2022), p. 7430.

[319] Maya W. Haaker, Arie B. Vaandrager, and J. Bernd Helms. “Retinoids in health and disease: A role for hepatic stellate cells in affecting retinoid levels”. *Biochimica et Biophysica Acta - Molecular and Cell Biology of Lipids* 1865.6 (2020), p. 158674.

[320] Marta Melis et al. “Retinoids in the Pathogenesis and Treatment of Liver Diseases”. *Nutrients* 14.7 (2022), p. 1456.

[321] Magnus Christensen et al. “The Karolinska cocktail for phenotyping of five human cytochrome P450 enzymes”. *Clinical Pharmacology and Therapeutics* 73.6 (2003).

[322] J. Y. Ryu et al. “Development of the "Inje cocktail" for high-throughput evaluation of five human cytochrome P450 isoforms in vivo”. *Clinical Pharmacology and Therapeutics* 82.5 (2007).